Resonant Inelastic X–ray Scattering at Small Hydrocarbon Molecules

Scattering Dynamics and Bonding to Silicon

Dissertation
zur Erlangung des Doktorgrades
des Fachbereichs Physik
der Universität Hamburg

vorgelegt von
Franz Hennies
aus Freiburg i. Brsg.

Hamburg
2005

Resonante inelastische Röntgenstreuung an kleinen Kohlenwasserstoffmolekülen: Dynamik des Streuprozesses und Bindung auf Silizium

In der vorliegenden Arbeit werden die dynamischen Eigenschaften der resonanten inelastischen Röntgenstreuung (RIXS) an kleinen Kohlenwasserstoffmolekülen untersucht. RIXS bietet einen experimentellen Zugang zur elektronischen Struktur in symmetrieaufgelöster und atomspezifischer Weise und erlaubt Rückschlüsse auf dynamische Prozesse, wie sie elementaren chemischen Vorgängen zugrundeliegen.

An kondensierten Molekülen wurde RIXS mit gezielter Anregung eines definierten resonanten Vibrationszwischenzustandes durchgeführt. Die experimentellen Ergebnisse werden mit Rechnungen verglichen, die auf einer Interpretation des Streuvorgangs als Ein–Stufen–Prozess basieren. Es wird gezeigt, dass der Streuvorgang von der dynamischen Entwicklung der Elektronen– und Kernwellenfunktion beeinflusst wird. Bei resonanter Anregung wird reine Vibrations–Raman–Spektroskopie im weichen Röntgenbereich beobachtet. Von den reinen Vibrationszuständen klar zu unterscheiden, tragen kombinierte vibrations- und elektronisch angeregte Zustände zum Spektrum bei. Die Adsorption auf einer Halbleiteroberfläche ändert die Dynamik des Streuprozesses im Vergleich zu den Kondensaten. Es sind experimentell Unterschiede in der resonanten Röntgenstreuung zwischen den Adsorptionssystemen C_2H_4/Si(001) und C_6H_6/Si(001) festgestellt worden. Diese werden im Vergleich zu Grundzustandsrechungen im Zwei–Stufen-Modell mit Relaxationseffekten im Streuzwischenzustand erklärt. Im Falle von Benzol auf Silizium kann *Participator*–Streuung mit Vibrationsverlusten nachgewiesen werden.

Resonant Inelastic X–ray Scattering at Small Hydrocarbon Molecules: Scattering Dynamics and Bonding to Silicon

In this work, the dynamic properties of resonant inelastic X–ray scattering (RIXS) at small hydrocarbon molecules in different environments are investigated. With RIXS, the symmetry selective, atom and chemical state specific electronic structure is experimentally accessible, as well as dynamic properties of the system under investigation.

RIXS at weakly interacting, randomly oriented molecules in a condensate has been performed with vibrational selective excitation of a resonant scattering intermediate state. A one–step scattering description including the electronic and nuclear wave function is applied to model the experimental spectra. The combined experimental and theoretical investigation shows that the resonant scattering at the condensed molecules is determined by combined vibrational and electronic dynamics in the scattering intermediate state. Upon resonant excitation, purely vibrational Raman scattering in the soft X–ray regime has been observed. Additionally, clear separated combined electronic and vibrational features contribute to the spectra. Adsorption on a semiconductor surface changes the scattering dynamics. Differences occur in the experimental RIXS between C_2H_4/Si(001) and C_6H_6/Si(001). Comparing to two–step simulations in the ground–state model, the relaxation dynamics of the scattering intermediate state are explained. For benzene on Silicon, *participator* RIXS with vibrational loss features is demonstrated.

List of papers

This thesis is based on the following papers. They will be referred to in the text by their roman numbers.

[Paper I] **Fully polarization resolved X–ray absorption spectroscopy of C_2H_4 on single-domain Si(001)–(2×1).**
Franz Hennies, Alexander Föhlisch, Wilfried Wurth, Nadine Witkowski, Mitsuru Nagasono, and Maria Novella Piancastelli.
Surface Science **529**, 144–150 (2003).

[Paper II] **Polarization and angle-resolved NEXAFS of benzene adsorbed on oriented single-domain Si(001)–(2×1) surfaces.**
N. Witkowski, F. Hennies, A. Pietzsch, S. Mattsson, A. Föhlisch, W. Wurth, M. Nagasono, and M. N. Piancastelli.
Physical Review B **68**, 115408 (2003).

[Paper III] **Adsorption geometry of C_2H_2 on the single-domain Si(001)–(2×1) surface: fully polarization resolved NEXAFS.**
Annette Pietzsch, Franz Hennies, Alexander Föhlisch, Wilfried Wurth, Mitsuru Nagasono, Nadine Witkowski, and Maria Novella Piancastelli.
Surface Science **562**, 65–72 (2004).

[Paper IV] **Nonadiabatic effects in resonant inelastic X–ray scattering.**
F. Hennies, S. Polyutov, I. Minkov, A. Pietzsch, M. Nagasono, F. Gel'mukhanov, L. Triguero, M.-N. Piancastelli, W. Wurth, H. Agren, and A. Föhlisch.
Physical Review Letters **95**, 163002 (2005).

[Paper V] **Dynamic interpretation of resonant inelastic X–ray scattering: Ethylene and benzene.**
F. Hennies, S. Polyutov, I. Minkov, M. Nagasono, A. Pietzsch, F. Gel'mukhanov, L. Triguero, M.-N. Piancastelli, W. Wurth, H. Agren, and A. Föhlisch. *In Manuscript*.

[Paper VI] **Electronic structure and screening dynamics of ethene on single-domain Si(001) from resonant inelastic X–ray scattering.**
A. Föhlisch, F. Hennies, W. Wurth, N. Witkowski, M. Nagasono, M. N. Piancastelli, L. V. Moskaleva, K. M. Neyman, and N. Rösch.
Physical Review B **69**, 153408 (2004).

[Paper VII] Intermediate State Relaxation in Resonant Inelastic X-ray Scattering of Silicon Surface Adsorbates
F. Hennies, M. Nagasono, A. Pietzsch, N. Witkowski, M. N. Piancastelli, W. Wurth, L. Triguero, and A. Föhlisch. *In Manuscript*.

[Paper VIII] Bonding Configuration of Benzene adsorbed on Si(001)–(2×1) refined from Resonant Inelastic X–ray Scattering.
F. Hennies, M. Nagasono, A. Pietzsch, N. Witkowski, M. N. Piancastelli, W. Wurth, L. Triguero, and A. Föhlisch. *In Manuscript*.

I have participated in the following projects related to my thesis. They cover aspects of dynamic spectroscopy and surface chemistry:

Direct observation of electron dynamics in the attosecond domain
A. Föhlisch, P. Feulner, F. Hennies, A. Fink, D. Menzel, D. Sanchez-Portal, P. M. Echenique, and W. Wurth. *Nature* **436**, 373 (2005).

Attosecond charge transfer in c(4×2)S/Ru(0001): Core hole clock spectroscopy using two independent clocks
A. Föhlisch, S. Vijayalakshmi, F. Hennies, W. Wurth, V. R. R. Medicherla, and W. Drube. *Submitted to Physical Review Letters*.

Surface projected electronic band structure and adsorbate charge transfer dynamics: Ar adsorbed on Cu(111) and Cu(100)
S. Vijayalakshmi, A. Föhlisch, F. Hennies, A. Pietzsch, M. Nagasono, W. Wurth, A. G. Borisov, and J. P. Gauyacq. *Submitted to Physical Review Letters*.

Electronic transfer processes studied at different time scales by selective resonant core hole excitation of adsorbed molecules
C. Keller, M. Stichler, A. Fink, P. Feulner, D. Menzel, A. Föhlisch, F. Hennies, and W. Wurth. *Applied Physics A* **78**, 125 (2004).

Energy dependence of resonant charge transfer from adsorbates to metal substrates
A. Föhlisch, D. Menzel, P. Feulner, M. Ecker, R. Weimar, K. L. Kostov, G. Tyuliev, S. Lizzit, R. Larciprete, F. Hennies, and W. Wurth. *Chemical Physics* **289**, 107 (2003).

Adsorption and thermal evolution of SO_2 on Ru(0001)
F. Hennies, A. Föhlisch, W. Wurth, P. Feulner, A. Fink, and D. Menzel. *In Manuscript*.

Surface photovoltage dynamics at the buried BaF_2/Si interface from time resolved laser-synchrotron 2 photon photoemission
A. Pietzsch, A. Föhlisch, F. Hennies, S. Vijayalakshmi, and W. Wurth. *Submitted to the Journal of Applied Physics*.

Contents

Chapter 1

Introduction

The electronic structure of matter defines most of its relevant attributes. Chemical reactions, the optical character, and magnetic properties are all constituted by interaction of the system's electrons. Their investigation thus plays a key role in an understanding of virtually any process relevant in nature or technical applications[1]. The determination of the electronic structure has been facilitated mainly by the application of spectroscopic techniques. Historically, static properties have been probed. Nowadays, the focus moves to dynamic processes influencing the electronic and nuclear configuration of the systems investigated.

In this thesis, I aim to examine the dynamics of resonant inelastic X–ray scattering (RIXS). I want to investigate how dynamic processes in the electronic and nuclear wave function influence the electronic structure information obtained with RIXS. This investigation is important for two aspects: The determination of dynamic properties of matter with RIXS depends on the accessibility of this information. And the reliability of the electronic structure information obtained with RIXS relies on the identification of dynamic contributions to the spectral profile.

I will apply RIXS to hydrocarbon molecules weakly interacting in a condensate and adsorbed on a Si(001) surface. The condensed molecules act as a model system for the general investigation of the dynamic contributions to the RIXS spectral profile. In the investigation of molecules, typically a purely electronic ground state interpretation of RIXS in the "adiabatic" limit is applied [12–16]. Although it is known that vibrational contributions influence the spectra, they are usually treated as negligible. The appropriateness of this approximation is

[1]This importance has been underlined by the various nobel prizes awarded recognizing the advances in this field. I just want to mention a few directly related to the methods and concepts applied in this thesis: The Nobel prize in 1924 for X–ray spectroscopy [9]; 1966 for the concept of molecular orbitals [10]; for density–functional–theory as the base of computational methods in 1998 [11].

proved here. If the pure electronic treatment turns out to be oversimplifying, this would have significant implications for the application of RIXS to any system. I will present a detailed systematic investigation of the resonant inelastic X–ray scattering applying a full treatment of the electronic and nuclear aspects of the scattering process.

Surface adsorbate systems employ complex bonding mechanisms. In the case of adsorbates on a metal surface, RIXS has allowed to refine and sharpen the concepts of chemical bond formation [17–20]. In these systems, dynamic processes have not found to be important to consider in the interpretation of RIXS. Less well described are semiconductor adsorbates. RIXS has so far not been used to investigate these systems. The nature of a semiconductor surface chemical bond is significantly different from that of a metallic bond. It has to be investigated how the RIXS process appears in these systems. In this work, resonant inelastic X–ray scattering at small hydrocarbons adsorbed on a silicon surface will be studied. I will investigate the characteristics of the scattering process and show how to utilize the knowledge of the dynamic properties to extract reliable electronic structure information from RIXS of hydrocarbons adsorbed on silicon. From this, a detailed picture of the surface chemical bond can be extracted.

Classical spectroscopic techniques probe static properties of matter. This can be the electronic structure of an atom before and after a certain chemical reaction. The lifetime of an electronically excited state can be determined from the spectral line width of the corresponding spectral feature. The investigation of molecular vibrations with infrared and Raman spectroscopy reveals the static properties of the nuclear wave function. Summarizing, classical spectroscopies probe the eigenfunctions of the electronic and nuclear wave functions, but not their temporal evolution. Photoelectron spectroscopy of core[2] and valence[3] electrons, X–ray absorption spectroscopy[4] (XAS) and X–ray emission spectroscopy (XES) are routinely used methods to study static properties of the electronic structure. Laser–Raman spectroscopy is used to probe molecular vibrations.

The knowledge of the start–point and the end–point of a chemical process, however, does not necessarily allow to describe the mechanism of that specific reaction. The functionality of complex molecular systems rather seems to be defined by the dynamic response to an external perturbation. Within the last years, increasing effort has therefore been put into the description of the temporal evolution of the electronic and nuclear wave function. Here, the pathways of a chemical reaction or triggered processes in atomic and molecular systems in

[2]XPS: X–ray photoemission spectroscopy; ESCA: Electron spectroscopy for chemical analysis
[3]UPS: Ultraviolett photoemission spectroscopy
[4]Also called NEXAFS: Near–edge X–ray absorption fine structure spectroscopy

general are of interest. Today, basically two methods are used for dynamic investigations: pump–probe spectroscopy and resonant spectroscopies [21], which include RIXS.

In the pump–probe techniques, extremely short laser pulses are applied to measure time–dependent properties. An optical pulse triggers ("pumps") the system and a second pulse probes the response of the system as a function of the time–delay between pump and probe [22, 23]. In "Femtochemistry"[5], "snap–shots" of a chemical reaction on ultra short time scales are made with pump–probe methods. The temporal resolution depends on the time structure of the laser pulses utilized and goes down to about a femtosecond. However, these sources are optical lasers and are thus limited to optical excitations in the systems probed[6].

Resonant spectroscopies have the advantage of being able to address element specific dynamic properties. With ultrashort laser–pulses, it is up to now not possible to probe atom specific information. In biological systems, it is an interesting question how certain atomic centers influence the function of the complex system. Atom specific and even chemical state sensitive information can be observed with soft X–ray spectroscopies. An alternative to laser pump–probe is the investigation of dynamic processes by using an *internal* reference clock of the investigated system. This is done by resonant spectroscopies, which include resonant photoemission or Auger–Raman spectroscopies and resonant X–ray scattering. One example for resonant Auger–Raman spectroscopy is the investigation of charge transfer processes at surfaces with the so called core–hole–clock method [27]. The unknown time constant of a charge transfer from an adsorbate in a resonantly excited atom to a substrate is measured on the time scale of the known core hole lifetime. This is spectroscopically done by comparing the intensities of the different final states linked to the decay channels. With this method, attosecond resolution can be obtained [28].

In the work presented here, I utilize resonant inelastic X–ray scattering. RIXS has a characteristic duration time [29]. This time results from the formulation of the channel interference in the time domain instead of the energy domain. The scattering duration time depends on the detuning of the energy of the exciting X–ray beam from an absorption resonance. By tuning the photon energy into or away from a scattering resonance it is possible to adjust the internal "egg–timer"

[5] With a nobel prize in 1999 [23].

[6] A recent, promising, development to overcome this restriction is high–harmonic generation (HHG) with ultrashort laser sources allowing to produce X–ray pulses [24, 25]. With this technique the laser sources expand into the domain of synchrotron sources, however, still missing their tunability and average brilliance. With the short wavelengths there, even shorter pulses can obtained as in the optical regime [26].

of the scattering process. This internal shutter determines the time on which dynamic processes during the scattering can take place. It thus allows to measure time dependent processes without need to apply an external time reference. RIXS clearly has the potential to be used as an explicitly dynamic spectroscopy. However, up to now it still excels in the static electronic structure determination. RIXS is atom specific and chemical state selective. The RIXS scattering profile exhibits a polarization anisotropy [30] that can be utilized to investigate the symmetry of the valence electronic excited final states of the scattering. In the case of ordered surface adsorbates — molecules fixed in space — the fully symmetry–resolved electronic valence density of states can be determined [31].

I will present an interpretation of the experimental RIXS data based on a comparison with simulated spectra. The theoretical model chosen determines the physical aspects that can be evaluated with RIXS. The simplest model that can be applied is the two–step model in the ground–state approach considering only the electronic wave function. Here, only the decay step in the scattering process is considered and approximated by using the ground state wave function representation of the system studied. Although this model makes very strong simplifications, it has been very successful describing RIXS of adsorbates on metals. I will investigate adsorbates on semiconductors. The semiconductor chemical bond is substantially different from the metal case. It can therefore not be assumed that this simple model will also work here. The best description possible is a one–step treatment considering both electronic and nuclear contributions. This treatment, however, is not available for complex systems with todays computational methods. A central topic of this thesis will be the application and comparison of different theoretical descriptions. It has to be determined from which model and under which conditions a valid description of the scattering process can be expected.

The simplest systems to study are free atoms and molecules. They have the advantage of providing well known systems of reasonable complexity. This allows in particular the investigation of fundamental processes. However, characteristic for matter is the *interaction* between atoms and molecules that can not be studied by only looking at the ‘building blocks’.

Surface adsorbates act as model systems to address basic questions of the interaction between atoms, molecules and bulk matter. Technologically important fields — e.g. heterogeneous catalysis, oxidation and corrosion, tailored surfaces, or self–organized layers — are directly based on surface chemical processes. At the same time, surfaces represent a difficult task to experimental and theoretical methods. Model surface systems with defined properties are experimentally quite troublesome to handle. A very clean ultra high vacuum is needed and the preparation is sophisticated. An adsorbate on a surface always represents

a dilute system. The spectroscopic technique applied thus has to be able to distinguish between adsorbate, surface, and bulk contributions to the overall electronic structure. The methods used in this thesis are atom specific and chemical state sensitive and thus fulfill this requirement. In a theoretical treatment, a small single molecule can completely be described considering each electron, a bulk crystal can be approximated in a periodic treatment. Surface systems, however, are too big for an all–electron treatment, and not periodic at the interface. In this work, a cluster model is applied to describe the properties of the adsorbate system[7]

This thesis is organized as follows: At first, I will give a short overview on the history and applications of RIXS. I will introduce the theoretical basis, the computational methods, and the experimental requirements of the work presented here (Chapter 2). The careful characterization of the adsorbate configuration is a necessary prerequisite for their investigation with RIXS. This is done in the NEXAFS studies presented in Chapter 3 [Paper I, Paper II, Paper III]. The NEXAFS information obtained there is also important for the interpretation of the RIXS process, and for the investigation of the bonding mechanism. Chapter 4 [Paper IV, Paper V] contains the investigation of the RIXS dynamics of weakly interacting condensed molecules. In Chapter 5, RIXS of silicon surface adsorbates is presented. In Paper VI and Paper VII, the specific aspects of the scattering process in these systems are discussed. A model for the configuration and surface chemical bond of benzene [Paper VIII] on Si(001) is derived. I will finally summarize and interpret the findings of this thesis in Chapter 6 and 7.

[7] The cluster calculations have inherent difficulties, though, that will be addressed in this work later.

Chapter 2

Resonant inelastic X-ray scattering (RIXS)

The spectroscopy of soft X–rays emitted from a sample is a classical technique[1]. It has been used for electronic structure determination since back in the 1920's [32, 33]. In the 1960's the "electron spectroscopy for chemical analysis" (ESCA) [34] began to attract broad attention and X–ray emission spectroscopy (XES) lost popularity. XES had its revival with the rapid evolution of synchrotron radiation sources making monochromatized X–rays of high intensity available in the 1980's [35]. This progress was facilitated by the development of new soft X–ray fluorescence spectrometers [36]. With monochromatized synchrotron radiation it was possible to selectively excite single atoms. Already in the first experiments a clear excitation energy dependence of the X–ray emission was observed on TiN [37]. It was interpreted as resonant behavior — the birth of resonant inelastic X–ray scattering as a spectroscopic technique. A little earlier theory — not being limited by inappropriate experimental conditions — began to investigate resonant effects in RIXS [38][2].

Nowadays, RIXS is a spectroscopic tool with a variety of applications. RIXS is a photon–in/photon–out technique with a large penetration depth. Among many other systems, buried layers [40] as well as liquids behind thin windows [12, 14] can be probed. RIXS can be applied independently from the sample environment: Experiments under external fields or on active devices have been proposed. Metals, semiconductors, and insulators are equally accessible. The scope of systems investigated with RIXS includes solids and compounds [41],

[1] This paragraph contains only a few milestones of personal choice in the development of X–ray fluorescence spectroscopy and can't give an exhaustive historical overview.

[2] A complete overview over the theoretical development has been given by Gel'mukhanov and Ågren [39].

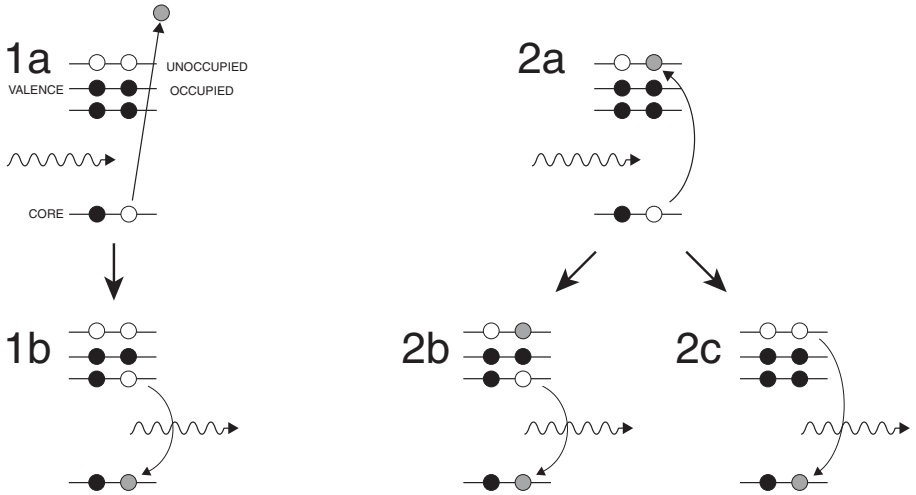

Figure 2.1: The two–step model of resonant inelastic X–ray scattering. 1a & 1b: X-ray emission spectroscopy (XES). 2a, 2b & 2c: Resonantly excited X–ray emission spectroscopy.

and extends to such exotic systems as paracetamol or bio–tissue like affected teeth [42].

This thesis wants to contribute to the dynamic aspects of RIXS of molecules[3] and semiconductor surface adsorbates. I will utilize the method to investigate the silicon surface chemical bond[4].

In this chapter, I will summarize the general theoretical, computational, and experimental basis for the RIXS investigations presented in this work. This thesis is to a large extend a compilation of papers. The particular experimental setup, computational details, and theoretical framework will thus be discussed in each section in direct relation to the corresponding studies.

2.1 X-ray absorption and emission. A two–step model.

In a simple picture soft X–ray scattering can be understood as a two–step process. In the first step, a core hole is created in an atom by absorbing a photon (Fig. 2.1 panel 1a & 2a). In the second step the created core vacancy is filled with an electron from the valence states under emission of a second photon (Fig. 2.1 panel 1b, 2b, 2c). Experimentally the spectral distribution of the outgoing photon is recorded for a certain fixed energy of the incoming photon.

[3] The most important work done on single molecules up to now is summarized in [43].

[4] A review of adsorbate systems probed with RIXS can be found in [44]. I will later cite the work related to this thesis in greater detail.

In this simple two–step model, the X–ray absorption and emission are considered to be decoupled, the emission is therefore independent of the specific character of the absorption. This model is fully valid for excitation far above threshold or for non–monochromatic excitation where no specific intermediate state can be prepared. It is also valid for systems with large core hole energy splitting, e.g. CO [45, 46], when no vibrationally excited intermediate state has to be considered. It is applicable in many more cases and can be considered as a special case of the models discussed in the following. This model has a strong historic justification. However, it fails to describe the experiments with narrow bandwidth monochromatic excitation. The simple two–step model has therefore been expanded to account for the character of the absorption process. The new models are called “generalized two–step model TS2” [30] or “resonantly excited X–ray emission” [45].

Phenomenologically, the two step picture can be improved by explicitly treating special cases: Depending on the energy of the incoming photon the atom can either be ionized (Fig. 2.1 panel 1a) or be resonantly excited into a neutral state (Fig. 2.1 panel 2a). The character of the core excited state strongly influences the scattering process. Typically, the first case is referred to as non–resonant and the second case is considered to be resonant. Only the non–resonant case can be treated in a simple two–step model. However, it is not as easy as it seems to draw the line between resonant and non–resonant intermediate cases. Indeed, one of the central points of this thesis is to investigate the resonance nature of actual RIXS experiments on molecules and semiconductor surface adsorbates.

The core hole of an ionized atom can only be filled from the occupied valence states (Fig. 2.1 1b). This case is called X-ray emission spectroscopy (XES) and gives a spectroscopic image of the occupied valence density–of–states (DOS) [47–49]. The core hole binding energy is an atomic property and depends on the chemical environment [50]. Considering the core orbitals having a somewhat local character (which is e.g. justified in case of CO on a metal surface [17]) only the part of the valence DOS with sufficient spatial overlap with the core orbital is probed, e.g. the part of the valence structure located at the adsorbate. This is called the local DOS. In addition, the core wave function has atomic properties, resulting in a survival of the atomic selection rules. If the core hole wave function has s–character, only the partial p–derived DOS is observed due to the $\Delta l = \pm 1$ selection rule. XES thus probes the local partial DOS (lpDOS). The final state in XES is a valence ionized final state. This is the same final state as in the case of valence band photo emission spectroscopy (UPS). UPS however probes the overall valence DOS of the system and can not separate the contributions from single atoms [47].

If the intermediate state is a core excited neutral state (Fig. 2.1 2a), the situation is different. Here, the properties of the specific occupied valence state influence the decay. As will be discussed later in this chapter, the excitation of a particular intermediate state of specific symmetry sets certain constraints for the decay considering the symmetry and polarization of the emission.

The core excited neutral state can decay by two different mechanisms: Either an electron from the occupied valence state (Fig. 2.1 panel 2b) or the initially excited electron itself (Fig. 2.1 panel 2c) fills the core hole. With the term "spectator" the electron involved in the former decay channel is referred to, and with "participator" the electron in the latter channel. The spectator decay leaves the atom in a valence excited final state. The participator decay brings the atom back into the electronic ground state. The latter channel is often considered as pure elastic scattering. This interpretation is not always true. In this channel vibrational loss processes can be present, which forbid to call it elastic [Paper IV].

2.2 Energy balance of RIXS

Generally, resonant inelastic X–ray scattering probes electronic and vibrational loss processes. In the scattering process the energy difference $\Delta\epsilon$ between incoming photon ω and outgoing photon ω' is transfered into the scatterer. The energy balance of RIXS is thus[5]

$$\Delta\epsilon = \omega' - \omega = \epsilon_0 - \epsilon_f \tag{2.1}$$

$\epsilon_f - \epsilon_0$ is the energy difference between the scatterer's initial state $|0\rangle$ and final state $|f\rangle$. $\Delta\epsilon$ can be called the energy loss. The energy loss corresponds to the energies of the nuclear (vibrational) and electronic excitations present in the final state:

$$\Delta\epsilon = \epsilon_{\text{nuclear}} + \epsilon_{\text{electronic}} \tag{2.2}$$

In the RIXS spectrum of a free molecule these contributions can be nicely separated. In Fig. 2.2, a sample experimental and computed spectrum of ethylene is shown [Paper IV]. The HOMO–LUMO separation in ethylene is ~ 6 eV. The energy loss features in the "participator" region are too small to correspond to electronic valence excitations, they have to arise due to pure vibrational excitations. The "spectator" region contains combined electronic and vibrational (vibronic) loss features. In case of larger systems — surface adsorbates etc. — additional electronic and vibrational losses mediated by the substrate can enter the energy balance.

[5] Without loss of generality I use the simplest possible units in this work and define $\hbar = 1$.

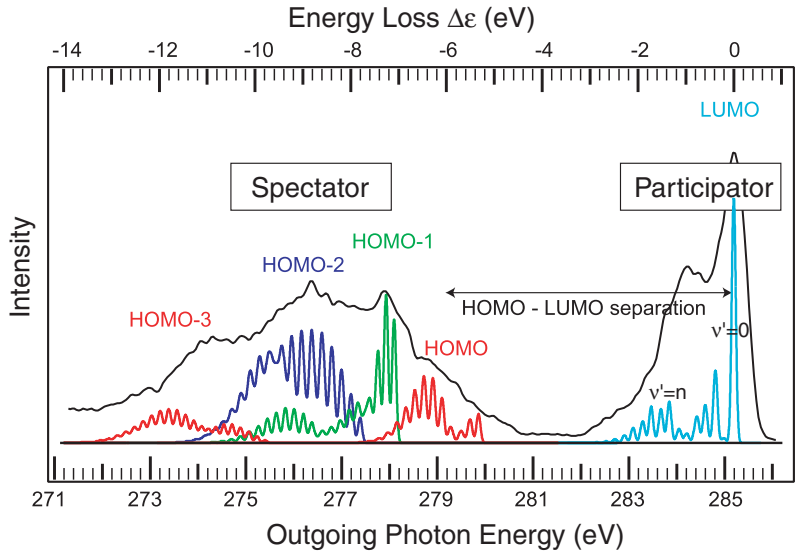

Figure 2.2: Sample RIXS spectrum of ethylene after C $1s$ core excitation into the vibrational progression of the LUMO π^* at 285.2 eV [Paper V]. The lower scale indicates the energy of the outgoing photon. The upper scale shows the energy loss, i.e. the energy difference between incoming and outgoing photon $\Delta\epsilon = \omega' - \omega$. The black solid line shows the measured spectrum. In the experiment, the single vibrational lines can not be resolved and only the vibrational envelope is observed. Beneath the experimental spectrum, the simulated spectrum is shown with the vibrational fine–structure.

2.3 The scattering description.

In a general picture, RIXS is considered as an one–step process. An incoming photon with energy ω scatters at a system in the initial state, which in the following is assumed to be the ground state $|0\rangle$. After the one–step scattering process the system is in a final state $|f\rangle$ and a photon with energy ω' is emitted.

The theory of the scattering of light by atoms goes back to the Kramers–Heisenberg description [51]. Based on second order perturbation theory, the scattering can be described with the double differential cross section for scattering into a solid angle Ω [31, 39],

$$\frac{d^2\sigma(\omega',\omega)}{d\omega' d\Omega} = \sum_f |F_f|^2 \delta(\omega' - \omega - \omega_{f0}) \tag{2.3}$$

where ω_{f0} is the energy difference between initial and final states. The energy conservation law is reflected by the delta function $\delta(\omega' - \omega - \omega_{f0})$. The energy difference between incoming and outgoing photon equals the excitation energy of the final state $\omega' - \omega = \omega_{f0}$. The intensity distribution of the outgoing photon is described by the Kramers–Heisenberg (KH) scattering amplitude F_f. In the

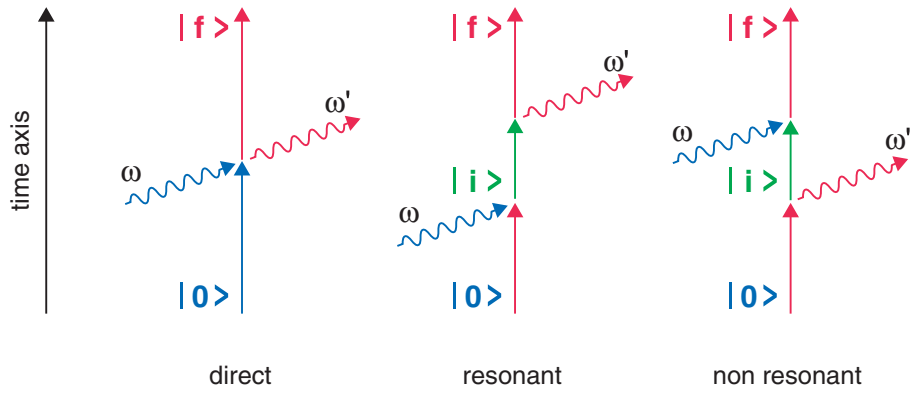

Figure 2.3: Time sequence of the scattering process. Since the scattering invokes a virtual state, the emission can take place before the adsorption, leading formally to the non–resonant case.

scattering amplitude, an explicit consideration of the scattering intermediate state $|i\rangle$ is introduced. F_f divides into three terms, the direct or Thompson scattering, the resonant scattering and the non–resonant scattering [39]:

$$F_f = \underbrace{\left[(\mathbf{e}'\cdot\mathbf{e})\langle f|0\rangle\right]}_{\text{direct}} + \sum_i \underbrace{\left[\frac{\langle f|\hat{\mathbf{p}}\cdot\mathbf{e}'|i\rangle\langle i|\hat{\mathbf{p}}\cdot\mathbf{e}|0\rangle}{\omega-\omega_{i0}+\imath\Gamma_i/2}\right.}_{\text{resonant}} + \underbrace{\left.\frac{\langle f|\hat{\mathbf{p}}\cdot\mathbf{e}|i\rangle\langle i|\hat{\mathbf{p}}\cdot\mathbf{e}'|0\rangle}{\omega'+\omega_{i0}}\right]}_{\text{non resonant}} \tag{2.4}$$

The introduction of the intermediate state is the inclusion of the second order term from time–independent perturbation theory [52]. The resonant and non–resonant part is summed over all intermediate states $|i\rangle$. Γ_i denotes the lifetime broadening of the intermediate state with excitation energy ω_{i0}. $\mathbf{e}$ and $\mathbf{e}'$ denote the polarization vector of incoming and outgoing photon, respectively. $\hat{\mathbf{p}}$ is the dipole operator. In the resonant term, channel interference can occur [39].

The meaning of the three terms in Eqn. (2.4) can best possible be understood considering the time sequence of the scattering (Fig. 2.3). The direct term corresponds to sudden scattering. The “normal” scattering sequence is the absorption of an incoming photon, followed by the emission of a second photon after some time. This is reflected in the resonant term. The intermediate state of the scattering process has virtual character. Thus, the sequence of adsorption and emission can be permuted, leading to the non–resonant contribution [39], where the specific information of the incoming photon is lost.

It is generally assumed that the direct term in case of soft x-ray scattering always collapses to purely elastic scattering with $\omega' = \omega$ [39]. This is only true if pure electronic excitations are considered. In Paper IV (Chapter 4.1), we show that in the limit of sudden scattering the resonant term converges to the direct

term. For short scattering duration times this term can describe scattering into vibronic — i.e. combined electronic and vibrational — final states.

2.3.1 Selection rules: Polarization resolved RIXS of oriented adsorbates.

In a gas phase experiment, the RIXS description has to be averaged over all molecular orientations. Neither the polarization of the incoming nor the outgoing photon can be determined with respect to the molecular orientation. The same is true for RIXS of randomly oriented condensed molecules as presented in this thesis (Chap. 4). In the case of an oriented adsorbate on the other hand, the adsorbed molecules can be considered as fixed in space. This experimentally defines the polarization of X–ray absorption and emission.

RIXS is governed by selection rules that have been extremely useful in the interpretation and utilization of this spectroscopy [30, 31]. The selection rules can be derived from the dipole matrix elements of the appropriate transitions [Eqn. (2.4)] in either the two–step or the one–step formalism. Group theory gives a tool for the investigation of the matrix elements. A matrix element does not vanish when it contains the total symmetric representation. This can be checked by calculating the direct product of the irreducible representations of the involved orbitals and the transition dipole components, i.e. the polarization vectors of incoming and outgoing photon.

Free molecules have to be averaged over spatial orientations. The transition dipole components are thus described by the total symmetric representation, and can be omitted in the treatment. Considering a valence electronically excited final state $|n^{-1}\, v\rangle$, where n and v denote occupied and unoccupied valence states, respectively, one finds that scattering into this state is allowed if $\Gamma_n \times \Gamma_v$ contains the total symmetric representation. This directly leads to the parity selection rule, demanding that n and v are of the same parity (either $g-g$ or $u-u$) for the excited final state to be allowed. The parity selection rule is very helpful in the discussion of the core hole localization or symmetry breaking effect (Paper IV and Paper V in Chap. 4) in case of weakly interacting condensed molecules.

The absorption of a molecule on a surface almost always lowers the symmetry compared to free molecules. Adsorbate systems have no inversion symmetry, and thus no parity selection rule can be applied. However, in many cases the adsorbed molecules retain their gas phase character to a wide extend. Within certain limits, the scattering can then successfully be interpreted using gas phase symmetries. Additionally, the fixing in space of the adsorbed molecules allows for the utilization of (further) polarization selection rules. The calculated spectra presented in Paper VII, and Paper VIII are based on the theory of polarized X–ray

emission developed by Triguero et al. [31]. I will give an exemplary discussion of the polarization selection rules for the case of ethylene adsorbed in a C_{2v} symmetry, which is the symmetry of the Si(001)–(2×1) substrate of the adsorption systems investigated in this work. Ethylene has two core holes of a_1 and b_1 symmetry. The polarization vectors along the directions x, y, and z are represented by $\mathbf{b_1}$, $\mathbf{b_2}$, and $\mathbf{a_1}$, respectively. Considering the decay as in the two–step model, only the following channels are allowed:

$$
\begin{aligned}
\Gamma_\beta \times \Gamma_n \times \Gamma_c = a_1 \quad &\Longleftrightarrow \quad \text{transition allowed} \\
\mathbf{x} - \text{polarization} : \Gamma_\beta = b_1 \quad &\Longrightarrow \quad \Gamma_n \times \Gamma_c = b_1 \times a_1 \\
&\qquad\quad\ \ \Gamma_n \times \Gamma_c = a_1 \times b_1 \\
\mathbf{y} - \text{polarization} : \Gamma_\beta = b_2 \quad &\Longrightarrow \quad \Gamma_n \times \Gamma_c = b_2 \times a_1 \\
&\qquad\quad\ \ \Gamma_n \times \Gamma_c = a_2 \times b_1 \\
\mathbf{z} - \text{polarization} : \Gamma_\beta = a_1 \quad &\Longrightarrow \quad \Gamma_n \times \Gamma_c = a_1 \times a_1 \\
&\qquad\quad\ \ \Gamma_n \times \Gamma_c = b_1 \times b_1
\end{aligned}
\tag{2.5}
$$

β denotes the emission dipole moment and corresponds to the polarization of the outgoing photon. n and c are occupied valence and core orbitals, respectively. Γ_x is the irreducible representation of element x. This analysis shows that the a_1 and b_1 states are observable with both x and z polarization, whereas the a_2 and b_2 states are only visible in the y polarized emission.

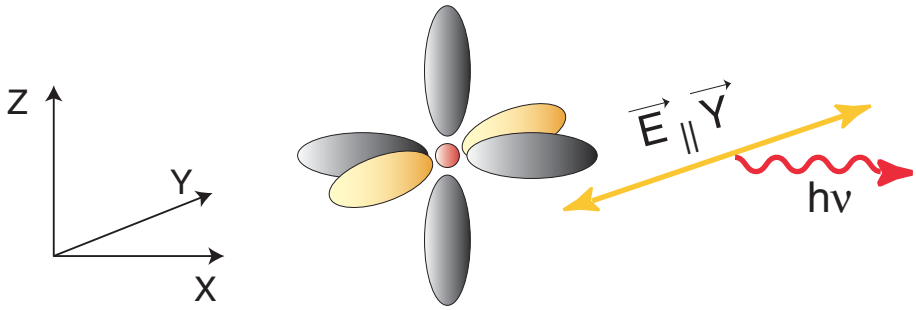

Figure 2.4: Polarization resolved X–ray emission. Depicted is the decay of a totally symmetric core excited state. The p–derived valence orbitals can only be observed with polarization parallel to their spatial orientation. In this figure the polarization vector of the emitted photon is aligned along the y direction. The photon stems from the decay transition of a p_y–derived valence orbital into an s–type core hole.

2.3.2 Polarization selective excitation

Using selective resonant excitation, a particular intermediate core excited state of defined symmetry can be prepared. This further reduces the allowed final states. In the experiments discussed here, the incoming photon has z–polarization. I will give an example for ethylene. Excitation into the π^* (LUMO) creates an intermediate state with b_1 symmetry. The emitted photons with x, y, and z polarization then have to correspond to the decay from occupied valence states with a_1, a_2, and b_1 symmetry, respectively. This is illustrated in Fig. 2.4. Polarization resolved resonantly excited X-ray emission gives an ideal tool for the symmetry decomposition of the occupied valence density–of–states of ordered adsorbates.

2.3.3 Interference between indistinguishable core holes

In molecules with (near) degenerate core levels of the same symmetry each of the core levels can be involved in the excitation. The square of the sum of the individual channel amplitudes $|F_f|^2$ in the scattering cross section (Eqn. (2.3)) gives rise to an interference term [31]. The same situation occurs if core holes of different symmetry mix due to a configurational change in the molecule, lowering the molecular symmetry. This is the case in the so called dynamic symmetry breaking that I will discuss below.

2.4 Vibrational RIXS and vibronic coupling.

In Paper IV and Paper V (Chapter 4), the scattering description is applied to the case of electronic and vibrational excitation. I will here summarize the theoretical description. A more detailed discussion can be found in Paper V. Ethylene is used as an example. It has two near degenerate core orbitals of different symmetry in delocalized representation. Without vibronic coupling, no interference between electronic channels can occur and the electronic dipole transition moments can be extracted in a factor ζ_{f0}[6]. The RIXS cross section then reads [Paper IV, Paper V]:

$$\sigma(\omega',\omega) = \sum_{f,\nu_f} \zeta_{f0}|F_{\nu_f}|^2 \Phi(\omega' - \omega + \omega_{f\nu_f,00} + \omega^e_{f0}, \gamma) \tag{2.6}$$

ω and ω_1 are the energies of incoming and outgoing photon, respectively. ω^e_{f0} is the electronic resonance energy, i.e. the energy difference of the minima of

[6]The mixing of electronic scattering channels involving both core holes is a dynamic effect and treated separately later in this section.

the potential surfaces of ground state and final state. $\omega_{f\nu_f,00}$ is the vibrational energy of the ν_f^{th} vibrational state. The spectral function $\Phi(\omega-\omega_0,\gamma)$ centered at ω_0 with width γ describes the energy distribution of the incoming photons.

Since the electronic transition moments have been extracted, $|F_{\nu_f}|$ becomes the pure Franck–Condon (FC) amplitude:

$$F_{\nu_f} \approx \sum_{\nu_i} \frac{\langle\nu_f|\nu_i\rangle\langle\nu_i|0_0\rangle}{\omega-\omega_0^i-\omega_{i\nu_i,00}+\imath\Gamma/2}, \tag{2.7}$$

$\Omega=\omega-\omega_0^i-\omega_{i\nu_i,00}$ denotes the detuning of the incident photon energy from a vibrational resonance. The vibrational spacing in ethylene is of the same order of magnitude as the intermediate state lifetime Γ. Thus, when the incident photon energy is tuned to the resonance energy ($\Omega\approx 0$), the FC amplitude is determined by interference between scattering channels including different vibrational states ν_i.

In the limit of large detuning ($\Omega\gg\Gamma$), the FC amplitude collapses:

$$\begin{aligned} F_{\nu_f} &\approx \sum_{\nu_i} \frac{\langle\nu_f|\nu_i\rangle\langle\nu_i|0\rangle}{\Omega} \\ &\approx \frac{\langle\nu_f|0\rangle}{\Omega}, \quad \text{with} \ \sum_{\nu_i}|\nu_i\rangle\langle\nu_i| = 1 \end{aligned} \tag{2.8}$$

This means that the FC amplitude in the limit of large detuning is equivalent to the direct scattering term of Eqn. (2.4) (The electronic dipole moment has been extracted before into the ζ_{f0} factor in eqn. (2.6)). In the case of the final state being the electronic ground state, the scattering profile collapses to pure elastic scattering since the ground state vibrational states are orthonormal $\langle 0,\nu_0|0,0\rangle = \delta_{\nu_0,0}$. But if the final state is valence excited, this term describes direct scattering into electronically and vibrational excited states.

The collapse can also be explained coming back to the time sequence of the scattering process. The duration time of the RIXS process depends on the detuning Ω and is defined by

$$\tau = 1/\sqrt{\Omega^2+\Gamma^2} \tag{2.9}$$

For large detuning, the scattering duration shortens and the resonant scattering converges to direct scattering (Fig. 2.1).

The above description has to be extended for the influence of the symmetry changes accompanied by the activation of an asymmetric vibration. The Jahn–Teller theorem [53] states that the degeneracy of the core orbitals is removed by such a vibration, effectively localizing the core holes. This acts as a mixing of

the core holes of different symmetry and they become inseparable, opening additional scattering channels. In Paper IV and Paper V (Chapter 4), it is discussed how this effect leads to additionally allowed final states, the detailed theoretical treatment can be found there. This vibronic coupling is only possible when tuning the incident photon energy into the resonance. Then the scattering duration becomes sufficiently long to change the molecular symmetry and to localize the core holes. Scattering detuned from the resonance suppresses the activation of vibrational motion and preserves the delocalized orbital representation in the undistorted molecular symmetry.

2.5 Computation

In this thesis, the experimental RIXS spectra of free molecules and surface adsorbates are discussed in comparison to simulated spectra. The computational models are based on the theory elements described above. The simulation of the RIXS spectra of free molecules presented here bases on the methods developed by Gel'mukhanov et al. [39, 54]. The first simulated RIXS spectra of semiconductor adsorbates are presented. I will briefly summarize the computational approach applied in the following.

2.5.1 Ground state interpretation of RIXS

A very good computational modeling of RIXS spectra of adsorbates on metals is possible in the framework of the ground state interpretation [45]. Within the ground state model, the absorption and emission transitions are simply described by the computation of the virtual and valence transition moments in the ground state wave function representation[7]. The transitions are thus interpreted as one electron processes in a frozen orbital picture without considering any relaxation processes. The excitation and decay energies are obtained from the ground state orbital energies. The RIXS spectra of metal adsorbates have been found to be well modeled in this approach. This is surprising because the creation of a core hole is a major perturbation of the electronic structure of an atom. It is therefore not to be expected that the total neglection of dynamic core hole effects and electronic relaxation can result in a valid description of the scattering process. The ground–state interpretation has nevertheless been demonstrated to be valid in the case of metal adsorbates. It has been assumed [45] that the fast metallic screening in these adsorbate systems accounts for an immediate response of the system to the perturbation in the scattering process.

[7] Virtual and valence transition moments are the transition moments from the unoccupied ("virtual") and occupied ("valence") molecular orbitals into the core orbitals.

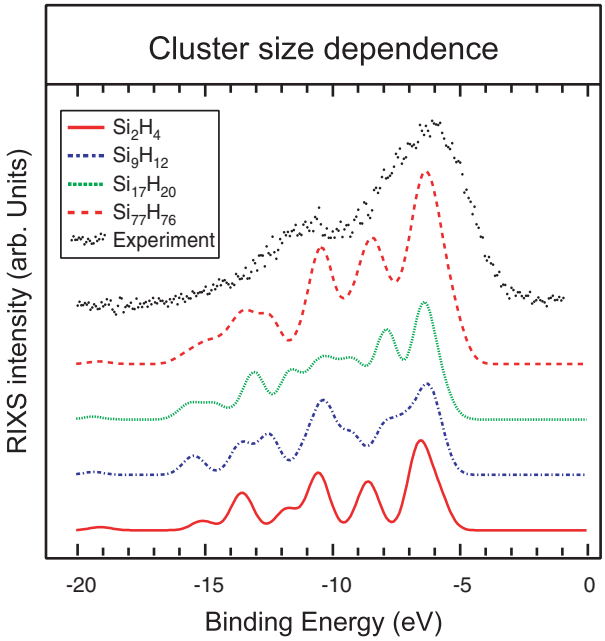

Figure 2.5: Cluster convergence for non–resonant X–ray emission simulations of C_2H_4/Si(001). The z component of the emission is plotted for the different cluster sizes.

Due to this fact, intermediate state dynamics and final state state screening effects cancel out and the ground state properties determine the scattering profile.

In the work presented here [Paper VI, Paper VII, Paper VIII], it has been found that the ground state model is applicable to adsorption on semiconductors. In particular, scattering above an adsorption resonance can in intensity and energy position well be described in this model. The specific screening and relaxation characteristics of resonantly excited intermediate states in semiconductor adsorbates can not be covered in the ground state simulations. They need an improved computational treatment.

2.5.2 DFT calculations on a silicon cluster

In Paper VI, Paper VII, and Paper VIII, calculations of RIXS spectra of adsorbates are presented. They have been performed in a density functional approach using a cluster representation of the substrate. For these calculations, the question of cluster convergence is generally interesting: From which size on, can a cluster be considered to be representative for the inherently periodic “real–world” substrate? The cluster model is established for the calculation of adsorbates on metals [31]. For ethylene on copper, it has been shown that the increase of the

cluster size does not significantly improve the modeling. This is at least true for the calculation of non–resonant X-ray emission spectra.

Performing the calculations for C_2H_4/Si(001) [Paper VII] strong variations of the non–resonant X–ray emission with the cluster size have been observed. In Fig. 2.5, the cluster size dependence of the z component of the X–ray emission is shown. The spectral shape differs significantly with the cluster size[8]. In particular, the Si_9H_{12} cluster exhibits a spurious signature. Very good correlation has been obtained between experimental data and the calculations on the largest cluster. The problem of cluster convergence in the case of a semiconductor cluster, however, has to to be addressed in future work.

A second problem of the Si cluster calculations is connected to the optimized adsorbate configuration. In this work, it has been found that the experimental RIXS spectra give an excellent measure to testify the theoretically optimized geometric structures. In an usual approach, the adsorbate geometry is optimized on the cluster model minimizing the total energy. The optimized cluster model is then taken to compute the spectra. However, with this approach, it has not been possible to optimize adsorbate structures, that result in spectra which really reflect the experimental data.

In C_2H_4/Si(001), e.g., the position of the $3a_g(\sigma)$ orbital in the X–ray emission spectra is extremely sensitive to the C–C bond length. The configuration optimized on the cluster model exhibits a C–C bond length too long to produce a correct appearance of the $3a_g(\sigma)$. The calculation of the X–ray spectra was therefore performed using a structure published by Birkenheuer et al. [56]. This structure was obtained from a slab calculation in the DFT–GGA (general gradient approximation). The slab–structure contains a C–C bond length that results in a good representation of the $3a_g(\sigma)$ orbital [Paper VII].

The geometry dependence of the RIXS spectral shape of C_6H_6/Si(001) is explicitly discussed in Paper VIII. The overall electronic character of this system strongly depends on the “butterfly” fold angle of the molecule. RIXS calculations performed using a geometry optimized on a cluster model [57] fail to reproduce the experimental spectra. Therefore, the adsorbate structure has been varied systematically [Paper VIII] to obtain the best match between experiment and calculations. It has been found, that the molecule is less distorted then the cluster calculations have shown.

[8] In this comparison, the silicon cluster geometries have been taken from ref. [55] and have not been further optimized. The adsorbate complex has always the same configuration (optimized by Birkenheuer et al. [56], see below). No relaxation of the cluster model has been allowed.

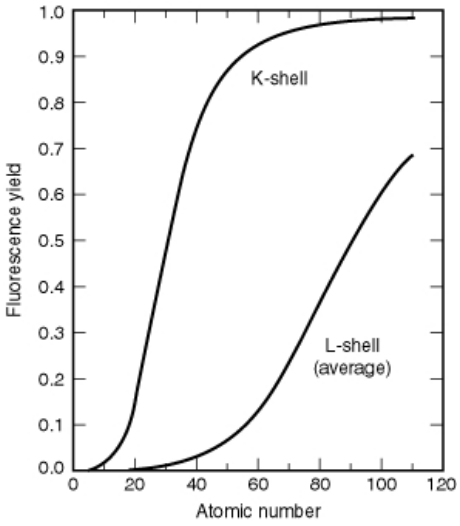

Figure 2.6: Fluorescence yields for K and L shells (From [58, 59]).

2.6 Experimental techniques

The specific experimental setup is described in detail in connection with the corresponding studies (Chap. 3 – 5). However, I will briefly sketch the general experimental requirements in this section: The demand for high–brilliance synchrotron radiation, the specifications of the experimental setup, and the sample mounting.

2.6.1 Low countrates

Measuring the X–ray emission of the core decay of light elements like carbon is a very time consuming task due to a multitude of experimental and physical restrictions reducing the count rate obtainable. A typical soft X–ray beamline — like beamline I-511 at MAXlab [60], where all experiments of this thesis have been performed — delivers 10^{11}–10^{13} photons / s. A soft X–ray beamline normally suffers from carbon contamination on the optical elements. Due to photo absorption in these contaminations, the flux at the carbon resonance energy is about ten times lower than in the other energy regions.

The X–ray spectrometer analyzing the emitted photons [35, 61, 62] has a very small acceptance angle of a few degree[9]. This is not really a disadvantage since it allows to measure with the very high angular sensitivity necessary for polarization resolved studies. But on the other hand, it reduces the count rate by a factor of 10^4. Other factors play a minor role. The detector sensitivity of the X–ray spectrometer is about 20%.

[9] For the actual model XES–350 of this spectrometer the azimuthal angle is given to be $\leq 5°$, the elevation angle to be $\leq 0.5°$ [62].

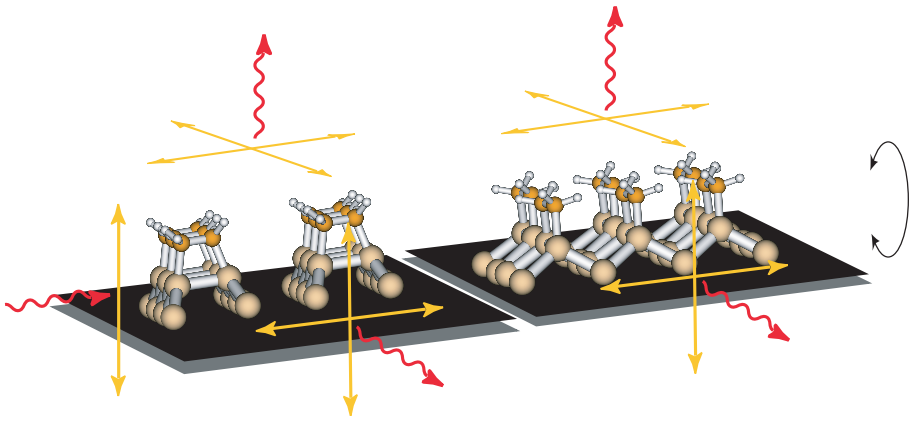

Figure 2.7: Si(001)–(2×1) sample mounting for full angle and polarization resolution. Incoming and emitted photons are graphed as rippled arrows. The polarization vector is represented by a double arrow.

The small acceptance angle results in the focus of the analyzer on the sample being typically in the μm–range, and thus much smaller than the spotsize of the incident beam. This directly leads to the demand for high brilliance synchrotron radiation sources having not only high flux, but also a small beam spot size on the sample.

A pure physical reason for getting low count rates in carbon K–emission can be found in Fig. 2.6, plotting the probability of a fluorescent decay as a function of the atomic number. In only 0.28% of the carbon 1s core decay processes, a photon is emitted, 99.72% of the core vacancies are filled by an auger decay. This reduces the count rate by a factor of 10^3.

On a high brilliance beamline like I-511, we can now estimate maximal possible count rate from the above discussed factors to be $\leq 10^3$ counts / s, depending on the spot size on the sample. The absorption cross section of the specific system is not taken into account in this estimate. It further reduces the obtainable count rate dependent on the target density. The target density is the lowest in case of the adsorbate measurements. The typical count rates of the experiments presented in this thesis were in the order of 10^2 counts / s for the condensed molecules and 10 counts / s for the surface adsorbates and are thus reasonable values.

2.6.2 Experimental design

In order to fully utilize the symmetry selectivity of RIXS and NEXAFS, it is mandatory to create an experimental setup with suitable geometry. The alignment of the polarization vector and the direction of propagation of incoming and outgoing photons has to be well–defined with respect to the molecular ad-

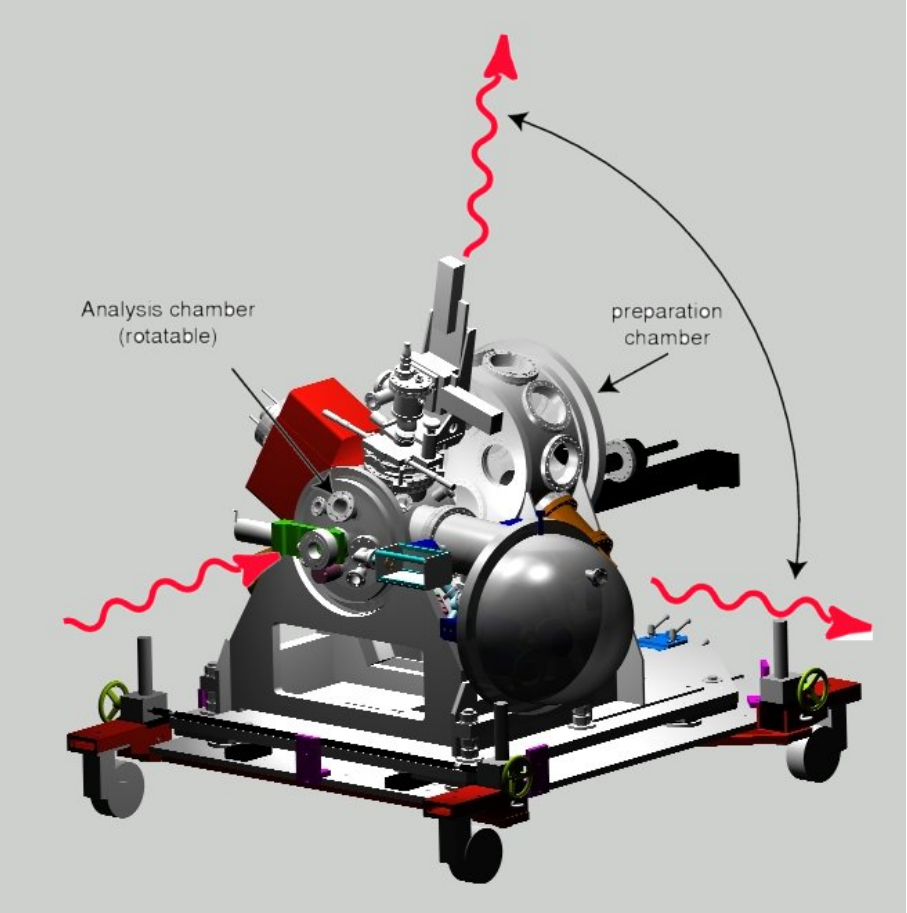

Figure 2.8: An end station suitable for angle resolved spectroscopy on surfaces under ultra–high–vacuum conditions: HIXSS

sorbate orientation. This is possible in a setup schematically depicted in Fig. 2.7. The here used vicinal cut Si(001)–(2×1) substrates exhibit a macroscopic single domain reconstruction. Two silicon samples rotated by 90° around the surface normal with respect to each other are mounted at 7° gracing incidence of the incoming photon beam. The samples can be rotated around the beam axis, allowing to orient the polarization vector freely in–plane or out–of–plane. With a X–ray emission spectrometer that, too, can be freely rotated around the beam axis, it is possible to detect the outgoing photons in all three directions in space with respect to the surface orientation. The beamline I-511 at MAXlab in Lund — where all experiments presented in this thesis have been performed — is equipped with an analysis chamber that can be rotated around the beam axis. An experimental chamber with a similar configuration is the HIXSS (Hamburg inelastic X–ray scattering station) that has been build with my substantial participation during the time of my PhD–thesis (Fig. 2.8).

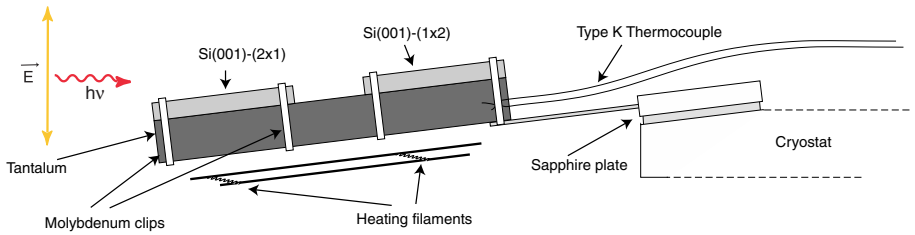

Figure 2.9: Schematic drawing of the sample mounting

2.6.3 Sample holder and sample preparation

Silicon is a critical sample, as it is forming surface alloys directly when coming in contact with many metals. In particular, Ni containing materials, like most of the usual metallic tools and the standard temperature probe used in UHV (AlNi–CrNi [63]), may not come in contact to the silicon sample. For the preparation of surface adsorbate systems, on the other hand, a reliable temperature control is needed.

For the here presented studies, a sample mounting has been developed that avoids contact between the thermocouples and the crystals and still allows for a precise temperature measurement. The geometry of the sample mounting follows the conditions sketched above (Fig. 2.7). The mounting of the silicon pieces (Fig. 2.10) has been adapted from Gokhale et al. [64] as sketched in Fig. 2.9. Gokhale et al. [64] “glue” the crystals using a silver bonding layer to the tantalum support. In the work presented here, the silicon wafer pieces have simply been clamped with Mo clips to the Ta support. The thermal contact between the silicon pieces and the tantalum support is good enough to heat and cool the samples in a controlled manner with good temperature measurement. The samples can be heated purely radiative with the filaments or with electron

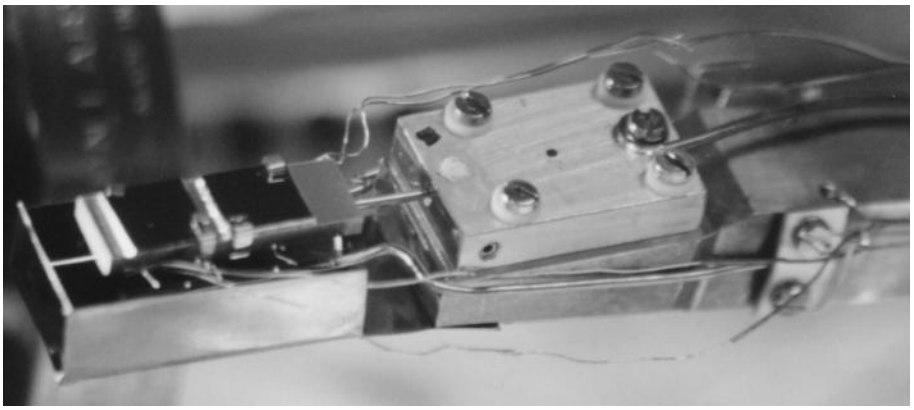

Figure 2.10: Photography of the sample holder (by courtesy of M. Nagasono).

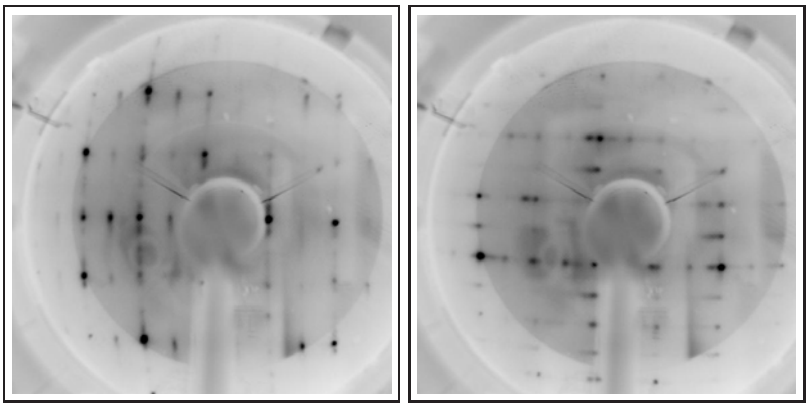

Figure 2.11: LEED pattern of clean Si(001)–(2×1). The two crystals mounted on the sample holder have been measured separately. The (2×1) domains of both crystals are rotated by 90° around the surface normal with respect to each other. The colors of the LEED image in the figure have been inverted.

bombardment heating by additionally applying a positive high voltage to the samples.

2.6.3.1 Preparation of clean Si(001)–(2×1)

Silicon is very sensitive to carbon contamination. I experienced that a silicon crystal contaminated with a certain amount of carbon can not be cleaned *in–situ* and has to be replaced by a new one. The fresh silicon wafer pieces are protected by a natural oxide layer. This layer desorbs from the surface at ~ 900 K. The removal of this layer has to take place in extremely good vacuum conditions.

In detail, the following steps have been performed to get a clean, ordered Si(001)–(2×1) surface: During the bake out of the experimental chamber, the samples were heated at 800 K for ~ 12 hours. In the very good vacuum after the bakeout ($P \leq 10^{-10}$ torr), the samples were flashed and annealed to 1350 K for $t > 10$ s. Then the samples had to be sputtered with Xe ions at room temperature and at 800 K for at least two cycles for $t = 20$ minutes at each temperature with subsequent annealing to 1350 K for $t > 10$ s. A good surface exhibits a LEED (low energy electron diffraction) pattern as depicted in Fig. 2.11.

2.6.3.2 Preparation of monolayers of ethylene and benzene on Si(001)–(2×1)

At room temperature, adsorption of C_2H_4 leads to a saturation coverage of one molecule per surface dimer [65]. In this thesis, the ethylene layers have been prepared by dosing $p = 5 \cdot 10^{-7}$ torr of high purity ethylene at room temperature for $t = 20$s into the chamber. This corresponds to a dose of 10 L (Langmuir).

Benzene was purified by freeze–pump–thaw cycles and dosed at room temperature by exposing the Si substrates to $p = (1 - 3) \cdot 10^{-7}$ torr for $t = 200$s ($\sim$20-60 L)). This procedure ensures a saturation coverage of about 0.25 carbon atoms per surface Si atom [66].

To clean the crystals before preparation of a new layer, the sample was flashed to 600–700 K by pure radiative heating, sputtered at room temperature and at 800 K each for 12 min, and subsequently annealed to 1350 K for $t > 10$ s.

Chapter 3

X-ray absorption spectroscopy: Structure of unoccupied electronic states

X–ray absorption spectroscopy (XAS) is a method for the determination of the unoccupied valence density–of–states (DOS)[1] [67]. The probability for the absorption of a X–ray photon is measured as a function of photon energy by monitoring secondary processes as Auger or fluorescence decay. In this chapter, I present XAS — or NEXAFS (near–edge X–ray absorption fine structure spectroscopy) — studies of small hydrocarbon molecules adsorbed on the single domain Si(001)–(2×1) surface.

Within the scope of this work the investigation of the unoccupied valence structure with XAS serves the following purposes: It allows the characterization of the scattering intermediate state, it provides further information about the

[1]The unoccupied DOS is in molecular orbital theory often referred to as the "virtual" molecular orbitals.

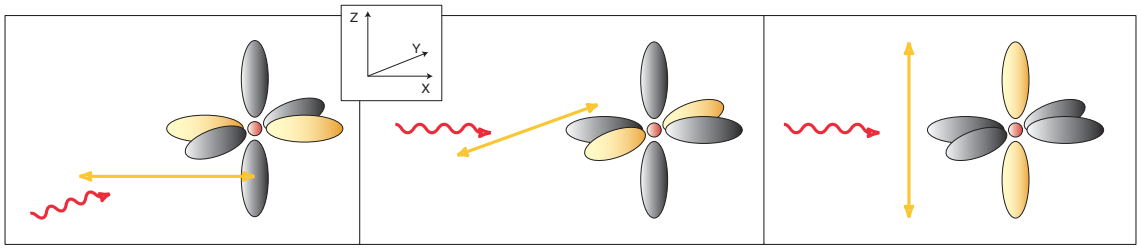

Figure 3.1: Polarization selective X–ray absorption at a carbon atom of an ordered adsorbate system. When exciting *s*–type core orbitals with an incoming photon of x, y, and z polarization, only transitions into *p*–type valence states with respective orientation are allowed.

electronic and/or vibrational properties of the system under investigation, and finally, it helps to determine the configuration of the studied adsorbate systems.

The detailed investigation of the unoccupied valence density of states is a premise for the understanding of the RIXS process. RIXS is determined by the scattering intermediate state $|i\rangle$, which is a core excited state $|\psi_{\mathrm{core}}^{-1}\psi_{\mathrm{unoccup.}}\rangle$. A decent knowledge of the virtual molecular orbitals — i.e. the unoccupied valence structure — is thus mandatory for the interpretation of RIXS. In this work, therefore X–ray absorption measurements of all systems investigated with RIXS have been performed. The XAS of condensed benzene and ethylene have carefully been reproduced and compared to literature [68–74]. These data are part of Paper IV and Paper V in Chap. 4.

The XAS investigations of hydrocarbons adsorbed on silicon have been published separately from the RIXS studies and can be found in this chapter [Paper I, Paper II, Paper III]. Polarization resolved XAS allows to determine the orientation of the unoccupied electronic states in space (Fig. 3.1) and thus the geometric configuration of the adsorbate [67]. The changes in the electronic valence structure of a molecule induced by the adsorption, combined with the knowledge of the adsorbate geometry, allow an insight into the mechanism of the formation of the surface chemical bond.

The clear identification of the adsorbate configuration is a prerequisite for the full utilization of RIXS. RIXS has the potential to determine the polarization and symmetry resolved electronic valence structure if applied to a fixed–in–space molecule. This can only be obtained on a macroscopically ordered structure, as it is possible for specific adsorbate systems. In the papers of this chapter, the adsorption geometry of ethylene (C_2H_4), benzene (C_6H_6), and acetylene (C_2H_2) on oriented single domain Si(001)–(2×1) substrates has been investigated with XAS. In all three cases, the XAS data show significant polarization anisotropy. Information about the adsorbed species and their configuration has been obtained. From this, it was possible to identify candidates for the RIXS investigations. Ethylene and benzene each adsorb in a single, fully ordered species and are thus suitable for a polarization resolved RIXS study. Acetylene adsorbes in a mixture of species, making a full polarization and symmetry deconvolution of the RIXS spectra impossible. C_2H_2/Si(001) has therefore not been investigated with RIXS in this thesis.

I will briefly summarize the findings of the papers in this chapter.

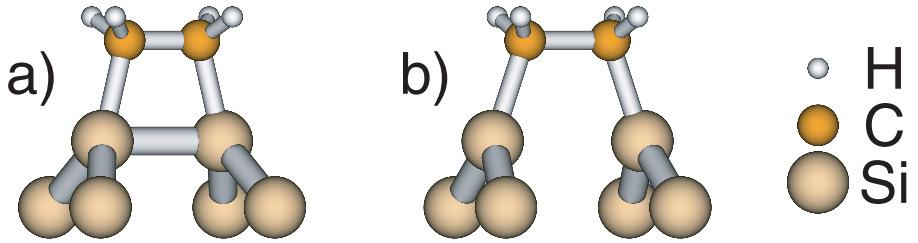

Figure 3.2: Historically competing adsorption models of ethylene on Si(001)–(2×1): a) dimerized; b) broken–dimer.

3.1 Electronic structure and bonding of small hydrocarbons on Si(001)

For ethylene and benzene it has been possible with XAS to identify the actual adsorption configuration within a set of competing models discussed in literature. Basic information about the nature of the chemical bond has been obtained. The adsorption models identified in the XAS studies were used as the base for the *ab–initio* calculations of the resonant and non–resonant RIXS spectra (Chap. 5), obtaining excellent agreement with the experiment and thus giving additional confirmation of the XAS analysis.

There has been a long debate concerning the question how ethylene adsorbs on the Si(001)–(2×1) surface. This surface exhibits a dimer reconstruction and the controversial issue was whether the dimers are cleaved and the ethylene inserted between the silicon atoms [75–78] or whether they stay intact with the ethylene adsorbing on top (Fig. 3.2). Although a trend in the latest work published favored the dimerized model [56, 79–90], direct experimental evidence was still missing. The NEXAFS study presented here [Paper I, Chap. 3.2] unambiguously identifies the dimerized configuration. The analysis of the electronic structure furthermore reveals strong indications for a re–hybridization of the carbon orbitals from sp^2 in the gas phase to sp^3 in the adsorbate. The ethylene inner π–bond is destroyed upon adsorption.

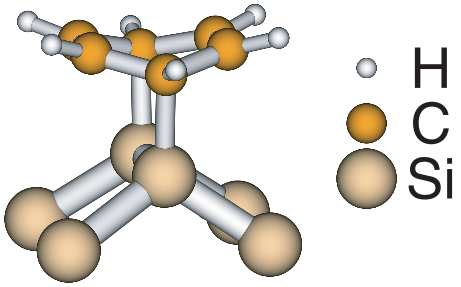

Figure 3.3: "Butterfly" adsorption model of benzene on Si(001)–(2×1).

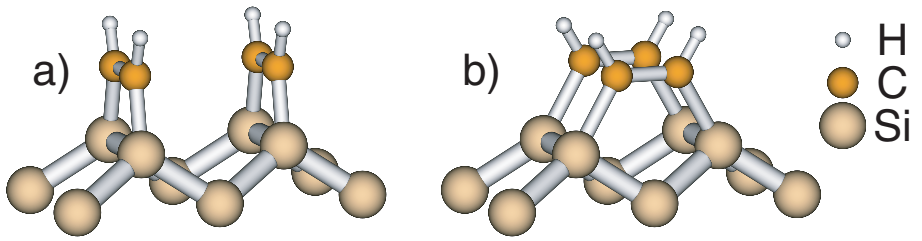

Figure 3.4: Coexisting adsorption species of acetylene on Si(001)–(2×1): a) dimerized; b) end–bridge.

In the case of benzene the adsorption configuration was likewise unsettled. An overview about the discussed adsorption models can be found in Fig. 3.9 (page 46). The XAS study presented here [Paper II, Chap. 3.3] determines the adsorption configuration to be the "butterfly" (Fig. 3.3). In the literature discussing this configuration so far, it has always been assumed that the C atoms coordinated to the Si surface atoms are re–hybridized from sp^2 in the gas phase to sp^3, and form surface chemical bonds similar to those of ethylene on Si(001). The analysis of the polarization anisotropy in the XAS clearly supports the "butterfly" configuration. But the XAS profile does not exhibit significant enough changes compared to gaseous benzene to definitely postulate a full sp^3 hybridization. In Paper II it has been carefully concluded that the experimental verification of the "butterfly" configuration implies the sp^3 hybridization of the surface coordinated C atoms. The RIXS experiments presented in [Paper VIII] reveal, that the re–hybridization of the C $2s$ and $2p$ orbitals is not fully sp^3.

The adsorption mechanism of acetylene [Paper III, Chap. 3.4] on Si(001) is comparable to that of ethylene. In both systems the out–of–plane π system is lost. In acetylene, the C atoms re–hybridize from sp to sp^2. The molecule adsorbs in a mixture of two structures (dimerized and end–bridge, see Fig. 3.4).

3.2 Fully polarization resolved X–ray absorption spectroscopy of C_2H_4 on single–domain Si(001)–(2×1)[2]

Abstract

We present a polarization resolved near edge X–ray absorption fine structure (NEXAFS) investigation of ethylene (C_2H_4) adsorbed on the oriented single domain Si(001)–(2×1) surface. From the detected resonances and their polarization dependences C_2H_4 is found to be strongly bound to the silicon dimers with the carbon atoms in a sp^3–hybridized state. The molecular axis is rotated around the surface normal with respect to the dimer axis.

Introduction

The adsorption of molecules on silicon surfaces has been the focus of many investigations over the last few years. The bonding of hydrocarbons to the Si(001)–surface is of particular interest due to the proposed technological potential of the hydrocarbon–silicon interface in bio–molecular sensors or even future integrated circuitry beyond today's silicon oxide based semiconductor manufacturing [91, 92].

The Si(001)–surface exhibits a reconstruction characterized by dimer formation [93]. Pairs of neighboring surface atoms form surface dimers saturating one of their dangling bonds. The still high reactivity of this surface originates from the remaining unsaturated bond per surface atom. Below 200 K a c(4×2) surface reconstruction is observed, formed of alternating flipped buckled dimers. At temperatures above 200 K these buckled dimers oscillate resulting in an average (2×1)–pattern [94].

The interaction of C_2H_4 with Si(001) was first examined more than ten years ago [95], leading to a bonding model where the C_2H_4 develops a di–σ bond to the dangling bonds of the Si dimers (Fig. 3.5). The C_2H_4 looses its double–bond and the carbon atoms rehybridize to an sp^3 state. Upon adsorption the dimer dangling bonds are saturated and the buckling of the silicon dimers is removed[87]. At room temperature adsorption of C_2H_4 leads to a saturation coverage of one molecule per surface dimer [65].

Although these results have been supported by many other studies [56, 75–78, 83, 84, 88–90] since then, about one central issue no consent has been achieved until recently: Do the surface dimers stay intact upon adsorption of C_2H_4 or is the dimer cleaved with new dangling bonds appearing in the adsorp-

[2] *Peer reviewed paper. This section has been published as Paper I:* Hennies, Föhlisch, Wurth, Witkowski, Nagasono, and Piancastelli [1], *Surface Science* **529**, 144–150 (2003).

doi:10.1016/S0039-6028(03)00079-7

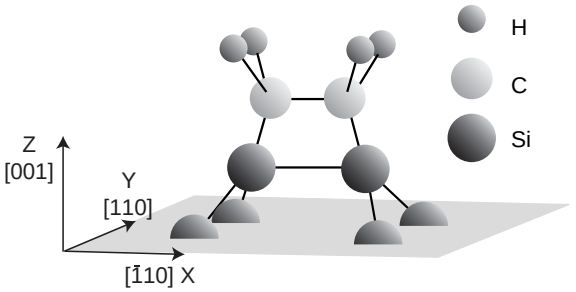

Figure 3.5: Adsorption model of ethylene C_2H_4 on Si(001)–(2×).

tion system? The latter model found strong support over some time, driven by the wish to explain the affinity of the C_2H_4–covered silicon surface to the coadsorption of atomic hydrogen without major changes in the initial adsorbate complex [76–78]. However, with the latest theoretical [90] and experimental results the intuitively convincing dimerized adsorption structure with the ethylene saturating the surface dangling bonds seems to be agreed upon. Experimental support for this bonding configuration is given among others by photoelectron diffraction measurements [87] and valence band photoemission (UPS) [84], where surface states resulting from the dangling bonds could no longer be detected. Theoretical investigations [79–82, 85, 86, 90, 96] quite consistently found the dimerized structure most stable.

With the UPS examination [84] and corresponding density functional calculations (DFT) [56] a more detailed adsorption geometry of C_2H_4 to Si(001) has been proposed. While the question of bonding geometries has been dominating the debate for many years, the last cited investigations focus on the electronic structure of this adsorbate system. The authors of the UPS study detected a 1D–band–like dispersion of two valence states. The DFT calculations support the interpretation of a delocalized one–dimensional adsorbate band structure along the dimer rows in C_2H_4 chemisorbed on Si(001)–(2×1). Lateral overlap of the $1b_{3u}$– and $1b_{2g}$–derived orbitals[3], which carry the bond to the hydrogen atoms, causes Pauli repulsion of the respective wave–functions. By an $11.4°$ rotation of the C–C–bond axis against the dimer axis around the surface normal and a further distortion of the molecule the Pauli repulsion is reduced and delocalized bands are formed.

These interesting new results demand for a further investigation of both the occupied and unoccupied valence structure in order to understand the complete spatial distribution of the valence states. A previous NEXAFS study [97, 98] showed general trends in the modification of the unoccupied valence states of

[3]This labeling of the orbitals corresponds to the notation used by Widdra et al. [84] and Birkenheuer et al. [56]. It is not compliant with the reference frame used in this paper and throughout the thesis. In the other papers presented in this thesis the in–plane orbitals of ethylene are thus denoted as $1b_{2u}$ and $1b_{1g}$.

doi:10.1016/S0039-6028(03)00079-7

C_2H_4 upon adsorption to Si(001). Since this investigation had been performed on a nominal plain (001)–surface with a mixing of (2×1)– and (1×2)–domains, the lateral adsorption directions have not been resolved therein.

We here present a fully polarization resolved NEXAFS investigation, allowing us to decide about the orientation of the unoccupied valence orbitals with respect to the substrate. We are making use of the possibility to prepare an oriented single–domain Si(001)–(2×1) crystal in order to distinguish between all excitation geometries with respect to the Si single domain surface coordinate system. On such a sample the full geometrical information about the orientation of the unoccupied valence structure can be obtained with NEXAFS [67].

Experimental methods

Setup

The experiments have been performed on beamline I511 [99] at MAX-Lab in Sweden. The beamline is equipped with a UHV–system for electron spectroscopy and X–ray emission studies on surfaces and surface adsorbates. A preparation chamber operated at a base pressure of low 10^{-10} torr is connected to an analysis chamber (at mid 10^{-11} torr). The analysis chamber can be rotated around the beam axis, allowing one to choose the detection angle freely with respect to the orientation of the electric field vector.

The samples used were cut from p–doped silicon with an intentional 5° deviation of the surface normal from the [001] direction to the [110] direction. This miscut (001) surface exhibits diatomic steps with terraces of 8.5 dimers width in a single (2×1) domain [100]. We mounted two samples with a 90° rotation around the surface normal with grazing incidence of the synchrotron light at an angle of 7° to the surface plane. This setup allows us to measure with the electric field vector of the incident light oriented normal to the surface and in the surface plane normal and parallel to the dimer axis.

Sample preparation

Samples were outgassed in the UHV by radiative heating at 800 K for 12 hours. The clean surface was prepared by cycles of sputtering with xenon at room temperature and at 800 K with subsequent annealing to 1250 K. The surface order was checked with LEED and surface cleanliness was monitored with XPS.

The C_2H_4 was dosed at room temperature with a capillary doser at a chamber background pressure of $P = 1.3 \cdot 10^{-7}$ torr for 15 min. These conditions lead to saturation coverage [101].

doi:10.1016/S0039-6028(03)00079-7

Absorption measurement and data analysis

The X–ray absorption spectra have been taken with the Scienta SES–200 hemispherical electron analyzer in constant final state mode. The pass energy was set to 500eV. In this setting an Auger yield is measured in an energy range of 50eV around the carbon KLL Auger at 252eV. Electrons were detected in an angle of 55° with respect to the polarization vector.

The photon flux was measured simultaneously by a reference gold mesh. The Auger yield spectra from the adsorbate system and from the clean silicon were first divided by the flux. All spectra were normalized to the flat region below threshold, before the clean sample spectra have been subtracted from the adsorption system spectra.

A total energy calibration of the photon energy has been performed making use of first– and second–order photons of the monochromator exciting the Si $2p$ electrons.

To rule out beam damage during measurements we compared the carbon $1s$ XPS–spectra before and after the X–ray absorption measurements for shape and intensity, but no difference was observed.

Results and discussion

Experimental results

In Fig. 3.6 a) and b) we show the spectra recorded with the $\vec{E}$–Vector oriented close to normal to the sample surface (z–direction along the [001] crystallographic axis) for each of our differently mounted samples (compare sketch). The incidence direction of the X–ray beam is grazing to the surface. The sample surface stands vertical, that is perpendicular to the horizontal polarization plane of the insertion device. Both spectra show the same two sharp resonances at 285.3 eV and 286.5 eV. These energies were calibrated with XPS as mentioned above, so this values represent the true energy with an error of $\leq \pm 100$ meV. In addition, weak appearances of two more features can be detected. In this excitation geometry the spectra obtained are independent of the azimuthal sample orientation (compare Fig. 3.6 a) and b)). This proves the comparability of the data collected from these two samples. These data are also similar to those published in a previous absorption study and measured in this geometry on a Si(001) surface with two domains [97, 98]. This assures the comparability of experiments performed on the nominal plane and on the oriented single domain terraced Si(001)–(2×1) surface and confirms that adsorption of ethylene on step–edges is negligible [102].

doi:10.1016/S0039-6028(03)00079-7

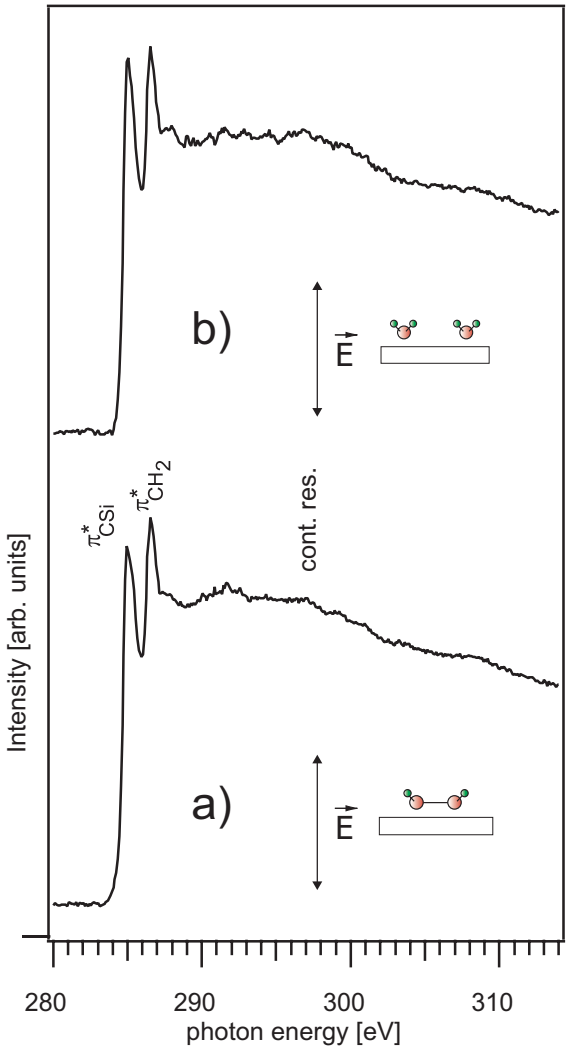

Figure 3.6: NEXAFS spectra of C_2H_4 adsorbed on Si(001)–(2×1) at room temperature measured on two samples with their (2×1) domains rotated 90° with respect to each other. The $\vec{E}$–vector of the incident photon beam is aligned along the z–Axis (compare sketch). Peak assignment see text.

The spectrum recorded with the electric field vector oriented in x–direction, i.e. parallel to the Si dimer axis (along $[\bar{1}10]$), is shown in Fig. 3.7. These measurements have been obtained from the same sample as the one in Fig. 3.6 b). The light is incident grazing to the surface perpendicular to the Si dimer axis. The sample surface is now parallel to the polarization plane of the synchrotron (compare sketch). Here we clearly observe a resonance at 291 eV. A smaller sharp resonance can be seen at 285.3 eV. A broad feature around 297 eV is also visible.

Fig. 3.8 shows the spectrum acquired with the $\vec{E}$–Vector aligned in y–direction (along $[110]$). These data now are collected on the same sample as the spectrum in Fig. 3.6 a). The polarization therefore is again parallel to the surface, but in this case perpendicular to the Si dimer axis. In this geometry we detect three features. The peak at 291 eV as well as the broad resonance around 297 eV can

doi:10.1016/S0039-6028(03)00079-7

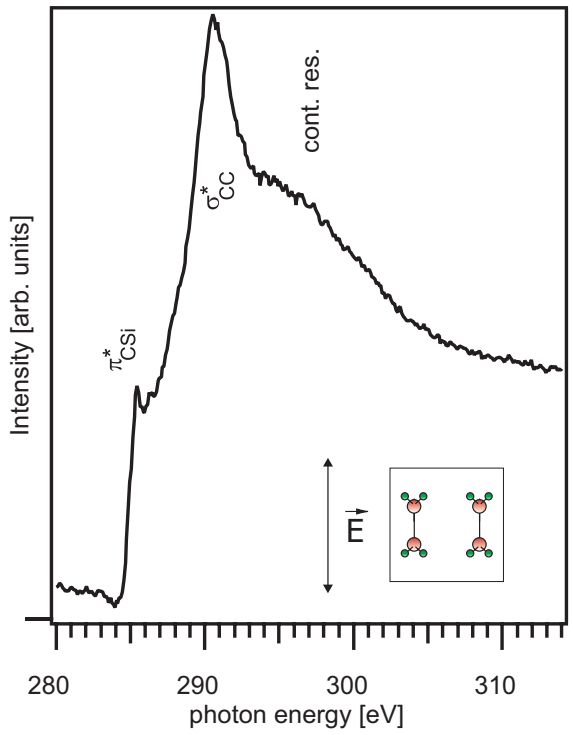

Figure 3.7: NEXAFS spectra of C_2H_4 adsorbed on Si(001)–(2×1) at room temperature. The E–vector of the incident photon beam is aligned along the x–Axis (compare sketch). Peak assignment see text.

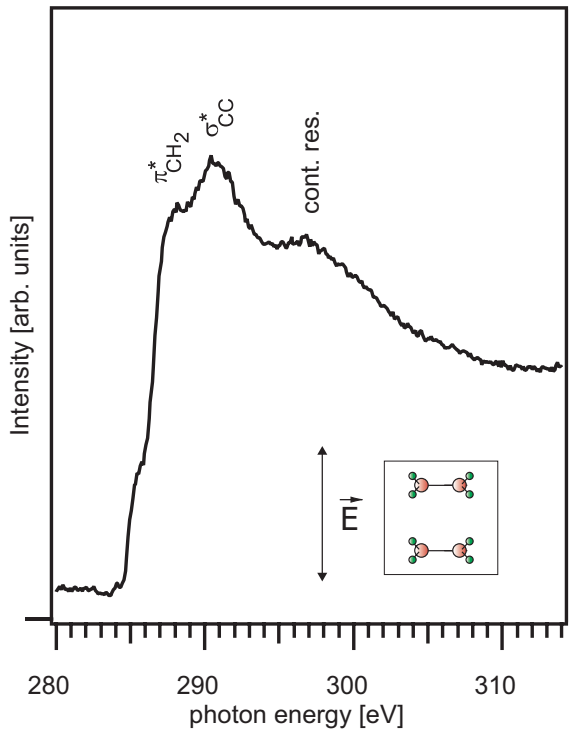

Figure 3.8: NEXAFS spectra of C_2H_4 adsorbed on Si(001)–(2×1) at room temperature. The E–vector of the incident photon beam is aligned along the y–Axis (compare sketch). Peak assignment see text.

be found again. A further feature appears at approximately 288 eV. At the onset of the X–ray absorption flank a weak shoulder can be seen.

doi:10.1016/S0039-6028(03)00079-7

Discussion

We start the discussion of our data with the resonance at 291 eV. This feature is dominant with x–polarization and can clearly be observed with y–polarization. Only a very small admixture of this state can be detected with z–polarization. The occurrence of this peak in the spectrum recorded with x–polarization can therefore be explained by assigning the feature to excitation into a σ^*–resonance. The corresponding bond is therefore parallel to the x–axis. We can interpret this σ^*–resonance as the antibonding orbital corresponding to the C–C bond. The direction of maximum intensity is given by the direction of the bond. Here in ethylene adsorbed on Si(001) the peak appears at 291 eV, that is 10 eV lower than in gas phase free ethylene [103]. The position is now comparable to the σ^*–resonance (at 291 eV) in free ethane C_2H_6 [104] which is sp^3–hybridized. The σ^*–resonance in simple hydrocarbons shifts to lower energies with increasing C–C bond length [105]. The shift in ethylene upon adsorption to Si(001) can therefore be taken as an experimental evidence for the loss of the C–C π–bond and the rehybridization of the carbon atoms.

We now have to understand why this resonance can be clearly seen with y–polarized light as well. If the bond is totaly aligned along the x–axis respectively if the C–C bond is parallel to the Si–Si dimer bond axis this transition would not be allowed. UPS investigations [56, 84] proposed a slight rotation of the ethylene molecule around the surface normal due to a lateral interaction of the molecules. This deviation of the C–C axis from the dimer orientation can explain the occurence of the σ^*–resonance in spectra recorded with y–polarization. Without any assumptions our NEXAFS measurements therefore give the direct experimental evidence for the rotation of the C–C bond axis against the Si dimer axis around the surface normal in C_2H_4 adsorbed on Si(001). The additional very small admixture of the σ^* resonance seen in the spectra recorded with polarization vector normal to the surface, is however most likely due to experimental restrictions, e.g. the angle between the macroscopic and microscopic surface plane on the terraced crystals and the incomplete polarization due to the grazing incidence of the X–rays. To check for out of plane tilting, we have also determined NEXAFS with the E–vector $\pm 45°$ off the surface normal. Here no variation is observed, which is an indication of in plane orientation.

Next we turn to the discussion of the "π"–type resonances at 285.3 eV and 286.5 eV which are seen prominently in Fig. 3.6a) and b). From the absorption measurements on free C_2H_4 [103] and on C_2H_4 in weakly bound systems [106] one would expect a very strong single π^*–resonance for orientation of the polarization vector perpendicular to the plane of the molecule. Our spectra instead show two resonances that are much weaker, even weaker than the σ^*–resonance

doi:10.1016/S0039-6028(03)00079-7

seen in Fig. 3.7. Here we can prove that C_2H_4 has lost its π–bond and is rehybridized when adsorbed to Si(001). In the absorption spectra we can see the antibonding counterparts of the tetrahedrally oriented sp^3–bonds, i.e. one C–Si bond directed towards the surface and two C–H bonds which are now seen to be lifted upwards. The fourth bond is the C–C σ–bond. The C–H bonds are equivalent and we assign one of the split π^* to the antibonding C–Si state and the other to the $C–H_2$, but there is no reason for which bond should be assigned to which resonance in the first place. Our fully polarization resolved measurements however give a certain way to identify the bonds in the observed resonances.

The first resonance at 285.3 eV is not only strongly enhanced with z–polarization but can also clearly be seen with x–polarization. As a slight shoulder it occurs very weakly in the spectra recorded with y–polarized light. That it is clearly visible with x–polarization but can hardly be seen with y–polarization gives a strong indication to identify this resonance to have predominant C–Si character. If this bond would be aligned with the Si dimer it would only be visible with z– and x–polarization. But since the molecule is rotated (see above) this explains the observation of this state as a shoulder in the spectrum recorded with y–polarization.

We then have to assign the second resonance at 286.5 eV to a state with major $C–H_2$ admixture. Its strong contribution to the spectra recorded with z–polarization gives an experimental evidence that this bond is not lying in the molecular plane any more, but that the H atoms are lifted out of the plane. This again confirms the sp^3 hybridization. As a $C–H_2$ bond it then should show up with x– as well as with y–polarization. Its part in the spectra measured with x–polarization is difficult to determine because it lies in the strong rise of the σ^* resonance. Anyhow the flank of the σ^*–resonance seems to include the part of another resonance. With y–polarization this state can clearly be seen, although it seems to be shifted to around 288 eV. Here probably the dispersion of the occupied states related to the $C–H_2$ bond as measured with UPS [56, 84] can be taken into account to explain this effect.

Finally the broad feature at approx. 297 eV can be more or less seen in all geometries. We attribute this state to the “continuum resonance” [107] called state exhibited by all simple hydrocarbons in the gas phase, which is caused by multiple excitations.

So far we have discussed our NEXAFS results assuming that the features result mainly from the ethylene species adsorbed on the terraces. In principle there could also be a sizeable contribution from step species. However, additional measurements at polarization angles of $\pm 45°$ with respect to the surface normal (not shown) which exhibit no difference indicate that this contribution must be small.

doi:10.1016/S0039-6028(03)00079-7

Conclusion

Using vicinal single domain Si(001) crystals we have been able to perform a fully polarization resolved NEXAFS study of C_2H_4 adsorbed on oriented Si(001)–(2×).

By investigating the unoccupied states our measurements not only prove the adsorption of C_2H_4 on top and along the Si surface dimers, but also give direct evidence of a slight rotation of the C_2H_4 C–C bond axis around the surface normal against the dimer axis. In addition we find the C–H_2 bond to be flipped out of the molecular plane by identifying the z–component of its corresponding antibonding state.

The full picture of the spatial orientation of the unoccupied states and the shift of the σ^*–resonance to lower energy support the bonding model of C_2H_4 adsorbed on Si(001) with sp^3–rehybridization of the carbon atoms and formation of a strong covalent bond to the Si surface dimer atoms.[4]

[4]**Acknowledgements:** We thank B. Naydenov, A. Fink and W. Widdra for providing the samples and preparation infrastructure. We acknowledge support from MAX-Lab staff during the beam-time. Financial support was given through the EU access to research infrastructure program (ARI), the DFG (grant Fo 343/1-1) and the "Grant–in–Aid for Japan Society for the promotion of Science Fellows".

doi:10.1016/S0039-6028(03)00079-7

3.3 Polarization and angle–resolved NEXAFS of benzene adsorbed on oriented single–domain Si(001)–(2×1) surfaces[5]

Abstract

We have investigated the adsorption of benzene on oriented single–domain Si(001)–(2×1) surfaces at room temperature by means of fully polarization–resolved near–edge X–ray–absorption fine–structure (NEXAFS) experiments. The present study reveals that benzene chemisorbs in a stable cyclohexadienelike configuration, labeled as a "butterfly" in the literature, which is di–σ bonded to silicon atoms.

Introduction

The understanding of hydrocarbon adsorption on semiconductors is of great interest, since the demand for Si–C containing devices has increased in opto-electronic applications.

The unsaturated hydrocarbons have been shown to be good candidates to modify the Si(001) surfaces via covalent bonds. A number of experimental and theoretical studies on the reconstructed Si(001)–(2×1) surface pointed out that alkenes react with the surface dangling bonds and form a pair of C–Si σ bonds[76, 78, 108]. In this class of molecules, complete understanding of the electronic structure is still under debate, but the geometry of the adsorption seems to have been clarified. This is not the case for benzene, which is the simplest molecule in the class of aromatic unsaturated hydrocarbons. Indeed, experimental and theoretical studies have revealed several possible adsorption models of benzene on the Si(001)–(2×1) surface.

The first experimental study of benzene on Si(001)–(2×1) surface from Taguchi et al. [66] was based on the combined use of techniques such as Auger electron spectroscopy, thermal desorption spectroscopy (TDS) and high–resolution electron energy loss spectroscopy (HREELS). They examined the chemisorption of benzene at room temperature with a saturation coverage of about 0.25 carbon atom per surface Si atom. Two thermal desorption peaks, at 460 K and 500 K, were assigned to benzene molecules adsorbed on terrace sites and defect sites respectively.

The HREELS analysis revealed the presence of a C=C double bond, and it was proposed that benzene is di–σ bonded to two adjacent Si atoms through

[5] *Peer reviewed paper. This section has been published as Paper II:* Witkowski, Hennies, Pietzsch, Mattsson, Föhlisch, Wurth, Nagasono, and Piancastelli [2], *Physical Review B* **68**, 115408 (2003).

doi:10.1103/PhysRevB.68.115408

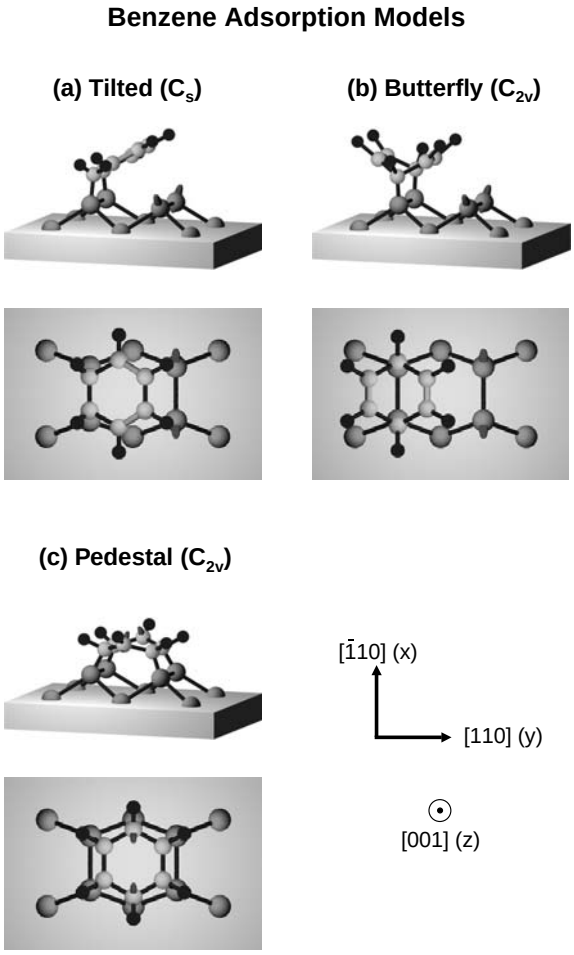

Figure 3.9: Schematic representation of the different structural models for the adsorption of benzene on Si(001)–(2×1): a) tilted (the gray bonds represent C=C double bonds), b) butterfly, and c) pedestal (from Ref. [101]).

the rehybridization of carbon states from sp^2 to sp^3. Based on these experimental results, the authors proposed two possible geometries for benzene adsorption, corresponding to the 1,4– and 1,3–cyclohexadiene–like structures (Figs. 3.9 b) and c) [101]) called "butterfly" and "tilted" structure, respectively. Theoretical investigations have been carried out to find out what is the most stable geometry of the adsorbed benzene. Craig [109] proposed an asymmetric "tilted" cyclohexadiene–like configuration which is fourfold bound to a Si surface dimer, whereas Jeong et al. [110] using different calculations, concluded that the most stable configuration is a "pedestal" geometry (Fig. 3.9 a). In this model, the benzene molecule lies flat on the surface and no carbon double bonds exist anymore. In a later study [57] the "pedestal" and "butterfly" configurations were found energetically favorable, but due to photoemission results [111] the "butterfly" structure model was preferred. At the same time, two independent scanning tunneling microscopy (STM) studies revealed that the benzene is initially adsorbed in a metastable "butterfly" configuration and proceeds to convert to

doi:10.1103/PhysRevB.68.115408

a stable final state which is attributed to a “pedestal” configuration [112] or a “tilted” configuration [113] according to the authors. This idea is also supported by a near–edge X–ray–absorption fine–structure (NEXAFS) study [114] where a second adsorbed species attributed to the “pedestal” configuration was reported.

In the present study, we have measured polarization dependent NEXAFS spectra of benzene adsorbed on Si(001)–(2×1) single–domain surfaces. We can thus examine the unoccupied states to determine their orbital symmetry and to derive the orientation and adsorption configuration of benzene on Si(001). We are able to assign unambiguously the adsorption configuration to one of the theoretical models previously described — namely, to the “butterfly” configuration.

Experimental details

The experiments have been carried out on the beamline I511 at the Swedish national synchrotron facility MAX-Lab providing linear polarized radiation [99]. The end station is composed of a preparation chamber for surfaces, operated at low 10^{-10} Torr, and an analysis chamber where combined X–ray photoemission spectroscopy (XPS), NEXAFS, and X–ray emission spectroscopy (XES) experiments can be performed in the middle–10^{-11}–Torr range. The analysis chamber can be rotated around the beam axis to measure polarization–dependent spectra.

The experiment was performed on single–domain Si(001)–(2×1) surfaces by using vicinal *p*–doped Si(001) substrates with a miscut angle of 5° in the [110] direction, which leads to single–domain terraces of 8.5 dimers with diatomic steps. The silicon substrate was fixed on a tantalum plate by using Mo clamps to avoid metal migration on the surface; the temperature reading was achieved by a *K*–type thermocouple spot–welded on the Ta plate.

Two single–domain samples were mounted both with a fixed grazing incidence of 7° to the incoming light and rotated by 90° with respect to each other within the surface plane. This setup allows us to perform measurements with the $\vec{E}$ vector of the incident radiation oriented normal to the surface and in the surface plane, along and perpendicular to the dimer axis.

The samples were outgassed at 800 K for 12 h under UHV conditions. After several cycles of Xe sputtering at room temperature and at 800 K followed by subsequent annealing at 1250 K, single–domain low–energy electron diffraction (LEED) patterns on each sample were observed and no contamination was visible in XPS. Benzene was purified by freeze–pump–thaw cycles and was dosed at room temperature on clean reconstructed surfaces by exposing the Si substrates to 10 L (1 L= 10^{-6} Torr/s). This procedure ensures a saturation coverage of the surfaces[66].

doi:10.1103/PhysRevB.68.115408

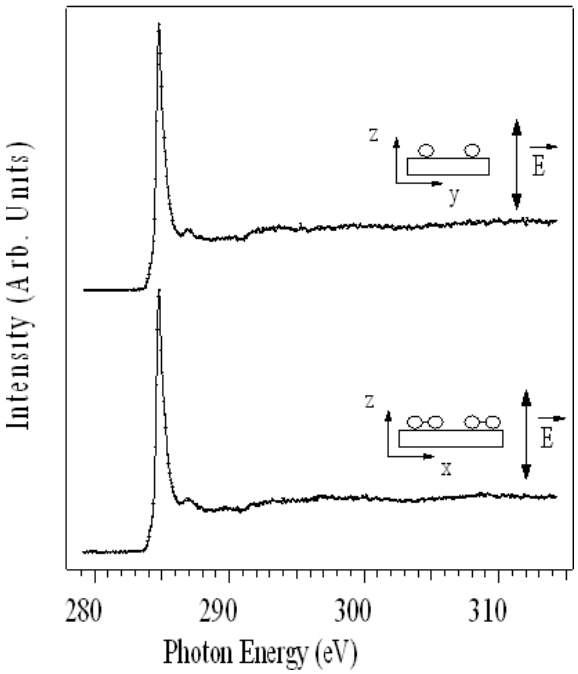

Figure 3.10: NEXAFS spectra of benzene adsorbed on Si(001)–(2×1) at room temperature measured on two samples with their (2×1) domains rotated 90° with respect to each other. The $\vec{E}$ vector of the grazing incident photon beam is aligned along the [001] direction.

The NEXAFS spectra were taken right after exposure with a Scienta SES–200 hemispherical electron analyzer at 500 eV pass energy in constant final–state mode monitoring the KLL carbon Auger peak at 252 eV±25 eV. The electrons were collected in a fixed angle of 55° with respect to the polarization vector. The bandwidth of the incoming photons was below 50 meV, and the energy calibration has been performed by using first– and second–order photons from the monochromator to measure the Si 2*p* electron emission, which allows us to obtain the true photon energy with an uncertainty of ≈100 meV.

Each NEXAFS spectrum on the adsorbate has been divided by the clean silicon surface measured in the same geometry as discussed in Ref. [115].

Results and Discussion

In Fig. 3.10, we present the NEXAFS spectra obtained for room–temperature benzene saturation coverage (10 L) taken with the electric field vector $\vec{E}$ normal to the surface or along the z direction, using the definition of x, y, and z relative to the crystallographic axis as given in Fig. 3.9 [6], where the (2×1) domains on the two samples are rotated by 90° inplane, respectively. In this excitation geometry, we are probing in the carbon K–edge absorption the unoccupied states of carbon 2*p* character, which are oriented normal to the surface. We observe that these spectra on the two samples are very similar. The peak at 284.8 eV

[6] Due to the sample tilt of 7°, $\vec{E}$ is also 7° off the surface normal.

doi:10.1103/PhysRevB.68.115408

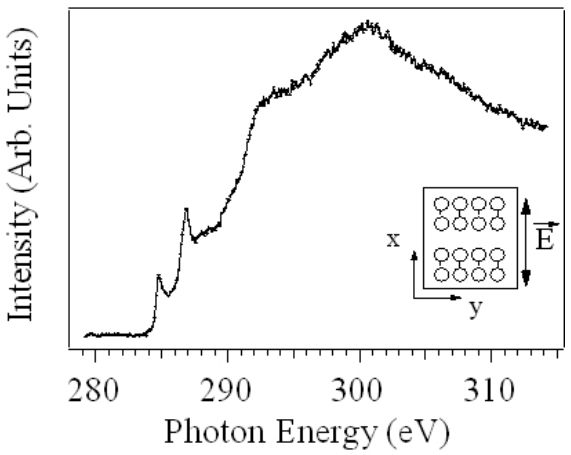

Figure 3.11: NEXAFS spectra of benzene adsorbed on Si(001)–(2×1) at room temperature. The $\vec{E}$ vector of the grazing incident photon beam is aligned along the x axis (i.e., parallel to the Si dimers).

is dominating next to as mall feature at 286.9 eV, whereas the rest of the spectrum is almost structureless, representing the continuum. In Figs. 3.11 and 3.12, we present the NEXAFS spectra taken for the $\vec{E}$ vector lying in the surface plane, along the Si dimers (the x axis) or normal to the Si dimers (the y axis), respectively. Here we observe very different spectral distributions and intensities. The peak at 284.8 eV, which we have observed strongly for out–of–plane polarization in Fig. 3.10, is also present in Figs. 3.11 and 3.12. However, for in–plane polarization the intensities are weak in comparison to the continuum step height. This clearly indicates a strong out–of–plane amplitude of this unoccupied state, which is in correspondence with the π^* orbital of a lying benzene molecule. However, a completely flat lying benzene would only show this π^* state for out–of–plane polarization and no intensity for in–plane polarization as has been reported for benzene adsorbed on metals[116]. We thus directly see that the benzene molecule either does not lie flat or is geometrically distorted upon adsorption. In particular for the in–plane polarization, the stronger appearance of the $\vec{E}$ vector normal rather than parallel to the Si dimers indicates that the π^* resonance has an in–plane component normal to the Si dimers. Therefore the adsorption configuration has to be either the benzene molecule “tilted” normal to the Si dimers or the benzene molecule in the “butterfly” configuration.

We also note that the shape of this peak at 284.8 eV isvery similar to the π_1^* peak observed in multilayers of benzene [116]. Furthermore, we do not find the asymmetric shape reported by Ref. [114], where a second structure 1 eV higher in the π^* tail has been attributed to a second adsorbed species, which at an energy resolution of about 50 meV we should have been able to resolve. In order to investigate the possible occurrence of a second adsorbed species reported first by TDS [66] we annealed the benzene monolayer at 480 K which is in between the two TDS peaks. The NEXAFS spectra, recorded in the same conditions as previously (not shown here), did not exhibit any visible changes which could

doi:10.1103/PhysRevB.68.115408

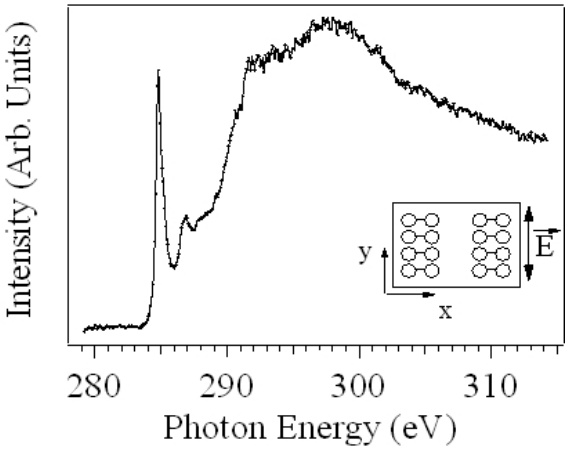

Figure 3.12: NEXAFS spectra of benzene adsorbed on Si(001)–(2×1) at room temperature. The $\vec{E}$ vector of the grazing incident photon beam is aligned along the y axis (i.e., perpendicular to the Si dimers).

be a signature for a second adsorption geometry. This absence of change can be due to the low concentration of the second species which is proportional to the number of surface defects [66]. However, this investigation ensures that the geometry of the adsorbed molecules is stable on the surface and not metastable as seen by STM [113].

To investigate the adsorbed species further, we now turn to the peak appearing at 286.9 eV, which is almost equally strong for all three polarizations in comparison to the continuum step height. This state has been previously assigned as due to the C–H* resonance[114]. As the C–H bonds are distorted from the planar geometry of the free benzene molecule upon adsorption, where the hydrogen atoms — independent of the adsorption model "pedestal", "tilted" or "butterfly" — are pointing away from the surface, we observe this state for both in–plane and out–of–plane polarization.

We also note that we do not observe a clear spectral feature around 289 eV which in gas phase and multilayers has been attributed to π^* conjugation [69, 116]. The absence of conjugation clearly shows that the aromatic π system is broken up upon adsorption, in full agreement with other investigations [57, 111].

Let us now turn to the spectral features towards higher photon energies. Here both spectra in Figs. 3.11 and 3.12 exhibit a broad structure around 292.5 eV and quite pronounced in Fig. 3.11, a feature around 300.7 eV, mainly seen for the $\vec{E}$ vector parallel to the Si dimers. In the framework of a localized bond description, the feature at 292.5 eV could be assigned to a σ^*_{C-C} resonance with an energy lower than in the gas phase, as the C–C bond in chemisorbed benzene has been elongated in comparison to the benzene gas phase, as is the case for the "butterfly" adsorption model [57]. The state at 300.7 eV would then be assigned to a $\sigma^*_{C=C}$ resonance of the carbon double bond, with a shorter C–C distance than in gasphase benzene [57], supporting HREELS measurements

doi:10.1103/PhysRevB.68.115408

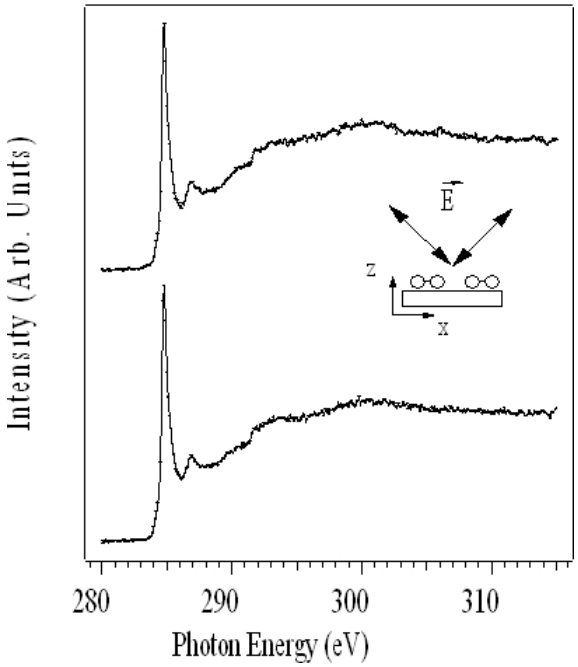

Figure 3.13: NEXAFS spectra of benzene adsorbed on Si(001)–(2×1) at room temperature. The $\vec{E}$ vector of the grazing incident photon beam is oriented ±45° from the z axis along the Si dimers as indicated in the sketch.

indicating a carbon double bond in the adsorbed molecule [66]. In particular the reduced intensity of the latter structure for the polarization normal to the Si dimers (Fig. 3.12) favors the "butterfly" model, where the carbon double bonds are parallel to the dimers and shorter as in the free molecule [57], and speaks against the "tilted" and "pedestal" configurations. In the case of a "tilted" configuration we would expect contributions of C–C double bonds for both in–plane polarizations, and for the "pedestal" configuration, we would expect as trong σ^*_{C-C} resonance and no structures for C–C double bonds around 300 eV as seen in the NEXAFS spectrum for the saturated ring C_6H_{12} in the gas phase [117].

We are aware of the fact that also σ conjugation can play a significant role in adsorbed benzene. Furthermore, the complex nature of continuum resonances (multiply excited states and shape resonances) does not directly link the number and position of resonant features and the type of chemical bonds.

To gain further information to distinguish between the "tilted" and "butterfly" adsorption models for benzene on the Si(001)–(2×1) surface, we also took NEXAFS data with the $\vec{E}$ vector oriented at ±45° from the (001) direction in order to distinguish an overall preferential orientation of the benzene molecules. The results are presented in Figs. 3.13 and 3.14. In Fig. 3.13, the examined sample is the same as presented in Fig. 3.11 and we analyze the symmetry of the molecules along the dimer (i.e., parallel to the x axis). In this figure, the two NEXAFS spectra presented for the two orientation of the $\vec{E}$ vector are totally superimpos-

doi:10.1103/PhysRevB.68.115408

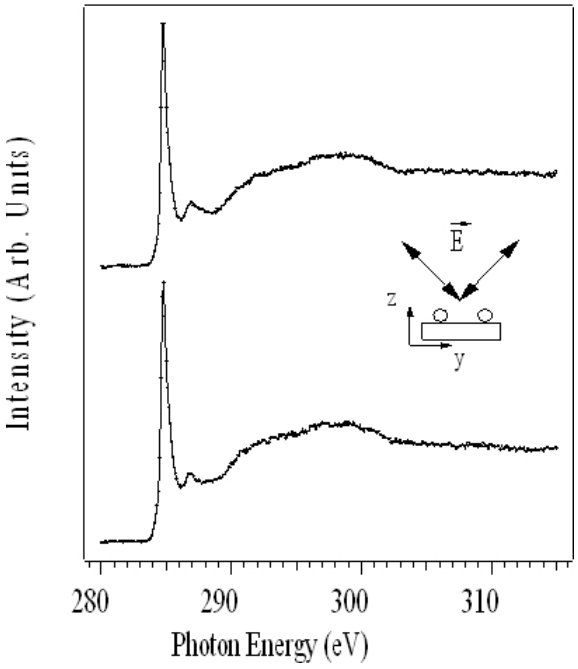

Figure 3.14: NEXAFS spectra of benzene adsorbed on Si(001)–(2×1) at room temperature. The $\vec{E}$ vector of the grazing incident photon beam is oriented ±45° from the z axis perpendicular to the Si dimers as indicated in the sketch.

able which indicates that the molecules are symmetric with respect to the plane which is perpendicular to the dimers. This would agree with both models, as the adsorption geometry has local mirror symmetry normal to the Si–Si dimers. The spectra in Fig. 3.14 are taken with the $\vec{E}$ vector ±45° around the Si–Si dimer, thus probing the orientation perpendicular to the dimers (i.e., parallel to the y axis). For the two angles of polarization, we can see that the two spectra are very similar. Assuming that the benzene molecules in the "tilted" configuration are all to be found at the same tilt angle, we would expect a strong difference in the NEXAFS spectra for the different polarizations $-45°$ and $+45°$ with respect to the [001] direction. The small variations observed in Fig. 3.14 prove that the molecules are symmetric with respect to the dimer axis. This is the case for the "butterfly" configuration. The small difference between the two spectra is mostly the spectral feature assigned to the C–H* resonance, which indicates that the C–H bonds might have a slight distortion on each side of the butterfly wings of the molecule. This could be the influence of the asymmetry of the surface induced by the step edges on the single–domain Si(001)–(2×1) surface.

Conclusion

We have performed fully polarization–resolved NEXAFS experiments on benzene adsorbed on oriented Si(001)–(2×1) single–domain surfaces. We find that the benzene ring lies distorted on the surface. In particular, the molecules are tilted on the surface as has been proposed for the "tilted" and "butterfly" configura-

doi:10.1103/PhysRevB.68.115408

tions, dismissing the "pedestal" adsorption model. From NEXAFS spectra with in–plane $\vec{E}$ vector we deduce that the C–C double bonds are preferentially oriented parallel to the dimer axis. And from NEXAFS spectra with the $\vec{E}$ vector oriented at $\pm 45°$ with respect to the surface normal, we determine the molecule to be symmetric with respect to the dimer axis, excluding an ordered, asymmetric "tilted" configuration. The geometry of adsorbed benzene on Si(001)–(2×1) is thus attributed to a stable "butterfly" configuration corresponding to a 1,4–cyclohexadiene–like structure where benzene is di–σ bound to Si dimers with the coordinating carbon atoms showing sp^3 rehybridization. We also find that only this adsorbed species occurs at room temperature and no evidence for a more stable adsorption geometry like the "tilted" and "pedestal" model after annealing at higher temperature has been found.[7]

[7]**Acknowledgements:** We thank L. Kjeldgaard and the MAX-Lab staff for scientific and technical support during the experiment. Financial support was given through the European Access to Research Infrastructure (ARI), the Grant–in–Aid for Japan Society for the Promotion of Science and the Deutsche Forschungsgemeinschaft through Grant No. Fo 343/1-1.

doi:10.1103/PhysRevB.68.115408

3.4 Adsorption geometry of C_2H_2 on the single–domain Si(001)–(2×1) surface: fully polarization resolved NEXAFS[8]

Abstract

The adsorption of acetylene on single–domain Si(001)–(2×1) surfaces has been investigated at room temperature using fully polarization resolved near edge x–ray absorption fine structure (NEXAFS) spectroscopy. Two coexisting adsorption species have been observed, which we ascribe to the dimerized and end–bridge structures. In both cases, the Si dimers remain intact and the acetylene carbon atoms rehybridize to sp^2.

Introduction

As the demand for Si–C containing devices has increased in optoelectronic applications, the understanding of hydrocarbon adsorption and bonding on semiconductors is of great interest. Especially acetylene (C_2H_2) adsorption has been the subject of investigation [79, 89, 97, 98, 118–125]. The precise adsorption geometry of acetylene is still under debate, since calculations show a multitude of possible structures; some being energetically very close to each other.

In an early study, Nishijima et al. [118] investigated acetylene adsorption on silicon using high resolution electron energy loss spectroscopy (HREELS) and low energy electron diffraction (LEED). It was determined that acetylene predominantly chemisorbs non–dissociatively on the Si(100) dimerized surface in the temperature range 80 K – 300 K. The acetylene molecule was found to adsorb on top of a Si dimer bound to two adjacent silicon atoms (*dimerized*, see Fig. 3.15a), saturating the dangling bonds and leaving the Si–Si dimer intact. A few years later, in a study of acetylene adsorption using Auger electron spectroscopy, temperature–programmed desorption (TPD), and HREELS [120, 121], it was proposed that the Si–Si dimer is cleaved by adsorption on top of the dimer (*broken–dimer structure*, as shown in Fig. 3.15b). Early classical trajectory and slab calculations [79, 122] also favored the broken–dimer structure, whereas subsequent density functional theory, first principles dynamics, and total energy surface studies [123–125] found the dimerized structure with an intact Si–Si dimer to be considerably more stable.

The dimerized configuration as the groundstate of chemisorption was also proposed by Hofer et al. [126] in simulating scanning tunneling microscopy

[8] *Peer reviewed paper. This section has been published as Paper III:* Pietzsch, Hennies, Föhlisch, Wurth, Nagasono, Witkowski, and Piancastelli [3], *Surf. Sci.*, 562:65–72, 2004.

doi:10.1016/j.susc.2004.05.007

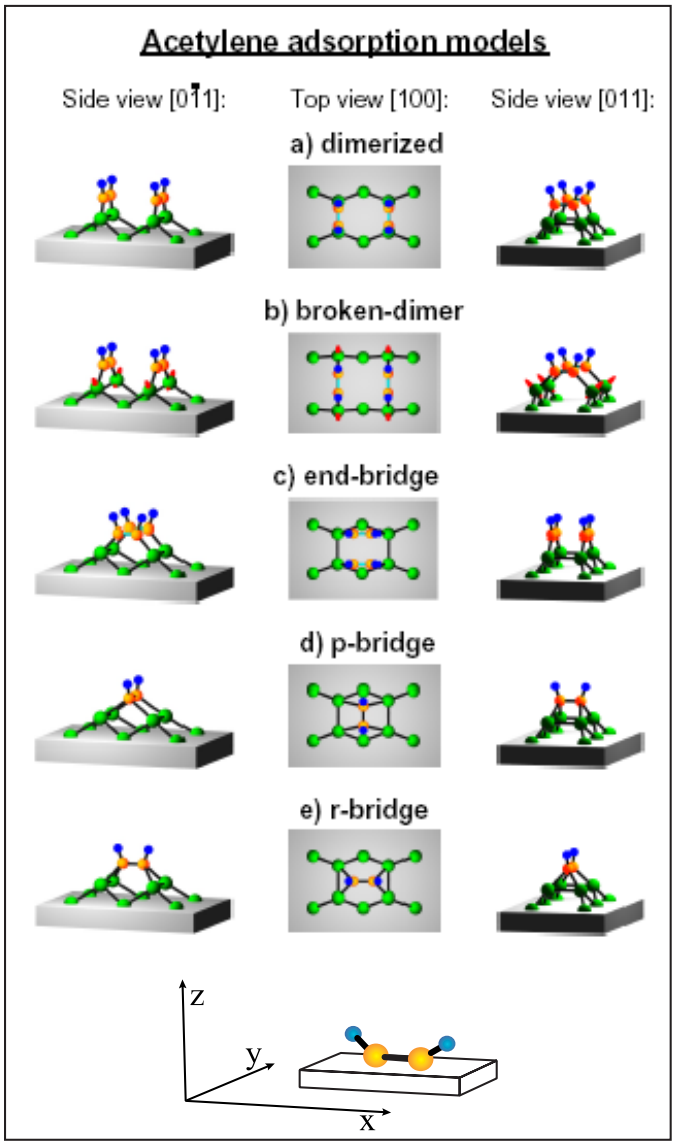

Figure 3.15: Acetylene adsorption models on Si(001)–(2×1); a)*dimerized* model with C_{2v} symmetry [118], b) *broken–dimer* model with C_{2v} symmetry [120], c) *end–bridge* model with C_s symmetry [89], d) *p–bridge* model with C_{2v} symmetry, and e) *r–bridge* model with C_{2v} symmetry; from [101]. At the bottom, the used coordinate system relative to the acetylene molecules is shown.

(STM) images and calculating adsorption energies. Apart from the broken–dimer structure and the dimerized structure with an adsorption energy of 2.97 eV, three alternative adsorption structures were considered: The *end–bridge structure* (Fig. 3.15c), with the C–C bond bridging the ends of two dimers and having 2.87 eV adsorption energy. There, the carbon atoms are sp^2 hybridized as supported by HREELS [78] (like in the dimerized and broken–dimer structures), thus the acetylene contains a C–C double bond. Apart from that, two fourfold bonded configurations (*tetra–σ bonds*) have been proposed by Xu et al. [89] based on photoelectron diffraction measurements. Here, the acetylene retains only a single C–C bond and is thus sp^3 hybridized. Two orientations were considered: The acetylene molecule bonds to two adjacent Si–dimers with the C–C bond par-

doi:10.1016/j.susc.2004.05.007

allel to the dimer axis (*p–bridge structure*, Fig. 3.15d), or the C–C bond axis is oriented perpendicular with respect to the dimer axis (*r–bridge structure*, Fig. 3.15e). The distance between the C atoms in sp^3 hybridization is increased by about 0.2 Å with respect to the sp^2 hybridization. The adsorption energies of the r–bridge and p–bridge species are found to be 2.00 eV and 1.20 eV, respectively [126].

It has also been considered that different adsorption species coexist on the surface: Using scanned–energy photoelectron diffraction, Terborg et al. [127] found evidence for the coexistence of at least two distinct species, which they determine to be the dimerized species and a tetra–σ configuration. By comparing calculated HREEL spectra with experimentally reported spectra, Morikawa [128] stated that at least two energetically very close stable adsorption states coexist: At a coverage of 0.5 ML, the dimerized structure is predicted to be the most stable configuration, while at 1 ML coverage in turn the end–bridge structure becomes the most stable configuration (that means a pair of end–bridge configurations occupying the same two Si–dimers), in agreement with the work of Sorescu and Jordan [129]. This configuration was also identified by Kim et al. [130] using STM and pseudopotential calculations. Recent first–principle calculations [131, 132] also favor the coexistence of the dimerized and end–bridge structures. Silvestrelli et al. [131] also found the lowest–energy end–bridge structure to be stable and non–metallic in contradiction to Miotto et al. [133].

In contrast, Yeom et al. [134] did not find any evidence for a coexistence of the end–bridge and dimerized species investigating the acetylene adsorption using core–level photoemission spectroscopy. They explained the discrepancy by the fact that coexistence may happen only for the very initial adsorption or that the C 1s binding–energy differences are too small to be resolved. However, they admit that the end–bridge structure is chemically very similar to the dimerized bonding and thus might not be distinguished.

NEXAFS on C_2H_2/Si(001)–(2×1) has been measured earlier by Matsui et al. [97, 98]. There, the adsorption of acetylene has been studied for different orientations of the polarization vector with respect to the surface normal. However, the spectra were not taken on samples with oriented dimers. Thus, the obtained information about the adsorption geometry is limited.

A complication in the study of the adsorption geometry is that the Si(001) surface exhibits a mixture of $90°$ rotated domains of Si dimers. To investigate the orientation of adsorbed C_2H_2, we need single domain Si(001) surfaces in order to determine the spatial orientation of the adsorbed molecule relative to the dimer reconstructed surface. A single domain Si(001)–(2×1) surface has been successfully prepared by using a Si(001) crystal miscut by $5°$. For a Si

doi:10.1016/j.susc.2004.05.007

crystal cut directly in (001), one atomic layer steps will occur at the surface and the formed silicon dimers will be rotated by 90° at every 1–layer step [100]. In the miscut crystal however, only 2–layer steps occur, leading to an uniform orientation of the dimer rows [100].

On vicinal cut Si(001)–(2×1) single domain surfaces, we have successfully used carbon K–edge NEXAFS to determine the unoccupied electronic structure and geometric orientation of adsorbed C_2H_4 [1] and C_6H_6 [2] on the Si(001)–(2×1)surface.

In the present paper, we investigate the bonding of C_2H_2 at saturation coverage on the Si(001)–(2×1) single–domain surface, using polarization dependent NEXAFS. This allows us to observe the unoccupied valence states of this adsorbate system and to determine the spatial orientation of the adsorbed acetylene relative to the Si(001) surface, going beyond NEXAFS using unoriented domains [97, 98], where the orientation of the adsorbate in the surface plane could not be distinguished. We interpret our NEXAFS data as due to the coexistence of two adsorption species, which we ascribe to the dimerized and end–bridge structures in a ratio of 5:4.

Experiment

The experiments have been carried out at the surface endstation on the undulator beamline I511 at the swedish national synchrotron facility MAX-Lab in Lund which provides linear polarized radiation in an energy range of 100 – 1500 eV [99]. The end station consists of two connected UHV chambers: a preparation chamber operated at low 10^{-10} Torr, and an analysis chamber where x–ray photoemission spectroscopy (XPS), NEXAFS, and x–ray emission spectroscopy (XES) experiments can be performed in the 10^{-11} Torr range. The analysis chamber is rotatable around the optical axis of the incoming beam. This allows to freely vary the relative angle between the electric field vector of the synchrotron radiation, the sample, and the angle of detection.

NEXAFS was carried out in constant final state mode detecting carbon KLL Auger decay in an energy interval of 228 eV to 278 eV with a Scienta SES200 electron analyzer. The band width of the incoming photons was set to 50 meV and the photon energy was determined to an accuracy of 0.1 eV using the first– and second–order of the beamline grating monochromator. The NEXAFS spectra were doubly normalized [67]: Each spectrum was normalized to the incident photon flux, measured on a reference gold mesh. Additionally, spectra of the clean substrate were subtracted from spectra of the adsorbate covered surface. Finally, all spectra have been normalized to unit height at the continuum region at $h\nu$ = 315 eV.

doi:10.1016/j.susc.2004.05.007

The molecules were adsorbed on $5°$ vicinal cut single domain Si(100)–(2×1). We mounted two 1×1 cm^2 single domain Si(100)–(2×1) crystals taken from the same $5°$ vicinal cut Si(100) wafer at 7° incidence angle on a tantalum plate with molybdenum clamps. The surface structure and the orientation was checked with LEED. For one Si crystal the [011] direction is along the incident photon beam, whereas for the other one the [$0\bar{1}1$] direction is along the incident photon beam. With this set–up, the electric field vector of the incident radiation can be oriented normal to the surface, and in the surface plane with the electric field vector either normal or parallel to the Si–Si dimers.

The samples were outgassed at 800 K for about 12 hours under UHV conditions. To clean the sample, several cycles of sputtering with Xe^+ ions at room temperature were applied, followed by subsequent annealing to 1250 K to reconstruct the surface. The sample cleanliness was checked using XPS. Saturation coverage of acetylene gas was dosed at room temperature.

Results and Discussion

In Fig. 3.16, carbon K–edge NEXAFS of C_2H_2 on Si(100)–(2×1) for out–of–plane polarization ($\vec{n}$) for the two samples are presented. As shown in the schematic drawing inset, the electric field vector is normal to the silicon dimers for both samples. In both cases, a similar spectral distribution is observed which further emphasizes the equivalence of the two Si(001) crystals. In particular, two sharp features at 283.8 eV and 286.7 eV and a broader structure at 288.4 eV have been observed.

Turning the electric field vector of the incident radiation into the surface plane, we obtain the NEXAFS spectra shown in Fig. 3.17. With the electric field vector along the Si dimers ($s_{||}$ polarization) we observe the three states at 283.8 eV, 286.7 eV, and 288.4 eV as for $\overrightarrow{n}$ polarization plus an additional broad feature at 299 eV. With the electric field vector perpendicular to the Si dimers ($s_\perp$ polarization) we also observe these four peaks. The first resonance at 283.8 eV has about 20% higher intensity with respect to the continuum step height at 315 eV for $s_\perp$ polarization.

The resonances at 283.8 eV and 286.7 eV show a strong variation of the peak intensities with polarization. The first resonance is dominating the spectra with $s_\perp$ and $s_{||}$ polarization, whereas it only contributes to a very small amount to the $\overrightarrow{n}$ spectra. On the other hand, the resonances at 286.7 eV and 288.4 eV are observed to increase for $\overrightarrow{n}$ polarization. The intensity of the second resonance at 286.7 eV is found to be about one and a half times as large in the $\overrightarrow{n}$ as in the $\overrightarrow{s}$ geometries.

doi:10.1016/j.susc.2004.05.007

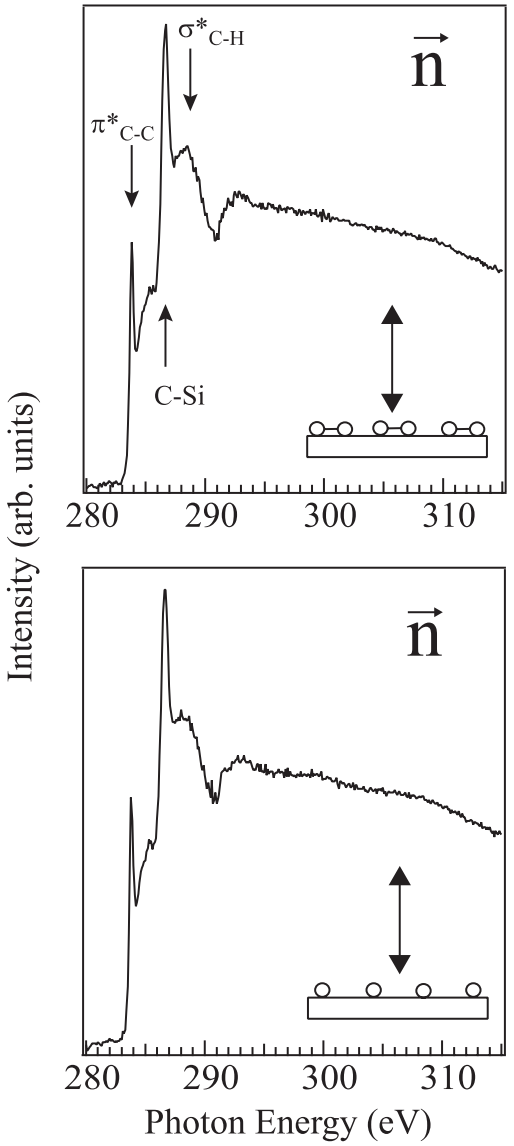

Figure 3.16: NEXAFS spectra of C_2H_2 on Si(001)–(2×1) for $\vec{E}$ vector normal to the surface.

Since the resonance at 283.8 eV is most pronounced in the $s_\perp$ and $s_{||}$ geometry, in–plane spatial orientation of this state is suggested. The resonance state at 286.7 eV, showing its maximum intensity for out–of–plane polarization, is thus stated to be oriented perpendicular to the surface. A similar behavior is observed for the peak at 288.4 eV.

For the following discussion, a coordinate system relative to the acetylene molecules is used; it is shown in the lower part of Fig. 3.15. Now, based on the polarization–dependence, we can directly assign the two observed sharp resonances at 283.8 eV and 286.7 eV to states which derive from the p–type π^*_{C-C} states perpendicular to the molecular axis which represent the antibonding part

doi:10.1016/j.susc.2004.05.007

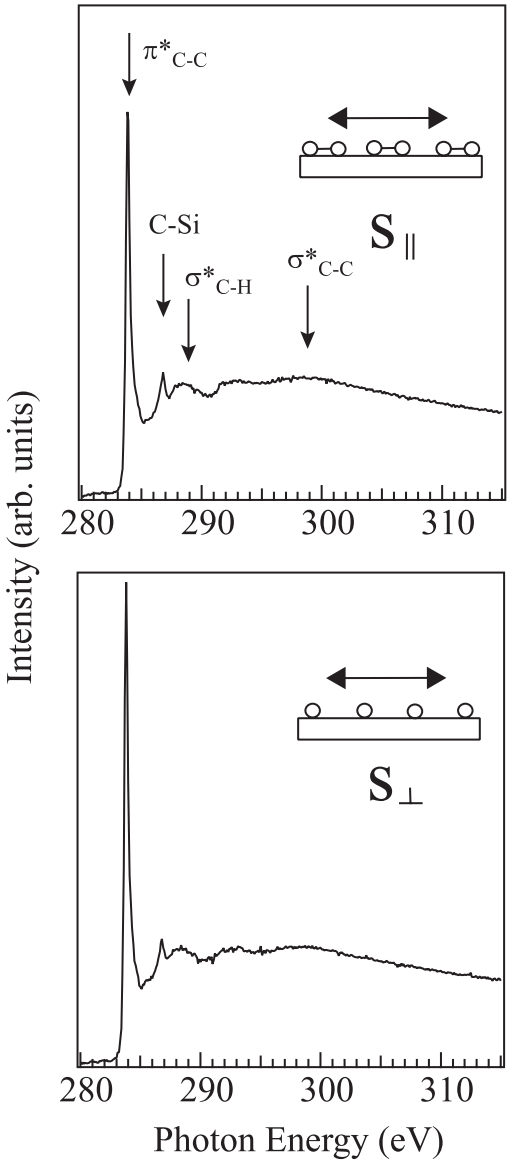

Figure 3.17: NEXAFS spectra of C_2H_2 on Si(100)–(2×1) for $\vec{E}$ vector parallel to the surface.

of the triple bond in the free acetylene molecule. The state at 283.8 eV is observed with very high intensity in the $s_\perp$ and $s_{||}$ geometries and with much lower intensities also in the $\overrightarrow{n}$ geometry. The intensity ratio is about 6:1 for $s_\perp : \overrightarrow{n}$ and 5:1 for $s_{||} : \overrightarrow{n}$. This confirms the orientation of this state parallel to the surface; it is thus assigned to a p_y–derived π^*_{C-C} state. The orientation of this π^*_{C-C} state implies the orientation of the C–C axis of the adsorbed molecules parallel to the surface.

Since the state at 286.7 eV is observed to be perpendicular to the surface, it is stated to be derived from the p_z states. Its orientation suggests that it is involved in the surface bond between the acetylene molecule and the substrate.

doi:10.1016/j.susc.2004.05.007

Matsui *et al.* [98] assign the second resonance at 286.7 eV to a state which they denote as σ^*_{C-Si}. From the observed polarization dependence, this resonance is denoted to be a C–Si resonance. Comparing this with ethylene adsorption on Si(001)–(2×1) [1], the C–Si state is also observed to be most prominent in the corresponding measuring geometry [98]. However, its energy is lower by 1.4 eV due to the weaker bonding.

As the free acetylene has a sp–hybridization, it will rehybridize to sp^2 or even sp^3 during bonding. The resulting hybridization depends on the structure of bonding: sp^3–hybridization allows bonding to four Si atoms, whereas sp^2–hybridization only leaves space for two new bonding partners. The sharp resonance peak at 283.8 eV representing an undisturbed π^*_{C-C} state is observed in every measurement geometry, thus a tetra–σ bond seems unlikely. The observation of two resonances resulting from the splitting of the π^* resonance of the free acetylene molecule further supports this statement. This leaves the dimerized, broken–dimer and end–bridge structures for the adsorption species. From the intensity variation of the C–Si resonance, it may be concluded that this bond is oriented mainly perpendicular to the surface. Its contribution to the spectra is highest for $\vec{n}$ polarization and decreases towards $\vec{s}$ polarization which coincides well with the dimerized and end–bridge structures. For the broken–dimer structure however, a C–Si bond with nearly $45°$ angle towards the surface is expected due to the larger Si–Si distance. Thus, this adsorption geometry can also be excluded.

As a consequence of the adsorption, also the C–H bond does not longer lie along the molecular axis. As the π–type unoccupied C–C orbital splits up, it not only forms the C–Si bond, but part of it joins the C–H bond and causes it to bend upwards away from the surface, as has also been observed for ethylene adsorption on Si(001)–(2×1) [1]. The feature at 288.4 eV shows exactly that behavior. Its intensity is strongest for excitation with $\vec{n}$–polarization and it is in good agreement with the data from [98]. Thus, this peak is assigned to be a σ^*_{C-H} state.

As noted above, the intensity of the first resonance is nearly equally large for both $s_{||}$– and $s_\perp$–polarization excitation, see Fig. 3.17. This indicates that the acetylene molecules do not adsorb on the surface in a defined azimuthal orientation, but are either randomly oriented or adsorb in at least two different structures which are rotated with respect to each other. Measurements of polarization resolved NEXAFS of ethylene on Si(001)–(2×1) performed by us [1] using the same wafer resulted in a clear difference between the $s_{||}$ and $s_\perp$ spectra, thus in contrast showing a single adsorption geometry with C_2 symmetry. Hence, a possible scenario would be the coexistence of the dimerized and the end–bridge structure (as proposed in [128, 130]), see Fig. 3.15. Alternative models de-

doi:10.1016/j.susc.2004.05.007

scribing a random orientation of the adsorbed molecules are not supported by theoretical investigations. An adsorption species oriented at $45°$ with respect to the Si dimers has been considered by Sorescu and Jordan [129] and has been found to be very unstable.

Turning to the continuum resonances, we observe a very broad feature at 299 eV. It is visible in both $s_\perp$ and $s_{||}$ polarization and weak in $\overrightarrow{n}$. The energy position of the peak at 299 eV is in quite good coincidence with the σ^*_{C-C} state in [98] where dimerized adsorption is stated. As this state is oriented along the C–C bond, its observation allows deductions about the orientation of these bonds: the peaks at 299 eV are most intense for $\overrightarrow{s}$ polarization, thus the C–C bond is oriented parallel to the surface further supporting our conclusions based on the behavior of the π^* resonance. The position of this resonance also allows some conclusions about the C–C bond length and therefore about the hybridization. Comparing the NEXAFS spectra for gas phase C_2H_2 (sp–hybridized, C≡C triple bond), C_2H_4 (sp^2–hybridized, C=C double bond), and C_2H_6 (sp^3–hybridized, C–C single bond), one notices the blue shift of the σ^*–resonance with increasing hybridization [67]. In the case of C_2H_4, the σ^*–resonance is shifted from about 300 eV for the free molecule to 291 eV for the adsorbed molecule [1]. This could be explained by the rehybridization of the C=C double bond of the free C_2H_4 molecule to a single bond of the adsorbate comparable to that of free C_2H_6, but still being somewhat shorter. In the case of C_2H_2, the σ^*–resonance is thus expected at about 300 eV for a ethylene–type sp^2 adsorption (i.e. dimerized, end–bridge) and at about 291 eV for a ethane–type sp^3 adsorption (i.e. r–bridge, p–bridge). Since in both spectra a σ_{C-C} resonance at 299 eV is observed, the acetylene hybridization is stated to be sp^2 for both adsorption species. The remaining π^*_{C-C} resonance confirms the existence of a C=C double bond. The sp^3 hybridization would lead to a tetrahedrical state which would also be observed in the $\overrightarrow{n}$ spectra. Thus it is concluded that the adsorption species aligned parallel to the Si dimers is a dimerized species. This structure has been calculated to be the most stable adsorption structure together with the end–bridge configuration [129, 131, 135]. The sp^2 hybridization of the C–C bond has also been observed using HREELS which identified the hybridization based on the C=C stretching frequency [78]. The latter being slightly lower for acetylene in gasphase or on metal surfaces, it indicates a weakened but still remaining C=C bond after adsorption.

Also the rotated (end–bridge) adsorption species contains a C=C double bond which should show in the $s_{||}$–excited spectrum as a pronounced π^*_{C-C} peak at 283.8 eV as is indeed observed. Investigating the different adsorption geometries, it is evident that the only structure aligned perpendicular to the Si dimers and leaving the observed π_{C-C} bond undisturbed is the end–bridge configura-

doi:10.1016/j.susc.2004.05.007

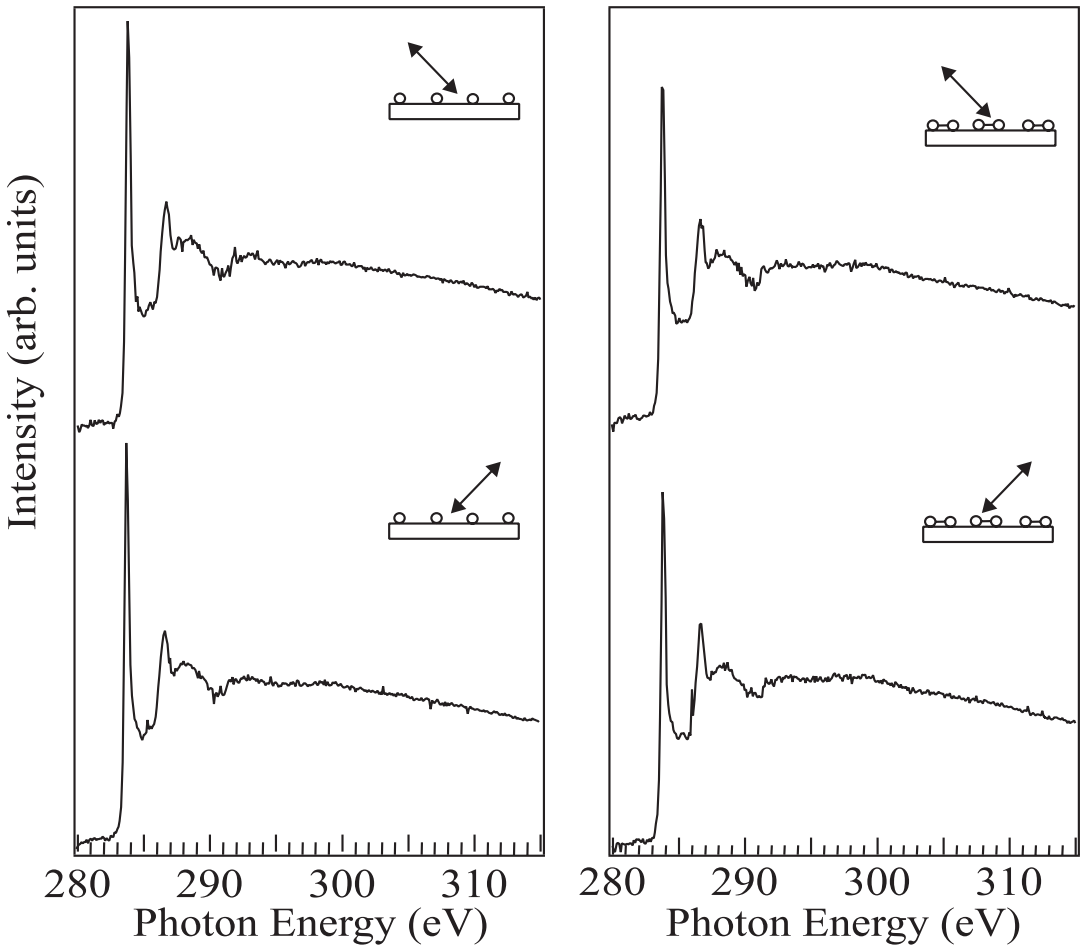

Figure 3.18: NEXAFS spectra of C_2H_2 on Si(001)–(2×1) for the incident beam in [0$\bar{1}$1] (left) and [011] (right) and polarization at $+45°$ and $-45°$ towards the surface.

tion. The C–C bond length for that geometry has been calculated to be about the same value as for the dimerized case (1.37 Å and 1.36 Å, respectively) [135]. Thus, the C–C bonds of both adsorption species contribute to the σ^* resonance at 299 eV; this is supported by the fact that the resonance is not visible in the $\vec{n}$–excited spectra, but observed for both $s_{||}$ and $s_\perp$ polarized excitation.

We can now estimate the relative coverage of the dimerized and the end–bridge adsorption species based on the relative peak intensity of the 283.8 eV π^*_{C-C} resonance in the $s_\perp$– and $s_{||}$–excited spectra. Since the corresponding orbital is oriented perpendicular to the acetylene molecular axis, the $s_\perp$ spectrum shows the contribution from the dimerized adsorbed molecules. The end–bridge adsorbed molecules then contribute to the $s_{||}$ spectrum. The π^*_{C-C} resonance is about 20% higher for $s_\perp$ polarization than for $s_{||}$ polarization. Assuming for both species the same transition strength, the ratio of dimerized to end–bridge species

doi:10.1016/j.susc.2004.05.007

is roughly 5:4 for measurement at room temperature. Changing the temperature will presumably shift the saturation coverage and equilibrium population of the two adsorption species.

Until now, the NEXAFS spectra are discussed assuming that all features arise from acetylene molecules adsorbed on the terraces. In principle, there might be some contribution from molecules situated at the step edges. In order to investigate this contribution we have taken spectra with a polarization angle of $\pm 45°$ towards the surface shown in Fig. 3.18. These spectra should show a clear difference if step species are important. However, this is not the case. Here we conclude that the spectral contribution from molecules adsorbed on the step edges has to be small.

Conclusion

In conclusion, acetylene adsorbs at room temperature and saturation coverage in more than one bonding configuration on the Si(001)–(2×1) surface where the carbon atoms are sp^2 hybridized and the C–C bond lies in the surface plane. This we interpret as due to a mixture of dimerized and end–bridge species in a ratio of 5:4, where the C–C axis is oriented in the surface plane parallel and perpendicular to the Si–dimers, respectively. Thus, the investigation of acetylene adsorption on single domain Si surfaces fully resolving the polarization dependence allows unambiguous determination of the adsorption geometries and gives clear evidence for the simultaneous existence of more than one adsorbate species.[9]

[9]**Acknowledgements:** We gratefully acknowledge help from Lisbeth Kjeldgaard and the MAX-Lab staff. This work was supported by the DFG grant Fo 343/1-1 and the Grant–in–Aid for Japan Society for the promotion of Science Fellows.

doi:10.1016/j.susc.2004.05.007

Chapter 4

Weakly interacting molecules: Vibronic scattering dynamics

One central question addressed in this work is: To what extend do the dynamic characteristics of RIXS influence the scattering profile? The applicability of RIXS for the electronic structure determination of any system depends on the answer to that question. RIXS data can only be interpreted reliably when knowing the mechanism of formation of the spectral profile. A deduction of electronic or geometric structure information or the nature of the chemical bonding from RIXS needs this basis. From a theoretical viewpoint, I have sketched the scattering in Chap. 2.

In the following, I will present a model investigation of the dynamic effects in the scattering process. I will demonstrate how the intermediate state dynamics influence the role of electronic and vibrational contributions to the scattering profile. Not every system is equally suited to address the question of dynamic influences on the RIXS profile. RIXS at the semiconductor surface adsorbate systems originally being the focus of this thesis can today not be accessed by a systematic theoretical investigation of the dynamic effects. In this chapter, I therefore present RIXS studies of condensed hydrocarbon molecules weakly interacting with their surroundings. It will be shown that the condensates can act as model systems for the free molecules when investigating the resonant scattering at the LUMO. Ethylene and benzene were chosen since they are also investigated when interacting with the silicon surface in this thesis. It has here been possible to apply a treatment, where vibrational and electronic contributions to the spectral profile are fully considered. In Paper IV, the necessity to account for vibrational band formation in the case of resonant scattering at ethylene is demonstrated and purely vibrational contributions in soft X–ray scattering pre-

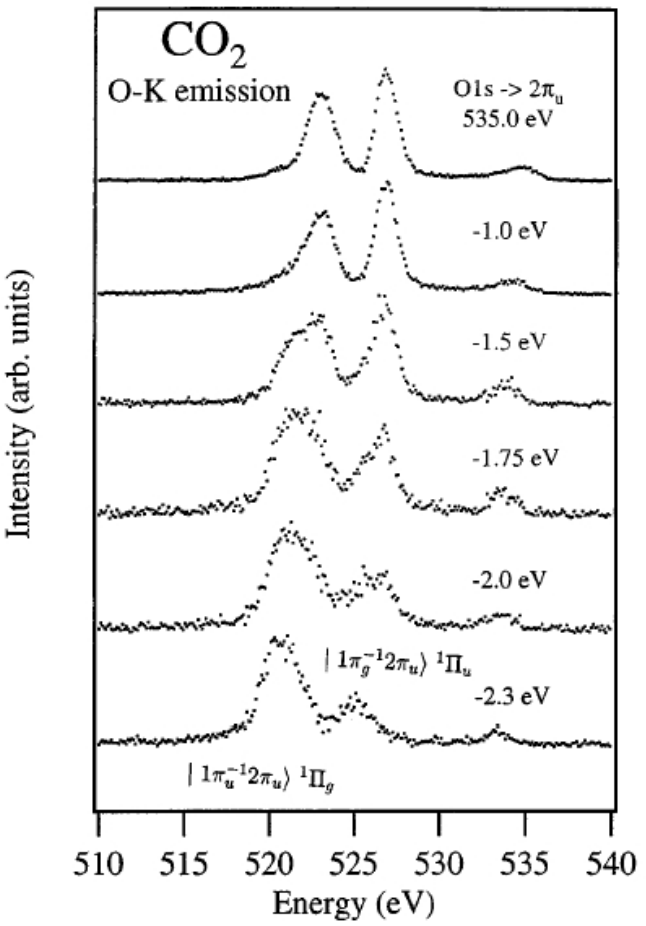

Figure 4.1: Oxygen K–edge resonant X–ray emission spectra of CO_2 with different detuning energies below the $2\pi_u$ resonance, from [136]. First observation of "symmetry breaking". According to the parity selection rule the $^1\Pi_u$ final state is electronically forbidden, but can be reached upon resonant excitation.

sented. In Paper V, the systematic application of this approach to ethylene and benzene is developed in detail.

In general, the total wave function can change in the scattering process. Staying in the Born–Oppenheimer approximation, the total wave function can be understood as the product of the nuclear and the electronic wave function. The RIXS profile can thus be expected to have vibrational and electronic — as well as combined, i.e. vibronic — contributions.

Vibronic effects in RIXS have been well known for a long time. Already in the early work on narrow bandwidth resonant excited soft X–ray emission, vibronic coupling in bulk carbon systems has been addressed [137][1]. Experimentally, in these investigations vibronic loss processes occur as additional loss contributions in the spectral profile resulting in an asymmetric line shape. With the routine application of RIXS to molecules, more studies have concentrated on the vibronic effects in RIXS. The breaking of the symmetry of electronic states in a

[1] Remarkably, vibronic processes in the same system have recently again been focus of investigations [138].

molecule in the resonant scattering process has been investigated [136, 139–141]. A configurational change of the molecule in the scattering intermediate state can open scattering channels to additional electronic final states (Fig. 4.1). This depends on the scattering duration and is thus a dynamic effect influencing the electronic selection rules (compare Chap. 2.4). The influence of changes in the nuclear wave function is here indirectly probed in the electronic scattering profile. The RIXS profile is directly influenced by lifetime–vibrational interference [46, 142].

Although established in principle, the importance of vibronic effects in RIXS has been neglected in a number of recent investigations of liquids [12–16]. This neglection can be understood by the fact that in all the work so far, vibronic effects appear as affecting the RIXS spectral profile only to a minor extend. The spectra, thus, seem to be dominated by the electronic states. The work presented in the following challenges the appropriateness of this approach.

4.1 Nonadiabatic Effects in Resonant Inelastic X-ray Scattering[2]

Abstract

We have studied the spectral features of resonant inelastic x-ray scattering of condensed ethylene with vibrational selectivity both experimentally and theoretically. Purely vibrational spectral loss features and coupled electronic and vibrational losses are observed. The one-step theory for resonant soft x-ray scattering is applied, taking multiple vibrational modes and vibronic coupling into account. Our investigation of ethylene underlines that the assignment of spectral features observed in resonant inelastic x-ray scattering of polyatomic systems requires an explicit description of the coupled electronic and vibrational loss features.

Resonant inelastic x-ray scattering (RIXS), also known as x-ray raman scattering (RXS), has evolved into a widely used spectroscopic tool to study electronic structure of matter [18, 39, 61]. This development has been promoted by the rapid evolution of high brilliance soft x-ray sources. The Raman selection rule in this photon-in/photon-out spectroscopy gives a high degree of polarization anisotropy and reveals symmetry–information of the systems under investigation. This is also true for the optical dipole transitions underlying the separate x-ray absorption and emission steps. Soft x-ray spectroscopies are element and chemical state selective. In the case of RIXS, these features are strongly enhanced due to the selective excitation of a particular intermediate core-excited state of defined symmetry.

In general, RIXS probes electronic and nuclear (vibrational) inelastic loss processes. In particular, the scattering process is governed by the total symmetry of the coupled nuclear and electronic wave functions. Therefore strong deviations from a case assuming purely electronic symmetry selection rules have been observed [136, 141]. Some studies have addressed the vibrational contributions to the spectral profile, e.g. vibrational broadening [137, 138] and life-time vibrational interference effects [46].

The investigation of condensates and liquids has recently drawn great attention, most prominently the detailed picture of hydrogen bonding in aqueous systems [12, 15]. The depth information necessary for such studies makes RIXS ideally suited. In these systems both the geometric configuration and the elec-

[2] *Peer reviewed paper. This section has been published as Paper IV:* Hennies, Polyutov, Minkov, Pietzsch, Nagasono, Gel'mukhanov, Triguero, Piancastelli, Wurth, Agren, and Föhlisch [4], *Physical Review Letters* **95**, 163002 (2005).

doi:10.1103/PhysRevLett.95.163002

tronic structure are under debate. The interpretation of the RIXS presented there bases upon the calculation of the electronic spectral states in the adiabatic limit for different molecular configurations which result from molecular dynamics simulations. RIXS spectra however contain coupled electronic and vibrational loss features. In this work, we aim to disentangle the electronic and vibrational contributions to RIXS spectra and investigate the interplay of electronic structure and nuclear dynamics. We have studied RIXS spectral features of condensed ethylene, with vibrational selectivity, in an exemplary way both experimentally and theoretically. We have chosen ethylene as a test-system due to its unambiguously characterized electronic and geometric structure [143]. We find in our joint experimental and theoretical investigation that explicit consideration of both the electronic and vibrational loss features is needed to assign spectral states. This is of general relevance for the interpretation of RIXS of any polyatomic system.

The experiments were carried out at MAX-lab, Sweden, on beamline I511-1. Bulk layers of condensed ethylene have been prepared by dosing 100 L onto a p-doped silicon substrate cooled to ≤ 25 K. The grazing incidence x-ray spectrometer [61] was operated with 0.4 eV (full-width-half-maximum FWHM, as all comparable values in this work) bandwidth in the direction perpendicular to the incident beam axis in magic angle geometry to the electric field vector of the incident radiation. The x-ray absorption spectra (XAS) have been measured with a Scienta SES-200 analyzer in constant final state mode. The excitation bandwidth was set to 35 meV for the x-ray absorption measurement and to 100 meV for RIXS.

The ethylene (C_2H_4) molecule has D_{2h} symmetry and the electronic ground state $|0\rangle$ configuration is $(1a_g)^2(1b_{3u})^2(2a_g)^2(2b_{3u})^2(1b_{2u})^2(3a_g)^2(1b_{1g})^2(1b_{1u})^2$. Ethylene has two symmetry adapted, near–degenerate core orbitals ($\psi_{\rm core}$: $1a_g, 1b_{3u}$), which result from the linear combination of the atomically localized C 1s orbitals. $1b_{1u}$ is the highest occupied molecular orbital (HOMO) and the $1b_{2g}$ is the lowest unoccupied molecular orbital (LUMO), also called the π^*. The HOMO–LUMO separation is ≈ 7 eV.

In our simulations of the resonant x-ray scattering amplitude F_{ν_f}, we have included the treatment of multiple vibrational modes and vibronic coupling based on the methods described in Refs. [39, 54]. The scattering amplitude F_{ν_f} for ethylene is described by the equation (in a.u.):

$$F_{\nu_f} = \frac{1}{2}\sum_{\nu_i} \frac{\Lambda^{(N-N_A)}(\nu_f,\nu_i)[\Lambda_2^{(N_A)}(\nu_f,\nu_i) + \mathcal{P}_f\Lambda_1^{(N_A)}(\nu_f,\nu_i)]}{\omega - \omega_{i\nu_i,00} + \imath\Gamma/2} \tag{4.1}$$

$\hbar\Gamma = 0.1$ eV is the lifetime broadening of the core excited state, $\mathcal{P}_f = \pm 1$ the parity of the final electronic state (+ gerade; – ungerade), $\nu_i = (\nu_{i,1}, \nu_{i,2}, \cdots)$

doi:10.1103/PhysRevLett.95.163002

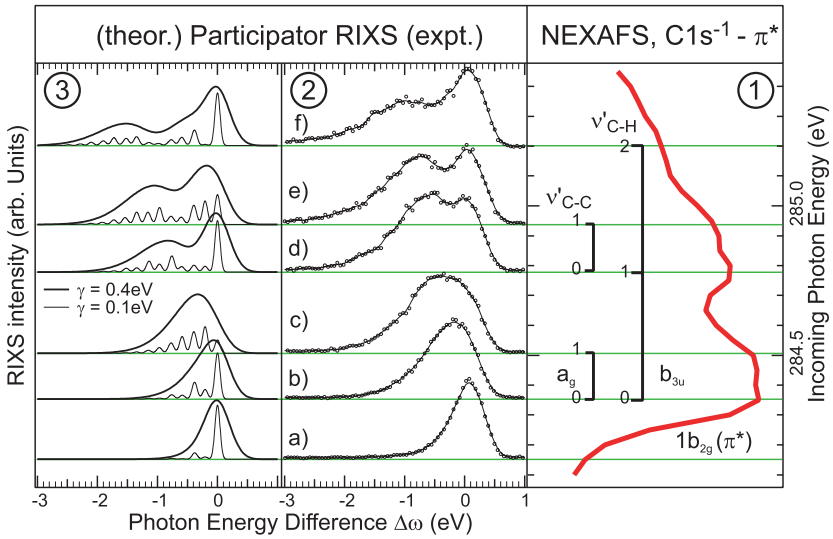

Figure 4.2: Participator RIXS of ethylene at the C K-edge (final state is electronic ground state). Panel (1): C 1s $\rightarrow \pi^*$ absorption spectrum; (2): RIXS spectra (exp.) with excitation at the energies indicated; (3): Simulated RIXS at the according energies. RIXS spectra are plotted vs. the energy difference of outgoing and incoming photon $\Delta\omega = \omega_1 - \omega$.

is the vector of the vibrational quantum numbers of all modes of the i^{th} electronic state and $\omega_{i\nu_i,j\nu_j}$ is the electron-vibrational transition energy. We have separated the product of the Franck-Condon (FC) amplitudes $\Lambda_n^{(N_A)}(\nu_f,\nu_i) = \prod_{q\subseteq A}\langle\nu_{f,q}|\nu_{i,q};n\rangle\langle\nu_{i,q};n|0_{0,q}\rangle$ of N_A asymmetric vibrational modes, that lead to the localization of the core hole in the n^{th} carbon atom from the product of the FC amplitudes for the corresponding symmetric vibrational modes $\Lambda^{(N-N_A)}(\nu_f,\nu_i) = \prod_{q\not\subseteq A}\langle\nu_{f,q}|\nu_{i,q}\rangle\langle\nu_{i,q}|0_{0,q}\rangle$. The scattering cross section for monochromatic excitation is then given by the equation:

$$\sigma_0(\omega,\omega_1) = \sum_{f,\nu_f}\zeta_{f0}|F_{\nu_f}|^2\delta(\omega_1-\omega+\omega_{f\nu_f,00}) \tag{4.2}$$

ω and ω_1 are the frequencies of the incident and scattered photons. The anisotropy factor $\zeta_{f0} = (d_{fi}^2 d_{i0}^2/9)\left[1+\frac{1}{10}(3\cos^2\varphi_{f0}-1)(1-3\cos^2\chi)\right]$ depends on the angle $\chi = 35.3°$ between the polarization vector of incident photon and the momentum of the scattered photon (set to the experimental value). The anisotropy factor also depends on the the angle φ_{f0} between the transition dipole moments of core excitation $\mathbf{d}_{i0}$ and emission $\mathbf{d}_{fi}$.

Computations of the valence and virtual transition moments were performed in the dipole approximation and have been done within the framework of the

doi:10.1103/PhysRevLett.95.163002

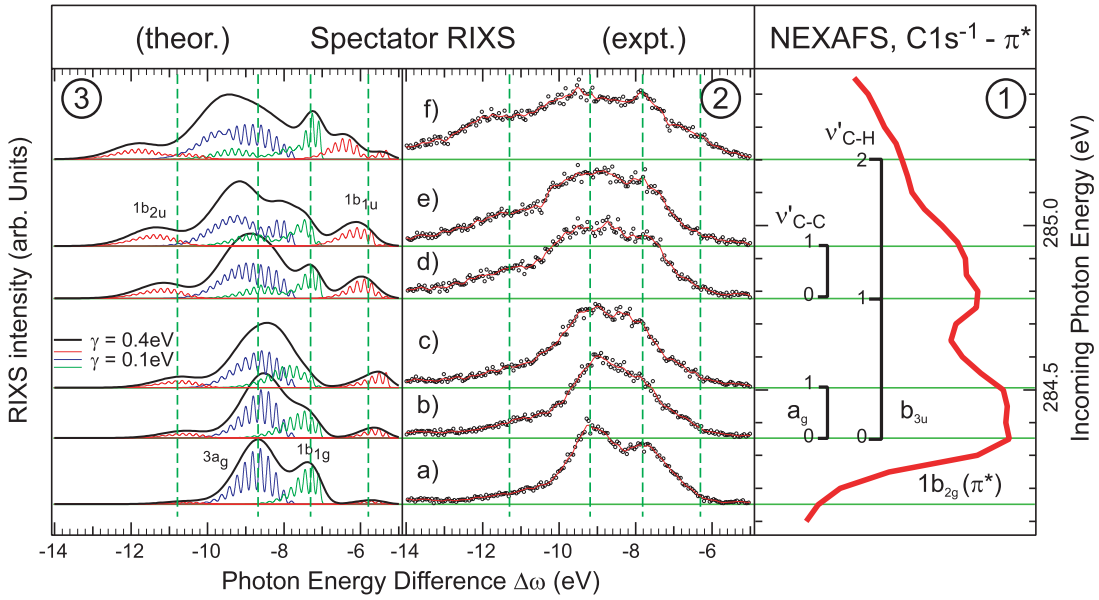

Figure 4.3: Spectator RIXS of ethylene at the C K-edge (final state is valence electronic excited). Panel (1): C 1s $\rightarrow \pi^*$ absorption spectrum; (2): RIXS spectra (exp.) with excitation at the energies indicated; (3): Simulated RIXS at the according energies. RIXS spectra are plotted vs. the energy difference of outgoing and incoming photon $\Delta\omega = \omega_1 - \omega$.

density functional theory (DFT) using the StoBe code [144]. The transition energies were taken directly from the Kohn-Sham orbital energies. Numerical analysis of the FC amplitudes reveals that only four in–plane vibrational modes, three a_g (C-C stretch, H-C-H scissor, and C-H stretch) and one b_{3u} (C-H asym. stretch), give major contributions to the x-ray absorption and RIXS spectra, therefore only these four modes were taken into account in the simulations. The FC amplitudes have been computed in the harmonic approximation without consideration of changes in the vibrational frequencies due to the electronic excitations.

In Fig. 4.2 panel 1 we show the vibrationally resolved x-ray absorption spectrum of ethylene at the π^* resonance, corresponding to the excitation of a $|\psi_{\rm core}^{-1} 1b_{2g}\rangle$ electronic state. We can directly assign this vibrational fine structure in agreement with literature [68, 74] to the a_g C-C stretch vibration and to the b_{3u} C-H asymmetric stretch vibrational mode. We measured RIXS spectra with the excitation energy tuned onto the vibrational modes of the first core excited electronic state $|\psi_{\rm core}^{-1} 1b_{2g}\rangle$.

The RIXS spectrum consists of two qualitatively different contributions, the participator or "elastic" band ($|0\rangle \rightarrow |\psi_{\rm core}^{-1} 1b_{2g}\rangle \rightarrow |0\rangle$) and the spectator or "inelastic" band ($|0\rangle \rightarrow |\psi_{\rm core}^{-1} 1b_{2g}\rangle \rightarrow |\psi_f^{-1} 1b_{2g}\rangle$) with $\psi_f = 1b_{1u}, 1b_{1g}, 3a_g, 1b_{2u}$, denot-

doi:10.1103/PhysRevLett.95.163002

ing valence electronic states. The participator scattering channel leads to the electronic ground state with energy loss features due to vibrational excitations (purely vibrational Raman), while the spectator channel is the scattering to electronically excited final states which is accompanied also by vibrational excitations (vibronic Raman). For clarity of presentation we show the participator RIXS in Fig. 4.2 and the spectator RIXS in Fig. 4.3 separately.

Both experiment and theory display a strong dependence of the participator band (Fig. 4.2 panel 2 and 3) on excitation energies. For scattering with an incident energy below the resonance energy (a), we see mainly a single resonance centered at 0 eV energy loss. This is what is usually referred to as the elastic peak which is the only feature in this channel in the case of single atoms. When exciting on top of the resonance and into higher levels of the vibrational progression (b–f), the participator profile becomes increasingly asymmetric toward lower energies and a band of inelastic loss features becomes observable. This band moves its center of gravity to lower energies with increasing excitation energy. For the limit of high positive detuning from the electronic resonance we observe decreasing intensity of the vibrational loss features. The cross section for scattering into vibrational excited final states is thus significantly enhanced upon resonant excitation.

The simulations of the participator band are depicted in panel 3 of Fig. 4.2. We obtain good agreement with the experiment when the simulated spectra are convoluted with a gaussian of γ=0.4 eV which mimics the total instrumental broadening and excitation bandwidth. Within this envelope we also show the vibrational progression with only γ=100 meV broadening. The spacing of the vibrational states corresponds to the electronic ground state vibrational modes. The intensities of the vibrational loss features is governed by the Kramers-Heisenberg scattering amplitude (eqn. 4.1). The lifetime vibrational interference influences strongly the spectral profile [38]. In particular, we find both in experiment and theory that the detuning $\Omega = \omega - \omega_{i0,00}$ of the incident photon energy from the electronic π^* resonance leads to only a single spectral line. The origin of this collapse of the vibrational structure is the shortening of the scattering duration [145] $\tau_{\text{eff}} = 1/\sqrt{(\Gamma/2)^2 + \Omega^2}$ with increase of $|\Omega|$. A short scattering duration will not allow the nuclear wave packet to dynamically evolve [39, 146], thus effectively suppressing vibrational motion during the scattering and letting vibrational contributions to the spectral profile vanish.

The physics of the formation of the spectator scattering channel is rather different from the participator scattering channel. The spectator channel corresponds to scattering into four different electronic final states: $|1b_{1u}^{-1}1b_{2g}\rangle$, $|1b_{1g}^{-1}1b_{2g}\rangle$, $|3a_g^{-1}1b_{2g}\rangle$, and $|1b_{2u}^{-1}1b_{2g}\rangle$. The scattering to the ungerade final states ($|1b_{1u}^{-1}1b_{2g}\rangle$, $|1b_{2u}^{-1}1b_{2g}\rangle$) is forbidden according to the parity selection rules. However, the ex-

doi:10.1103/PhysRevLett.95.163002

periment as well as the theory (Fig. 4.3) show the breakdown [147] of these selection rules when exciting resonantly into the π^* and its vibrational progression (Fig. 4.3 b–f). The origin of this effect is the mixing of near–degenerate gerade and ungerade core excited states ($|1b_{3u}^{-1}1b_{2g}\rangle$, $|1a_g^{-1}1b_{2g}\rangle$) by the activation of the ungerade b_{3u} vibration, effectively localizing the core excited state. We clearly can see the restoration of the selection rules for large detuning (Fig. 4.3 a), i.e. the quenching of the symmetry forbidden transitions. This "purification" of the spectator spectrum happens due to the shortening of the scattering duration, leaving no time for the b_{3u} vibration to mix the core excited states with different parities [136]. If the detuning is sufficiently large, the spectator RIXS (Fig. 4.3 panel 2, 3 (a)) is restricted to the electronic final states $|3a_g^{-1}1b_{2g}\rangle$ and $|1b_{1g}^{-1}1b_{2g}\rangle$.

Taking vibronic coupling into consideration, our theoretical approach can fully describe all spectral features in the RIXS spectra (a - f) in panel 2 and 3 of Fig. 4.3. In particular, the nominal adiabatic transition, defined by the purely electronic transitions can become very small in comparison to the vibrationally excited final states. Taking spectra (d–f) in Fig. 4.3 as an example, we can illustrate how crucial it is to take the full vibronic spectral profile into consideration in the interpretation of experimental RIXS. For the electronically excited final states, we observe vibrational progressions extending over 2 eV$\sim$ 4 eV, with a bimodal vibrational envelope. Moreover, the spectral shape of each excited final state changes with photon energy (d–f) significantly and differently for each of them.

In summary, we have studied RIXS spectral features of condensed ethylene with vibrational selectivity, both experimentally and theoretically. The theoretical model of the inelastic scattering process takes multiple vibrational modes and vibronic coupling into account. We have obtained excellent agreement between experiment and simulations for the purely vibrational spectral loss features in the RIXS participator channel, reaching the electronic ground state as a final state. We have also observed the coupled electronic and vibrational loss features of the spectator RIXS channel, reaching electron–hole final states combined with vibrational excitation. We have disentangled these contributions and investigated the interplay of electronic structure and nuclear dynamics in an exemplary way. We find the excited electronic final states to split significantly into broad vibrational bands with a complicated, partly bimodal, envelope structure. This goes beyond the spectral distribution expected from an adiabatic model, where vibronic effects are only implicitly treated in a broadening of states. In conclusion, we find that the explicit consideration of coupled electronic and vi-

doi:10.1103/PhysRevLett.95.163002

brational states in the one-step theory of resonant inelastic x-ray scattering is required to fully assign RIXS spectral states of ethylene.[3]

[3]**Acknowledgements:** This work was supported by the Access to Research Infrastructure (ARI) Program of the EU, the Swedish National Research council (VR) and the Deutsche Forschungsgemeinschaft (Grant DFG Fo343/1-1). M.N. acknowledges support from MEXT Japan, Grant in aid for Young Scientists (B) 2003. Valuable support from Lisbeth Kjeldgaard and MAX-lab staff is gratefully acknowledged.

doi:10.1103/PhysRevLett.95.163002

4.2 Dynamic Interpretation of Resonant Inelastic X-ray Scattering: Ethylene and Benzene[4]

Resonant inelastic X–ray scattering (RIXS) or X–ray raman scattering (RXS) is used to probe stationary and dynamic properties of matter [18, 39, 41, 61]. RIXS as a photon–in–photon–out method provides a large penetration depth. It has the advantage of being applicable to a wide range of systems, including semiconductors and insulators, and in various environments, e.g. systems in external magnetic fields. RIXS probes electronic and nuclear (vibrational) inelastic loss processes. Most work so far has focused on the investigation of the electronic structure.

In the present paper, we systematically develop a complete interpretation of RIXS on condensed ethylene and benzene based on the consideration of electronic structure, nuclear dynamics and vibronic coupling. We will show how RIXS can be utilized to probe nuclear dynamics in terms of an atom specific, chemical sensitive Raman spectroscopy. It will further be discussed under which conditions the consideration of nuclear dynamics is indispensable and when it can be omitted.

The absorption and emission of X–ray photons are governed by the dipole selection rules. Spectroscopy based on these processes therefore provides symmetry, orientation, and polarization selectivity. Soft X–ray spectroscopies are element and chemical state selective, since they involve transitions from core orbitals with atomic properties. In the RIXS process, a particular intermediate core–excited state of defined symmetry is prepared by selective excitation, thus enhancing the former properties. The selection rules of excitation and decay converge in this coherent one–step scattering process to a Raman selection rule, giving a high degree of polarization anisotropy and providing symmetry–information of the systems under investigation. The scattering process is ruled

[4] *Paper in manuscript. This section is intended for publication as Paper V:* Hennies, Polyutov, Minkov, Nagasono, Pietzsch, Gel'mukhanov, Triguero, Piancastelli, Wurth, Agren, and Föhlisch [5].

This paper is based on an ongoing collaboration with the theoretical chemistry group at the KTH Stockholm. The manuscript as included in my thesis contains the description and discussion of the experimental work and the theory and simulations of the ethylene molecule, and thus reflects the biggest part of my contribution to this project. In the final version of this paper, also calculations for the benzene molecule will be included. They are not finished at the time this thesis is handed in. The problem of the benzene calculations is the presence of degenerate core orbitals of the same symmetry. Ethylene has two core–holes of different symmetry. No interference between electronic core–excited states can occur in the unchanged configuration. In benzene — already without core–hole localization — electronic interference can occur. This demands for an extension of the here presented approach describing the core hole localization.

by the symmetry of the system's total wave function including all nuclear and electronic contributions.

RIXS has been applied to a wide range of systems, including crystalline solids, surface adsorbates and free molecules [41, 43, 44, 61]. Spectra of crystalline solids have been interpreted based on the description of electronic states in band structure calculations [41]. Utilizing the atom specificity, it has been possible to examine the electronic density–of–states (DOS) projected on the contributions of different atoms in a compound system. This has been extremely useful in the case of surface adsorbates [18, 31, 45, 148], where the electronic structure of the adsorbed molecule can be investigated suppressing the vast majority of substrate contributions. Combined with the symmetry selectivity, this has allowed to study the formation of the surface chemical bond in great detail. For the case of adsorbates on metals it has been shown that the spectral profile can fully be described in the so called "ground state interpretation" [45]. Here, the energy distribution of the scattering spectra is directly derived from the difference of ground state orbital energies, e.g. obtained from Density Functional Theory (DFT) calculations. The selectivity of the excitation is explicitly taken into account in this model, modulating the intensity distribution of the spectral profile [31]. In this pure electronic interpretation, the selection rules for the scattering process are applied only to the electronic part of the systems total wave function.

The influence of nuclear motion on RIXS spectra has been discussed as phonon side bands in RIXS of diamond and graphite [137, 138]. The vibrational loss processes are identified in an asymmetric tail of the recombination emission. For molecules, the shaping of the RIXS bands due to lifetime–vibrational interference has been demonstrated [46, 142]. In this case, the core hole lifetime broadening is of the same order of magnitude as the vibrational spacing in the core excited intermediate state which gives rise to channel interference in the scattering process. In these works, the vibrational effects are discussed as additional contributions to the electronic states in RIXS. In a general treatment of RIXS, always the changes in the combined nuclear and electronic contributions to the systems total wave function have to be considered. In the RIXS profile of molecules, therefore, strong deviations from a model accounting only for electronic symmetry selection rules have been observed and discussed as bond length dependent core hole localization [141] and breaking of electronic symmetry [136, 139]. Nevertheless, here too, only the influence of these effects on the electronic spectral structure is discussed.

In two recent publications [13, 15], the electronic and geometric structure of liquids has been investigated with RIXS. In both studies, the spectral profile has been interpreted on the basis of calculations of the ground state electronic struc-

ture in the adiabatic limit disregarding vibrational effects [16]. In particular, the low count rate achieved for X–ray emission on light elements in todays setups has for a long time not allowed to interpret the scattering spectra of a system completely in all aspects of vibrational band formation, interference effects, and vibronic coupling. We have recently demonstrated that in the case of molecules, vibrational influences on the spectral profile can not only be considered as additional effects in the electronic features visible in the spectra, but have to be understood as constituting the spectral profile [4].

Our paper is organized as follows: We will develope the theoretical framework in Sec. 4.2.1. The technical aspects of experiment and computation are addressed in Sec. 4.2.2 and 4.2.3, respectively. In Sec. 4.2.4, we present and analyze the experimental findings and the results of the computations before jointly discussing and interpreting the electronic and vibrational structure for both molecules in Sec. 4.2.5. In Sec. 4.2.6, we finally summarize.

4.2.1 Methodical Framework

Kramers–Heisenberg formalism for RIXS

We investigate the resonant inelastic scattering of a X–ray photon at a molecule initially in the electronic and vibrational ground state $|0,0\rangle$. The absorption of the incident photon with energy ω promotes the scatterer into an intermediate core excited state $|i\rangle$ with vibrational excitation $|\nu_i\rangle$, coherently followed by the decay of the excited state into the electronic and vibrational final state $|f,\nu_f\rangle$ under emission of a second photon ω_1. The "scattering of radiation by atoms" [51] is generally treated in the Kramers–Heisenberg formalism. The spectral distribution of the emitted photon ω_1 is accordingly given by the RIXS cross section [39] containing the spectral function Φ, the scattering amplitude F_{ν_f} and the electronic factor ζ_{f0}:

$$\sigma(\omega,\omega_1) = \sum_{f,\nu_f} \zeta_{f0} |F_{\nu_f}|^2 \Phi(\omega_1 - \omega + \omega_{f\nu_f,00} + \omega^e_{f0}, \gamma) \tag{4.3}$$

RIXS probes inelastic loss processes. The spectral function $\Phi(\omega - \omega_0, \gamma)$ centered at ω_0 with line width γ (full–width–half–maximum FWHM, as all comparable values in this work) describes the energy distribution of the spectral features. For each electronic and vibrational final state $|f,\nu_f\rangle$, the spectral line occurs at an energy difference $\Delta\omega = \omega_1 - \omega$ equaling the sum of the electronic and vibrational excitations $\omega^e_{f0} + \omega_{f\nu_f,00} = -\Delta\omega$ present in the final state. Here, ω^e_{f0} denotes the difference between the minima of the potentials of electronic final and ground state, and $\omega_{j\nu_j}$ the vibrational energy of the ν_j^{th} vibrational level in the j^{th} electronic state.

The absorption of the incoming and the emission of the outgoing photon, respectively, happen very fast compared to the speed of the nuclear motion. We consider the changes of the electronic wave function therefore as sudden and without any change of the nuclear wave function [29]. The total wave function of the system is thus written in the Born–Oppenheimer approximation as the simple product of both. The vibrational transitions are accordingly treated following the Franck–Condon (FC) principle. We want to point out that excitation and decay transitions each for themselves are considered as sudden. Nevertheless, the whole scattering process can effectively be associated with a total scattering duration time allowing vibrational motion to take place (see Discussion Sec. 4.2.5). The probability for scattering into a specific vibrational final state ν_f is then given by the FC amplitude F_{ν_f}:

$$F_{\nu_f} \approx \sum_{\nu_i} \frac{\langle \nu_f | \nu_i \rangle \langle \nu_i | 0_0 \rangle}{\omega - \omega_0^i - \omega_{i\nu_i,00} + i\Gamma/2} \tag{4.4}$$

F_{ν_f} is here stated for the limit of small bandwidth excitation and for the case of a single vibrational mode. Γ is the lifetime broadening of the core excited intermediate state. If the lifetime broadening Γ is comparable to the energy spacing $\omega_{i\nu_i',i\nu_i}$ of the vibrational intermediate states $i\nu_i$, multiple scattering channels open and give rise to channel interference. We will show in the following that interference effects predominantly determine the spectral appearance of RIXS spectra.

The FC amplitude F_{ν_f} [Eq. (4.4)] only accounts for the vibrational transitions, the electronic transitions are described by the anisotropy factor $\zeta_{f0} = \overline{(\mathbf{d}_{fi} \cdot \mathbf{e}_1)^2 (\mathbf{d}_{i0} \cdot \mathbf{e})^2}$. In our case ζ_{f0} is averaged over the molecular orientations. It depends on the polarization vectors of incident $\mathbf{e}$ and emitted $\mathbf{e}_1$ X–ray photons and the transition dipole moments of core excitation $\mathbf{d}_{i0}$ and decay $\mathbf{d}_{fi}$.

RIXS is governed by a Raman selection rule operating on the total wave function of the system [39, 149]. For our present discussion, we consider the investigated molecules to be "non"–interacting and have preserved their molecular symmetry. Both molecules have inversion symmetry. In particular, the parity of the total wave function can, thus, not differ in the scattering final state from the initial state. In a scattering process not changing the symmetry of the nuclear wave function, this parity conservation has to be strictly fulfilled by the electronic wave function.

Multi–mode scattering amplitude and vibronic coupling

A molecule containing more than two atoms needs consideration for multiple vibrational modes. The FC amplitude thus contains the product of the transi-

tion matrix elements $\prod_q \langle \nu_{f,q}|\nu_{i,q}\rangle\langle\nu_{i,q}|0_{0,q}\rangle$ of all vibrational modes q. If symmetry equivalent atoms are present, we get (near) degenerate core orbitals in a delocalized representation. According to the Jahn–Teller theorem [53], an asymmetric vibrational motion or "distortion" can remove this degeneracy and lower the total energy, thus effectively localizing the core wave functions. This so called "vibronic coupling" then opens additional scattering channels through the localized core holes. In the FC amplitude F_{ν_f} we now have to distinguish the scattering through symmetric vibrational modes from scattering through asymmetric vibrational modes for each core–hole separately:

$$\begin{aligned} F_{\nu_f} &\approx \frac{1}{2}\sum_{\nu_i} \frac{\Lambda^S(\Lambda_1^A + \mathcal{P}_f\Lambda_2^A)}{\omega - \omega_0^i - \omega_{i\nu_i,00} + \imath\Gamma/2} \\ \Lambda^S &= \prod_{q\nsubseteq A} \langle \nu_{f,q}|\nu_{i,q}\rangle\langle\nu_{i,q}|0_{0,q}\rangle \\ \Lambda_n^A &= \prod_{q\subseteq A} \langle \nu_{f,q}|\nu_{i,q};n\rangle\langle\nu_{i,q};n|0_{0,q}\rangle,\ n=1,2 \end{aligned} \tag{4.5}$$

Λ^S is the product of the symmetric modes and Λ_n^A the product of the scattering paths involving asymmetric modes. Here, $|\nu_{i,q};n\rangle$ is the vibrational wave function of the q^{th} asymmetric mode in the core excited state with the core hole localized on the n^{th} atom (given for two equivalent atoms). $\mathcal{P}_f$ is the parity of the final electronic state ν_f:

$$\mathcal{P}_f = \begin{cases} 1, & f = g, \\ -1, & f = u \end{cases} \tag{4.6}$$

We will discuss how additional electronic final states become possible due to vibronic coupling and demonstrate on our results that vibronic coupling is a dynamic effect and strongly depends on the detuning of incident photon energy from the absorption resonance of the scatterer (sec. 4.2.5)

4.2.2 Experimental Setup and Data Treatment

The experiments have been performed at the Swedish national laboratory MAX-lab in Lund at beamline I511–1. The beamline is equipped with an end station operated in UHV dedicated for X–ray absorption spectroscopy (XAS), photoelectron spectroscopy (XPS) and X–ray emission spectroscopy (XES) measurements on adsorbate, surface and bulk samples. The station consists of a preparation chamber operated at a base pressure of low 10^{-10} torr connected to an analysis chamber (at mid 10^{-11} torr). The analysis chamber is equipped with a Scienta

SES 200 hemispherical electron analyzer for XPS and partial electron yield XAS measurements. XES is detected with a grazing incidence soft X–ray fluorescence spectrometer [61].

For the XAS, the excitation bandwidth was set to ~ 35 meV. For the excitation of the resonant X–ray scattering spectra, the bandwidth of the incident photons was set to ~ 100 meV in the case of the ethylene measurements and and ~ 250 meV in case of benzene. The overall instrumental resolution of the X–ray emission spectra was ~ 400 meV (FWHM), as determined by measuring reflected light on a silicon substrate in the first order.

The X–ray absorption spectra have been recorded with the Scienta Analyzer in constant final state mode with a pass energy of 500 eV. In the case of the benzene measurements, we detected electrons in an energy window of 50 eV width centered around the Carbon KLL Auger. The ethylene multilayer was found to charge too much during irradiation with synchrotron light to be able to detect the Carbon Auger properly. Therefore, we have chosen to measure the yield of low energy electrons in an energy range of $(120\,\mathrm{eV} \leq E_{Kin.} \leq 168\,\mathrm{eV})$ where charge effects were found not to disturb the absorption spectra. For normalization purposes we measured the photon flux simultaneously with a reference gold mesh. The partial yield spectra shown here have been normalized by division by the flux signal. The X–ray emission spectra have not further been treated except for the correction to a calibrated energy scale. A total energy calibration of the incoming photon energy has been performed by exciting Si 2p electrons with first– and second–order light passing the monochromator.

The samples were prepared by exposing a silicon substrate at a temperature $T \leq 100$ K to gaseous ethylene and benzene at a pressure of $P = 5 \cdot 10^{-7}$ torr for 200 s (100 L). The high purity liquid benzene was further purified by repeated freeze–pump–thaw cycles, gaseous ethylene (purity 2.8) was directly used. Cleanliness of the gases was assured by checking with a mass spectrometer. Physisorbed benzene has a sticking coefficient near 1 [150], thus, our preparation conditions lead to the formation of a ~ 100 ML thick multilayer of benzene with a randomly tilted orientation of the molecules [150]. We believe that also the ethylene multilayer is randomly ordered, as the comparison between our XAS data and XAS measured on statistically distributed gas–phase ethylene [74] shows no difference (see below). To avoid beam damage, we scanned the samples during the measurements. We found no indication of beam induced processes in the condensed layers, as the XE spectra did not change during long exposure to the synchrotron light.

	ω^v (eV)	d (a.u.)	$\cos\varphi_{f0}$	ζ_{f0} (10^{-6} a.u.^{2})
$1b_{2g}$	283.92	0.0733^z	1	2.558
$1b_{1u}$	278.27	0.0765^z	-1	2.788
$1b_{1g}$	276.55	0.0586^y	0	2.254
$3a_g$	274.97	0.0822^x	0	4.435
$1b_{2u}$	273.69	0.0658^y	0	2.839

Table 4.1: Excited state parameters: vertical excitation energy (ω^v), transition dipole moments (d), $\cos\varphi_{f0}$, where φ_{f0} is the angle between the transition dipole moments of core excitation and decay, and the anisotropy factor ζ_{f0}. $1b_{2g}$ denotes the core excited state produced by the 1s $\rightarrow$ LUMO transition, while the rest of the states are valence excited and produced by a decay transition from an orbital with the respective symmetry to the core hole. Only non–zero components of the transition dipole moment are listed: d^z, d^y, d^x.

			F_{iq} (10^{-3} a.u.)				
mode	symm.	$\omega_q(eV)$	$1b_{2g}$	$1b_{1u}$	$1b_{1g}$	$3a_g$	$1b_{2u}$
3 (C-H sym. stretch)	a_g	0.379	1.498	0.624	-0.881	0.063	-0.784
4 (C-H asym. stretch)	b_{3u}	0.379	1.098	-0.023	0.031	0.039	0.007
5 (C-C stretch)	a_g	0.207	-0.498	-1.424	0.152	-2.127	-0.522
7 (H-C-H scissoring)	a_g	0.165	-0.106	-0.701	-0.750	0.420	-1.527

Table 4.2: Vibrational normal modes excited in X–ray absorption and X–ray Raman scattering. ω_q denotes the vibrational frequency, $F_{iq} = dE_i/dQ_q$ represents the gradient along the particular mode for the vertical core excitation $1b_{2g}$ state and for decay to four final states: $|1b_{1u}^{-1}1b_{2g}\rangle$, $|1b_{1g}^{-1}1b_{2g}\rangle$, $|3a_g^{-1}1b_{2g}\rangle$, $|1b_{2u}^{-1}1b_{2g}\rangle$. The b_{3u} mode vibronically couples core excited states of *gerade* and *ungerade* symmetry.

4.2.3 Computational Details

We have simulated the spectra utilizing strict *ab initio* methods based on the wave packet technique described in [39, 54, 151] and the theoretical description given here. Computations of the valence and virtual transition moments from the C 1s were performed in the dipole approximation and have been done within the framework of the density functional theory (DFT) using the StoBe code [152] and employing the PW91 density functional for both exchange and correlation contributions. The transition energies were taken directly from the

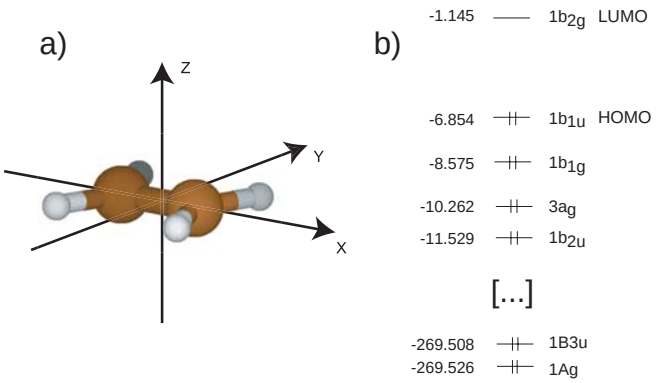

Figure 4.4: a) The ethylene molecule with the coordinate system used in our work. b) The energy levels of ethylene involved in the scattering process (in eV). The two inner shell orbitals ($2a_g$ and $2b_{3u}$) are omitted as irrelevant.

ground state Kohn–Sham orbital energies. The gradients of the core excited potential along normal modes were computed using an effective core potential for the non–excited carbon, thus effectively localizing the core hole. The core excited center was described by a rather large IGLO–III basis set.

The RIXS spectral profile was computed making use of the scattering cross section [Eq. (4.3)] and the Franck–Condon amplitude including the treatment of the vibronic coupling [Eq. (4.5)]. The spectral function $\Phi(\omega_1 - \omega, \gamma)$ was modeled by a gaussian with $\gamma = 0.1\ eV$. We considered RIXS from randomly oriented molecules and averaged the electronic factor ζ_{f0} over all molecular orientations for the experimental geometry $\chi = 35.3°$, where $\chi = \angle(\mathbf{k}_1, \mathbf{e})$ is the angle between the wave vector $\mathbf{k}_1$ of the emitted photon and the polarization vector of the incident photon $\mathbf{e}$. The core hole lifetime broadening was set to $\Gamma = 0.1$ eV, corresponding to the estimated Carbon 1s core hole lifetime for ethylene [153, 154].

The Franck–Condon amplitudes were computed in harmonic approximation making use of the gradient $F_{iq} = dE_i/Q_q$ along mode q in the equilibrium geometry of the ground state. The changes of the vibrational frequencies under electronic excitations are ignored in our simulations. We have only taken into account those four vibrational modes which were found to give significant contribution to the XAS and RIXS spectra (see Table 4.2). All modes have been computed up to $N_{\nu_j} = 11$.

The energy scale of the computed spectra was adjusted with respect to the experimental values by a constant offset to match the top of the absorption resonance.

4.2.4 Results and Analysis

Ethylene belongs to the D_{2h} symmetry group, the ground state $|0\rangle$ electronic configuration is:

$$\begin{aligned} \text{Core}: \quad & (1a_g)^2(1b_{3u})^2 = \psi_{\text{core}} \\ & [...] \\ \text{Valence}: \quad & (1b_{2u})^2(3a_g)^2(1b_{1g})^2(1b_{1u})^2 \end{aligned}$$

In Fig. 4.4, we show the molecule and its energy levels in the reference frame used in this work. Ethylene has two near degenerate core orbitals in delocalized representation, here referred to as ψ_{core}. They result from the linear combination of the C 1s atomic orbitals. The HOMO ($1b_{1u}$) has π character. The LUMO with π^* character is the $(1b_{2g})$ orbital.

The benzene molecule has D_{6h} symmetry and its electronic configuration in the ground state $|0\rangle$ is:

$$\begin{aligned} \text{Core}: \quad & (a_{1g})(e_{2g})(b_{1u})(e_{1u}) = \psi_{\text{core}} \\ & [...] \\ \text{Valence}: \quad & (2e_{1u})^4(2e_{2g})^4(3a_{1g})^2(2b_{1u})^2(1b_{2u})^2 \\ & (3e_{1u})^4(1a_{2u})^2(3e_{2g})^4(1e_{1g})^4 \end{aligned}$$

The HOMO ($1e_{1g}$) is a π orbital. The lowest unoccupied molecular orbitals $(1e_{2u})$ and $(1b_{2g})$ have π^* character.

We first measured the absorption spectra in the region of the carbon K–edge to characterize the scattering intermediate state for ethylene and benzene. In the following, we performed RIXS at both molecules with selective excitation of defined intermediate states.

Ethylene

In Fig. 4.5, we show carbon K–edge X–ray absorption spectroscopy (XAS) of condensed ethylene and theoretical simulations in the resonance region. The spectrum shows an absorption resonance at 284.37 eV with fine structure. The resonance is clearly separated from a continuum region at higher energies with two broad resonances at 287.8 eV and 288.68 eV. We will at first discuss the resonance and turn to the higher energy states later. We compared the spectra with high–resolution XAS of ethylene measured in the condensed phase [68] and in the gas–phase [74]. The first resonance represents the C 1s $\rightarrow \pi^*(1b_{2g})$

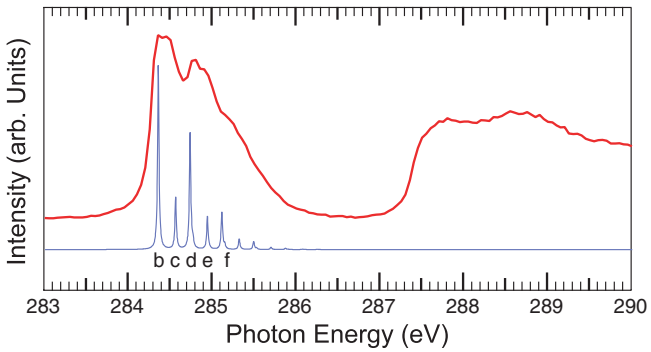

Figure 4.5: X–ray absorption spectrum of condensed ethylene. Thick line: experiment; thin line: simulation in the region of the π^*–resonance. Four modes are calculated (see Tab. 4.2): b) 0→0; c) $\nu_5(0\rightarrow1)$; d) 60% $\nu_3(0\rightarrow1)$ / 40% $\nu_4(0\rightarrow1)$; e) $\nu_5(0\rightarrow1)$ + [60% $\nu_3(0\rightarrow1)$ / 40% $\nu_4(0\rightarrow1)$]; f) $\nu_3(0\rightarrow1)$ + $\nu_4(0\rightarrow1)$

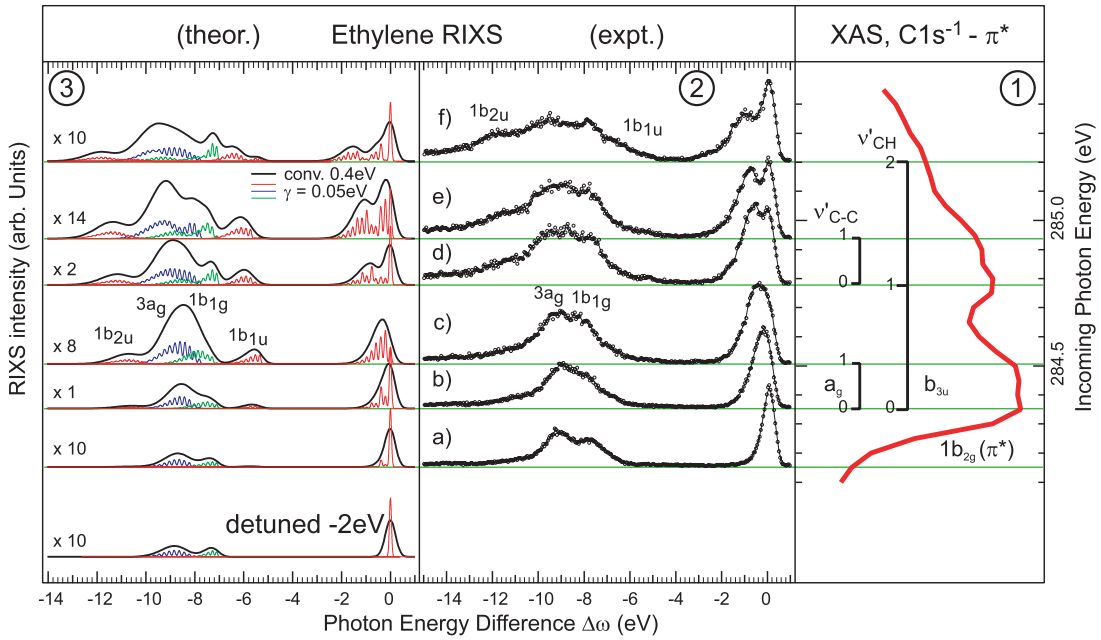

Figure 4.6: RIXS of ethylene at the C K–edge in the region of the C 1s → π^* resonance. Panel (1): Absorption spectrum with partly assigned vibrational states; (2): RIXS spectra (exp.) with excitation at the energies indicated; (3): Simulated RIXS at the according energies. RIXS spectra are plotted vs. the energy difference of outgoing and incoming photon $\Delta\omega = \omega_1 - \omega$. The experimental spectra are arbitrarily scaled to equal maximum height.

transition, i.e. excitation into an electronic state $|\psi_{\mathrm{core}}^{-1} 1b_{2g}\rangle$. The appearance of this feature is identical in the gas phase and condensed phase measurements. This assures the properness of our preparation and affirms that the condensed ethylene in the region of the π^*–resonance can act as a model for a free molecule.

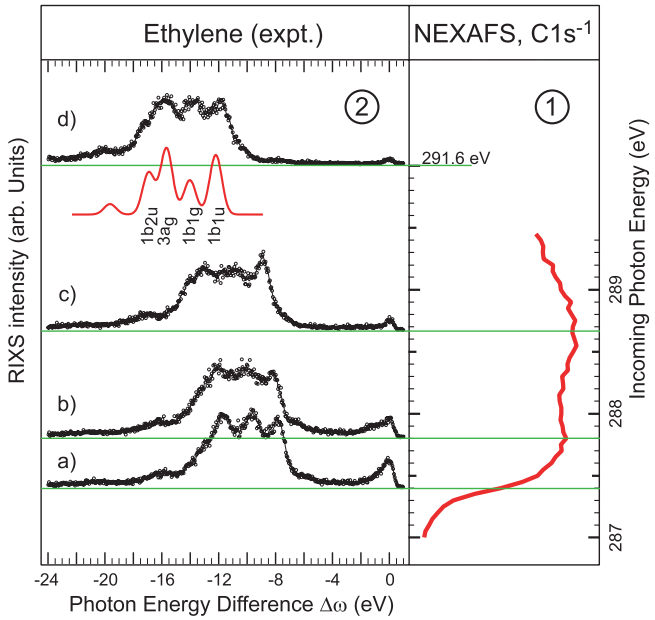

Figure 4.7: RIXS of ethylene at the C K–edge in the rydberg region. Panel (1): Absorption spectrum; (2): RIXS spectra (exp.) with excitation at the energies indicated, plotted vs. the energy difference of outgoing and incoming photon $\Delta\omega = \omega_1 - \omega$. The inset shows non–resonant calculations from [155]. The spectra are arbitrarily scaled to equal maximum height.

The resonance fine structure stems from vibrational excitations. We also show our simulations of the XAS. Our theoretical simulation has shown that only four vibrational modes are active in the scattering process (see Sec. 4.2.3). According to our simulations and in agreement with Gadea et al. [74], we can assign the vibrational states: Maximum (b) corresponds to the $0 \rightarrow 0$ transition, (c) to the excitation of an a_g C–C stretch mode, (d) contains the excitation of a b_{3u} CH_2 mode, and (e) the combined excitation of the C–C and the CH_2 mode (see figure caption).

We have measured RIXS for selective excitation into the vibrational states of the π^*–Resonance and performed RIXS simulations at the according energies. The resonant scattering with excitation into the π^* resonance is presented in Fig. 4.6. Panel 1 contains the XA spectrum from Fig. 4.5 in the π^* resonance region, with the vibrational progression assigned in the plot. Panel 2 contains experimental RIXS spectra, taken at excitation energies indicated in the XA spectrum by the horizontal lines. Panel 3 contains the corresponding simulations. We convoluted the simulated spectra with a gaussian of 0.4 eV to mimic the spectral distribution of the incident photon and the instrumental broadening. In addition, we show the computations with only 0.1 eV broadening to illustrate the underlying spectral structure. The RIXS spectra are displayed on an energy

loss scale corresponding to the energy difference between outgoing and incoming photon.

The experimental RIXS data and the theoretical simulations both show strong excitation energy dependence. We first turn to the experimental data (Fig. 4.6 panel 2). When exciting below the resonance energy (a), an isolated, nearly symmetric peak centered at 0 eV energy loss with FWHM of 0.4 eV and two broad features at -7.8 eV and -9.4 eV can be seen. The feature centered at 0 eV is commonly called the “elastic” peak. This band corresponds to scattering into the electronic ground state ($|0\rangle \rightarrow |\psi_{\mathrm{core}}^{-1} 1b_{2g}\rangle \rightarrow |0\rangle$). The features at -7.8 eV and -9.4 eV correspond to scattering into electronically valence excited final states ($|0\rangle \rightarrow |\psi_{\mathrm{core}}^{-1} 1b_{2g}\rangle \rightarrow |3a_g^{-1} 1b_{2g}\rangle$ and $|1b_{1g}^{-1} 1b_{2g}\rangle$). We have tentatively assigned the corresponding states following our simulations and in agreement with Gunnelin et al. [141] and Triguero et al. [155] as marked in the figure.

When increasing the excitation energy, two qualitatively different effects can be observed: a broadening of the features that is asymmetric toward lower energies, and the appearance of additional features. After resonant excitation on top of the electronic resonance (b), the peak at 0 eV becomes asymmetric toward lower energies. Exciting into the higher vibrational resonances (c–g), this feature splits into two contributions, one staying at 0 eV and one moving toward lower energies with increasing excitation energy. The lower energy fraction decreases in intensity with increasing excitation energy compared to the part at 0 eV. The features representing the valence electronically excited final states $|1b_{1g}^{-1} 1b_{2g}\rangle$ and $|3a_g^{-1} 1b_{2g}\rangle$ broaden and merge when increasing the excitation energy to the electronic resonance (b) and further to the first vibrational level (c). They become increasingly asymmetric and their center of gravity moves toward lower energies. Increasing the incident photon energy to higher vibrational levels (d–f) not only changes the appearance of the states visible with detuned excitation: Additional features show up, assigned to the valence excited final states $|1b_{1u}^{-1} 1b_{2g}\rangle$ and $|1b_{2u}^{-1} 1b_{2g}\rangle$. These features gain intensity with increasing excitation energy.

Our simulations (panel 3 of Fig. 4.6) agree well with the experimental spectra. In particular, the observed increasing asymmetry and the separation of a band of loss features of the scattering into the electronic ground state is resembled in the simulations. They also reflect the reduction of the intensity of these loss features with increasing excitation energy as well as the collapse of the loss features upon negatively detuned excitation. Simulations for an energy value detuned by -2 eV from the resonance position, where we have no experimental data for comparison, show that for this hypothetical detuning, the band at 0 eV collapses completely and only a single elastic scattering line remains.

The valence electronically excited final states are found to be formed by bands of closely spaced loss features. These bands undergo strong modulations when

tuning the excitation energy: They broaden and the intensity is strongly redistributed within each band. They move their center of gravity and even shape a bimodal structure in some states. After excitation negatively detuned from the absorption resonance, the bands narrow and form clear maxima. This can e.g. be seen nicely in case of the $|1b_{1g}^{-1}1b_{2g}\rangle$ final state in ethylene (Fig. 4.6). This band is approx. 1 eV wide with a sharp maximum when exciting detuned (a). When tuning the incident photon energy resonantly into the vibrational progression of the intermediate state $|\psi_{\mathrm{core}}^{-1}1b_{2g}\rangle$, this band broadens (b–c). Upon further increase of the excitation energy, it splits into a bimodal shape consisting of a narrow contribution with a sharp maximum staying at fixed energy and a less intense broad band at lower energies.

The convolution of these states resembles the experimental data in high detail, in particular the broadening and merging of the states, the increasing asymmetry and the overall broadening of the whole spectral range. Also reflected is the formation of special features in the spectra, e.g. the sharp ridge at -7.8 eV in the spectra (f) that can be found in both experiment and simulations. Upon excitation detuned, only the final states $|1b_{1g}^{-1}1b_{2g}\rangle$ and $|3a_{g}^{-1}1b_{2g}\rangle$ contribute to the spectra, whereas after excitation with higher energies, the additional final states $|1b_{1u}^{-1}1b_{2g}\rangle$ and $|1b_{2u}^{-1}1b_{2g}\rangle$ show up.

We now turn to RIXS at energies in the Rydberg or continuum region. A comparison of the higher energy region in the XAS (Fig. 4.5) with data published by Gadea et al. [74], Rabus et al. [156] shows significant differences between gas phase and condensed ethylene. Our spectra agree with the condensed measurements published before [68]. In the region above 287 eV, the gas–phase molecules show several discrete resonances, whereas in the condensed case only two very broad states remain. The Rydberg states here overlap due to van–der–Waals interaction of the closed packed molecules and the fine structure quenches and broadens [67].

RIXS spectra measured after excitation into the Rydberg region are depicted in Fig. 4.7 panel 2. The excitation energies are indicated in the XA spectrum in panel 1 by the horizontal lines. The experimental spectra show only weak excitation energy dependence and resemble the non–resonant X–ray emission spectrum (XES) of ethylene [141] very closely. For a tentative assignment of the emission from the valence orbitals we have inserted purely electronic XES calculations from [155]. The peak around 0 eV for scattering into the electronic ground state is at first (a) quite strong, although weaker as on resonant excitation into the π^*. With increasing excitation energy its intensity then decreases. Exciting detuned (a), the peak is clearly asymmetric and on top of the first resonance (b), the formation of a second band centered at ≈ -0.6 eV can be seen. After increasing the excitation energy further it again becomes symmetric. We

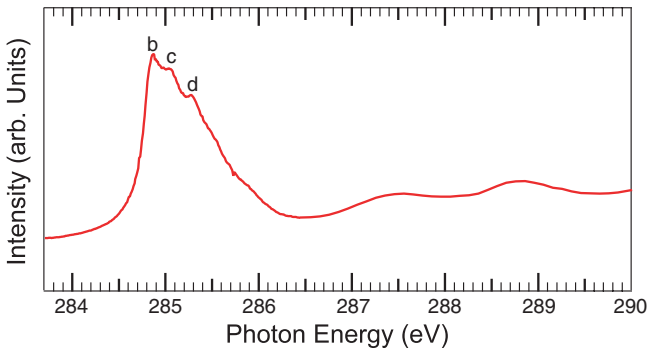

Figure 4.8: X–ray absorption spectrum of condensed benzene.

observe emission from the $2b_{3u}$, $1b_{2u}$, $3a_g$, $1b_{1g}$ and $1b_{1u}$ electronic orbitals, roughly equally strong for all excitation energies. Tuning the excitation energy into the rising flank (a) of the Rydberg region, these states are quite well separated. Scattering on top of the two broad resonances, these states broaden and smear out, while after excitation above these resonances (d) they again separate. When exciting at the second broad resonance (c), the emission from the $1b_{1u}$ orbital is found to be slightly enhanced above the others.

Benzene

Carbon K–edge XAS of condensed benzene is presented in Fig. 4.8. As in ethylene, we can separate the resonance with a maximum at 284.85 eV and a higher energy region with two broad features around 287.5 eV and 288.8 eV. We again discuss the resonance region first. We compared the spectra to XAS reported for condensed [68] and free [72] benzene with similar result as for ethylene. The shape of the C 1s $\rightarrow \pi^*(1e_{2u})$ resonance agrees for condensed and gas phase with our measurement, backing our preparation and the model function of the condensate for the isolated molecule in the π^* resonance region. Our spectrum resolves all reported features except for a small state right above the absorption maximum reported by Ma et al. [68]. The fine structure represents the vibrational progression of the π^* resonance. Following the discussion summarized by Rennie et al. [72], we can assign (b) to the $0 \rightarrow 0$ transition and (c) to an e_{1u} ring stretch and deformation. (d) combines the former mode with an a_{1g} C–H stretch mode.

Fig. 4.9 shows the resonant scattering data for condensed benzene. For comparison, we again show the XA spectrum in panel 1 and indicate the excitation energies with horizontal lines. The RIXS spectral distribution changes strongly with excitation energy. For scattering into the electronic ground state, we observe a behavior very similar to ethylene. Excitation detuned from the electronic

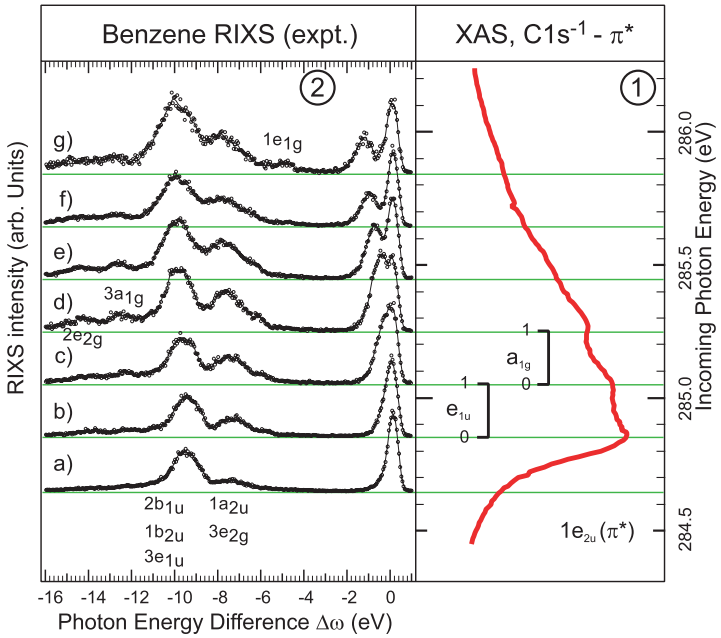

Figure 4.9: RIXS of benzene at the C K–edge in the region of the C 1s $\rightarrow \pi^*$ resonance. Panel (1): Absorption spectrum with partly assigned vibrational states; (2): RIXS spectra (exp.) with excitation at the energies indicated. RIXS spectra are plotted vs. the energy difference of outgoing and incoming photon $\Delta\omega_1 = \omega - \omega$. The spectra are arbitrarily scaled to equal maximum height.

resonance (a) gives rise to a single, slightly asymmetric peak at 0 eV ("'elastic peak"'). The 0 eV feature broadens and becomes more asymmetric when tuning the excitation energy on top of the resonance (b) and into the first level of the vibrational progression (c). Upon excitation with higher energies (d–g), it splits into two contributions, one staying at 0 eV and one moving toward lower energies similar to the ethylene case. The intensity of the moving fraction decreases with increasing excitation energy.

The region of valence excited final states between -16 eV and -3 eV were compared to data published [139] and electronic simulations from [155] for a tentative assignment of the spectral features as labeled in the plot. Due to the multitude of valence orbitals in benzene, these features convolute several final states. Exciting detuned from the resonance (a), we see two broad peaks: The first at -9.4 eV we assign to the $|2b_{1u}^{-1}1e_{2u}\rangle$, $|1b_{2u}^{-1}1e_{2u}\rangle$ and $|3e_{1u}^{-1}1e_{2u}\rangle$ final states, the other peak at -7.4 eV is assigned to $|1a_{2u}^{-1}1e_{2u}\rangle$ and $|3e_{2g}^{-1}1e_{2u}\rangle$. Upon excitation on top (b) of the resonance and into the vibrational progression (c–g), these two features change their shape and width and their relative intensity ratio. The states represented by these features show different excitation energy dependence; the changes in peak shape and in relative intensity reflect this.

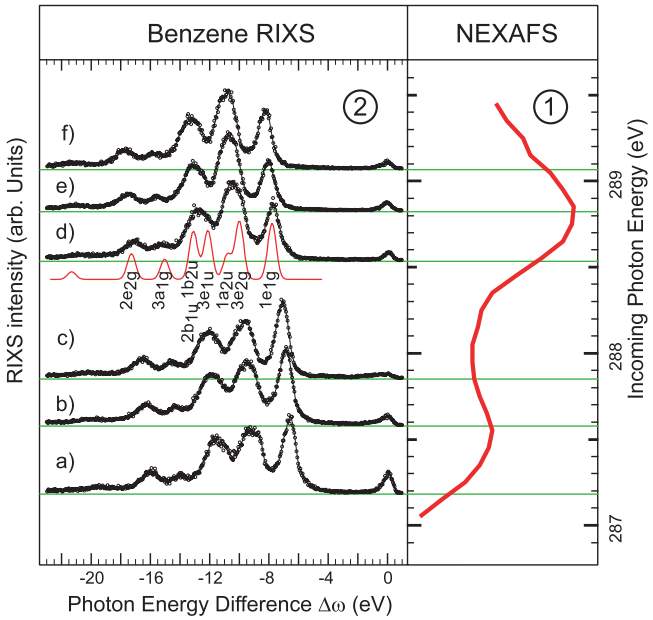

Figure 4.10: RIXS of benzene at the C K–edge in the rydberg region. Panel (1): Absorption spectrum; (2): RIXS spectra (exp.) with excitation at the energies indicated, plotted vs. the energy difference of outgoing and incoming photon $\Delta\omega = \omega_1 - \omega$. The inset shows non–resonant calculations from [155]. The spectra are arbitrarily scaled to equal maximum height.

Upon resonant excitation into the vibrational progression (b–g), additional features show up. They increase in relative intensity to the other features with increasing excitation energy. We assign the features at -14.4 eV to $|2e_{2g}^{-1}1e_{2u}\rangle$, at -12.6 eV to $|3a_{1g}^{-1}1e_{2u}\rangle$ and at -5 eV to $|1e_{1g}^{-1}1e_{2u}\rangle$. The intensity ratio between the peaks at -9.4 eV and -7.4 eV is roughly $4:1$ below resonance (a). On top (b) and above resonance (c–g), the peak at -7.4 eV gains relative intensity and the ratio alters to about $2:1$. In agreement with the increasing intensity of ungerade final states, we conclude that this intensity change reflects an increase of scattering into the $|3e_{2g}^{-1}1e_{2u}\rangle$ final state.

The higher energy part of the XAS spectra (Fig. 4.8 and Fig. 4.10 panel 1) reflects the condensed case [157] missing some fine structure visible in the gas phase [72]. Comparing to Rennie et al. [72] we assign the peak at 287.5 eV to the broadened $3s$ Rydberg state and the peak at 288.8 eV to the $\pi^*(1b_{2g})$ excitation. In benzene, the ionization potential lowers below the C–H* resonance [67].

RIXS at the Rydberg states is displayed in Fig. 4.10. The inset shows non–resonant XES calculations [155] in the adiabatic limit neglecting changes in the vibrational wave function and allowing for a tentative assignment of the spectral features. In benzene, stronger variations of the relative intensity of the peaks with the excitation energy can be observed as compared to ethylene, whereas

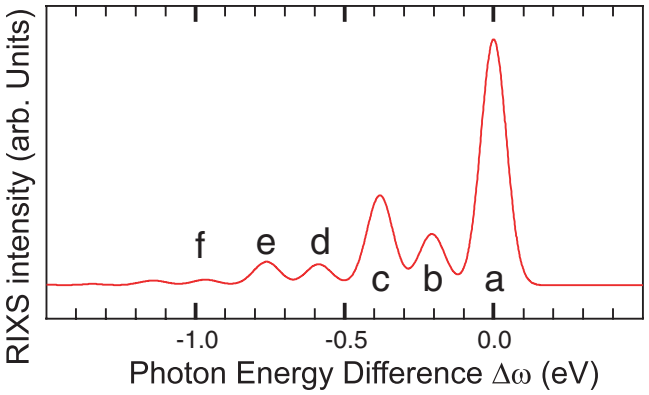

Figure 4.11: Participator channel: Purely vibrational inelastic X–ray scattering (Soft X–ray vibrational Raman) at C_2H_4 at 284.37 eV (compare Fig. 4.6). The vibrational modes 3, 4, and 5 (Tab. 4.2) contribute to the spectra: a) 0→0; b) ν_5(0→1); c) 93% ν_3(0→1) / 7% ν_5(0→2); d) ν_3(0→1) + ν_5(0→1); e) 69% ν_3(0→2) / 20% ν_4(0→2) / 11% [ν_3(0→1) ν_5(0→2)]; f) ν_3(0→2) + ν_5(0→1)

the separation and width of the features do not change noticeable. The feature at 0 eV varies a little bit with excitation energy without a clear trend and keeps its overall shape and width. Its center of gravity stays at 0 eV. Upon excitation into the region of the $3s$ Rydberg resonance at 287.5 eV (a–c), the π ($1e_{1g}$) peak at -7 eV is enhanced compared to the other features. Exciting around the $\pi^*(1b_{2g})$ resonance at 288.8 eV, the peak at -9 eV ($1a_{2u}$ or $3e_{2g}$) is enhanced over the others.

4.2.5 Discussion

Both ethylene and benzene show partly very similar effects in the RIXS. We will jointly discuss both molecules to work out the analogies and differences. The RIXS scattering depends strongly on the excitation energy. In the π^* resonance region, even small variations of the incident photon energy have big influence on the scattering profile. In the energy region > 2 eV above the resonance, the variations are smaller but still significant. The simulations only cover the region of the absorption resonance. We will first evaluate the π^* region and than discuss how the interpretation can be extended to the region of continuum excitation.

Generally, the scattering simulations reflect the experimental data good in shape, intensity, and position of the spectral features. In the following discussion, we will, thus, jointly discuss both data sets and not distinguish between experiment and calculations. In the RIXS spectra two energy regions can be separated: A region of small energy losses between -4 eV and 0 eV and a region of higher energy losses. The energy loss features in the region at 0 eV origi-

nate from vibrational excitations, since electronic excitations in both molecules require higher energies. We call this the participator region, since the underlying electronic transition is the decay of the initially excited ("participating") electron. The final state of the scattering represented by this energy region is the electronic ground state. The region of higher energy losses contains combined electronic and vibrational — i.e. vibronic — loss features. It corresponds to scattering into optically and vibrationally excited final states.

The participator region shows a single line when scattering far detuned from an absorption resonance that is usually called the elastic peak. Upon resonant excitation into the vibrational progression of the π^* resonance we find vibrational features appearing in this channel. The vibrational band becomes wider with increasing incident energy. The intensity is redistributed between these vibrational states when tuning the excitation energy across the π^* resonance, at higher energies the vibrational band exhibits a bimodal envelope structure. In Fig. 4.11 we show a detail of the RIXS spectra of ethylene. The participator band consists of distinct vibrational lines. Only the peak at 0 eV corresponds to elastic scattering.

To understand the origin of this vibrational lines, we look at the scattering cross section (Eq. (4.3)). For scattering into the electronic ground state, the electronic final state coincides with the electronic initial state ($|f\rangle = |0\rangle$). The spectral function then becomes $\Phi(\Delta\omega + \omega_{0\nu_0,00}, \gamma)$. From this, we can see that this band composes of vibrational lines that represent direct excitations $0 \rightarrow \nu_0$ of vibrational states in the electronic ground state. The energy spacing of the lines corresponds to the vibrational energy of ground state vibrational modes. In the participator channel, we, thus, observe purely vibrational Raman spectra in the soft X–ray regime, that are resonantly enhanced tuning into a molecular resonance. As normal Raman spectroscopy, this allows to investigate ground state vibrational properties of a system. This observation of purely vibrational states is in principal possible only in a photon–in–photon–out spectroscopy, where electronically not excited final states can be reached. Basing on the theoretical analysis we have assigned the vibrational states as indicated in Fig. 4.11. The mode analysis reveals, that only those final states are active in the scattering, where the parity of the total wave function is conserved.

The spectator region contains combined electronic and vibrational loss features. The vibrational band belonging to a specific electronic final state is relatively narrow and have a single maximum when scattering with an incident energy away from the absorption resonance. The vibrational bands widen, when tuning the excitation energy into the π^* resonance. Similar to the purely vibrational band, some vibronic bands form a bimodal structure. The spectator channel corresponds to scattering into electronically excited final. Looking at

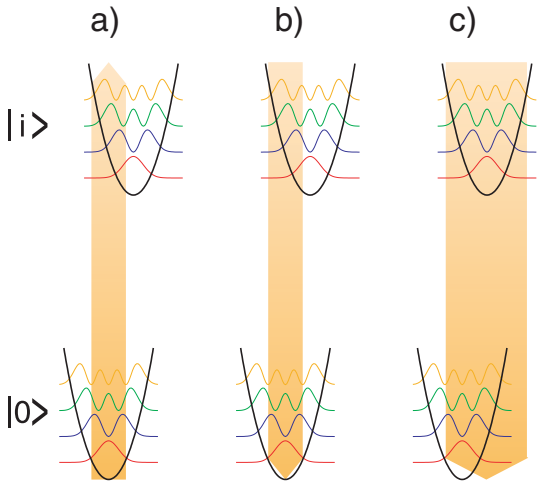

Figure 4.12: Scheme of transitions. Displayed is the case for $|f\rangle = |0\rangle$. Panel a) shows the excitation into the core excited intermediate state $|i\rangle$. Panels b) and c) show the decay into the final state with different excitation energies and thus scattering duration. b) Detuned scattering / short duration: The intermediate state wave packet had no time to evolve in the intermediate state, the initial probability density is down projected onto the final state $|f\rangle$. c) Resonant scattering / long duration: The nuclear wave packet has equilibrated in the intermediate state, before the decay takes place.

the spectral function in Eq. (4.3) we see that the energy position of a single vibrational line represents the sum of the energies of the vibrational and electronic excitation present in the particular final state. In the spectator channel, we, thus, probe the vibrational properties of valence excited final states.

The mechanism of the vibrational band formation is similar for the participator and the spectator channel. The intensity of the vibrational states arises from the scattering amplitude (Eq. (4.4)) and (Eq. (4.5)). From this expression, we get in general a scattering amplitude for vibrationally excited final states. For the limit of large detuning compared to the vibrational spacing in the intermediate state ($\Omega = \omega - \omega_0^i \gg \omega_{i\nu_i,00}$) and to the intermediate state lifetime $\Omega \gg \Gamma$, the scattering amplitude [Eq. (4.4)] collapses from the sum over all channels to a direct term due to the condition of completeness (we discuss the case for a single vibrational mode for clarity):

$$\begin{aligned} F_{\nu_f} &\approx \sum_{\nu_i} \frac{\langle \nu_f|\nu_i\rangle\langle\nu_i|0\rangle}{\Omega} \\ &\approx \frac{\langle \nu_f|0\rangle}{\Omega}, \quad \text{with} \quad \sum_{\nu_i} |\nu_i\rangle\langle\nu_i| = 1 \end{aligned} \tag{4.7}$$

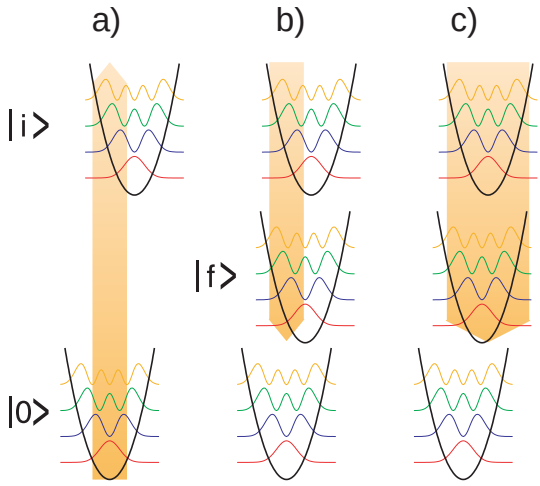

Figure 4.13: Scheme of transitions. Displayed is the case for $|f\rangle \neq |0\rangle$. Panel a) shows the excitation into the core excited intermediate state $|i\rangle$. Panels b) and c) show the decay into the final state with different excitation energies and thus scattering duration. b) Detuned scattering / short duration: The intermediate state wave packet had no time to evolve in the intermediate state, the initial probability density is down projected onto the final state $|f\rangle$. c) Resonant scattering / long duration: The nuclear wave packet has equilibrated in the intermediate state, before the decay takes place.

This has different consequences for the participator and the spectator channels. In the purely vibrational Raman or participator channel, the electronic initial and final state is the same, the ground state. The vibrational states of a particular electronic state are orthonormal ($\langle 0, \nu_0 | 0, 0\rangle = \delta_{\nu_0,0_0}$), thus the matrix element of pure vibrational transitions in Eq. (4.7) vanishes for all but the $0 \to 0$ transition, which is the elastic scattering. This results in a complete collapse of the vibrational structure. The spectator channel contains transitions between vibrational states belonging to different electronic states. They are not orthonormal and, thus, even allowed for detuned excitation.

We demonstrate the formation of the vibrational bands in Fig. 4.12 (participator channel) and Fig. 4.13 (spectator channel). In panel a) of both figures the excitation transition into the core excited intermediate state is shown. As mentioned before, the excitation is considered as sudden. In the Franck–Condon picture, thus, the probability density of the vibrational ground state is projected onto the core excited state. To understand the difference between detuned and resonant scattering we invoke the scattering duration time concept. The duration time τ of the scattering process is defined by:

$$\tau = 1/\sqrt{\Omega^2 + (\Gamma/2)^2} \tag{4.8}$$

The time scale of the nuclear motion is defined by the period of vibration ω_ν. In the limit of large detuning the total scattering time is too short for the vibrational wave packet to evolve in the intermediate state. In this case, excitation and decay follow each other suddenly and the nuclei cannot move in between. In the immediate decay, the initial probability density of the ground state is unchanged projected on the final state. This is equivalent to a direct transition from the initial to the final state. In the participator channel (Fig. 4.12 b) the final state is the electronic ground state. The potential surfaces coincide and according to the Franck–Condon principle only a single line corresponding to the $0 \rightarrow 0$ transition is observed. For the valence excited final states in the spectator channel (Fig. 4.13 b), the potential surfaces do not coincide. Therefore, transitions into vibrationally excited states are possible. In the case of detuned excitation, the formation of the spectrum can be understood as a result of a direct Franck–Condon transition between the initial ground state and the final state.

On resonant excitation, the scattering duration τ becomes sufficiently large for the nuclei to move on the potential surface of the core excited intermediate state. The decay thus takes place in a different configuration than the excitation. This situation is depicted in panel c) of Fig's. 4.12 and 4.13. Now the probability density is redistributed in the intermediate state. The RIXS spectral profile is determined by channel interference between scattering over different vibrationally excited intermediate states $|\nu_i\rangle$. Additional vibrational excited final states become allowed in the decay transition — which again follows Franck–Condon. The formation of a bimodal structure in some vibrational bands in this situation can now be explained qualitatively. The probability density is highest at the turning points of the oscillator. The decay thus takes preferable place at these two coordinates, leading to two band maxima.

We now turn to the discussion of the selection rules applicable for electronic transitions. If only the electronic wave function is considered, the Raman selection rule would allow only scattering into those final states where the total parity of the electronic wave function is not changed with respect to the ground state. In ethylene this is the case for the $|1b_{1g}^{-1}1b_{2g}\rangle$ and the $|3a_g^{-1}1b_{2g}\rangle$ final states, in Benzene for the $|2b_{1u}^{-1}1e_{2u}\rangle$, $|1b_{2u}^{-1}1e_{2u}\rangle$, $|3e_{1u}^{-1}1e_{2u}\rangle$ and the $|1a_{2u}^{-1}1e_{2u}\rangle$ final states. Nevertheless, upon resonant excitation scattering into the "dipole forbidden" final states $|1b_{2u}^{-1}1b_{2g}\rangle$ and $|1b_{1u}^{-1}1b_{2g}\rangle$ in ethylene and $|2e_{2g}^{-1}1e_{2u}\rangle$, $|3a_{1g}^{-1}1e_{2u}\rangle$, $|3e_{2g}^{-1}1e_{2u}\rangle$, and $|1e_{1g}^{-1}1e_{2u}\rangle$ in benzene can be observed.

Instead, the scattering process is governed by the total wave function of the scatterer, including electronic and nuclear wave function. The activation of asymmetric vibrational modes can couple core excited states of different symmetry, effectively localizing the core excited state (Jahn–Teller–effect, see 4.2.1).

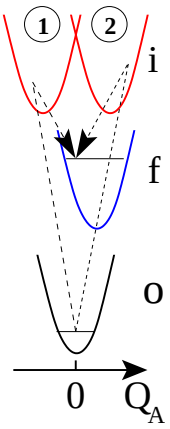

Figure 4.14: Core hole localization in ethylene: Due to vibronic coupling through the asymmetric mode b_{3u} (see Table 4.2), the core excited state localizes in the carbon atom 1 or 2. The scattering can now happen through interfering scattering channels.

The transition dipole moment of the decay transition $\mathbf{d}_{fi}$ then becomes non–zero for gerade and ungerade final states:

$$\mathbf{d}_{fi} \equiv \begin{cases} \langle \psi_f | \mathbf{r} | 1b_{3u} \rangle, & if \quad f = g \\ \langle \psi_f | \mathbf{r} | 1a_g \rangle, & if \quad f = u \end{cases} \tag{4.9}$$

and the multi mode scattering amplitude [Eq. (4.5)] opens additional scattering paths for each localized core hole (Fig. 4.14). In the limit of large detuning $|\Omega|$, all intermediate state vibrational modes are excited equally and the scattering amplitude (4.5) reduces to

$$F_{\nu_f} \approx \frac{\langle \nu_f | 0_0 \rangle}{2\Omega} \, (1 + \mathcal{P}_f). \tag{4.10}$$

One can see that we here converge to the case of pure electronic selection rules because the amplitude vanishes ($F_{\nu_f} = 0$) for ungerade final states $f = u$. Both simulation and experiment clearly demonstrate this effect.

This process of vibronic coupling upon resonant excitation and “sharpening” of the selection rules is to be understood as a dynamic process. If the scattering duration is sufficiently large — as it is the case in resonant excitation — the molecule has enough time to distort to a non–symmetric configuration, where the core excited states are no longer represented in the ground state symmetry of the molecule and thus the selection rules can no longer operate on the delocalized representations. When we detune from resonant excitation, the scattering duration becomes too short for the molecule to change symmetry. In a sudden scattering process, the molecular configuration symmetry and, thus, the according selection rules are conserved.

We can test our interpretation model for the case of RIXS of ethylene and benzene in the Rydberg and continuum region. Here, different effects can be observed. In both molecules, these spectra roughly resemble the non–resonant

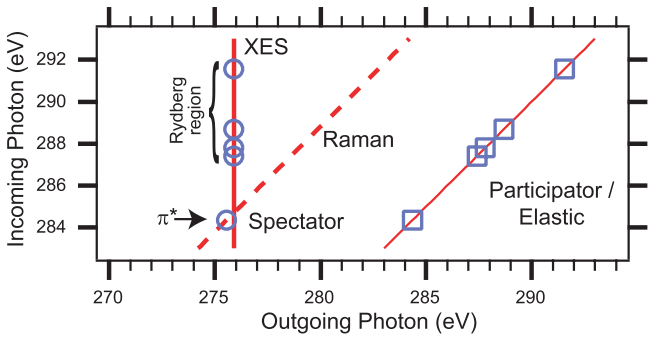

Figure 4.15: Schematic plot of the energy dispersion of spectator and participator / elastic contribution. The markers indicate the position of the participator (squares) and the $3a_g$ (circles) in ethylene (Fig's. 4.6 and 4.7) as an example. The dashed line represents Raman dispersion, the thick solid line fixed emission energy (XES).

XES spectrum, indicating the joint excitation of intermediate states with different electronic symmetry. The enhancement of specific final states then indicates the slight pronunciation of an intermediate state with a certain symmetry. In ethylene, e.g. the $1b_{1u}$ orbital is enhanced upon excitation into the upper resonance (Fig. 4.7 c). This resonance contains large contributions from the $3p$ Rydberg state [158], that corresponds in molecular orbital description to the $3b_{3u}$ orbital [143]. The enhancement, thus, represents the parity selection rule for the $|1b_{1u}^{-1}3b_{3u}\rangle$ final state. Similar effects can be observed in benzene.

In the ethylene Rydberg region, we can also find the effect of strong vibrational contributions to all final states upon excitation into the lower resonance (b). This state corresponds to the $3s\sigma$ Rydberg orbital and $4a_g$ molecular orbital. The intensity enhancement of the 0 eV feature scattering at this energy indicates a strong participator decay contribution. Above this outer resonance, the 0 eV feature becomes weaker and converges to elastic scattering. The fingerprints of resonant scattering involving vibrational dynamics can be nicely summarized here: Firstly, the formation of broad vibrational bands causing a merging of the electronic excited final states; Secondly, the formation of a vibrational loss band in the scattering channel representing the ground state final state, even with a visible bimodal structure; and, thirdly, a clear reduction of these effects when detuning from the resonance (spectrum (a) in Fig. 4.7).

So far, we have not discussed the energy position of the spectral lines. The energy dispersion of the spectra is different for resonant excitation and excitation in the Rydberg region. We have plotted the energy dispersion of the different features in Fig. 4.15 schematically. In the resonant scattering at the π^*, the observed spectral bands become wider with increasing excitation energy and their

center of gravity moves toward higher energy losses. But, the position of a specific vibronic transition — as visible in the calculations — stays at fixed energy difference of incoming and outgoing energy. At the resonance, these features, thus, follow the Raman law. In the Rydberg region, all features except for the 0 eV line move to higher energy losses with increasing excitation energy. The outgoing photons of the valence ionized final states, thus, stay at fixed emission energy (XES features). The crossing point between the Raman and the XES dispersion indicates a threshold value, e.g. the conduction band edge, above that the energy of the excitation relaxes before the decay. Above this threshold, the initially excited participator electron relaxes and its energy information is lost before the decay. Below the threshold Raman scattering is observed and the 0 eV feature is participator decay. Above the threshold the scattering converges to the XES case and the 0 eV feature is simply elastic scattering.

4.2.6 Conclusion

We have observed and explained purely vibrational and vibronic Raman scattering in RIXS. The resonant enhancement of the vibrational contributions to the RIXS profile opens a perspective for new applications of RIXS. The availability of high brilliance light sources and the upcoming development of X–ray spectrometers with improved resolution will allow for the use of RIXS as an element specific vibrational spectroscopy, opening fantastic perspectives in the investigation of large complex molecules.

Our investigation of ethylene and benzene evidences the potential and the necessity of a dynamical interpretation of resonant inelastic X–ray scattering. Ethylene is a linear hydrocarbon with near degenerate core orbitals, benzene a cyclic aromatic molecule with both degenerate and near degenerate core orbitals. A comparative discussion of these two quite different molecules supports the general relevance of our interpretation for RIXS on any molecule.

The nature of the scattering process changes significantly with the duration of the scattering. On resonant excitation, indeed, even in the soft X–ray regime, the scattering duration becomes sufficiently large to probe nuclear dynamics with RIXS. Tuning the photon energy away from the resonance shortens the scattering duration. A similar effect has been observed 32 years ago in conventional resonance Raman spectroscopy [159]. However in RIXS, the pure vibrational Raman collapses in the limit of large detuning.

Upon resonant scattering, the RIXS spectral profile becomes constituted by the intermediate state dynamics and the formation of vibrational bands. The increasing possibility to utilize RIXS with small bandwidth resonant excitation,

thus, requires an interpretation based on a complete treatment of coupled electronic and vibrational processes[5].

[5]**Acknowledgements:** This work was supported by the Access to Research Infrastructure (ARI) Program, the Swedish National Research council (VR) and the Deutsche Forschungsgemeinschaft (Grant DFG Fo343/1-1). M.N. acknowledges support from "Grant in aid of Japan Society of science fellows". Valuable support from Lisbeth Kjeldgaard and MAXlab staff is gratefully acknowledged.

Chapter 5

RIXS of hydrocarbon adsorbates on Si(001)

The first white light excited soft x-ray emission spectra of metal surface adsorbates already illustrated the potential to examine the local partial density of states (local p-DOS) of a selected adsorbate atom [48]. With the availability of tunable and highly brilliant synchrotron radiation in the following years, the experiments first focused on the symmetry selectivity of XES (demonstrated for CO [160]), followed by experiments utilizing the ability to selectively excite inequivalent atoms (N_2 [161]). A very nice example illustrating the power of RIXS as a method to investigate the atom and chemical state specific valence structure is the case of glycine adsorbed on Cu(110) [162]. Glycine (OCOH–CH_2–NH_2) binds trough the NH_2–group and the two oxygen atoms — becoming equivalent upon adsorption — to the surface. By selective excitation at the atomic resonances, it is possible to deconvolute the overall valence electronic structure into the four components arising from the O atoms, the C atom in the OCOH–group, the C atom in the CH_2–group, and the N atom. For the bonding of CO to metal surfaces, the application of RIXS has led to a re–consideration of the mechanism establishing the surface chemical bond [17–20].

In this chapter, I present the application of resonant inelastic X–ray scattering to determine the electronic structure of hydrocarbons on a silicon surface. Here, one can tap the full power of the method lying in the polarization resolved and symmetry selective, atom specific determination of the valence electronic structure. From this, a detailed picture of the chemical bond will be drawn.

Moving the focus from metallic systems to adsorbates on semiconductors has demanded to look closer at the dynamic properties of RIXS. While in the case of metallic systems, the interpretation of the scattering as a two–step process

has been quite successful, the investigations on semiconductors presented here demand for deeper consideration of the full scattering description.

At first, I will briefly summarize the literature on RIXS investigating the chemical bonding of these molecules to a transition metal surface. The following sections then contain the semiconductor adsorbate studies performed in this thesis. In Paper VI, the first general application of RIXS to a semiconductor adsorbate is presented. The screening situation is found to be different from the metal case. The experimental RIXS spectra are compared to simulations invoking a detailed bonding model of ethylene on silicon. Paper VII illustrates the dynamic and screening properties of RIXS at molecular adsorbates on silicon, in particular emphasizing the vibrational contribution and the conditions for a loss of coherence in the scattering process. In Paper VIII finally, the chemical bonding of benzene to Si(001) will be discussed based on the electronic structure determined with RIXS. In section 5.5, I summarize the findings about the bonding of small hydrocarbon molecules to the Si(001) surface and compare to the bonding situation on metals.

5.1 Hydrocarbon adsorbates on metals

The electronic structure of benzene and ethylene adsorbed on metals has been experimentally and theoretically studied with RIXS [31, 148, 163, 164]. It has been possible to determine the nature of the new electronic orbitals formed upon

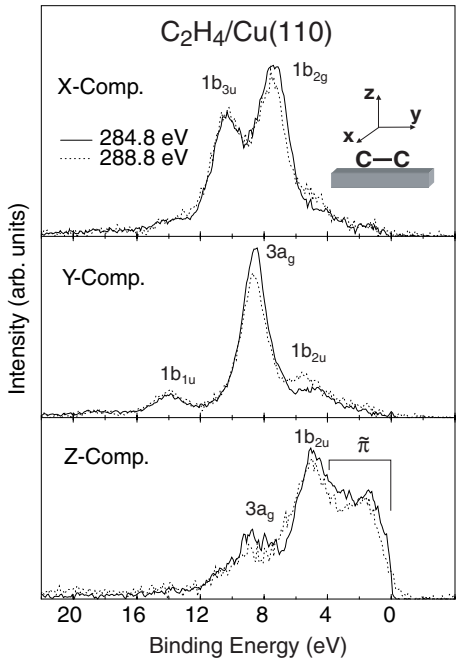

Figure 5.1: Polarization resolved RIXS of C_2H_4/Cu(110), from [148].

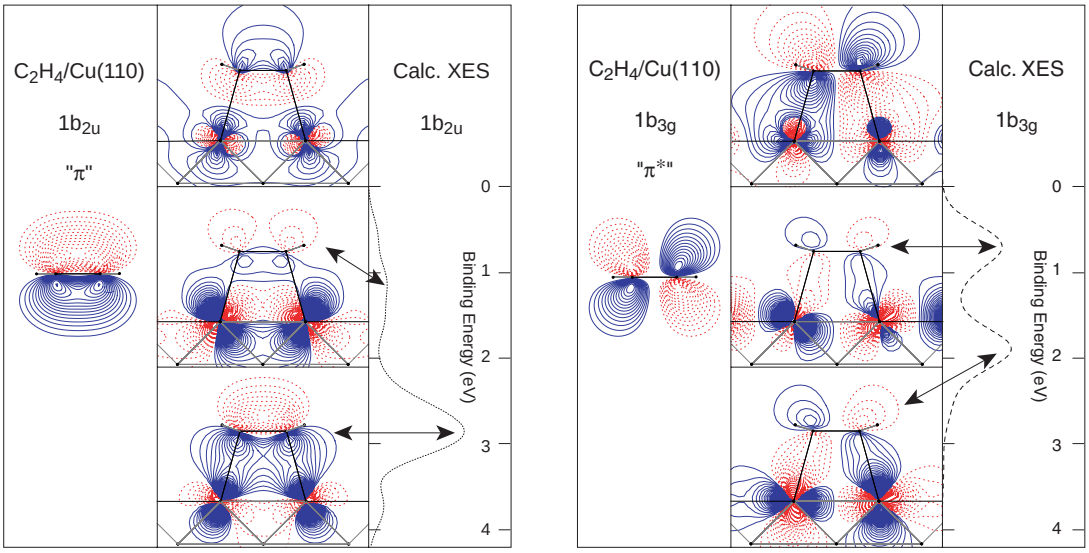

Figure 5.2: Molecular orbital plots of the π and π^* orbitals of ethylene adsorbed on Cu(110), from [148]. In the left panel, the orbitals of free ethylene are shown, the middle panel contains combinations of these orbitals with substrate d–states upon adsorption. In the right panel, the binding energy and intensity of the corresponding RIXS features is indicated.

adsorption. Triguero et al. [31] have presented a model theory for soft x-ray scattering in the case of metal adsorbates.

The bonding of unsaturated hydrocarbons to metals has been described in the so called DCD model developed by Dewar [165] and Chatt and Duncanson [166], commonly called the donation/back-donation mechanism. The bonding is mediated by the adsorbate π-system: electrons from the occupied molecular π orbital are donated into the metal d-band, and in exchange, electrons are back-donated from the metal into the former unoccuopied π^* orbital. By means of the atom specificity and orbital symmetry selectivity of XES and utilizing the polarization selective excitation of the RIXS process, it has been possible to experimentally verify the DCD model [148].

Fig. 5.1 shows the x, y and z components[1] of the X–ray emission spectra from C_2H_4/Cu(110) after resonant excitation into the first molecular π-resonance (284.8 eV) and after non-resonant excitation with 5 eV higher photon energy. The upper two panels show the x– and y–components and thus the orbitals lying parallel to the surface. The states visible in the y–spectrum[2] reflect the C–C

[1]The reference frame used in ref. [148] differs from the one used throughout this thesis. The x and y axis are permuted. This also has influence on the notation of the molecular orbitals. The CH orbitals denoted as $1b_{3u}$ and $1b_{2g}$ (ref. [148]) are called $1b_{2u}$ and $1b_{1g}$ in this thesis.

[2]The notation of the first state in the y spectrum as $1b_{1u}$ is wrong, this is the $2b_{1u}$ orbital.

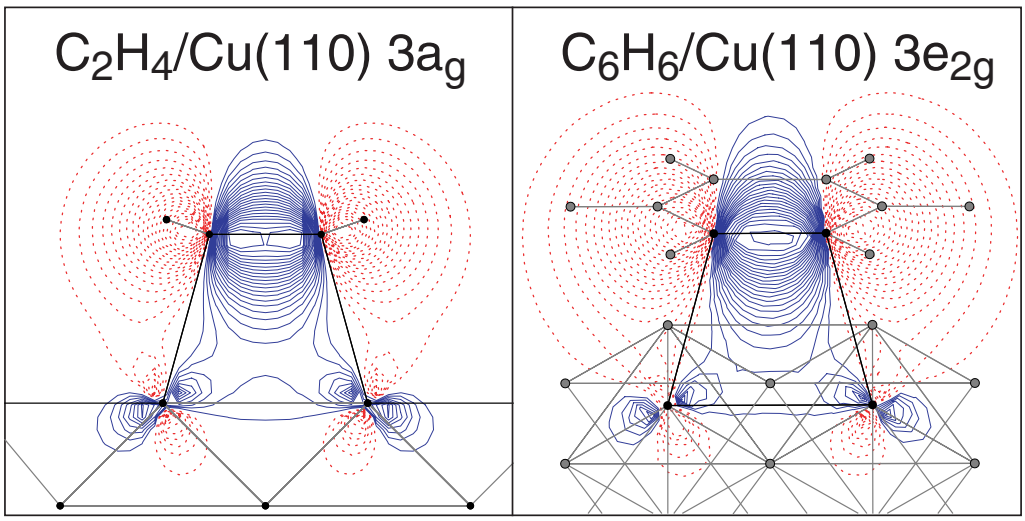

Figure 5.3: Molecular orbital plots of the σ–orbitals of ethylene and benzene adsorbed on Cu(110), from [148].

bonding σ-system ($2b_{1u}$ and $3a_g$). The C-H bonding moiety ($1b_{3u}$ and $1b_{2g}$) can be observed with x–polarization. The z-component exhibits not only the expected π orbitals $1b_{2u}$ and the $3a_g$ as in free ethylene, but also broad band–like state denoted as $\tilde{\pi}$. This state arises from the interaction of the molecular π–system with the Cu d–orbitals and reflects the DCD model.

The interaction of the ethylene π–orbitals with the substrate d–states is illustrated in the molecular orbital plots in Fig. 5.2. For both cases, π and π^* form strong binding combinations with the Cu d–orbitals at high binding energies and weaker combinations when going upwards in energy toward the fermi edge. Additionally, a σ–π mixing is observed and an according distortion of the ethylene σ orbital upon interaction with the surface (Fig. 5.3).

For the case of benzene adsorbed on Cu(110), much weaker changes from the gas–phase case have been observed. The σ–π mixing is smaller and the σ–orbital less distorted (Fig. 5.3). This observation corresponds to the amount of donation/back–donation in the DCD model experimentally determined by Triguero et al. [148]. Here, the respective values per carbon atom are only half as large in benzene as in ethylene. This is also in line with the chemisorption energies per carbon atom, being more than two times higher for ethylene than for benzene.

5.2 Electronic structure and screening dynamics of ethene on single–domain Si(001) from resonant inelastic x-ray scattering[3]

Abstract

We present a resonant inelastic x-ray scattering (RIXS) study of a strongly bound adsorbate on a semiconductor surface, C_2H_4/Si(001). The valence electronic structure as well as the photon energy dependence in RIXS can be studied without the dominating effect of dynamic metallic screening. We demonstrate that for this strongly coupled system the RIXS spectrum resulting from a selective excitation into the unoccupied σ^*_{CSi} resonance can be interpreted with the help of density-functional calculations. In addition, we show how excitation into different resonances leads to a significant photon energy dependence of the RIXS spectral features, not seen in strongly coupled adsorbate systems on metals.

The investigation of resonant inelastic scattering in the soft x-ray spectral range using third-generation synchrotron radiation sources has recently attracted great interest as a powerful method for detailed electronic structure determination [61, and references therein]. The inelastic-scattering process can be described as a transition from the electronic ground state of a system via an intermediate resonant core-excited state into a final state which is electronically and/or vibrationally excited. This event can be studied by either detecting scattered photons or secondary Auger electrons. The former case involving photons in the incoming as well as the outgoing channel has the advantage of being almost independent of the sample environment, thus enabling even electronic structure studies of complex interfaces and liquids. Resonant inelastic x-ray scattering (RIXS) is governed by the dipole operator, and therefore has a well-defined polarization dependence and anisotropy, which provides insight into spatial orientation and symmetry properties of the systems studied [45]. Furthermore, due to the element specificity of the resonant excitation process, one is able to probe the electronic structure of complex heteronuclear systems for selected states [18, 61]. In crystalline solids, momentum conservation in RIXS can be used to access the k-resolved band structure [167]. In adsorption systems, RIXS effectively suppresses contributions from the much larger number of substrate atoms and thus permits to access the atom-specific va-

[3] *Peer reviewed paper. This section has been published as Paper VI:* Föhlisch, Hennies, Wurth, Witkowski, Nagasono, Piancastelli, Moskaleva, Neyman, and Rösch [6], *Physical Review B* **69**, 153408 (2004).

doi:10.1103/PhysRevB.69.153408

lence electronic structure of the adsorbate [17, 18, 45], allowing significantly improved understanding of the surface chemical bond [17, 18].

In free molecules, RIXS depends strongly on the energy of the incoming photon as a result of the interference of degenerate or near-degenerate intermediate states in the scatteringprocess [39, and references therein]. Furthermore, excitation to different resonances leads to significant differences in the spectral shape of the scattering spectra because of strong symmetry selection rules [39]. For adsorbed molecules, this situation changes because coupling to the substrate, which modifies the dynamic response of the core-hole RIXS intermediate state, has to be taken into account. To date only adsorbates on metallic substrates have been investigated with RIXS. For these adsorbates, dynamic metallic screening leads to a significant loss of coherence in the scattering process. Fully angle resolved RIXS investigations were performed for weakly coupled C_2H_4 (Refs. [148] and [31]) and C_6H_6 (Refs. [148] and [163]) on Cu(110). In case of C_2H_4/Cu(110), the excitation to two different resonances is reflected only weakly in the spectral shape, which was attributed to the highly efficient screening in the core-hole intermediate state [31, 148]. For C_6H_6/Cu(110) a stronger photon energy dependence was observed, most likely due to the weaker coupling of the aromatic C_6H_6 which preserves the localized, molecular nature of the adsorbate [148, 163].

This is in line with the present understanding of the femtosecond dynamics of the adsorbate/substrate charge transfer in the intermediate core excited state, achieved in resonant inelastic-scattering studies with Auger electrons [27, 168, 169] where a direct correspondence between coupling strength and chargetransfer probability was found [27].

In the following we will present a RIXS study for an adsorbate on a semiconductor surface, where for a strongly bound adsorbate the valence electronic structure as well as the photon energy dependence in RIXS can be studied without the dominating effect of dynamic metallic screening. As a model system for the early stages of the formation of Si-C layers, we investigated an ordered C_2H_4 adsorbate layer on a single-domain Si(001) surface. This system has been thoroughly characterized experimentally and theoretically [1, 56, 84]. We demonstrate that for this strongly coupled surface complex, the RIXS spectrum resulting from selective excitation into the unoccupied σ^*_{CSi} resonance can be interpreted with the help of density-functional (DF) calculations. In addition, we show how excitation into different resonances leads to a significant photon energy dependence of the RIXS spectral features, even though the molecule is strongly perturbed upon interaction with the substrate.

The experiments were performed at beamline I511 at Max-Lab, Sweden. The bandwidth of the exciting radiation was set to 0.2 eV for the C K edge. The

doi:10.1103/PhysRevB.69.153408

x-ray emission spectrometer[35] can be rotated around the optical axis of the exciting synchrotron radiation and was operated at 0.5 eV bandwidth. Switching the direction of observation relative to the surface of the sample results in the detection of valence molecular orbitals (MO's) of different orientation. In normalemission, valence states in plane are probed while in grazing emission in-plane and out-of-plane orbitals contribute to the spectrum [45]. Assuming a linear superposition of these contributions, a subtraction procedure allows us to separate the spatial contributions to the valence states [45]. The quality of the sample was assured through repeated x-ray photoelectron spectroscopy (XPS) measurements and the spectra were collected by scanning the sample in front of the spectrometer to minimize beam damage. We used p-doped Si(001) surfaces, 5° miscut towards the [110] direction, yielding a single (2 × 1) domain orientation over the whole Si surface [100], as verified by low energy electron diffraction. Two of these single-domain crystals were mounted at 7° grazing incidence rotated 90° around the surface normal, permitting to excite and detect in the direction parallel to the surface (along and perpendicularto the Si-dimer rows) as well as perpendicular to the surface.

The molecule C_2H_4 belongs to symmetry group D_{2h} with the electronic configuration $(1a_g)^2\ (1b_{3u})^2\ (2a_g)^2\ (2b_{3u})^2\ (1b_{2u})^2\ (3a_g)^2\ (1b_{1g})^2\ (1b_{1u})^2$ (footnote[4]), where the MO $1b_{1u}$ is denoted as π orbital; the lowest unoccupied MO is $1b_{2g}$ (π^*). The adsorption system of C_2H_4 on Si(001)-(2 × 1) exhibits local C_2 symmetry according to angle-resolved UV photoemission spectroscopy (ARUPS) [56, 84]. In combination with first-principles calculations, C_2H_4 was shown to be adsorbed on top of a Si(001)-(2 × 1) dimer, with the C-C bond axis rotated in the surface plane by 11.4° relative to the Si-Si dimer axis [56, 84]. This rotation, originally attributed to the spatial overlap of valence MO's between neighboring C_2H_4 adsorbates, leads to the formation of a one-dimensional band-like dispersion of the $1b_{2u}$- and $1b_{1g}$-derived C-H bonding states along the dimer rows of the Si(001)-(2 × 1) surface. Our recent polarization-dependent near-edge x-ray-absorption fine-structure investigation of the unoccupied adsorbate states [1] confirms the picture of the surface chemical bond derived in those earlier studies. In absorption with the electric-field vector oriented normal to the surface, two equally strong absorption resonances were observed below the ionization threshold at 285.3 eV and 286.5eV. Assuming sp^3 hybridized carbon atoms [1, 56, 84] with tetrahedrally oriented bonds, the resonance at 285.3 eV was assigned to the π^*-derived states related to C-Si (σ^*_{CSi}) bonds. The resonance at 286.5 eV was assigned to a state that results from the coupling to a C-H antibonding state involving CH_2 moieties which are bent away form the surface [1].

[4]The notation reflects the choice of axes shown in Figs. 1 and 3, which differs from the conventional choice for ethene molecule, see Merer and Mulliken [143]

doi:10.1103/PhysRevB.69.153408

To interpret the present RIXS spectra, all-electron DF calculations, using a local-density approximation, were carried out [170, 171] for the substrate model cluster Si_9H_{12}. The same basis set as in Ref. [172] was employed. The Si9H12 cluster was derived from a previously used model [172] by reducing the top layer representation to six Si atoms. First, a C_{2v} symmetry constraint was applied to the cluster C_2H_4/Si_9H_{12} , with the C-C bond of ethene oriented along the Si-Si dimer bond (x direction) nearest to the adsorbate and with the C_2H_4 moiety parallel to the (001) surface. The geometry of ethene as well as the dimer Si-Si and Si-C distances were allowed to relax (within C2v constraints). This cluster model was also considered in reduced (C_2) symmetry, but calculated spectral features showed only minor differences, despite the resulting noncollinearity of C-C and Si-Si bonds (see below). For clarity, we discuss the C_{2v} data.

The RIXS spectra were modeled invoking the commonly used ground-state approximation [17, 45, 148, 173], which is believed to furnish a sufficiently accurate description of experimental x-ray data. Thus, the dipole matrix elements for transitions between the C 1s levels and valence MO's of the adsorption complex were calculated using ground-state orbitals. The transition energies were approximated by differences between the Kohn-Sham energies of the valence orbitals and C 1s a_1 and b_1 symmetry-adapted orbitals. Within the dipole approach, the intensity $I(\epsilon)$ of a transition from a valence orbital $|f\rangle$ of energy ϵ_f to a previously generated hole in the core state $|i\rangle$ of energy ϵ_i is $I(\epsilon) \propto (\epsilon_i - \epsilon_f)^4 \langle i|\mathbf{r}|f\rangle^2$ [17, 45, 148, 173].

In Fig. 1, we show the anisotropy of our angle-resolved spectra for scattering into the σ^*_{CSi} excitation resonance at 285.3 eV. Due to symmetry selection rules for scattering off the C 1s core level, the RIXS spectral features with the electric-field vector in a given direction stem from C 2p-type valence orbitals oriented in the same direction. Using the known ultraviolet photoemission spectroscopy (UPS) binding energies[84] and the results of our calculations, we can assign the spectral features to the adsorbate valence level structure. MO's of free ethene are invoked to assign the UPS spectrum of the adsorption system, assuming that they contribute preferentially to the corresponding states of the coupled system. For direct comparison, Fig. 2 shows simulated RIXS spectra for the C_{2v} cluster model; they exhibit the same strong polarization dependence as the experimental results, yielding very similar overall profiles.

To elucidate this, we illustrate the relationship between MO symmetry and angular anisotropy for a few examples. For the $1b_{2g}$ (π^*) derived MO (b_2 character in C_{2v} symmetry), which becomes occupied upon interaction with the Si substrate, we experimentally observe a strong RIXS signal for z polarization, but only weak contributions for the polarization vector along x and y directions. This is also found in the simulated RIXS spectra, which reflect the fact that only the C

doi:10.1103/PhysRevB.69.153408

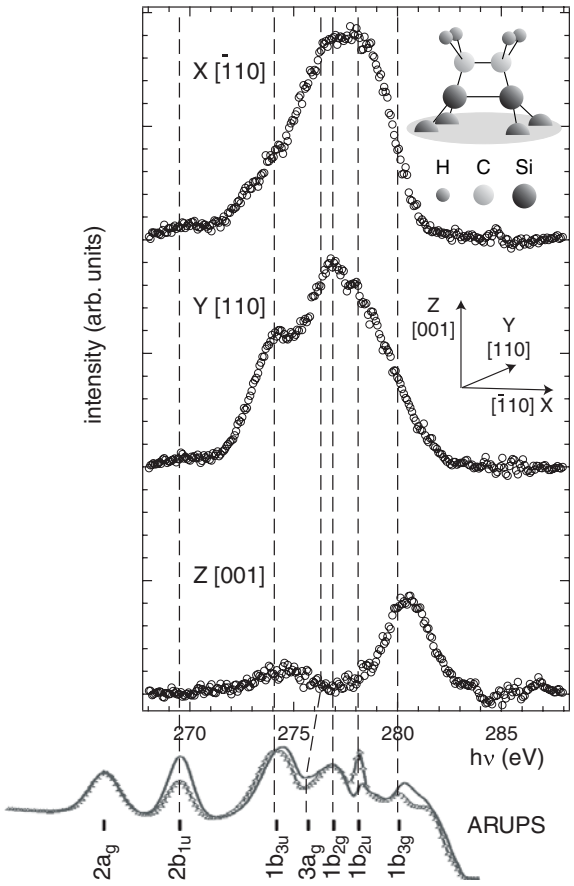

Figure 5.4: Angle-resolved carbon K-edge RIXS excited at the σ^*_{CSi} resonance (285.3 eV) on single-domain C_2H_4/Si(001), resolving the adsorbate valence electronic structure along the crystallographic axes. Below ARUPS spectra recorded in s and p symmetries [84].

2_{p_z} orbitals contribute to this state. The spectral assignment is more difficult for the x- and y-polarized cases because here several states, closely spaced in energy, contribute. With the computational model, we assign the two strong bands, observed only for y polarization, to contributions derived from the $1b_{2u}$ (b_1) and $1b_{1g}$ (a_2) MO's. These bands directly reflect C-H bonding MO's which are antisymmetric with respect to the C-C bond; these MO's are only moderately perturbed upon adsorption, thus keeping their dominant C 2_{p_y} character. In contrast, the former σ(CC) and π(CC) MO's, 3_{ag} and $1b_{1u}$, respectively, undergo strong mixing of C 2_{p_x} and C 2_{p_z} components (a_1 in C_{2v} symmetry) due to chemisorption and therefore appear with different intensities under z and x polarizations. Thus, we can directly observe how strongly the valence electronic structure of ethene is modified upon adsorption. The optimized nonplanar geometry of the adsorbed C_2H_4 moiety manifests a considerable sp^3 character of the carbon atoms. Thus, the RIXS anisotropy directly reflects the spatial orientation of particular C 2p orbitals. In view of earlier findings [56, 84], we reoptimized the adsorption cluster model in C_2 symmetry, allowing a rotation of the ethene moiety about the Si surface normal. The resulting structure features two methylene groups twisted

doi:10.1103/PhysRevB.69.153408

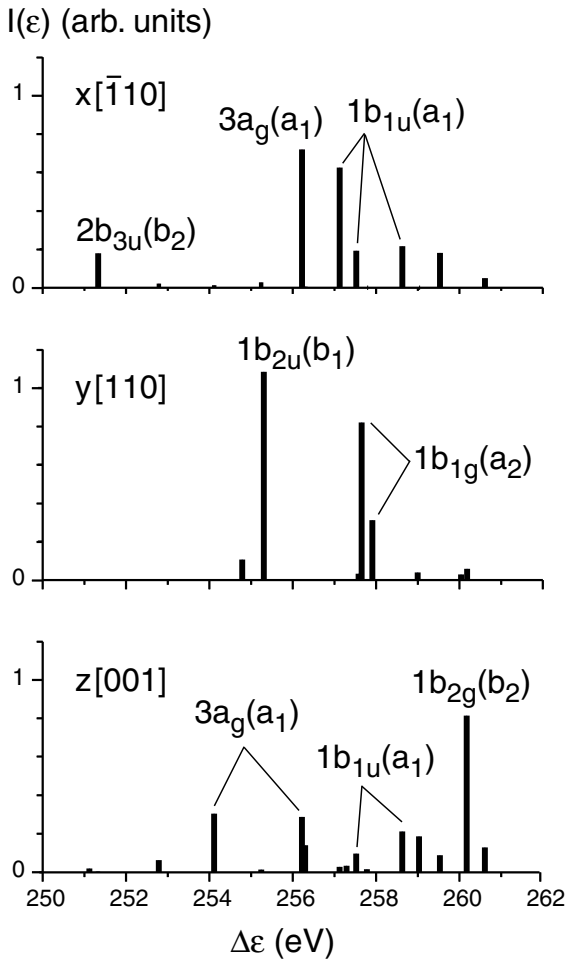

Figure 5.5: Simulated carbon K-edge RIXS spectra from a C_{2v} model of the C_2H_4/Si(001) adsorption complex. $\Delta\epsilon$ is the energy difference between valence and core (C 1s) Kohn-Sham levels. The labels give the dominant ethylene contributions to the respective orbitals (symmetry shown in parentheses) of the adsorbate-substrate complex.

with respect to one another. The C-C axis is rotated relative to the Si-Si bond by 15.4°°, in satisfactory agreement with the result of periodic calculations [56]. This suggests that the symmetry reduction is an inherent feature of the ethene adsorption complex, which distorts from an energetically unfavorable collinear conformation; interadsorbate repulsion at high coverage may enhance this effect.

We also performed angle-resolved RIXS for scattering into the CH_2^* excitation resonance at 286.5 eV, which we compare in Fig. 3 directly to RIXS results from the lower lying σ^*_{CSi} excitation resonance. The two RIXS spectral distributions vary significantly. In the picture of femtosecond charge transfer on the time scale of the core-hole lifetime, spectral features which change with the photon energy are related to the coherent RIXS process, whereas spectral features independent of excitation energy are related to radiative decay processes associated with loss of coherence in the core–excited intermediate state. Thus we conclude that ethene on Si falls into the former category where a significant contribution

doi:10.1103/PhysRevB.69.153408

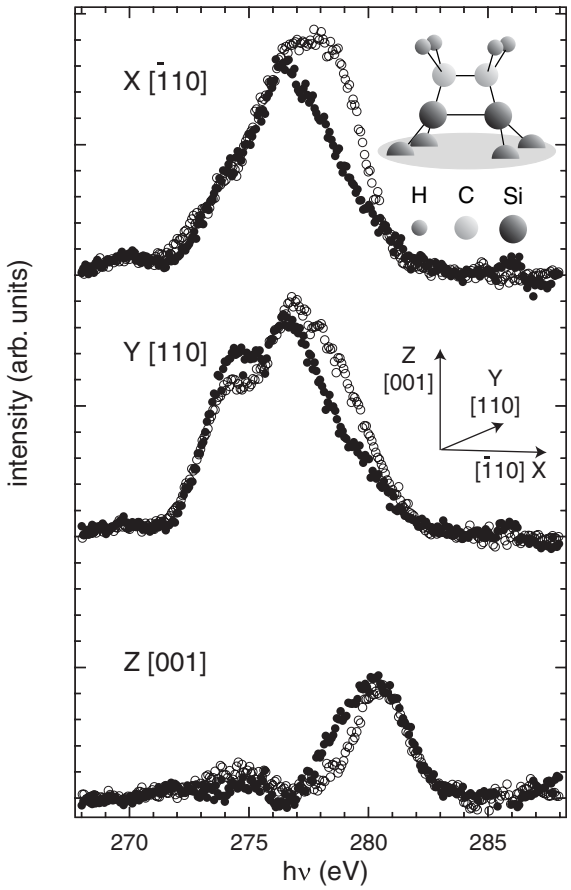

Figure 5.6: Excitation energy dependence of RIXS on single-domain C_2H_4/Si(001) for scattering into the σ^*_{CSi} (285.3 eV) (open circles) and the CH^*_2 (286.5 eV) (full circles) excitation resonances.

of coherent scattering processes is observed for a strongly coupled adsorbate, which shows notable electronic rehybridization in the ground state as discussed above. In particular, the spectral intensities of some of the valence states vary significantly, whereas energetic shifts are less pronounced. Comparing with our assignment given above, the most prominent effects occur in the spectral region of the $1b_{1g}$ and $1b1u$ derived MO's. This may reflect the fact that those states couple most efficiently to the respective core excited states, but a more elaborate theoretical description is needed to elucidate this problem.

In summary, we demonstrated that the valence electronic structure, and hence the chemisorption of a strongly bound adsorbate on a semiconductor surface [C_2H_4 /Si(001)], can be studied in detail with the help of RIXS experiments and DF calculations. In addition, we showed how excitation into different resonances leads to a significant photon energy dependence of the RIXS spectral features, not seen in strongly coupled adsorbate systems on metals. This indicates

doi:10.1103/PhysRevB.69.153408

a very different dynamic screening response for strongly coupled adsorbates on semiconductors as compared to metal surfaces.[5]

[5]**Acknowledgements:** This work was supported by Access to Research Infrastructure (ARI) Program, Deutsche Forschungsgemeinschaft, Fonds der Chemischen Industrie, and the "Grant-in-Aid for Japan Society for the promotion of Science Fellows."Valuable support from Max-lab staff is gratefully acknowledged. L.V.M. thanks the Alexander von Humboldt foundation for financial support.

doi:10.1103/PhysRevB.69.153408

5.3 Intermediate State Relaxation in Resonant Inelastic X-ray Scattering of Silicon Surface Adsorbates[6]

The electronic structure of matter is routinely determined by means of resonant inelastic X–ray scattering (RIXS) [18, 39, 41, 61]. RIXS excels as well in being element and chemical state selective as a soft X–ray spectroscopy, as in its advantages as a photon-in/photon-out spectroscopy. RIXS can be applied independently of the sample environment, e.g. to semiconductors, insulators and liquids [12, 15]. RIXS is governed by selection rules giving detailed symmetry information of the systems under investigation. Resonant, polarization selective excitation in ordered adsorbates facilitates a strict symmetry decomposition of the electronic density of states by selective excitation of a particular intermediate core excited state of defined symmetry [31]. The local probe character of RIXS allows for a determination of the adsorbate electronic structure separately from the contribution of the larger number of substrate atoms [45].

In most cases, RIXS is applied to investigate electronic properties, disregarding nuclear (vibrational) inelastic loss processes. Generally coupled electronic and vibrational, i.e. vibronic, loss processes are probed in RIXS [4, 46, 137, 138]. In the case of free ethylene e.g., the explicit consideration of coupled electronic and vibrational states is required to fully assign RIXS spectral states [4]. For the case of metal surface adsorbates, however, a purely electronic treatment in the framework of the ground state interpretation has successfully been applied (CO/Cu(100) [45]; C_2H_4/Cu(110) and C_6H_6/Cu(110) [31]). Little dependence of the scattering profile on the choice of the intermediate state has been observed. This is explained by the fast metallic screening leading to a full relaxation of the scattering intermediate state. The RIXS spectral profile in case of metal adsorbates thus converges to the non resonant scattering case.

In this work we demonstrate the characteristics of the RIXS process at semiconductor surface adsorbates. We will show, that the intermediate state screening dynamics differ significantly from the case of metal adsorbates and depends on the interaction strength between adsorbate and semiconductor substrate. We have carried out an experimental and theoretical study on the excitation energy dependence of RIXS at C_6H_6/Si(001) and C_2H_4/Si(001) and distinguished resonant and non–resonant scattering processes. Electronic and vibrational spectral features have been identified.

The hydrocarbon surface chemical bond in a transition metal system is carried by the d–states, whereas the itinerant sp–band mediates the fast metallic

[6] *Paper in manuscript. This section is intended for publication as Paper VII:* Hennies, Nagasono, Pietzsch, Witkowski, Piancastelli, Wurth, Triguero, and Föhlisch [7].

screening. For adsorbates on semiconductor surfaces, having a different band–structure, strong differences in the resonant scattering profile can be observed [6]. The specific character of the resonantly excited intermediate state determines the RIXS spectral profile. This has strong influence on the electronic and vibrational scattering profile.

Experiment

The experiments have been performed at beamline I511-1 at MAX-lab, Sweden. The samples used were cut from a P–doped silicon crystal with an intended deviation of 5° of the [001] direction, yielding a single domain (2×1) surface dimer reconstruction. Benzene (C_6H_6) and ethylene (C_2H_4) were absorbed at room temperature. C_6H_6 adsorbs on Si(001)–(2×1) in an ordered butterfly configuration, i.e. an 1,4–cyclohexadiene like structure [2, 8]. C_2H_4 was shown to adsorb in a single species on top of a Si(001)–(2×1) dimer [1, 56]. Two single domain Si(001) crystals were mounted at 7° grazing incidence rotated 90° around the surface normal. The grazing incidence X–ray spectrometer [61] was detecting X–ray emission with the propagation vector in the plane perpendicular to the incident beam axis and could be rotated around the beam axis. This setup allows to detect the X–ray emission in all three directions in space with respect to the single domain surface orientation. The polarization vector of the emitted photons lies in the plane perpendicular to the direction of detection. It is possible to separate the single polarization components assuming a linear combination of these contributions [45].

For the excitation of the resonant X–ray scattering spectra the bandwidth of the incident photons was set to $\sim$ 500 meV for ethylene ($\sim$ 250 meV for benzene). The overall instrumental resolution of the X–ray emission spectra was $\sim$ 1 eV ($\sim$ 470 meV). All respective values in this work denote the full–width–at–half–maximum (FWHM).

Calculations

We have simulated the RIXS spectral profile on the base of the ground state interpretation applying the theory of polarization resolved RIXS with selective resonant excitation [31]. Computations of the valence and virtual transition moments were performed in the dipole approximation and have been done within the framework of the density functional theory (DFT) using the StoBe code [144]. The transition energies were taken directly from the ground state Kohn-Sham orbital energies. The substrate was in the case of C_6H_6 represented by a $Si_{17}H_{20}$ cluster model with the molecule absorbed in the structure from Hennies et al.

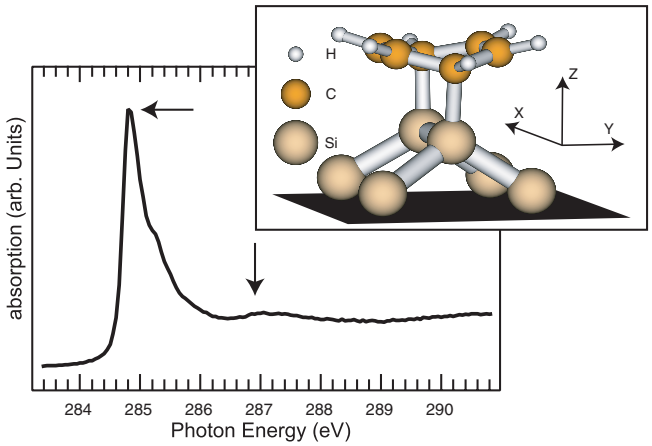

Figure 5.7: X–ray absorption spectrum of C_6H_6 / Si(001). The polarization vector of the incident photon is aligned along the z direction. The arrows indicate the excitation energies chosen for the RIXS. The inset shows the adsorption configuration with the reference frame used in this work.

[8]. C_2H_4 was modeled on a $Si_{77}H_{76}$ cluster in the C_{2v} configuration obtained from DFT slab calculations by Birkenheuer et al. [56]. The three layers silicon cluster contains a central subunit of six Si atoms, which are described at the all-electron level and form the centers of the interaction with the chemisorbed ethylene. The surrounding Si atoms are described by using a four-electron modified core potential (MCP) model developed by Suzanne, et al. [174], here only the $3sp$ valence electrons are treated explicitly. Hydrogen atoms are introduced to the silicon cluster to saturate the Si atoms. The all-electron basis set for Si was the triplet-zeta valence polarization (TZVP) [175] in a generalized [$5s$,$4p$] contraction and with one added d function. For the benzene molecule we used for the carbon atom the TZVP in a generalized [$4s$,$3p$] contraction and with one added d function; while for hydrogen the primitive ($5s$) basis set from ref [176] was used contracted to [$3p$,$1s$], augmented with one p function. All calculation were done using the gradient corrected BP86 [177, 178] exchange and correlation potentials.

Results and Analysis: C_6H_6 / Si(001)

At first, we performed X–ray absorption spectroscopy (XAS) to determine the polarization resolved unoccupied valence density–of–states (DOS) of the adsorbate system (Fig. 5.7). The polarization vector of the incoming photon was aligned perpendicular to the surface. In this geometry excitation into π–type unoccupied orbitals is performed. C_6H_6 / Si(001) exhibits a strong π^* type resonance at

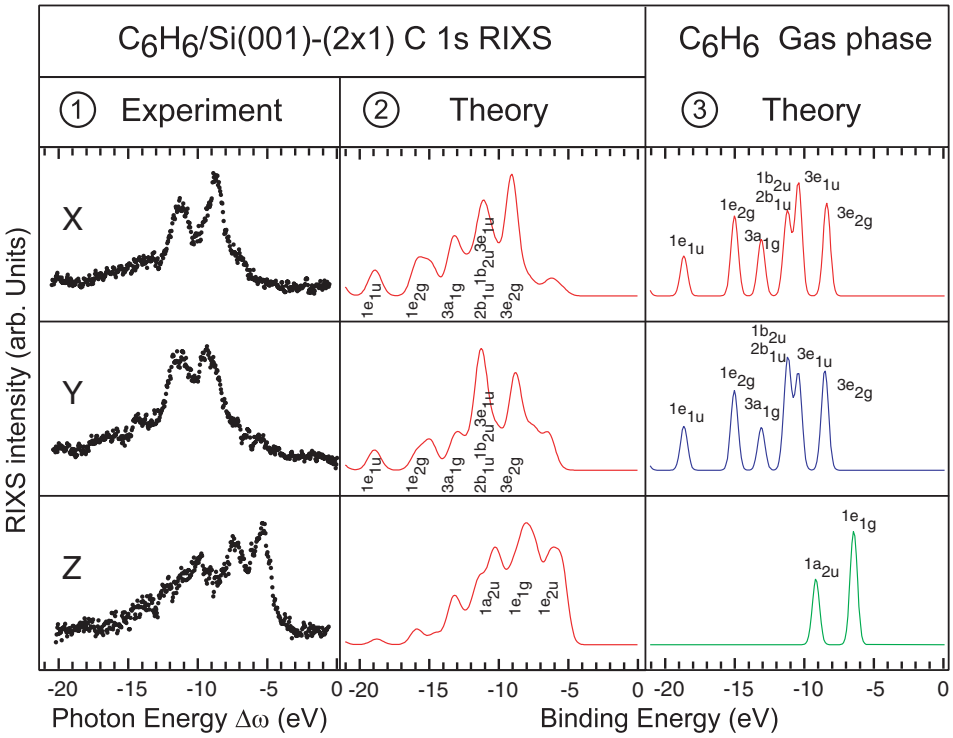

Figure 5.8: Polarization resolved carbon K–edge RIXS spectra of C_6H_6 / Si(001)–(2x1). Panel 1: Experimental data excited at 286.9eV. Panel 2: Calculations of the non–resonant scattering profile. Panel 3: Non–resonant calculations of gas–phase benzene [155].

284.8eV [2]. We have performed RIXS selectively exciting into this resonance and at 286.9eV, corresponding to excitation above this resonance.

In Fig. 5.8 panel 1 we show the polarization resolved RIXS spectra taken with an excitation energy of 286.9eV. The experimental RIXS data are plotted on a photon energy difference scale, indicating the difference in energy ($\Delta\omega$) between incoming (ω) and outgoing (ω') photon. The spectra for x, y, and z components show strong anisotropy, assuring the symmetry selectivity of the method and the ordering of the adsorbate. The x and y spectra, with the polarization vector lying in the surface plane, show the states with major σ contribution. The z spectra contain the out–of–plane polarization, and thus the π derived states. In order to assign and interpret the experimental data we have computed the polarization resolved non resonant X–ray emission spectra of C_6H_6 / Si(001) (Fig. 5.8 panel 2). Here, the energy scale denotes the binding energy. We get good agreement between experiment and theory[7] when the simulated spectra are convoluted with a gaussian of $\gamma = 0.5$ eV. In particular, the general shape and width of the

[7] At the time I hand in this thesis only calculations with an "butterfly" fold angle of 152° are available, which most probably do not reflect the perfect geometry. Nevertheless, the agreement

spectra is well modeled by the calculations. The broadening of the simulated spectra reflects the total instrumental broadening and the excitation bandwidth. The experimental broadening can also contain vibrational contributions.

The isolated benzene (C_6H_6) molecule has D_{6h} symmetry and the electronic ground state $|0\rangle$ configuration is $(1a_{1g})^2\ (1e_{1u})^4\ (1e_{2g})^4\ (1b_{1u})^2\ (1a_{1g})^2\ (2e_{1u})^4\ (2e_{2g})^4\ (3a_{1g})^2\ (1b_{2u})^2\ (2b_{1u})^2\ (3e_{1u})^4\ (1a_{2u})^2\ (3e_{2g})^4\ (1e_{1g})^4$. The HOMO ($1e_{1g}$) is a π orbital. The lowest unoccupied molecular orbitals ($1e_{2u}$) and ($1b_{2g}$) have π^* character. C_6H_6 has six symmetry adapted (near) degenerate core orbitals, two pairs of same symmetry. In the adsorbate, the symmetry is reduced to C_{2v}.

We use the gas phase (D_{6h}) notation tentatively assigning the spectral features as indicated in the figure, in order to illustrate the origin of the electronic states of the adsorbate system. We briefly summarize the differences in the electronic structure of C_6H_6 / Si(001) compared to the case of free benzene [155]. The x and y components do not change much, indicating that the σ system of benzene keeps its character upon adsorption. Clear changes occur in the spectral z component representing the "π" system. The π states $1a_{2u}$ and $1e_{2u}$ lower in energy and a strong contribution arises from the former π^* ($1e_{2u}$ LUMO), becoming partly occupied upon interaction with the substrate silicon dimer atoms. A slight σ–π mixing can be observed. A detailed discussion of the chemical bond formation of benzene on Si(001) can be found in [Paper VIII][8].

The RIXS profile for scattering 2.1 eV above the absorption resonance exhibits a definite non–resonant shape. This is comparable to the case of adsorbates on metals. We will now evaluate, how the choice of the intermediate state influences the scattering process. The excitation energy dependence of the polarization resolved RIXS for scattering into the π^* resonance and above we show in Fig. 5.9. Panel 2 contains the RIXS spectra recorded with an excitation energy of 286.9eV as discussed above. Panel 1 contains RIXS spectra taken with resonant excitation into the π^* resonance at 284.8eV. We see a clear excitation energy dependence of the RIXS spectral shape mostly pronounced for the x and z components. The $3e_{2g}$ state in the x spectra and the $1e_{1g}$ and $1e_{2u}$ states in z decrease in intensity when scattering into the π^* resonance. The spectral features in both x and z are significantly broadened upon resonant excitation, causing a merging of the states in the z component. These states can clearly be separated when scattering at the higher energy. The y states undergo only subtle modifications, neither intensity changes nor a clear broadening can be observed.

We have performed calculations based on the theory developed in [31] of the RIXS spectra for selective excitation into the π^* resonance taking interference between degenerate core orbitals into account. In Fig. 5.10 we show the com-

is already very good. It is intended to perform additional simulations before submission of this paper.

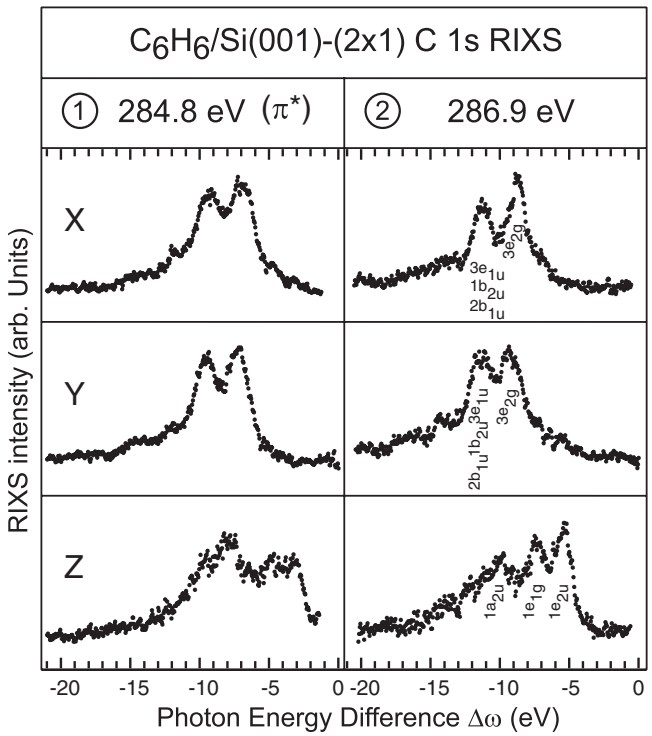

Figure 5.9: Excitation energy dependence of the experimental K–edge RIXS spectra of C_6H_6 / Si(001).

puted resonant spectra. In the x and z component, we have observed significant changes in the experimental data. We find the main spectral changes when scattering at the π^* reflected by the calculations, namely the enhancement of states derived from *ungerade* orbitals. The simulations verify the selective character of the resonant excitation into the LUMO π^*.

So far we have analyzed the excitation energy dependence of the shape and intensity of single features, but not their energy position. The scattering simulations only account for the intensity changes arising from the selective excitation. The energy position of a spectral feature in the ground state model is always the same and thus independent from the excitation. In the simulations (Fig's. 5.8 and 5.10), in principle no energy dispersion can be observed. In the experiment, a dependence of the emission energy from the excitation energy can be seen. The difference between the two excitation energies is $\Delta E = 2.1eV$. The RIXS spectral features shift by 0.3eV in emission energy. Thus, they appear at 1.8eV higher photon energy difference (Fig. 5.9). This is a clear indication for additional loss processes that can be observed as an energy shift of the whole spectrum. They are neither electronic nor vibrational excitations in the benzene molecule. These

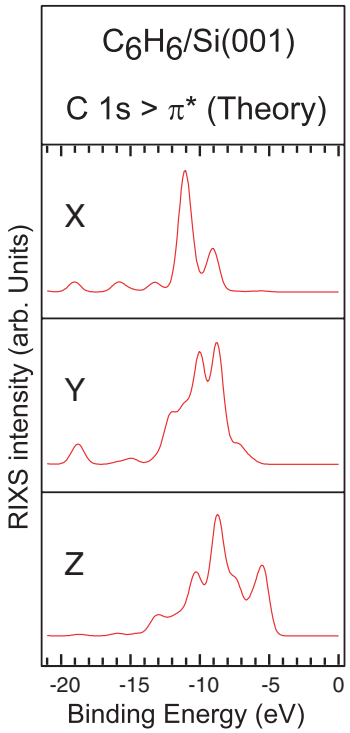

Figure 5.10: Resonant scattering simulation for excitation into the π^* of C_6H_6 / Si(001)–(2×1).

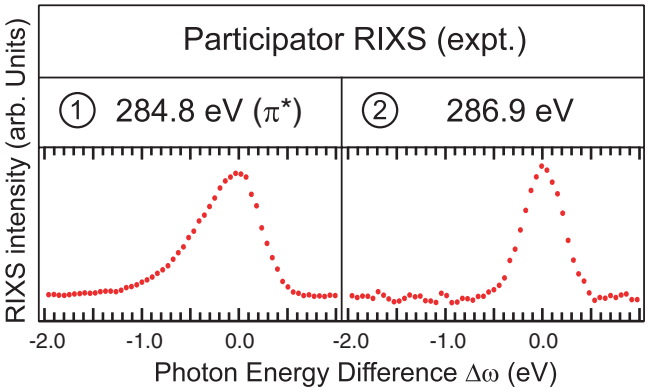

Figure 5.11: Participator channel in experimental K–edge RIXS spectra of C_6H_6 / Si(001). The scattering final state is the electronic ground state.

excitations could be identified in the spectra. The losses therefore have to belong to electronic or vibrational substrate excitations.

RIXS spectra consist of two qualitatively different parts. Additionally to the above discussed valence excited inelastic spectral features, a feature around 0 eV energy loss can be observed. This stems in the case of surface and bulk systems usually from elastic scattering of the incident photon beam and is nor-

mally removed from the data before analysis [6, 18, 164, 173, e.g.]. We have looked at the experimental excitation energy dependence of this feature (Fig. 5.11) in C_6H_6/Si(001). The "elastic" peak shows a significant excitation energy dependence. Scattering into the π^* resonance (panel 1) results in a clear asymmetric shape of the peak. When tuning the energy above the π^* absorption resonance, as in panel 2, the asymmetry is removed.

Results and Analysis: C_2H_4/Si(001)

A similar analysis has been performed for C_2H_4/Si(001). Fig. 5.12 shows the XAS spectrum [1]. In contrast to C_6H_6/Si(001), in the adsorbed ethylene molecule the π^* resonance looses its molecular character and splits into two contributions. We have performed RIXS selectively exciting into the two new resonances formed upon adsorption.

The isolated molecule C_2H_4 belongs to the symmetry group D_{2h} with the electronic configuration $(1a_g)^2(1b_{3u})^2(2a_g)^2(2b_{3u})^2(1b_{2u})^2(3a_g)^2(1b_{1g})^2(1b_{1u})^2$. Ethylene has two symmetry adapted, near–degenerate core orbitals, which result from the linear combination of the atomically localized C 1s orbitals. The MO $1b_{1u}$ is denoted as π orbital; the lowest unoccupied MO is $1b_{2g}$ (π^*). In the adsorbate, the symmetry is reduced to C_{2v}.

The polarization resolved RIXS spectra for scattering at the higher energy of 286.9eV we show in Fig. 5.13 panel 1 (footnote[8]). Here, too, a clear spatial anisotropy can be observed. Panel 2 contains the simulated polarization resolved non resonant X–ray emission spectra of this system, again revealing good agreement with the experiment. A tentative assignment of the spectral features following gas–phase notation (D_{2h}) is given in the figure. In ethylene, a strong σ–π mixing between states with x and z polarization can be observed. The y spectrum, containing the C–H binding states, changes less.

To further investigate the nature of the scattering process, RIXS has been performed with selective excitation into the two absorption resonances. In Fig. 5.14, the energy dependence of the RIXS spectra for scattering at two energies, 285.3 eV and 286.5 eV, is shown. The spectra show clear differences of the intensity of the observed spectral features between the excitation energies. For scattering at 285.3 eV, the π^* feature in the z spectra is clearly enhanced, with respect to the second excitation at higher energy. This is also the case for the $1b_{1g}$ peak in the y spectrum. In the x spectrum, a strong intensity gain is observed for the $1b_{1u}$ (π). At the same energy, some intensity fills into the high energy flank of the y spectrum.

[8] For the present work the symmetry deconvolution procedure for the ethylene spectra was carefully re–evaluated and yields slightly different results as in an analysis published earlier [6].

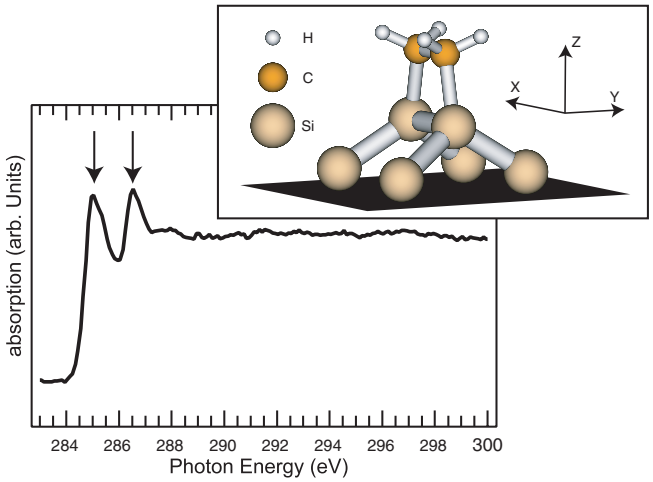

Figure 5.12: X–ray absorption spectrum of C_2H_4/Si(001). The polarization vector of the incident photon is aligned along the z direction. The arrows indicate the excitation energies chosen for the the RIXS. The inset shows the adsorption configuration with the reference frame used in this work.

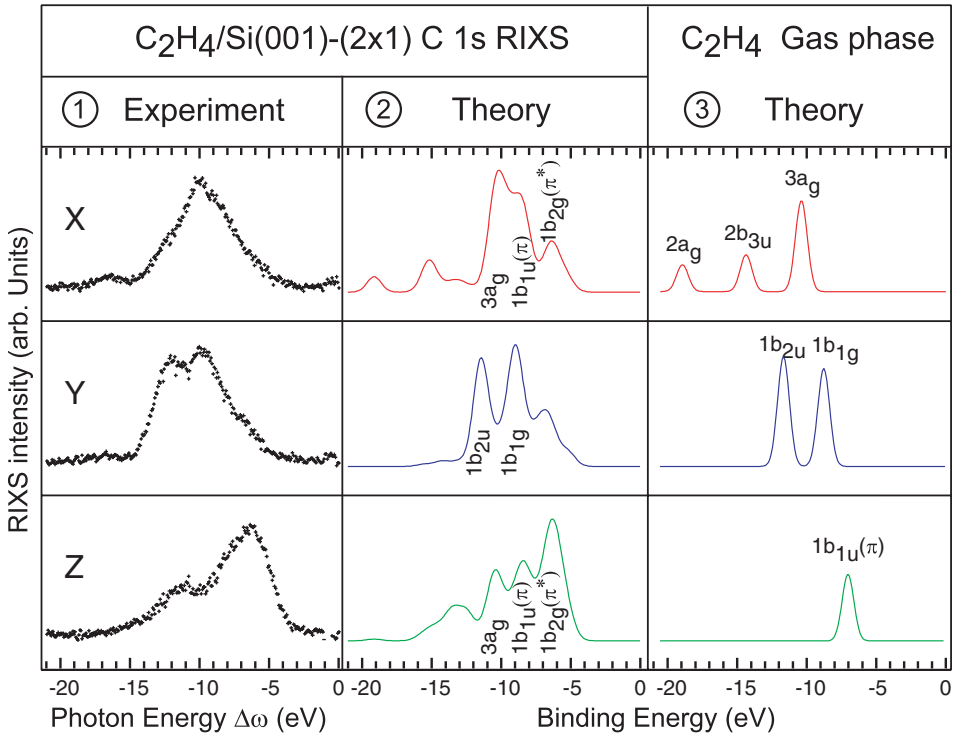

Figure 5.13: Polarization resolved carbon K–edge RIXS spectra of C_2H_4/Si(001)–(2x1). Panel 1: Experimental data excited at 286.5eV. Panel 2: Calculations of the non–resonant scattering profile. Panel 3: Non–resonant calculations of gas–phase ethylene [155].

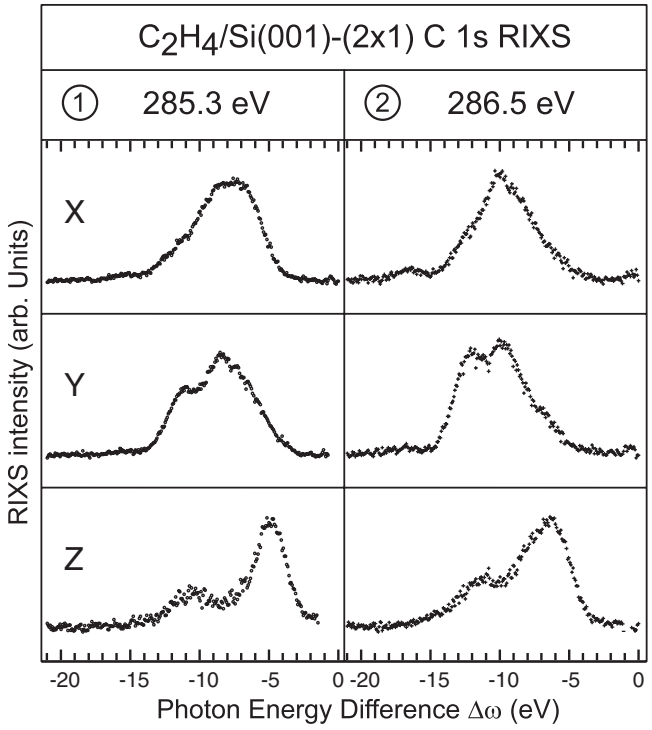

Figure 5.14: Excitation energy dependence of the experimental K–edge RIXS spectra of C_2H_4 / Si(001).

We performed resonant scattering simulations for selective excitation into the LUMO to model the experimental excitation of 285.3 eV. They are shown in Fig. 5.15. The $1b_{1g}$ feature with y polarization at -8 eV is strongly enhanced for excitation with 285.3 eV, as well as the π^* peak in z polarization, resembling the photon energy dependence of the experimental data. The observed differences in the x component are not reflected by the calculations.

The ethylene RIXS spectral features occur at constant emission energy, independent from their excitation energy. They thus shift in photon energy difference (Fig. 5.14) by exactly -1.2 eV, equaling the difference in excitation energy.

In Fig. 5.16 we show the elastic scattering at ethylene on silicon for excitation with the two different excitation energies. No significant changes in this feature can be observed.

Discussion and Conclusion

In both adsorbate systems, C_6H_6 / Si(001) and C_2H_4 / Si(001), the scattering profile for excitation at the higher energy is clearly non–resonant, as the comparison of experimental data, non–resonant, and resonant calculations reveals. This indicates that upon scattering at this energy a relaxed intermediate state is

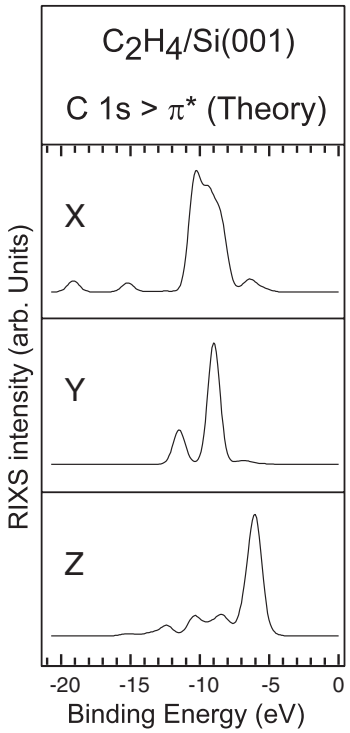

Figure 5.15: Resonant scattering simulation of carbon K-edge RIXS spectra of C_2H_4 / Si(001)–(2×1) excited with 285.3 eV.

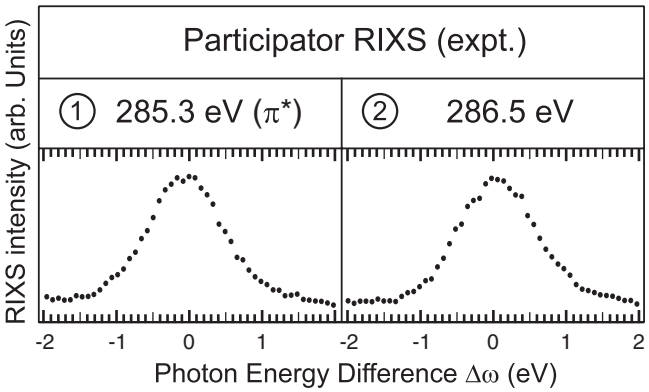

Figure 5.16: Elastic scattering in experimental K–edge RIXS spectra of C_4H_2 / Si(001).

reached, which carries no specific symmetry information. A similar observation has been made for adsorbates on metals [31, 45]. There always a fully relaxed intermediate state has been reached, independently from the excitation energy.

In the here observed semiconductor adsorbate systems, however, the RIXS profile is clearly excitation energy dependent. Scattering with the lower energy at the π^* resonance strongly enhances selected electronic final states, indicating

a preferred symmetry of the intermediate state. In the case of C_6H_6 / Si(001), the π^* ($1e_{2u}$) has *ungerade* character. Due to dipole selection rules the decay accordingly has to occur from *ungerade* valence orbitals to preserve the symmetry of the systems total wave function. These orbitals are enhanced upon resonant scattering. In the case of benzene on silicon thus, this interpretation using the symmetry of the molecular states of a free molecule works very well. The π^* ($1b_{2g}$) of C_2H_4 / Si(001) has *gerade* symmetry. Scattering at this resonance, nevertheless, enhances the $1b_{1u}$ (π) in x, the $1b_{1g}$ in y, and the $1b_{2g}$ (π^*) in z. Here the parity selection rule is obviously no longer valid. These states have a_1, a_2 and b_1 symmetry in the C_{2v} notation, respectively. Applying selection rules on the reduced adsorbate symmetry, the selectively excited unoccupied valence state has to be of b_1 symmetry. The first NEXAFS resonance (Fig. 5.12) at 285.3 eV can thus be attributed to have major $1b_{2g}$ (π^*) character.

In both systems, the intermediate state reached with the lower excitation energy has clearly a preferred symmetry. Benzene seems to keep its molecular character to a wide extend and the parity of the molecular states still influences the scattering. The ethylene molecule is stronger distorted upon adsorption and the parity of the orbitals is no longer defined. Instead, the symmetry selectivity of the resonant scattering can be explained invoking the orbital representations in the reduced adsorbate symmetry group.

The intermediate state reached by resonant excitation into the π^*, relaxes differently in both adsorbates. In ethylene on silicon, the emission features occur at constant emission energy. In benzene, the RIXS spectral profile shifts in energy with the excitation energy, even though not by the same amount.

The RIXS spectrum consists of two qualitatively different contributions, the participator or “elastic” band and the spectator or “inelastic” band. The participator scattering channel corresponds to the decay of the initially excited electron and leads to the electronic ground state. This feature is located at 0 eV energy loss (Fig’s. 5.11 and 5.16). The spectator channel is the scattering to valence electronically excited final states as shown in Fig’s 5.8, 5.9, 5.13 and 5.14. The resonant scattering participator channel of a free hydrocarbon contains energy loss features due to vibrational excitations (purely vibrational Raman), while the spectator channel contains combined electronic and vibrational excitations (vibronic Raman) [Paper IV][4]. The 0 eV feature in benzene exhibits a clear asymmetry upon resonant scattering. This asymmetry can only be due to vibrational loss processes. The intensity ratio between the peak maximum and the asymmetric tail indicates, that this feature has major participator character and only minor elastic scattering contribution. This is clear evidence for the initially excited electron to be still present at the time of the decay. At higher energy, the

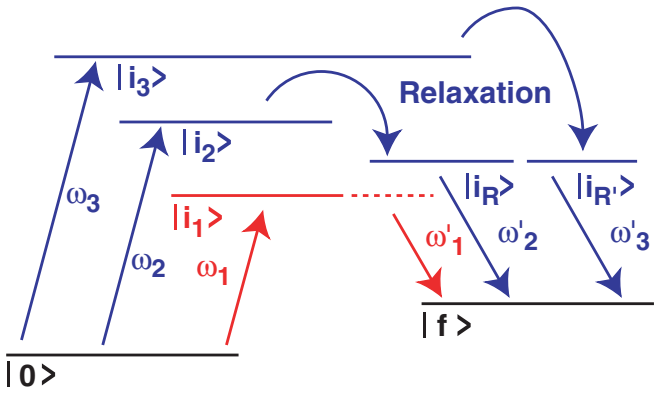

Figure 5.17: Simple model for the relaxation of the scattering intermediate state and energy balance of the scattering process.

asymmetry is lost in benzene, and the feature collapses to pure elastic scattering. In ethylene on silicon at neither energy a asymmetry can be observed.

We interpret these findings strictly phenomenologically and discuss them in a simple model as sketched in Fig. 5.17. In ethylene, the excitation energies correspond to ω_2 and ω_3 in the figure. In the absorption step the intermediate states $|i_2\rangle$ and $|i_3\rangle$ are reached. Both intermediate states relax, before the decay of the core excited state takes place. Defining $|\psi_{\mathrm{core}}^{-1}\pi^*\rangle = |i_2\rangle$ as the core–LUMO excitation, $|i_R\rangle$ is not fully symmetry relaxed and conserves the *gerade* character. The decay profile of this relaxed intermediate state has, thus, a preferred symmetry. The intermediate state $|i_3\rangle$ reached by higher excitation fully relaxes and $|i_{R'}\rangle$ has no specific symmetry. Both relaxed intermediate states are of the same energy, thus, the emission occurs at fixed energy ($\omega_2' = \omega_3'$).

In the benzene case, the intermediate state ($|\psi_{\mathrm{core}}^{-1}\pi^*\rangle = |i_1\rangle$) reached after resonant excitation directly decays and does not relax. After excitation above the resonance (ω_3) the intermediate state ($|i_3\rangle$) fully relaxes in energy and symmetry ($|i_{R'}\rangle$). The difference in emission energy corresponds to the energy difference of $|i_1\rangle$ and $|i_Res\rangle$, and, thus, does not equal the energy difference of the excitation.

The relaxation of the intermediate state is mediated by the substrate. The adsorbate–substrate interaction is differently strong for the two adsorption systems. In the case of ethylene [Paper I][1], the carbon atoms re–hybridize to a state near sp^3, and the molecular π system is destroyed upon adsorption. This strong interaction is reflected in the X–ray scattering and leads to a full energy relaxation of the intermediate state. The bond formation of benzene on silicon is different, the π system is retained and the carbon atoms binding to the surface are only slightly hybridized away from their gas–phase sp^2 state. This weak interaction accounts for the conservation of the scattering intermediate state.

The intermediate states lying higher in energy in both systems fully relax. Here, in the adsorption step multiple continuum states are excited. These states have a wide spatial extension and can overlap with the substrate conduction band states, opening various relaxation channels. Even in weakly interacting condensed molecules [Paper V][5], scattering at these states leads to a full relaxation of the intermediate state.

Comparing to adsorbates on metals, we seemingly have to invoke different relaxation mechanism. In metals, the bonding is carried by the d–states and the intermediate state relaxes trough metallic screening mediated by the itinerant metal sp–bands. A semiconductor has a different band structure. Near the adsorbate π–resonances, the substrate DOS has a band–gap. The whole substrate band–structure (s and p states) is involved in the surface chemical band. The relaxation there is mediated by the substrate chemical bond.

In the present study vibrational contributions have been identified in the resonant scattering spectra of a surface adsorbate (C_6H_6 / Si(001)) for the first time. Atomic center specific vibrational contributions are resonantly enhanced in RIXS [Paper IV][4], when the scattering intermediate state survives long enough for the excited nuclear wave packet to evolve. The participator asymmetry directly images scattering into carbon contributed ground state vibrational modes, the vibronic bands image vibrational properties of valence excited final states. With increased resolution, RIXS at this and similar systems could be utilized as an adsorbate and atom specific vibrational spectroscopy.

In the valence excited RIXS final states (Fig. 5.9) we find the vibrational profile reflected in the observed broadening of the states upon resonant excitation, causing the combined electronic and vibrational bands to merge and smear out. The vibrational envelope of one specific electronically excited final state can be wider than the spacing between the electronic final states. Upon scattering at the higher energy, the vibronic profile narrows and the states become clearly separable.

The scattering calculations of the resonant and non–resonant spectral profile resemble the experimental findings. The comparison of DFT based simulations and experimental data leads to the conclusion that by resonant scattering at the LUMO an intermediate state of preferred symmetry is reached and by positively detuned excitation the intermediate state relaxes in symmetry. The relaxation in energy and the vibrational band formation can not be accounted for in these computations. To investigate the relaxation process in greater detail, calculations of the surface density of states for the different adsorbate systems would be necessary to identify the screening and relaxation pathways. This could be done in band structure calculations performed in a solid–state code. The screening of excited electronic states in metal adsorbates depends on the surface projected

band structure [179, 180]. Although the semiconductor situation is different (as discussed above), it be can assumed, that the surface band structure here, too, influences the screening of the excited state. Furthermore, for the a bonding situation as in the present case, the surface band structure can be expected to be strongly influenced by the specific adsorbate. An extension of the theoretical treatment in this direction is a necessary next step.

Summarizing, we find the resonant inelastic X–ray scattering at adsorbate systems to be dependent on the specific system. Different substrates, but also the particular bonding situation, influences the characteristics of RIXS. To understand the relaxation mechanism in greater detail, an improved computational treatment is required.[9]

[9]**Acknowledgements:** This work was supported by the Access to Research Infrastructure (ARI) Program of the EU, the Swedish National Research council (VR) and the Deutsche Forschungsgemeinschaft (Grant DFG Fo343/1-1). M.N. acknowledges support from "Grant in aid of Japan Society of science fellows". Valuable support from Lisbeth Kjeldgaard and MAX-lab staff is gratefully acknowledged.

5.4 Bonding Configuration of Benzene adsorbed on Si(001)–(2×1) refined from Resonant Inelastic X–ray Scattering[10]

Abstract

The bonding configuration and electronic structure of benzene adsorbed on Si(001)–(2×1) is investigated with resonant inelastic X–ray scattering (RIXS). The two–step model of resonant soft X–ray spectroscopy implemented within the Density Functional Theory (DFT) framework is applied to simulate the non–resonant spectral profile. The aromatic system of the benzene molecule keeps its character to a wide extend upon adsorption. The comparison of experimental data and theoretical computations allows to determine the molecule to adsorb in a slightly folded "butterfly" configuration with an opening angle of near 152°.

Benzene is the smallest and simplest aromatic hydrocarbon and thus acts as a model adsorbate for the wider class of cyclic hydrocarbons interacting with semiconductor surfaces. Its interaction with the technologically important Si(001) surface has been subject of several studies [2, 57, 66, 109–114]. In these studies, there has been a long debate about the actual adsorption configuration of benzene on Si(001). The latest experimental studies [2, 111] prefer a distorted configuration in the so called "butterfly" structure, but the exact amount of distortion of the molecule upon adsorption could by now not experimentally be determined.

We present here a polarization resolved resonant inelastic X–ray scattering study of benzene adsorbed on the single domain Si(001)–(2×1) surface. RIXS is a tool allowing for a detailed investigation of the adsorbate specific valence electronic structure in a symmetry resolved manner [20, 31, 44, 45]. By comparison with simulated RIXS spectra obtained from density functional theory (DFT) [31, 155] we can examine different bonding configurations and determine the chemical bonding and exact geometric structure of the adsorbed molecule. By this, we try to refine the understanding of the adsorption configuration of benzene on Si(001).

The Si(001) surface exhibits a (2×1) reconstruction with two silicon surface atoms forming a Si dimer and, thus, saturating one dangling bond. One dangling bond per Si atom remains and accounts for the high reactivity of the surface. Taguchi et al. [66] have investigated the adsorption of benzene on

[10] *Paper in manuscript. This section is intended for publication as Paper VIII:* Hennies, Nagasono, Pietzsch, Witkowski, Piancastelli, Wurth, Triguero, and Föhlisch [8].

silicon in a combined thermal desorption spectroscopy (TDS), high resolution electron energy loss spectroscopy (HREELS) and low energy electron diffraction (LEED) study. They found the benzene molecule from the TDS to adsorb non–dissociatively with nearly one molecule per two Si dimers. The analysis of the C–H and C–C stretching frequencies, particularly the appearance of the existence of C=C double bonds reveals the presence of sp^2 and sp^3 hybridized C atoms in the adsorbed molecule. The LEED pattern gave strong evidence for the preservation of the Si dimers upon adsorption. The authors propose two possible adsorption models, a tilted structure in a 1,3–cyclohexadiene–like configuration and a structure in later work called "butterfly" that is 1,4–cyclohexadiene–like. The adsorbate–substrate bonding is believed to be established by two sp^3 hybridized carbon atoms forming di–σ bonds to the silicon dimer atoms. In theoretical investigations a long time no consensus could be achieved between the tilted [109], the butterfly [57], and a flat lying "pedestal" [57, 110] structure. A comparative experimental valence band photo emission (UPS) and DFT study [111] has preferred the "butterfly" structure and confirmed the di–σ bonds arising from the interaction of the C and Si π lobes building new bonding ("σ") orbitals. Contradictory findings from two independent scanning tunneling microscopy (STM) studies [112, 113] and a NEXAFS (near–edge X–ray absorption fine–structure) study [114], however, still left ambiguities about the real model. The "butterfly" structure has qualitatively been confirmed by our polarization resolved NEXAFS study [2], but, the NEXAFS does not allow to quantitatively determine the bonding configuration.

The "butterfly" model as proposed by Birkenheuer et al. [57] is depicted in Fig. 5.18. From the DFT structure optimizations the surface coordinated C_d

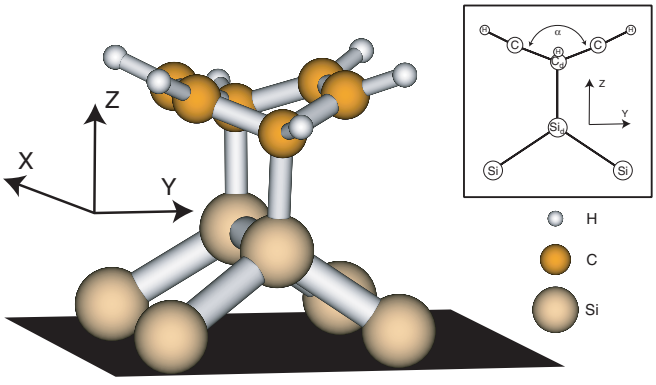

Figure 5.18: "Butterfly" adsorption configuration of C_6H_6 / Si(001) with the reference frame used in this work. The inset shows the structure in y–z–projection. α indicates the "fold–angle" of the "butterfly" and is in this figure set to 137° as proposed by Birkenheuer et al. [57].

atoms are found to be nearly sp^3 hybridized with their bond angles close to the ideal sp^3 hybridization angles. Gokhale et al. [111] have supported this model by comparison to UPS. The electronic valence structure of the adsorbed molecule reveals more similarities with 1,4–cyclohexadiene than with free gas–phase benzene. Other configurations, like the "pedestal" or "tilted", have been ruled out by, claiming that there the electronic structure is significantly different. The accuracy of this comparison facilitates a decision between the competing adsorption models, but can not evaluate details of a certain structure.

It is worth to mention that UPS only probes the overall valence structure of the adsorbate and the substrate. An advantage of our RIXS study over the UPS measurements is that we are able to resolve the adsorbate specific valence structure.

In the case of ethylene adsorbed on Si(001) we found in an other study that the C atoms strongly re–hybridize upon adsorption and that both the π and σ characters are completely distorted [1]. From TPD measurements it is known that benzene desorbs purely molecularly [66, 111] from Si(001) at about 200K lower temperatures than ethylene [75, 78] — which partly dissociates before desorption. The TPD indicates a much weaker interaction of the the Si(001) surface with the benzene molecule than with ethylene.

Experimental Setup and Data Treatment

The experiments have been performed at the Swedish national laboratory MAX-lab in Lund at beamline I511-1. The beamline is equipped with an end station operated in UHV dedicated for X–ray absorption spectroscopy (XAS), photoelectron spectroscopy (XPS) and X–ray emission spectroscopy (XES) measurements on adsorbate, surface and bulk samples. The station consists of a preparation chamber operated at a base pressure of low 10^{-10} torr connected to an analysis chamber (at mid 10^{-11} torr). The analysis chamber is equipped with a Scienta SES 200 hemispherical electron analyzer for XPS and constant final state XAS measurements. XES is detected with a grazing incidence soft X–ray fluorescence spectrometer [61]. The analysis chamber can be rotated allowing to choose the direction of detection freely in the plane perpendicular to the beam axis.

For the excitation of the resonant X–ray scattering spectra, the bandwidth of the incident photons was set to ~ 250 meV. The overall instrumental resolution of the X–ray emission spectra was ~ 470 meV. All respective values in this work denote the full–width–at–half–maximum (FWHM).

As substrate, we used P–doped silicon with a (2×1) single domain surface reconstruction. The (001) surface of Si crystals cut with an intentional 5° deviation of the surface normal from the [001] direction to the [110] direction exhibits

diatomic steps with terraces of 8.5 dimers width in a single (2x1) domain [100]. We mounted two samples with a 90° rotation around the surface normal with grazing incidence of the synchrotron light at an angle of 7° with respect to the surface plane. This setup allowed to measure angle resolved X–ray emission spectra with the direction of detection oriented normal to the surface and in the surface plane normal and parallel to the dimer axis.

To obtain a defect depleted, clean Si(001)–(2×1) surface, the crystals were first heated in the UHV at 800 K for 12 hours, followed by cycles of sputtering with xenon at room temperature and at 800 K with subsequent annealing to 1250 K. The surface ordering was checked with LEED and surface cleanliness was monitored with XPS. Saturated monolayers C_6H_6 were prepared by exposing the silicon substrate at room temperature to gaseous benzene at a pressure of $P = 5 \cdot 10^{-7}$ torr for 200 s.

The high purity liquid benzene was further purified by repeated freeze–pump–thaw cycles. Cleanliness of the adsorbate was assured by checking the vapor with a mass spectrometer. To avoid beam damage, the samples were scanned during the measurements and fresh systems were prepared in short intervals. XPS measurements assured that no photon induced reactions occurred in the adsorbate complex during measurements.

We have detected the X–ray emission in all three directions in space separately, corresponding to the propagation vector of the scattered photon. The polarization of the outgoing photon lies in a plane perpendicular to the direction of propagation. Each measured spectra in x, y and z direction thus represents a superposition of contributions with two polarization vectors, yz, xz and xy, respectively. Assuming a linear combination of these components, we can separate the single polarization components with a simple procedure [6, 45]. In the following, we will only discuss the separate components for each polarization.

Computational Details

In the present study, we apply the two–step model of resonant soft X–ray spectroscopy to simulate the non–resonant X–ray emission spectra [31, 155]. In order to evaluate the non–resonant X–ray emission spectra, it is necessary to compute the dipole transition moments between the valence and core orbitals, as well as the de–excitation energies. The calculation of these quantities is performed in the framework of DFT using the optimized Kohn–Sham SCF ground state orbital (DFT–Frozen approximation). All calculations are carried out with the StoBe program [144].

We used a silicon cluster to model the interaction of benzene with the (001)–(2×1) silicon surface. The silicon cluster contains seventeen silicon atoms. A

central subunit of six Si atoms, which are described at the all-electron level, forms the centers of the interaction with the adsorbed benzene. The surrounding Si atoms are described using a four-electron modified core potential (MCP) model developed by Suzanne, et al [174], here only the $3sp$ valence electrons are treated explicitly. The all–electron basis set for the central Si atoms was the triplet–zeta valence polarization (TZVP) [175] in a generalized [$5s$,$4p$] contraction and with one added d function. For the benzene molecule we used for the carbon atom the TZVP in a generalized [$4s$,$3p$] contraction and with one added d function; while for hydrogen the primitive ($5s$) basis set from ref [176] was used contracted to [$3p$,$1s$], augmented with one p function. The basis set described were used both for the geometry calculations and for the determination of the spectra. All calculation were done using the gradient corrected BP86 [177, 178] exchange and correlation potentials.

The starting configuration was taken from Birkenheuer et al. [57], based on their comparison of the simulated photoemission spectra and vibrational spectra. They arrive at the conclusion that the benzene forms an adsorption complex of local C_{2v} symmetry with one Si surface dimmer in a 1,4–cyclohexadine–like fashion and with the adsorbate plane parallel to the the surface. This structure is named the "butterfly" configuration. In the present study, we have further refined the butterfly configuration to account for the spectral features observed in the non–resonant experiment. This is done by varying the benzene plane angle. In Fig. 5.18 we show a projection of the adsorbate complex in the y–z–plane with the varied angle α indicated.

The coupling of the vibrational and electronic wave functions influences the RIXS process [4]. Upon resonant scattering in free molecules, the electronic spectral states evolve into broad bands with vibrational structure, which can merge and smear out the spectral envelope profile. Our analysis of the excitation energy dependence of RIXS of C_6H_6 / Si(001) — published in [7] — reveals that excitation at 286.9eV leads to an emission profile similar to the non–resonant case. By detuning from the absorption resonance — as it is the case for the spectra presented here — this vibrational structure collapses and the electronic character of the spectral states is restored to a wide extend. We can therefore base a reliable discussion of the data on a solely electronic interpretation of the data as expressed by the ground state interpretation DFT calculations.

Results and Analysis

The benzene molecule has D_{6h} symmetry and its electronic configuration in the ground state $|0\rangle$ is:

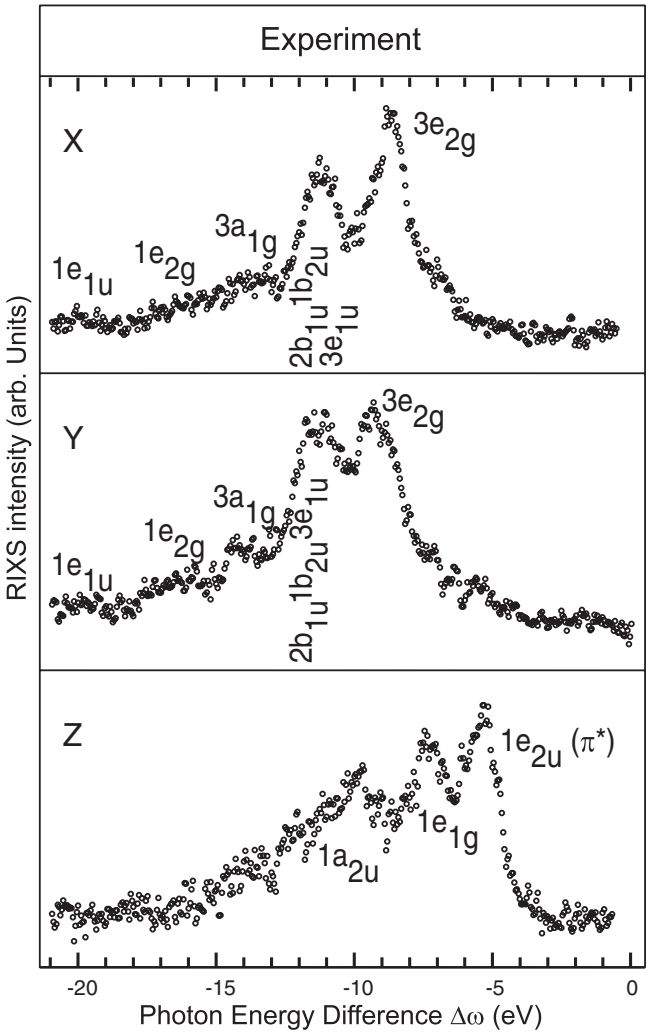

Figure 5.19: Polarization resolved carbon K–edge RIXS spectra of C_6H_6 / Si(001)–(2x1) excited at 286.9eV. The polarization vector of the outgoing photon reflects the orientation of the corresponding valence electronically excited final state.

$$\begin{aligned} \text{Core}: \quad & (1a_{1g})^2(1e_{1u})^2(1e_{2g})^4(1b_{1u})^2 \\ \text{Valence}: \quad & (1a_{1g})^2(2e_{1u})^4(2e_{2g})^4(3a_{1g})^2(1b_{2u})^2 \\ & (2b_{1u})^2(3e_{1u})^4(1a_{2u})^2(3e_{2g})^4(1e_{1g})^4 \end{aligned}$$

The highest occupied molecular orbital (HOMO) is the $1e_{1g}$ (π), the lowest unoccupied molecular orbitals have π^* character.

In Fig. 5.19, we show the polarization resolved RIXS spectra taken with an excitation energy of 286.9 eV. The data show strong polarization anisotropy. The x and y spectra, with the polarization vector lying in the surface plane,

show the states with major σ contribution. The z spectrum contains the out-of-plane polarization, and, thus, shows the π derived states. The x spectra show two intense broad features with maxima at -8.7 eV and -11.3 eV. The asymmetric shape of these two features indicate that they are composed of more than one contribution. The peak at -8.7 eV has a clearly visible high energy shoulder at -7 eV. Toward lower energies between -13 eV and -18 eV, a broad and decreasing band of states shows up. The spectra with y polarization show similar states with different intensity distribution. At low energies, two maxima at -16.5 eV and -14.5 eV are distinguishable. The feature at -11.3 eV is broader as in the x polarization. For y polarization, the higher energy feature has its maximum at -9.3 eV. The high energy shoulder of this peak is broader and more intense than for x polarization. The spectra with z polarization show a different set of features. We can distinguish three clear maxima with decreasing intensity from -5.2 eV, -6.3 eV, to -10 eV. At the lower energy side a band of states is visible with decreasing intensity down to -14 eV.

To assist in the assigning and in the interpretation of the experimental data, we compute the polarization resolved non–resonant X–ray emission spectra of C_6H_6 / Si(001) (Fig. 5.20). We get good agreement between experiment (Fig. 5.19) and theory (Fig. 5.20). In particular, the shape of the spectra with the main features discussed above is reflected by the calculations. To facilitate the discussion we have plotted the symmetry resolved XES spectra of free Benzene (dashed lines) beneath the adsorbate spectra. We use the gas phase (D_{6h}) notation to keep the discussion simple and to illustrate the origin of the electronic states of the adsorbate system. The peak assignment presented here bases on an in–detail analysis of those molecular orbitals contributing to the calculated spectra with a large dipole transition moment. We concentrate on the states that can be clearly identified in the experimental spectra.

We start our discussion with the low energy features at -19 eV, -15.5 eV, and -12 eV, which are derived from the $1e_{1u}$, $1e_{2g}$, and $3a_{1g}$ states, respectively. These features change their position and shape only little upon adsorption. The degeneracy of the $1e_{1u}$ and $1e_{2g}$ states is lifted and they split by 0.5 eV and 1 eV, respectively. In the case of free benzene all these are pure in–plane states. In the adsorbate calculations a clear out–of–plane component (z polarization) can be observed. Comparing with the experimental data, we find the admixture of the lower two states $1e_{1u}$ and $1e_{2g}$ to the z spectra clearly overestimated by the simulation, whereas the z intensity of the $3a_{1g}$ feature is reproduced correctly. The higher energy features between -12 eV and -5 eV are discussed for in–plane and out–of–plane polarization separately.

In x and y polarization, features at -11 eV, -9 eV, and -6 eV can be identified. The peak at ~ -11 eV stems from the $1b_{2u}$, $2b_{1u}$, and $3e_{1u}$ orbitals. The degeneracy

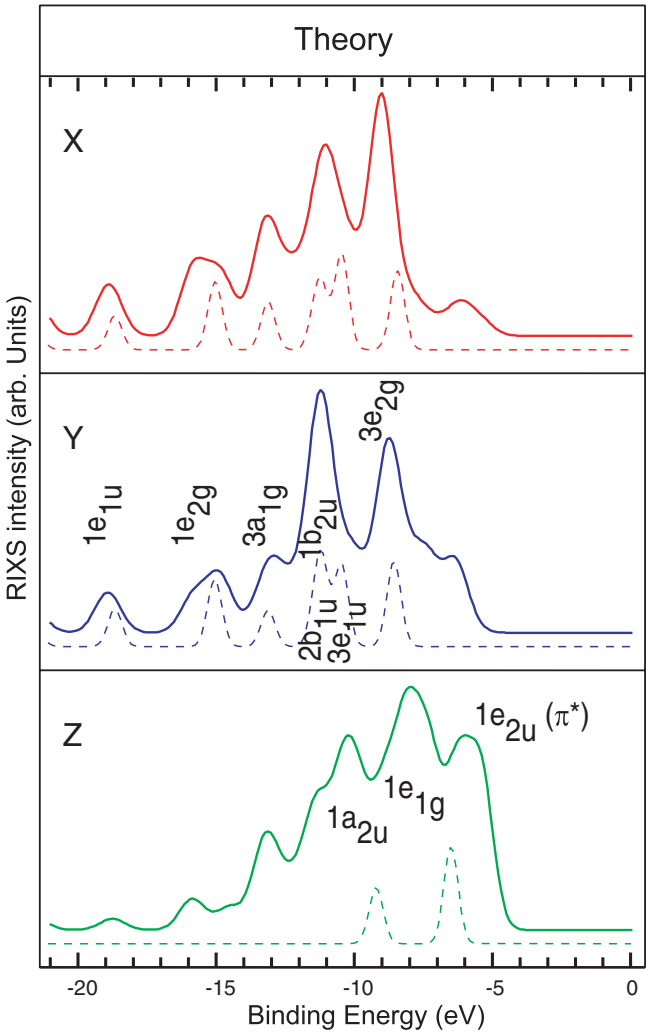

Figure 5.20: Calculated polarization resolved non–resonant X–ray emission spectra of a C_{2v} C_6H_6 / $Si_{17}H_{20}$ cluster modeling the adsorption on Si(001)–(2x1) (solid lines). The fold angle α was set to 152°. Beneath each spectra we show the calculated corresponding components of the X–ray emission from free benzene (dashed lines). The peak assignment follows gas phase notation.

of the $3e_{1u}$ is lifted and all these states split into overlapping bands of states in the region of -12.2 eV to -9.7 eV. The y spectrum has some ($\approx 10\%$) additional contribution from the $1a_{2u}$ (π) at this energies. The peak at ~ -9 eV only contains the former $3e_{2g}$ state.

Upon adsorption a new band of states occurs at -6 eV. It has a different origin in the x and y component. The y contributions stem from the former $3e_{2g}$ and $3e_{1u}$ orbitals, the x spectra is composed of $3e_{2g}$ and has some admixture from the formerly unoccupied LUMO $1e_{2u}$. This band is a little stronger pronounced in the calculations compared to the experimental data.

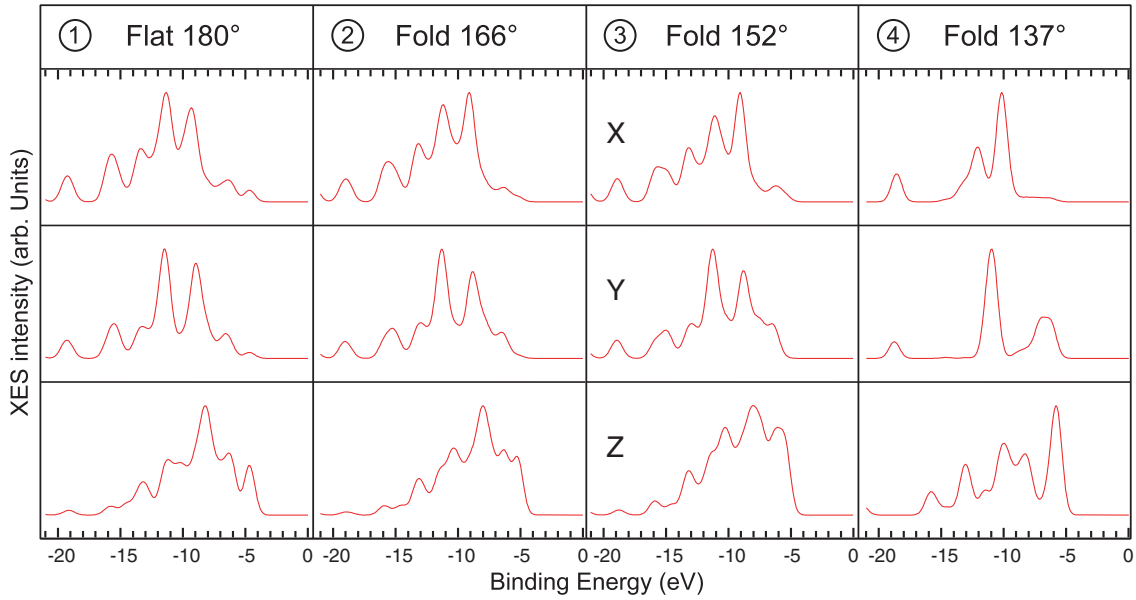

Figure 5.21: Variation of the adsorbate configuration. Each panel contains the calculated spectra (similar to Fig. 5.20) for the indicated value of the "butterfly" fold angle of the adsorbed benzene molecule.

The z spectrum exhibits three peaks at -10.3 eV, -8 eV, and -6 eV and a shoulder at -11.3 eV. This shoulder stems from the $3e_{1u}$, the peak at -10.3 eV from the $1a_{2u}$. The feature at -8 eV has mainly $1e_{1g}$ character. To this also the $3e_{1u}$, $1a_{2u}$, and $3e_{2g}$ contribute, in decreasing amount. The feature centered at -6 eV contains major contributions from the LUMO $1e_{2u}$ and the $3e_{1u}$ and some minor ones from the $3e_{2g}$.

The analysis of experimental data and theoretical simulations shows a strong in–plane anisotropy and only a weak mixing of π derived states into the in–plane x and y polarizations. Previous studies [57, 181] have analyzed the adsorption of benzene on different substrates, both metals and semiconductors, resulting in different possible stable chemisorption structures. These structures differ mainly in the degree of re–hybridization within the benzene molecule upon chemisorption. This degree of internal re–hybridization is strongly related to the "fold" angle of the benzene molecule. In the case of XES, it gives rise to a σ–π symmetry breaking with an altered angular dependence for the emitted X–ray photons [181].

In Fig. 5.21, we show the computed polarization resolved non–resonant XES spectra for four different fold angles, 180°, 166°, 152°, and 137°. 180° corresponds to an adsorbed planar molecule, where the H atoms are slightly lifted away from the surface. Comparing the calculations for 180°, 166°, and 152°, we see a rather similar general trend in the spectral shape with some changes

in intensity. Particularly, the intensity ratio between the most intense peaks in x and z polarization shows strong variations, as well as the spectral region between -5 eV and -10 eV in the z component. The spectra with a fold angle of 137° show a significantly different signature. The spectral shape of all three spatial components changes drastically compared to the less distorted geometries. The double peak structure at ~ -9 eV and ~ -11 eV changes significant in x polarization and vanishes in the y spectrum. The π^* contribution to the y and z spectrum is strongly enhanced. The best agreement between experiment and simulations is obtained for the spectra calculated with a fold angle of 152°.

The character of the surface chemical bonding is reflected in the occupied as well as in the unoccupied valence density of states. In Fig. 5.22, we show a carbon K-edge XAS spectrum of C_6H_6 / Si(001) from [2], resolving the atom specific unoccupied valence states with out–of–plane orientation. The system exhibits a strong π^* resonance, comparable to the case of free benzene, also indicating that the nature of the aromatic π–system is conserved to a wide extend.

Discussion

The absorption of the benzene molecule onto the Silicon substrate is found to have different influence on the in-plane and out-of-plane electronic states. The profile of the z polarized spectrum changes significantly. The in-plane-states of adsorbed benzene, visible with x and y polarization, keep to a large extend their gas phase spectroscopic appearance. By taking a closer look at the molecular orbital plots, we can obtain further information about the interaction and therefore the orbital character reflected in the spectral features. We can separate two effects: A change of the states within one symmetry and a mixing of states of different symmetry. For simplicity reasons we keep gas phase notation, therefore

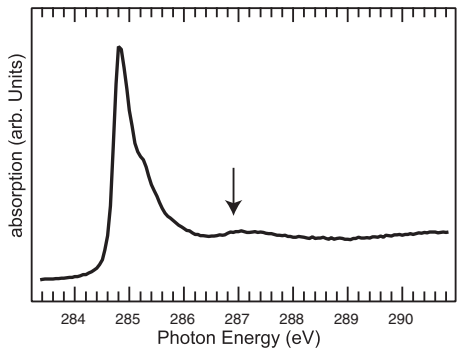

Figure 5.22: Carbon K–edge NEXAFS of C_6H_6 / Si(001)-(2x1). The polarization vector of the incident light has been aligned along the z axis. RIXS was performed at the energy indicated by the arrow.

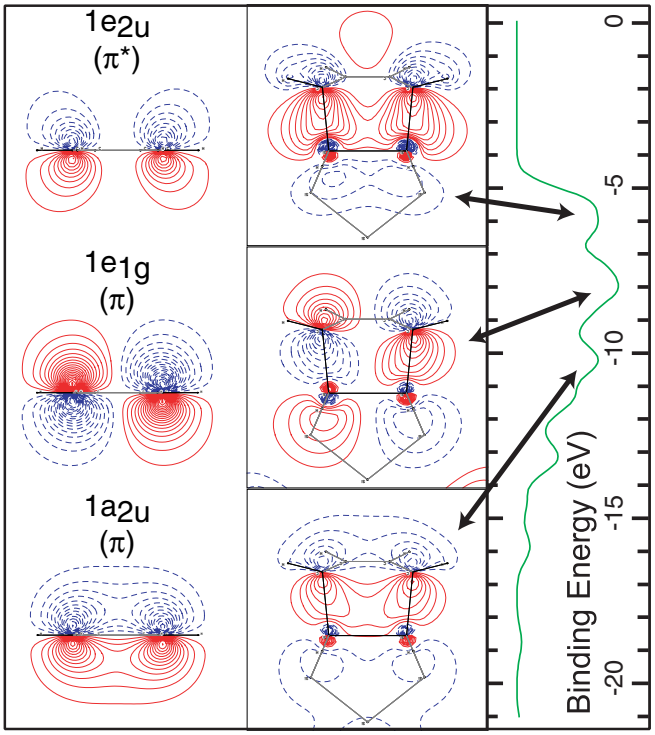

Figure 5.23: Comparison of the π–orbitals of benzene in gas–phase (left) and adsorbed on Si(001) (middle). The right panel shows the z component of the calculated RIXS spectra and indicates the binding energy of the according orbitals. The plane of projection is the x–z–plane with the substrate coordinated C_d atoms and the Si dimer atoms.

the in–plane states are denoted as σ states and the out–of–plane are denoted π states.

In the z spectrum the spectral features change strongly. The π states $1a_{2u}$ and $1e_{1g}$ move significantly toward lower energies. The π^* — unoccupied in free benzene — becomes partly occupied. These changes are clearly induced by the interaction with the substrate as comprised in the established Dewar [165] and Chatt and Duncansson model (DCD) [166] or by the alternative "spin–uncoupling" description [182].

The π/π^* states form strong bonding combinations with the Si $3p_z$ orbitals. In Fig. 5.23 we show molecular orbital plots of the $1a_{2u}$, $1e_{1g}$, and $1e_{2u}$ states interacting with the silicon surface. The $1a_{2u}$ (π) in the lowest panel hybridizes with the substrate p state to a combination bonding vertically between adsorbate and substrate and laterally within the C ring and between the Si dimer atoms. Going higher in energy, the $1e_{1g}$ (π) is found to be strongly bonding in the adsorbate complex, but anti–bonding between the C_d and the Si_d atoms, respectively. The $1e_{2u}$ (π^*), which has become occupied upon adsorption, forms a combina-

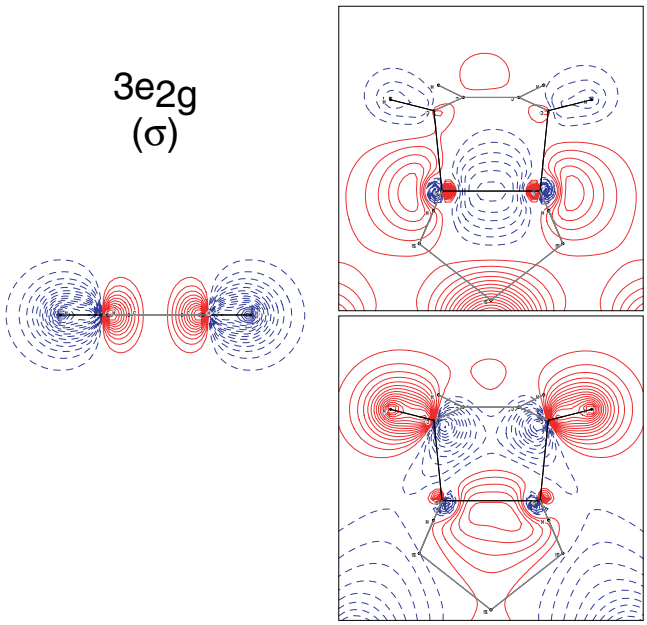

Figure 5.24: Comparison of the $3e_{2g}$ (σ)–orbital of benzene in gas–phase (left) and adsorbed on Si(001) (right). The plane of projection is the x–z–plane with the substrate coordinated C_d atoms and the Si dimer atoms.

tion binding within the adsorbate complex, within the C ring, and between the Si dimer.

These orbitals strongly interact with the substrate, but keep their molecular character to a wide extend, as a comparison of the molecular orbital plots of the free molecule and the adsorbate reveals. This is compliant with the unoccupied valence structure of adsorbed benzene as can be seen from the XAS data [2] (Fig. 5.22). Here the π^* resonance is nearly unperturbed compared to the free molecule.

The main changes of the x and y spectra are due to a rearrangement of the σ states and, where applicable, the removal of their degeneracy. These states barely change their energy position. The changes within the σ can be understood as a consequence of internal re–hydridization leading to changes of the molecular symmetry. Upon absorption the molecular symmetry reduces from D_{6h} to C_{2v}, thus, the partly degenerate σ states mix and rearrange. Nevertheless, these changes do not alter significantly the overall character of the σ–states. Some admixture of π and π^* states to the in–plane states can be observed. y gets some π and x gets some contribution from π^*. As we see from the fold–angle dependence (Fig. 5.21), the π–admixture to the y polarization stems from the inward fold of the π–lobes and increases with stronger folding. The π^* appear-

Table 5.1: Optimized parameters for the "butterfly" adsorption structure of C_6H_6 / Si(001) refined in this work by comparison of calculated and experimental RIXS spectra and obtained from "first principles" calculations reported by Birkenheuer et al. [57]

Property	This work	Birkenheuer et al. [57]
$\angle(CC_dC)$	117.9	109.9
$\angle(CC_dSi_d)$	99.5	104.8
$\angle$ dihedral α	152.0	$\sim$137.0[11]

ance in the x component on the other hand is due to the interaction with the substrate and reflects that the Si-C bond is inwardly oriented along the x axis.

In Fig. 5.24 two sample orbitals arising from the $3e_{2g}$ (σ) interacting with the silicon substrate atoms are sketched. They are very similar to the free benzene orbitals. They polarize in the presence of the silicon surface, due to the repulsive interaction with the substrate states. This results in the upward lift of the H atoms. The lower panel shows a bonding combination with the Si $3p_x$ orbitals. They are partly hybridized with the Si $3s$ orbitals, resulting in a slight rotation of the p_x lobes. The upper panel shows a combination basically non–bonding of the nearly undistorted σ states of adsorbate and substrate. Both plots illustrate the σ–π mixing in the adsorbed benzene as well as in the silicon substrate.

We find the admixture of out–of–plane (z) states to the in–plane (x and y) polarizations not perfectly modeled by the simulations compared to the experimental data. The π/π^* contribution is overestimated. The in–plane states at higher binding energy broaden in the calculations due to a removal of their degeneracy, but still occur as separate features. In the experimental data instead, these states build a broad, not separable band. These states have wide lateral dimensions in the adsorbate layer as well as in the substrate. This sets limits to their calculation in the confined cluster model. The out–of–plane states are found to be represented much better in the simulations. These states have strong local character (Fig. 5.23). Since they carry the surface chemical bond, an analysis of the bonding mechanism can be relied on this simulations.

The computational variation of the fold angle and the good agreement with the experimental data allows us to refine the adsorption configuration of benzene adsorbed on Si(001). The fold angle in the butterfly configuration has,

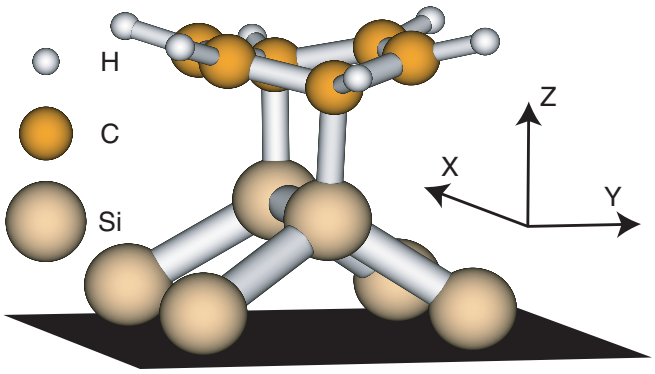

Figure 5.25: Adsorption model of C_6H_6 on Si(001)–(2×1) in the flattened "butterfly" configuration as evaluated in the present paper.

according to our finding, to be close or above 152°[12]. This finding differs from the geometry reported by Birkenheuer et al. [57] with a fold angle of 137°. In Tab. 5.1 the parameters optimized in our work are listed. When calculating the RIXS spectra in the strongly distorted geometry proposed there, we find e.g. the π^* contribution to the spectra with y and z polarization strongly enhanced. This indicates a very strong π^* back–donation in the chemisorption process, a fact not reflected in the experimental X–ray emission spectra. Furthermore, the σ states change completely compared to the free molecule in this strong folded configuration and appear significantly different in x and in y polarization, both not observable in the experimental spectra.

Conclusion

Our investigation of the electronic structure of benzene adsorbed on Si(001) allow us to provide a detailed picture of the adsorption of benzene on Si(001). From the spectroscopic finding, the molecule keeps its σ character to a wide extent and undergoes some modifications in the π system. The π^* orbital becomes occupied, π and π^* orbitals lower in energy. The π and π^* orbitals are mainly involved in the bonding. Although they hybridize with the Si $3p_x$ and $3p_z$ states, they keep their molecular character to a wide extend. We find a slight re–hybridization of the surface coordinated C_d atoms, as a result of the σ–π mixing and thus the folding of the molecule. The configuration is clearly not sp^3. Instead, the bond angles (Tab. 5.1) indicate a configuration close to sp^2.

[12] At the time I hand in this thesis only calculations with the values for α presented here are available. The optimal angle is most probably slightly smaller than 152°. Nevertheless, the agreement is already very good. It is intended to perform additional simulations before submission of this paper.

We have demonstrated that the RIXS spectroscopic signature is very sensitive to small changes in the adsorbate configuration, allowing us to systematically optimize the adsorbate geometry. We find the wings of the "butterfly" flapped toward the horizontal with a dihedral angle α of 152°.[13]

[13]**Acknowledgements:** This work was supported by the Access to Research Infrastructure (ARI) Program and the Deutsche Forschungsgemeinschaft (Grant DFG Fo343/1-1). M.N. acknowledges support from "Grant in aid of Japan Society of science fellows". Valuable support from Lisbeth Kjeldgaard and MAXlab staff is gratefully acknowledged.

5.5 Summary: Small hydrocarbons adsorbed on different surfaces

In the preceding papers, I have discussed the electronic structure and bonding of ethylene and benzene on Si(001). Scattering at hydrocarbons adsorbed on silicon above threshold can be described in pure ground–state X–ray emission calculations. By this means, the symmetry and polarization resolved atom specific electronic valence structure can be obtained. This allows to check and improve the concepts describing the surface chemical bonds formed by ethylene and benzene on Si(001).

Both molecules bind to the substrate in a similar manner, but with different strength. The bonding is formed by a hybridization of the σ and π orbitals of the adsorbate with the Si $3p_{x,z}$ and $3s$ states. The formerly unoccupied π^* orbital of ethylene and benzene becomes partly occupied upon adsorption. For the bonding of ethylene, the simple concept of an interaction involving only the π orbitals of adsorbate and substrate [98] has been replaced by a detailed description of the changes in both σ and π systems. The character of the π system is completely lost upon adsorption. A strong mixing of σ and π character can bee seen. In the benzene molecule, a distortion is evident. However, the spectral signature differs only in the π^* states significantly from the free molecule. Only little σ–π mixing can be observed. The carbon atoms that bind to the surface Si atoms are only slightly hybridized away from the gas–phase sp^2 state.

The interaction of small hydrocarbon molecules with transition metal surfaces has successfully been interpreted in the Dewar [165] and Chatt and Duncanson (DCD) model [166]. Here, the prototype system is ethylene on Cu(110) [148]. This concept has been extended to other molecules and metal surfaces [148, 164, 183]. In the DCD model, the surface chemical bond is formed by a donation/back–donation mechanism involving the “frontier orbitals” of adsorbate and substrate. Molecular π electrons are donated into the metal, while electrons from the metallic d–states are back–donated into the unoccupied anti–bonding molecular π^* orbital. The donation/back–donation is accompanied by a σ–π mixing. This causes the H atoms to lift upwards out of the surface plane. The bonding mechanism includes, strictly spoken, not only the “frontier” π orbitals of ethylene, but also the σ states by re–hybridization.

The hydrocarbon molecules adsorbed on silicon are stronger distorted than on metal. In ethylene, the H atoms are lifted higher away from the surface. The benzene molecule is not planar, as in the case of a metal adsorbate, but folded like a “butterfly”. In both molecules, the degree of re–hybridization and the amount of donation/back–donation is higher than in the Cu adsorbate. σ and π states mix in the spectra stronger than in the metal case. In the hydrocarbon

bonding to the silicon substrate, not only the silicon "frontier" $3p_{x,z}$, but also the $3s$ orbitals are involved. This indicates a re–hybridization also of the substrate states.

The DCD model, thus, can be invoked to describe the interaction of benzene with the Si(001) surface, where the internal changes in the adsorbate electronic valence structure can be approximated by a separate external π–interaction with the substrate in a donation/back–donation picture, accompanied by a σ–π mixing leading to a internal configuration change in the geometry of the adsorbate. In ethylene on silicon the electronic structure of adsorbate and substrate changes too much, to be satisfyingly described in a frontier orbital approach.

Chapter 6

Summary: Coherence in resonant inelastic X–ray scattering

For the modeling and interpretation of a specific RIXS experiment, one decision has to be made: Is it necessary to treat the scattering process fully coherent in an one–step description, or is an approximation justified? In nearly all systems but the simplest molecules, a one–step full scattering description is up to now virtually impossible. In most cases, it therefore has to be decided whether an approximated description is appropriate. The scattering itself coherently links the initial and final states. In other words, the symmetry of the total wave function and the energy are naturally conserved. But it is possible to observe a loss of coherence — i.e. a loss of information between incoming and outgoing photon. In this case, the initial excitation has relaxed in the system. The information about the participator electron is lost and the scattering final state cannot fully be described. The case of a scattering process appearing coherent is usually called resonant. This case is characterized by the possibility to derive the full symmetry and energy information of the scattering final state from the incoming and outgoing photon. The case where the specific information about the incoming photon is lost in the scattering profile is called non–resonant.

In this thesis, I have presented RIXS of hydrocarbon molecules. The nature of the scattering process depends on the sample and the type of excitation of the system. In the case of weakly interacting condensed molecules, the scattering at a molecular resonance appears to be fully resonant. Scattering at close lying continuum states at higher energies shows strong non–resonant behavior. Upon resonant scattering, the intermediate state dynamics in the nuclear wave function govern the scattering process. The spectral profile becomes deter-

mined by the formation of broad vibrational bands. Vibronic coupling changes the selection rules for the allowed electronic scattering transitions. An one–step treatment considering the electronic and nuclear wave function has been successfully applied.

I want to emphasize that vibrational effects can always influence the scattering profile. This is in principle independent from the intermediate state scattering dynamics and the kind of theoretical model applied to the scattering process. But — as pointed out in Paper IV — only under certain conditions, the vibrational contributions can implicitly be treated as a broadening of the electronic spectral states. In this case a pure electronic treatment is appropriate. This situation can be found for detuned excitation in free molecules, for non–resonant scattering at semiconductor adsorbates or in the case of metal adsorbates. In the free molecules, the changes of the nuclear wave function in the resonant scattering intermediate state are so strong that the vibrational band formation becomes constitutive for the spectral profile. In this case, the nuclear wave function has to be explicitly treated in the scattering description. This is the reason why the demand for a one–step treatment and for the consideration of the total wave function accompany each other in the systems presented here.

A similar observation has been made for hydrocarbons adsorbed on Si(001). Tuning the incident photon energy into the first molecular resonance leads to clear resonant contributions to the scattering profile. This makes at least a treatment in the coupled two–step model (TSII [30, 31]) necessary. In the case of C_6H_6 / Si(001), a full one–step description including vibrational effects would be desirable. If the incident photon energy is increased over the X–ray absorption edge, the scattering profile becomes non–resonant and can be described in pure ground state X–ray emission calculations.

In the case of transition metal adsorbates the scattering profile matches the non–resonant case, independent of the excitation energy [45]. This is explained by the fact that due to the fast screening in a metallic adsorbate system always a fully relaxed — and thus always the same — intermediate state is reached. The specific information of the incident photon is lost into the substrate on a time scale much faster than the scattering process. A rough estimate can be made of this effect. The C $1s$ core hole lifetime is ~ 6 fs [184]. Tuning the incident photon energy into the resonance makes the scattering duration time ~ 6 fs, too. For CO adsorbed on Ru the transfer time of an electron from the LUMO to the metal substrate has been determined to be 0.6 fs [168]. Independent of the excitation energy, always a fully relaxed intermediate state is reached. This state carries neither energy nor symmetry information about the initially exciting photon. Thus, the emission profile is that of an ionized system. A detuning of the incident photon energy shortens the scattering duration time. A detuning

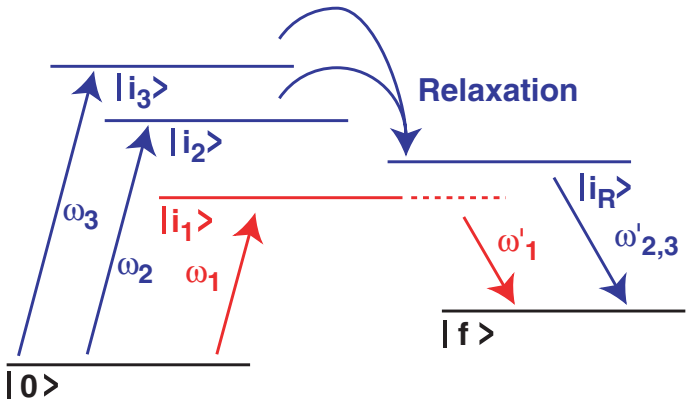

Figure 6.1: Relaxation model for scattering resonantly (ω_1) vs. non–resonantly (ω_2). The intermediate states $|i_2^n\rangle$ reached by ω_2 relax to $|i_R\rangle$.

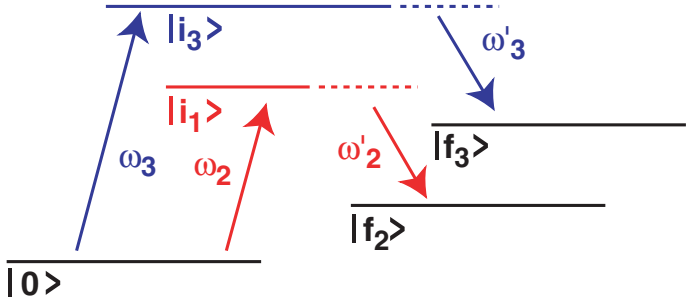

Figure 6.2: Continuum excitation model for scattering above the resonance.

of 1 eV e.g. would lead to a shortening by a factor of ten in the C $1s$ case. Turning back to the estimate given, this means that in such a detuned case, the scattering duration would have roughly the same time scale as the electron transfer process. This should have a significant influence on the scattering profile. However, no such data exists for adsorbates on metals.

In a free molecule and in the case of semiconductor adsorbates, the electron excited into the LUMO can not decay through such fast channels. When no relaxation can take place, the intermediate state survives long enough to determine the decay process. Thus, in the intermediate state both energy and symmetry of the excitation process is retained. Benzene and ethylene adsorbed on silicon show differences in the RIXS excitation energy dependence. These have in detail been discussed in Paper VII. In benzene, clear vibrational contributions to the resonant scattering profile have been observed; in ethylene, these could not be identified. In benzene, the emission energy of the electronically excited final states is different for resonant excitation and excitation above; in ethylene, it is not. Scattering at the higher lying continuum states has to be treated differently. In all cases — metal and semiconductor adsorbates and condensed molecules — the spectral profile matches the non–resonant one.

In the condensed molecules clear Raman scattering has been identified at the resonant and XES behavior exciting above. The case of adsorbed benzene

is similar. Two different pictures can be drawn to explain this behavior: The relaxation picture (Fig. 6.1) and the continuum model (Fig. 6.2).

The relaxation picture is model is sketched in Fig. 6.1. When exciting into a molecular resonance with an energy ω_1 below the relaxation threshold, the intermediate state decays directly and the emission occurs at an energy ω_1'. The spectral distribution in this case shows a resonant signature, i.e. carries clear symmetry information. Excitation at higher energies ω_2 and ω_3 above a relaxation threshold leads to the intermediate states $|i_2\rangle$ and $|i_3\rangle$, respectively. These intermediate states relax on a time scale much faster than the scattering duration, e.g. by a fast charge transfer to the substrate. The relaxed intermediate state $|i_R\rangle$ is independent of the incident photon energy $\omega_{2,3}$. The emission appears at fixed energy $\omega_2' = \omega_3'$. The emission profile corresponds to the non–resonant case and the information of the initially excited electron is lost.

In the continuum picture (Fig. 6.2), scattering into a resonant state with the incident energy ω_1 is treated as in the relaxation picture. Excitation into the continuum states leading to the XES case with energy ω_2 and ω_3 is treated different from the former model. The initially excited electron is always fully described in the final state. This electron can be relaxed, removed (as a photo electron) or in a molecular state. It's symmetry is not well defined and the emission spectra show the XES profile. Exciting with two different energies ω_1 and ω_2 leads to the final states $|f_1\rangle$ and $|f_2\rangle$ including the energy of the excited electron — equal, if it is relaxed, removed or in a molecular state. The emitted photon occurs at fixed energy independent of the excitation.

These two models are strictly spoken equivalent. The relaxation in the first model corresponds to an additional excitation present in the scattering final state of the second model. This could e.g. be an excitation of the substrate continuum states by the transfer of an electron. The final state $|f\rangle$ in the continuum model thus equals the sum of the final state $|f\rangle$ in the relaxation model plus the additional excitation performed by the relaxation process. Dependent on the application, each model has its advantages. The relaxation model is well suited to explain why the interpretation of the chemical bonding in Paper VI and Paper VIII works so well. There, scattering at higher energies is successfully interpreted with the non–resonant calculations and thus corresponds to a fully relaxed intermediate state. Scattering at the molecular LUMO resonance consequently needs a resonant treatment.

In the case of free molecules, the continuum model has the advantage of not needing an external relaxation channel like a charge transfer to explain the non–resonant behavior. Instead, the excitation of a multitude of molecularly located final states can account for the non–resonant emission profile. Nevertheless, in the case of condensed molecules presented here, a relaxation of the interme-

diate state due to decay into neighboring molecules is also possible. However, the question of the interplay of intra–molecular and inner–molecular relaxation processes is too complex to be addressed within this work[1].

[1]This question is a central topic of the PhD project of S. Vijayalakshmi on resonant photo emission and core–hole–clock spectroscopy and is discussed in [185]

Chapter 7

Conclusion

The starting hypothesis that dynamic processes in the scattering intermediate state have significant influence on the RIXS profile has been proven true. Nuclear dynamics in the resonant scattering intermediate state of free hydrocarbons and of benzene adsorbed on silicon enhance significantly the vibrational contributions to the spectral profile. Thus, in the interpretation of RIXS, the electronic and vibrational wave functions have to be considered. For excitation detuned far above an absorption resonance, the RIXS profile of adsorbates on semiconductors can be approximated by purely electronic simulations in the ground–state interpretation. This facilitates a study of the symmetry and polarization resolved electronic valence structure and allows for an interpretation of the surface chemical bond.

In this thesis, I have concentrated on basic aspects of the spectroscopical method and their interpretation. The hydrocarbon molecules in different chemical environments act as model systems for the characterization of the scattering process. I have summarized these findings in Chap. 6. The investigation of the surface chemical bond in this context serves as a sample application. The chemical bonding of small hydrocarbon molecules is summarized and compared in Chap. 5.5. Small hydrocarbons and semiconductor surface adsorbates have turned out to be suitable systems for this model investigation.

The vibrational modes of the hydrocarbon molecules are spaced wide enough to be accessible within the given limits of experimental resolution. The spacing allowed for a selective excitation of vibrational states. The ethylene molecule has shown to be reasonably complex for a theoretical treatment including coupled vibrational and electronic contributions. The benzene molecule, however, is already too complex for the approach presented here. It could by now not been simulated and waits for an improvement of the theoretical model. This is work to be done in the near future.

The screening and bonding situation on silicon allowed for an identification of resonant scattering phenomena in the adsorbed molecules. For the first time, a vibrational contribution to the RIXS profile of an adsorbate has been reported. To interpret these experimental data, a resonant but purely electronic treatment in the ground–state approach has been applied. Although this model cannot account for any vibrational effects, it has still turned out to be a good choice. Carefully considering the boundary conditions of the RIXS spectral profile formation, this model gives a very good approximation. It has, on this base, a justification to be applied to RIXS on surface adsorbate systems. However, there already exist e.g. time–dependent solid state computational tools. An application of these methods to the calculation of RIXS spectra opens an interesting perspective.

Experimentally, RIXS is still limited by the resolution that can be achieved. This makes the interpretation of the spectra difficult and leaves last ambiguities. Here, it can be trusted that the ongoing development of light–sources and spectral analyzers will improve the method.

The element specific enhancement of the inelastic scattering cross section of the vibrational contributions to the RIXS profile opens a perspective to new applications of RIXS. Supposing an ongoing rapid evolution of high brilliance soft X-ray sources based on synchrotron storage rings and the upcoming Free-Electron-Lasers, it becomes possible to study purely vibrational excitations by means of RIXS. The development of new soft X–ray spectrometers could vivify this evolution. With improved experimental techniques, purely vibrational soft X–ray Raman spectroscopy allows to directly link vibrational information to a selected atomic center. With soft X–ray spectroscopies, the large number of chemically relevant elements are addressable. This application of RIXS would be of high interest for a large class of investigations in materials science, chemistry, biology and environmental sciences.

In the investigation of surface adsorbate systems, RIXS has demonstrated its superiority over other tools for valence electronic structure determination. It has been shown that the specific advantages of RIXS — known from the investigation of adsorbates on metals — can also be employed investigating semiconductor surface adsorbates. The polarization and symmetry separation possible with RIXS facilitates the interpretation of the surface chemical bond. RIXS thus excels UPS, where the contributions from different atoms cannot be separated and the symmetry interpretation is much more difficult. Implying necessary technical improvements, RIXS could develop into a routinely used surface chemistry tool.

The RIXS investigation presented in this work has a little bit further elucidated the interplay of electrons in matter. This study has enlightened certain

mechanisms and opened perspectives to further applications of systems with higher complexity. At the same time, the restrictions of experimental and theoretical methods have been illustrated and the demand for an ongoing development in this field has been emphasized.

Comment on my contribution

This thesis represents an interpretation of RIXS based on experimental data and theoretical simulations. The experimental work was performed in a research team, the theoretical work in close cooperation with other groups. I was lucky to have the opportunity to play a central role in this joint effort. I actively participated in all experimental work — which was performed at MAXlab in Lund, Sweden. I shared the responsibility for the preparation and realization of the experiments with my advisor Alexander Föhlisch. In the period dedicated to analysis and interpretation in the last year of my thesis, I was working closely together with the theoretical chemistry groups in Stockholm during two stays in Sweden. The calculation of the vibrational RIXS of the free molecules has been performed by the team around Faris Gel'mukhanov. The DFT cluster calculations of the surface adsorbates in [Paper VII] and [Paper VIII] have been performed by Luciano Triguero with my participation. I have prepared the theoretical data for publication and analyzed and discussed them as presented here. I have only included papers in this thesis where I have contributed essentially in the experimental work, analysis, interpretation and writing. This is also reflected by the rank of my name in the respective author lists.

Acknowledgements

I have been working during my diploma and as a PhD student under supervision of Wilfried Wurth and Alexander Föhlisch from 2001 to 2005. During this five years I worked and learned as much as never before still having great fun. At the same time I had a very happy time with my family, I married my wife Martje and my daughters Eefje and Emma were born. This was only possible together, because I found at work the best scientific and personal environment I can think of and because Martje supported me with all her power. This was great fortune and I don't know how to thank for it.

But I thank Wilfried for having his office doors open late at the autumn evening in 2000 when I – by chance – knocked to see if the "'new professor"' might have an interesting project — I found your office doors open every time I tried since then for discussions about physics and university politics and I will continue knocking.

I thank Alexander for teaching me nearly everything I know about spectroscopy and surface science and for discussing (not only) his morning ideas with me. I think there is not a single hour on not a single weekday, where we have not discussed and the occasions include swimming in sight of the Miramare and the Øresundsbron (beside sitting at beamlines, of course). I hope we stay in contact realizing our vision of doing science and I am looking forward to many more discussions (at exotic places) with you.

I thank Mitsuru and Annette for the uncountable (night) shifts we shared at the beamline. We can really work together like a well-oiled machine and I hope we will never become to old to share night shifts.

I thank Sven and Holger for doing the difficult at once — when I hit the lottery jackpot I will hire you. Sven, I will always remember the experience we shared in drilling holes and threads. I thank Marlis for tons of gummi bears and fighting the university administration – without this I wouldn't have succeeded.

I thank Luciano and Faris for the theoretical work and the discussions about our common project. Traveling to Stockholm in the dark time of the year enlightened me.

I thank Viji and Edlira for our many common projects — whenever I need to know where the double bond is in x,y–cyclohexadiene, I will call you, Viji.

I thank Leif, the both Michaels, Jon, Matthias and Stina for the fun we had at work — Leif, when I am really in need of a cheer up, I will come to one of your barbecues.

I thank Luciano, Tobias, Annette and Johannes for reading my manuscript.

I enjoyed working with many more people: Maria-Novella, Nadine, Lisbeth, Ivo, Kai, Peter, Sergey, Svante – just to mention a few.

Bibliography

[1] Franz Hennies, Alexander Föhlisch, Wilfried Wurth, Nadine Witkowski, Mitsuru Nagasono, and Maria Novella Piancastelli. Fully polarization resolved X-ray absorption spectroscopy of C_2H_4 on single-domain Si(001)–(2×1). *Surf. Sci.*, 529: 144–150, 2003. URL http://dx.doi.org/10.1016/S0039-6028(03)00079-7.

[2] N. Witkowski, F. Hennies, A. Pietzsch, S. Mattsson, A. Föhlisch, W. Wurth, M. Nagasono, and M. N. Piancastelli. Polarization and angle-resolved NEXAFS of benzene adsorbed on oriented single-domain Si(001)–(2×1) surfaces. *Phys. Rev. B*, 68:115408, 2003. URL http://dx.doi.org/10.1103/PhysRevB.68.115408.

[3] Annette Pietzsch, Franz Hennies, Alexander Föhlisch, Wilfried Wurth, Mitsuru Nagasono, Nadine Witkowski, and Maria Novella Piancastelli. Adsorption geometry of C_2H_2 on the single-domain Si(001)-(2×1) surface: fully polarization resolved NEXAFS. *Surf. Sci.*, 562:65–72, 2004. URL http://dx.doi.org/10.1016/j.susc.2004.05.007.

[4] F. Hennies, S. Polyutov, I. Minkov, A. Pietzsch, M. Nagasono, F. Gel'mukhanov, L. Triguero, M.-N. Piancastelli, W. Wurth, H. Agren, and A. Föhlisch. Nonadiabatic Effects in Resonant Inelastic X-ray Scattering. *Phys. Rev. Lett.*, 95:163002, 2005. URL http://dx.doi.org/10.1103/PhysRevLett.95.163002.

[5] F. Hennies, S. Polyutov, I. Minkov, M. Nagasono, A. Pietzsch, F. Gel'mukhanov, L. Triguero, M.-N. Piancastelli, W. Wurth, H. Agren, and A. Föhlisch. Dynamic Interpretation of Resonant Inelastic X-ray Scattering: Ethylene and Benzene. In Manuscript, 2005.

[6] A. Föhlisch, F. Hennies, W. Wurth, N. Witkowski, M. Nagasono, M. N. Piancastelli, L. V. Moskaleva, K. M. Neyman, and N. Rösch. Electronic structure and screening dynamics of ethene on single-domain Si(001) from resonant inelastic x-ray scattering. *Phys. Rev. B*, 69:153408, 2004. URL http://dx.doi.org/10.1103/PhysRevB.69.153408.

[7] F. Hennies, M. Nagasono, A. Pietzsch, N. Witkowski, M. N. Piancastelli, W. Wurth, L. Triguero, and A. Föhlisch. Intermediate State Relaxation in Resonant Inelastic X-ray Scattering of Silicon Surface Adsorbates. In Manuscript, 2005.

[8] F. Hennies, M. Nagasono, A. Pietzsch, N. Witkowski, M. N. Piancastelli, W. Wurth, L. Triguero, and A. Föhlisch. Bonding Configuration of Benzene adsorbed on

Si(001)–(2×1) refined from Resonant Inelastic X–ray Scattering. In Manuscript, 2005.

[9] Manne Siegbahn. The X-ray Spectra and the Structure of the Atoms - Nobel Lecture 1924. In *Nobel Lectures, Physics 1922-1941*. Elsevier Publishing Company, Amsterdam, 1965. URL http://nobelprize.org/physics/laureates/1924/siegbahn-lecture.html.

[10] Robert S. Mulliken. Spectroscopy, Molecular Orbitals, and Chemical Bonding - Nobel Lecture 1966. In *Nobel Lectures, Chemistry 1963-1970*. Elsevier Publishing Company, Amsterdam, 1972. URL http://nobelprize.org/chemistry/laureates/1966/mulliken-lecture.html.

[11] Walter Kohn. Electronic Structure of Matter - Wave Functions and Density Functionals - Nobel Lecture 1998. In Ingmar Grenthe, editor, *Nobel Lectures, Chemistry 1996-2000*. World Scientific Publishing Co., Singapore, 2003. URL http://nobelprize.org/chemistry/laureates/1998/kohn-lecture.html.

[12] M. Odelius, H. Ogasawara, D. Nordlund, O. Fuchs, L. Weinhardt, F. Maier, E. Umbach, C. Heske, Y. Zubavichus, M. Grunze, Jonathan D. Denlinger, L.G.M. Pettersson, and A. Nilsson. Ultrafast Core-Hole-Induced Dynamics in Water Probed by X-Ray Emission Spectroscopy. *Phys. Rev. Lett.*, 94:227401, 2005. URL http://dx.doi.org/10.1103/PhysRevLett.94.227401.

[13] Ph. Wernet, D. Nordlund, U. Bergmann, M. Cavalleri, M. Odelius, H. Ogasawara, L. Å. Näslund, T. K. Hirsch, L. Ojamäe, P. Glatzel, L. G. M. Pettersson, and A. Nilsson. The Structure of the First Coordination Shell in Liquid Water . *Science*, 304: 995, 2004. URL http://dx.doi.org/10.1126/science.1096205.

[14] S. Kashtanov, A. Augustsson, Y. Luo, J.-H. Guo, C. Såthe, J.-E. Rubensson, H. Siegbahn, J. Nordgren, and H. Ågren. Local structures of liquid water studied by x-ray emission spectroscopy. *Phys. Rev. B*, 69:024201, 2004. URL http://dx.doi.org/10.1103/PhysRevB.69.024201.

[15] J.-H. Guo, Y. Luo, A. Augustsson, S. Kashtanov, J.-E. Rubensson, D. K. Shuh, H. Ågren, and J. Nordgren. Molecular Structure of Alcohol-Water Mixtures. *Phys. Rev. Lett.*, 91:157401, 2003. URL http://dx.doi.org/10.1103/PhysRevLett.91.157401.

[16] J.-H. Guo, Y. Luo, A. Augustsson, J.-E. Rubensson, C. Såthe, H. Ågren, H. Siegbahn, and J. Nordgren. X-Ray Emission Spectroscopy of Hydrogen Bonding and Electronic Structure of Liquid Water. *Phys. Rev. Lett.*, 89:137402, 2002. URL http://dx.doi.org/10.1103/PhysRevLett.89.137402.

[17] A. Föhlisch, M. Nyberg, P. Bennich, L. Triguero, J. Hasselström, O. Karis, L.G.M. Pettersson, and A. Nilsson. The Bonding of CO to metal surfaces. *J. Chem. Phys.*, 112:1946, 2000. URL http://dx.doi.org/10.1063/1.480773.

[18] A. Föhlisch, M. Nyberg, J. Hasselström, O. Karis, L. G. M. Pettersson, and A. Nilsson. How Carbon Monoxide Adsorbs in Different Sites. *Phys. Rev. Lett.*, 85:3309, 2000. URL http://dx.doi.org/10.1103/PhysRevLett.85.3309.

[19] A. Föhlisch, W. Wurth, M. Stichler, C. Keller, and A. Nilsson. X-ray emission spectroscopy of (2×2)R30∘CO/Ru(0001): Comparison to c(2×2)CO/Ni(100) and c(2×2)CO/Cu(100). *J. Chem. Phys.*, 121:4848, 2004. URL http://dx.doi.org/10.1063/1.1778380.

[20] A. Nilsson, J. Hasselström, A. Föhlisch, O. Karis, L.G.M. Pettersson, M. Nyberg, and L. Triguero. Probing chemical bonding in adsorbates using X-Ray emission spectroscopy. *J. Electron Spectrosc. Relat. Phenom.*, 110:15, 2000. URL http://dx.doi.org/10.1016/S0368-2048(00)00155-9.

[21] Nils Mårtensson, Olof Karis, and Anders Nilsson. Resonant processes in the soft X-ray regime. *J. Electron Spectrosc. Relat. Phenom.*, 100:379, 1999. URL http://dx.doi.org/10.1016/S0368-2048(99)00056-0.

[22] A. Pietzsch, A. Föhlisch, F. Hennies, S. Vijayalakshmi, and W. Wurth. Surface photovoltage dynamics at the buried BaF_2/Si interface from time resolved laser-synchrotron 2 photon photoemission. submitted to the Journal of Applied Physics, 2005.

[23] Ahmed Zewail. Femtochemistry: Atomic-Scale Dynamics of the Chemical Bond Using Ultrafast Lasers - Nobel Lecture 1999. In Ingmar Grenthe, editor, *Nobel Lectures, Chemistry 1996-2000*. World Scientific Publishing Co., Singapore, 2003. URL http://nobelprize.org/chemistry/laureates/1999/zewail-lecture.html.

[24] Donald Umstadter. Review of physics and applications of relativistic plasmas driven by ultra-intense lasers. *Phys. Plasmas*, 8:1774–1785, 2001. URL http://dx.doi.org/10.1063/1.1364515.

[25] A. Tarasevitch, A. Orisch, D. von der Linde, Ph. Balcou, G. Rey, J.-P. Chambaret, U. Teubner, D. Klöpfel, and W. Theobald. Generation of high-order spatially coherent harmonics from solid targets by femtosecond laser pulses. *Phys. Rev. A*, 62:023816, 2000. URL http://dx.doi.org/10.1103/PhysRevA.62.023816.

[26] M. Hentschel, R. Kienberger, Ch. Spielmann, G. A. Reider, N. Milosevic, T. Brabec, P. Corkum, U. Heinzmann, M. Drescher, and F. Krausz. Attosecond metrology. *Nature*, 414:509–513, 2001. URL http://dx.doi.org/10.1038/35107000.

[27] W. Wurth and D. Menzel. Ultrafast electron dynamics at surfaces probed by resonant Auger spectroscopy. *Chem. Phys.*, 251:141, 2000. URL http://dx.doi.org/10.1016/S0301-0104(99)00305-5.

[28] A. Föhlisch, P. Feulner, F. Hennies, A. Fink, D. Menzel, D. Sanchez-Portal, P. M. Echenique, and W. Wurth. Direct observation of electron dynamics in the attosecond domain. *Nature*, 436:373, 2005. URL http://dx.doi.org/10.1038/nature03833.

[29] P. Salek, A. Baev, F. Gel'mukhanov, and H. Ågren. Dynamical properties of X-ray Raman scattering. *Phys. Chem. Chem. Phys.*, 5:1, 2003. URL http://dx.doi.org/10.1039/b209717f.

[30] Yi Luo, Hans Ågren, and Faris Gel'mukhanov. Polarization anisotropy in resonant x-ray emission from molecules. *Phys. Rev. A*, 53:1340, 1996. URL http://dx.doi.org/10.1103/PhysRevA.53.1340.

[31] L. Triguero, Y. Luo, L.G.M. Pettersson, H. Ågren, P. Väterlein, M. Weinelt, A. Föhlisch, J. Hasselström, O. Karis, and A. Nilsson. Resonant soft-x-ray emission spectroscopy of surface adsorbates: Theory, computations, and measurements of ethylene and benzene on Cu(110). *Phys. Rev. B*, 59:5189, 1999. URL http://dx.doi.org/10.1103/PhysRevB.59.5189.

[32] H. W. B. Skinner. The soft x-ray spectroscopy of solids. I. K- and L-emission spectra from elements of the first two groups. *Trans. Roy. Soc. (London)*, A239: 95–134, 1940.

[33] H. M. O'Bryan and H. W. B. Skinner. Characteristic X-Rays from Metals in the Extreme Ultraviolet. *Phys. Rev.*, 45:370–378, 1934. URL http://dx.doi.org/10.1103/PhysRev.45.370.

[34] A. Fahlman, K. Hamrin, J. Hedman, R. Nordberg, R. Nordling, and K. Siegbahn. Electron Spectroscopy and Chemical Binding. *Nature*, 210:4, 1966.

[35] J. Nordgren, G. Bray, S. Cramm, R. Nyholm, J.-E. Rubensson, and N. Wassdahl. Soft x-ray emission spectroscopy using monochromatized synchrotron radiation (invited). *Review of Scientific Instruments*, 60:1690, 1989. URL http://dx.doi.org/10.1063/1.1140929.

[36] J. Nordgren, H. Ågren, L. Petterson, L. Selander, S. Griep, C. Nordling, and K. Siegbahn. A new 10m grazing incidence instrument for molecular X-ray studies. *Phys. Scr.*, 20:623, 1979. URL http://www.physica.org/.

[37] J.-E. Rubensson, N. Wassdahl, G. Bray, J. Rindstedt, R. Nyholm, S. Cramm, N. Mårtensson, and J. Nordgren. Resonant behavior in soft x-ray fluorescence excited by monochromatized synchrotron radiation. *Phys. Rev. Lett.*, 60:1759, 1988. URL http://dx.doi.org/10.1103/PhysRevLett.60.1759.

[38] F. K. Gel'Mukhanov, L. N. Mazalov, and A. V. Kondratenko. A theory of vibrational structure in the X-ray spectra of molecules . *Chem. Phys. Lett.*, 46:133, 1977. URL http://dx.doi.org/10.1016/0009-2614(77)85180-4.

[39] Faris Gel'mukhanov and Hans Ågren. Resonant X-Ray Raman scattering. *Phys. Rep.*, 312:87, 1999. URL http://dx.doi.org/10.1016/S0370-1573(99)00003-4.

[40] P. O. Nilsson, J. Kanski, J. V. Thordson, T. G. Andersson, J. Nordgren, J. Guo, and M. Magnuson. Electronic structure of buried Si layers in GaAs(001) as studied by soft-x-ray emission. *Phys. Rev. B*, 52:8643, 1995. URL http://dx.doi.org/10.1103/PhysRevB.52.R8643.

[41] Akio Kotani and Shik Shin. Resonant inelastic x-ray scattering spectra for electrons in solids. *Rev. Mod. Phys.*, 73:203, 2001. URL http://dx.doi.org/10.1103/RevModPhys.73.203.

[42] E. Z. Kurmaev, J. P. Werner, A. Moewes, S. Chiuzbian, M. Bach, W. Y. Ching, W. Motozaki, T. Otsuka, S. Matsuya, K. Endo, and M. Neumann. Soft X-ray emission studies of biomaterials. *J. Electron Spectrosc. Relat. Phenom.*, 137-140: 811–815, 2004. URL http://dx.doi.org/10.1016/j.elspec.2004.02.122.

[43] J. Nordgren, P. Glans, K. Gunnelin, J. Guo, P. Skytt, C. Såthe, and N. Wassdahl. Resonant soft X-ray fluorescence spectra of molecules. *Appl. Phys. A*, 65:97, 1997. URL http://dx.doi.org/10.1007/s003390050550.

[44] Anders Nilsson and Lars Gunnar Moody Pettersson. Chemical bonding on surfaces probed by X-ray emission spectroscopy and density functional theory. *Surf. Sci. Rep.*, 55:49, 2004. URL http://dx.doi.org/10.1016/j.surfrep.2004.06.002.

[45] A. Föhlisch, J. Hasselström, P. Bennich, N. Wassdahl, O. Karis, A. Nilsson, L. Triguero, M. Nyberg, and L.G.M. Pettersson. Ground-state interpretation of x-ray emission spectroscopy on adsorbates: CO adsorbed on Cu(100). *Phys. Rev. B*, 61:16229, 2000. URL http://dx.doi.org/10.1103/PhysRevB.61.16229.

[46] P. Skytt, P. Glans, K. Gunnelin, J. Guo, and J. Nordgren. Lifetime-vibrational interference effects in the resonantly excited x-ray-emission spectra of CO. *Phys. Rev. A*, 55:146, 1997. URL http://dx.doi.org/10.1103/PhysRevA.55.146.

[47] J. E. Rubensson. Soft X-ray emission spectroscopy. *J. Electron Spectrosc. Relat. Phenom.*, 92:189, 1998. URL http://dx.doi.org/10.1016/S0368-2048(98)00121-2.

[48] N. Wassdahl, A. Nilsson, T. Wiell, H. Tillborg, L.-C. Duda, J. H. Guo, N. Mårtensson, J. Nordgren, J. N. Andersen, and R. Nyholm. Soft X-Ray Emission Studies of Adsorbates. *Phys. Rev. Lett.*, 69:812, 1992. URL http://dx.doi.org/10.1103/PhysRevLett.69.812.

[49] J. Nordgren and N. Wassdahl. Current status and future prospects for ultra-soft X-ray emission spectroscopy. *Phys. Scr.*, T31:103, 1990. URL http://www.physica.org/asp/TopicalArticleList.asp?Vol=T31.

[50] Ingvar Lindgren. Chemical shifts in X-ray and photo-electron spectroscopy: a historical review. *J. Electron Spectrosc. Relat. Phenom.*, 137-140:59–71, 2004. URL http://dx.doi.org/10.1016/j.elspec.2004.02.086.

[51] H. A. Kramers and W. Heisenberg. Über die Streuung von Strahlung durch Atome. *Z. Phys.*, 31:681, 1925.

[52] J. J. Sakurai. *Modern Quantum mechanics*. 1985.

[53] H. A. Jahn and E. Teller. Stability of Polyatomic Molecules in Degenerate Electronic States. I. Orbital Degeneracy. *Proc. R. Soc. London A*, 161:220–235, 1937.

[54] F. Gel'mukhanov, T. Privalov, and H. Ågren. Restoration of selection rules in nonadiabatic resonant inelastic x-ray scattering. *Zh. Eksp. Teor. Fiz.*, 112:37, 1997. URL http://dx.doi.org/10.1134/1.558310. [JETP, 85, 20 (1997)].

[55] P. R. Watson, M. A. Van Hove, and K. Herrmann, editors. *Atlas of Surface Structures*, volume Monograph No. 5 of *J. Phys. Chem. Ref. Data, Monograph*. ACS, NSRDS, AIP, 1994.

[56] U. Birkenheuer, U. Gutdeutsch, N. Rösch, A. Fink, S. Gokhale, P. Trischberger, D. Menzel, and W. Widdra. Density Functional Investigation of the Geometric and Electronic Structure of Ethylene Adsorbed on Si(001). *J. Chem. Phys.*, 108:9868, 1998. URL http://dx.doi.org/10.1063/1.476425.

[57] U. Birkenheuer, U. Gutdeutsch, and N. Rösch. Geometrical structure of benzene absorbed on Si(001). *Surf. Sci.*, 409:213, 1998.

[58] A. Thompson, editor. *X-Ray Data Booklet*. Lawrence Berkeley National Laboratory, Berkeley, 2001. URL http://xdb.lbl.gov.

[59] M. O. Krause. Atomic Radiative and Radiationless Yields for K and L Shells. *J. Phys. Chem. Ref. Data*, 8:307, 1979. URL http://link.aip.org/link/?JPR/8/307/1.

[60] Beamline I511-1 and I511-3 - Short information, 2003. URL http://www.maxlab.lu.se/beamline/max-ii/i511/i511.html. Website, (2005-09-24).

[61] J. Nordgren and J. Guo. Instrumentation for soft X-ray emission spectroscopy. *J. Electron Spectrosc. Relat. Phenom.*, 110-111:1, 2000. URL http://dx.doi.org/10.1016/S0368-2048(00)00154-7.

[62] Gammadata Scienta AB. SOFT X-RAY EMISSION SPECTROMETER. Website (2005-10-05), 2004. URL http://www.gammadata.se/ULProductFiles/XES350_0412.pdf.

[63] P Pirro. The use of thermocoax Chromel-Alumel thermocouples for the measurement of small temperature differences. *J. Sci. Instrum.*, 44:1055–1056, 1967. URL http://dx.doi.org/10.1088/0950-7671/44/12/435.

[64] Shubha Gokhale, Andreas Fink, Peter Trischberger, Karl Eberle, and Wolf Widdra. Silicon bonding for ultrahigh vaccuum surface science studies. *J. Vac. Sci. Technol. A*, 19:706, 2001. URL http://dx.doi.org/10.1116/1.1350997.

[65] C. C. Cheng, R. M. Wallace, P. A. Taylor, W. J. Choyke, and J. T. Yates. Direct determination of absolute monolayer coverages of chemisorbed C_2H_2 and C_2H_4 on Si(100). *J. Appl. Phys.*, 67:3693, 1990. URL http://dx.doi.org/10.1063/1.345326.

[66] Y. Taguchi, M. Fujisawa, T. Takaoka, T. Okada, and M. Nishijima. Adsorbed state of benzene on the Si(100) surface: Thermal desorption and electron energy loss spectroscopy studies. *J. Chem. Phys.*, 95:6870, 1991. URL http://dx.doi.org/10.1063/1.461498.

[67] Joachim Stöhr. *NEXAFS Spectroscopy*. Springer, Berlin, 1992.

[68] Y. Ma, F. Sette, G. Meigs, S. Modesti, and C. T. Chen. Breaking of ground-state symmetry in core-excited ethylene and benzene. *Phys. Rev. Lett.*, 63:2044, 1989. URL http://dx.doi.org/10.1103/PhysRevLett.63.2044.

[69] A. P. Hitchcock, P. Fischer, Aharon Gedanken, and M. B. Robin. Antibonding σ^* valence MOs in the inner-shell and outer-shell spectra of the fluorobenzenes. *J. Phys. Chem.*, 91:531, 1987.

[70] J. A. Horsley, J. Stöhr, A. P. Hitchcock, D. C. Newbury, A. L. Johnson, and F. Sette. Resonances in the K shell excitation spectra of benzene and pyridine: Gas phase, solid, and chemisorbed states. *J. Chem. Phys.*, 83:6099, 1985. URL http://dx.doi.org/10.1063/1.449601.

[71] R. Püttner, C. Kolczewski, M. Martins, A. S. Schlachter, G. Snell, M. Sant'Anna, J. Viefhaus, K. Hermann, and G. Kaindl. The C 1s NEXAFS spectrum of benzene below threshold: Rydberg or valence character of the unoccupied -type orbitals. *Chem. Phys. Lett.*, 393:361, 2004. URL http://dx.doi.org/10.1016/j.cplett.2004.06.053.

[72] E. E. Rennie, B. Kempgens, H. M. Köppe, U. Hergenhahn, J. Feldhaus, B. S. Itchkawitz, A. L. D. Kilcoyne, A. Kivimäki, K. Maier, M. N. Piancastelli, M. Polcik, A. Rüdel, and A. M. Bradshaw. A comprehensive photoabsorption, photoionization, and shake-up excitation study of the C 1s cross section of benzene. *J. Chem. Phys.*, 113:7362, 2000. URL http://dx.doi.org/10.1063/1.1290029.

[73] H. Köppel, F. X. Gadea, G. Klatt, J. Schirmer, and L. S. Cederbaum. Multistate vibronic coupling effects in the K-shell excitation spectrum of ethylene: Symmetry breaking and core-hole localization. *J. Chem. Phys.*, 106:4415, 1997. URL http://dx.doi.org/10.1063/1.473488.

[74] F. X. Gadea, H. Köppel, J. Schirmer, L. S. Cederbaum, K. J. Randall, A. M. Bradshaw, Y. Ma, F. Sette, and C. T. Chen. Vibronic coupling and core-hole localization in K-shell excitations of ethylene. *Phys. Rev. Lett.*, 66:883, 1991. URL http://dx.doi.org/10.1103/PhysRevLett.66.883.

[75] L. Clemen, R. M. Wallace, P. A. Taylor, M. J. Dresser, W. J. Choyke, W. H. Weinberg, and J. T. Yates. Adsorption and thermal behavior of ethylene on Si(100)-(2×1). *Surf. Sci.*, 268:205, 1992. URL http://dx.doi.org/10.1016/0039-6028(92)90963-7.

[76] C. Huang, W. Widdra, and W. Henry Weinberg. Adsorption of ethylene on the Si(100)–(2×1) surface. *Surf. Sci.*, 315:L953, 1994. URL http://dx.doi.org/10.1016/0039-6028(94)90524-X.

[77] W. Widdra, Chen Huang, and W.H. Weinberg. Reply to "Comment on 'Adsorption of ethylene on the Si(100)–(2×1) surface' by B.I. Craig". *Surf. Sci.*, 329:295, 1995. URL http://dx.doi.org/10.1016/0039-6028(95)00105-0.

[78] W. Widdra, C. Huang, S. I. Yi, and W.H. Weinberg. Coadsorption of hydrogen with ethylene and acetylene on Si(10)–(2×1). *J. Chem. Phys.*, 105:5605, 1996. URL http://dx.doi.org/10.1063/1.472817.

[79] B. I. Craig and P. V. Smith. Structures of small hydrocarbons adsorbed on Si(001) and Si terminated β-SiC(001). *Surf. Sci.*, 276:174, 1992. Erratum: Surface Science **285**, 295 (1993).

[80] Pei-Lin Cao and Ru-Hong Zhou. Ethylene adsorption and decomposition on Si(100) 2x1: a semi-empirical quantum chemical study. *J.Phys.: Condens. Matt.*, 5:2887, 1993.

[81] B. I. Craig. Comment on 'Adsorption of ethylene on the Si(100)-(2×1) surface' by C. Huang, W. Widdra and W. Henry Weinberg. *Surf. Sci.*, 329:293, 1995.

[82] Ke-An Feng, Z. H. Liu, and Zhangda Lin. A theoretical study of the initial stage of diamond film growth on Si(001). I. Adsorption processes of some hydrocarbon fragments. *Surf. Sci.*, 329:77, 1995.

[83] A. J. Fisher, P. E. Blöchl, and G. A. D. Briggs. Hydrocarbon adsorption on Si(001): When does the Si dimer bond break? *Surf. Sci.*, 374:298, 1997.

[84] W. Widdra, A. Fink, S. Gokhale, P. Trischberger, U. Gutdeutsch, U. Birkenheuer, N. Rösch, and D. Menzel. One-Dimensional Delocalized Adsorbate Bloch States on a Semiconductor Surface: C_2H_4/Si(001)–(2×1). *Phys. Rev. Lett.*, 80:4269, 1998. URL http://dx.doi.org/10.1103/PhysRevLett.80.4269.

[85] F. Rochet, F. Jolly, F. Boumel, G. Dufour, F. Sirotti, and J. L. Cantin. Si(001)-2x1 and Si(111)-7x7: X-ray photoemission spectroscopy with synchrotron radiation. *Phys. Rev. B*, 58:11029, 1998. URL http://dx.doi.org/10.1103/PhysRevB.58.11029.

[86] G. A. D. Briggs and A. J. Fisher. STM experiment and atomistic modelling hand in hand: individual molecules on semiconductor surfaces. *Surf. Sci. Rep.*, 33:1, 1999.

[87] P Baumgärtel, R Lindsay, O Schaff, T Gießel, R Terborg, J T Hoeft, M Polcik, A M Bradshaw, M Carbone, M N Piancastelli, R Zanoni, and R L Toomes. The dimers stay intact: a quantitative photoelectron study of the adsorption system Si(100)–(2×1)–C_2H_4. *New Journal of Physics*, 1:20, 1999. URL http://dx.doi.org/10.1088/1367-2630/1/1/320.

[88] M. P. Casaletto, R. Zanoni, M. Carbone, M. N. Piancastelli, L. Aballe, K. Weiss, and K. Horn. Ethylene adsorption on Si(100)2x1: A high resolution photoemission study. *Phys. Rev. B*, 62:17128, 2000. URL http://dx.doi.org/10.1103/PhysRevB.62.17128.

[89] S. H. Xu, M. Keeffe, Y. Yang, C. Chen, M. Yu, G. J. Lapeyre, E. Rotenberg, J. Denlinger, and J. T. Yates. Photoelectron Diffraction Imaging for $C_2H_2$and C_2H_4 Chemisorbed on Si(100) Reveals a New Bonding Configuration. *Phys. Rev. Lett.*, 84:939, 2000. URL http://dx.doi.org/10.1103/PhysRevLett.84.939.

[90] J.-H. Cho, L. Kleinman, C. T. Chan, and K. S. Kim. First-principles study of the adsorption of C_2H_2 and C_2H_4 on Si(100). *Phys. Rev. B*, 63:073306, 2001. URL http://dx.doi.org/10.1103/PhysRevB.63.073306. Erratum: Phys. Rev. B **64**, 199902 (2001).

[91] J T Yates. A New Opportunity in Silicon-Based Microelectronics. *Science*, 279:5349:335, 1998.

[92] MAX SCHULZ. The end of the road for silicon? *Nature*, 399:729, 1999. URL http://dx.doi.org/10.1038/21526.

[93] R.J. Hamers, R.M. Tromp, and J.E. Demuth. Scanning tunneling microscopy of Si(100). *Phys. Rev. B*, 34:5343, 1986.

[94] Robert A. Wolkow. Direct observation of an increase in buckled dimers on Si(001) at low temperature. *Phys. Rev. Lett.*, 68:2636, 1992.

[95] J. Yoshinobu, H. Tsuda, M. Onchi, and M. Nishijima. The adsorbed states of ethylene on Si(100)c(4×2), Si(100)(2×1), and vicinal Si(100) 9○: Electron energy loss spectroscopy and low-energy electron diffraction studies. *J. Chem. Phys.*, 87: 7332, 1987. URL http://dx.doi.org/10.1063/1.453327.

[96] N. Pangher, L. Wilde, M. Polcik, and J. Haase. Structure determinations of SO_2 and its decomposistion product SO adsorbed on Cu(100) by use of X-ray absorption fine structure measurements. *Surf. Sci.*, 372:211, 1997. URL http://dx.doi.org/10.1016/S0039-6028(96)01109-0.

[97] F. Matsui, H. W. Yeom, A. Imanishi, K. Isawa, I. Matsuda, and T. Ohta. Adsorption and reaction of acetylene and ethylene on the Si(001)2x1 surface studied by NEXAFS and UPS. *Surf. Sci.*, 401:L413, 1998. URL http://dx.doi.org/10.1016/S0039-6028(98)00038-7.

[98] F. Matsui, H. W. Yeom, I. Matsuda, and T. Ohta. Adsorption and reaction of acetylene and ethylene on the Si(001)2x1 surface. *Phys. Rev. B*, 62:5036, 2000. URL http://dx.doi.org/10.1103/PhysRevB.62.5036.

[99] R. Denecke, P. Väterlein, M. Bässler, N. Wassdahl, A. Nilsson, J.-E. Rubensson, J. Nordgren, N. Mårtensson, and R. Nyholm. Beamline I511 at MAX II, capabilities and performance. *J. Electron Spectrosc. Relat. Phenom.*, 101-103:971, 1999.

[100] S. van Dijken and H. J. W. Zandvliet und B. Poelsema. Energetics and structure of the stable and unstable biatomic step edges of Si(001). *Surf. Rev. Lett.*, 5:15, 1998.

[101] Andreas Fink. *Organische Moleküle auf Halbleitern: Adsorption und elektronische Struktur ungesättigter Kohlenwasserstoffe auf Si(100), Ge/Si(100) und Ge(100) Oberflächen*. PhD thesis, TU München, 2001.

[102] A. Fink, R. Huber, and W. Widdra. Ethylene adsorption on Ge(100)-(2×1): A combined angle-resolved photoemission and thermal desorption spectroscopy study. *J. Chem. Phys.*, 115:2768, 2001. URL http://dx.doi.org/10.1063/1.1384552.

[103] R. McLaren, S. A. C. Clark, I. Ishii, and A. P. Hitchcock. Absolute oscillator strengths from K-shell electron-energy-loss spectra of the fluoroethenes and 1,3-perfluorobutadiene. *Phys. Rev. A*, 36:1683, 1987. URL http://dx.doi.org/10.1103/PhysRevA.36.1683.

[104] A. P. Hitchcock and I. Ishii. Carbon K-shell excitation spectra of linear and branched alkanes. *J. Electron Spectrosc. Relat. Phenom.*, 42:11, 1987. URL http://dx.doi.org/10.1016/0368-2048(87)85002-8.

[105] J. Stöhr, F. Sette, and A.L. Johnson. Near-Edge X-Ray-Absorption Fine-Structure Studies of Chemisorbed Hydrocarbons: Bond Lengths with a Ruler. *Phys. Rev. Lett.*, 53:1684, 1984. URL http://dx.doi.org/10.1103/PhysRevLett.53.1684.

[106] H. Rabus, D. Arvanitis, M. Dohmke, and K. Baberschke. High resolution x-ray absorption spectroscopy of linear hydrocarbons adsorbed on noble metal surfaces. *J. Chem. Phys.*, 96:1560, 1992. URL http://dx.doi.org/10.1063/1.462140.

[107] S.L. Sorensen, M. Wiklund, S. Sundin, A. Ausmees, A. Kikas, and S. Svensson. Continuum resonance in ethylene: Evidence from vibrationally resolved core photoionization. *Phys. Rev. A*, 58:1879, 1998. URL http://dx.doi.org/10.1103/PhysRevA.58.1879.

[108] Robert J. Hamers, Jennifer S. Hovis, Seung Lee, Hongbing Liu, and Jun Shan. Formation of Ordered, Anisotropic Organic Monolayers on the Si(001) Surface. *J. Phys. Chem. B.*, 101:1489, 1997. URL http://dx.doi.org/10.1021/jp9626778.

[109] B. I. Craig. A theoretical examination of the chemisorption of benzene on Si(100)-(2×1). *Surf. Sci.*, 280:L279, 1993. URL http://dx.doi.org/10.1016/0039-6028(93)90675-A.

[110] Hyun Dam Jeong, Seol Ryu, Yoon Sup Lee, and Sehun Kim. A semi-empirical study of the chemisorbed state of benzene on Si(100)-(2×1). *Surf. Sci.*, 344:L1226, 1995. URL http://dx.doi.org/10.1016/0039-6028(95)00931-0.

[111] S. Gokhale, P. Trischberger, D. Menzel, W. Widdra, H. Dröge, H.-P. Steinrück, U. Birkenheuer, U. Gutdeutsch, and N. Rösch. Electronic structure of benzene adsorbed on single-domain Si(001)-(2×1): A combined experimental and theoretical study. *J. Chem. Phys.*, 108:5554, 1998. URL http://dx.doi.org/10.1063/1.475945.

[112] G. P. Lopinski, T. M. Fortier, D. J. Moffatt, and R. A. Wolkow. Multiple bonding geometries and binding state conversion of benzene/Si(100). *J. Vac. Sci. Technol. A*, 16:1037, 1998. URL http://dx.doi.org/10.1116/1.581228.

[113] Brian Borovsky, Michael Krueger, and Eric Ganz. Metastable adsorption of benzene on the Si(001) surface. *Phys. Rev. B*, 57:R4269, 1998. URL http://link.aps.org/abstract/PRB/v57/pR4269.

[114] Maynard J. Kong, Andrew V. Teplyakov, Julia G. Lyubovitsky, and Stacey F. Bent. NEXAFS studies of adsorption of benzene on Si(100)-2×1. *Surf. Sci.*, 411:286, 1998. URL http://dx.doi.org/10.1016/S0039-6028(98)00336-7.

[115] D. A. Outka and J. Stöhr. Curve fitting analysis of near-edge core excitation spectra of free, adsorbed, and polymeric molecules. *J. Chem. Phys.*, 88:3539, 1988. URL http://dx.doi.org/10.1063/1.453902.

[116] J. L. Solomon, R. J. Madix, and J. Stöhr. Orientation and absolute coverage of benzene, aniline, and phenol on Ag(110) determined by NEXAFS and XPS . *Surf. Sci.*, 255:12, 1991. URL http://dx.doi.org/10.1016/0039-6028(91)90008-G.

[117] A. P. Hitchcock, D. C. Newbury, I. Ishii, J. Stöhr, J. A. Horsley, R. D. Redwing, A. L. Johnson, and F. Sette. Carbon K-shell excitation of gaseous and condensed cyclic hydrocarbons: C_3H_6, C_4H_8, C_5H_8, C_5H_{10}, C_6H_{10}, C_6H_{12}, and C_8H_8. *J. Chem. Phys.*, 85:4849, 1986. URL http://dx.doi.org/10.1063/1.451719.

[118] M. Nishijima, J. Yoshinobu, H. Tsuda, and M. Onchi. The adsorption and thermal decomposition of acetylene on Si(100) and vicinal Si(100)9 degrees. *Surf. Sci.*, 192: 383, 1987.

[119] L. Li, C. Tindall, O. Takaoka, Y. Hasegawa, and T. Sakurai. STM study of C_2H_2 adsorption on Si(001). *Phys. Rev. B*, 56:4648, 1997. URL http://dx.doi.org/10.1103/PhysRevB.56.4648.

[120] P. A. Taylor, R. M. Wallace, C. C. Cheng, W. H. Weinberg, M. J. Dresser, W. J. Choyke, and J. T. Yates. Adsorption and decomposition of acetylene on Si(001)-(2×1). *J. Am. Chem. Soc.*, 114:6754, 1992. URL http://dx.doi.org/10.1021/ja00043a020.

[121] C. Huang, W. Widdra, X. S. Wang, and W. H. Weinberg. Adsorption of acetylene on the Si(100)-(2×1) surface. *J. Vac. Sci. Technol. A*, 11:2250, 1993. URL http://dx.doi.org/10.1116/1.578356.

[122] C. S. Carmer, B. Weiner, and M. Frenklach. Molecular dynamics with combined quantum and empirical potentials: C2H2 adsorption on Si(100). *J. Chem. Phys.*, 99:1356, 1993. URL http://dx.doi.org/10.1063/1.465381.

[123] Qiang Liu and Roald Hoffmann. The Bare and Acetylene Chemisorbed Si(001) Surface, and the Mechanism of Acetylene Chemisorption. *J. Am. Chem. Soc.*, 117: 4082, 1995. URL http://dx.doi.org/10.1021/ja00119a024.

[124] Y. Imamura, Y. Morikawa, T. Yamasaki, and H. Nakatsuji. First-principles molecular dynamics study of acetylene adsorption on the Si(001) surface . *Surface Science*, 341:L1091, 1995. URL http://dx.doi.org/10.1016/0039-6028(95)00792-X.

[125] Ru-Hong Zhou, Pei-Lin Cao, and Lie-Quan Lee. Total-energy calculations for acetylene adsorption and decomposition on Si(100)-2x1. *Phys. Rev. B*, 47:10601, 1993. URL http://dx.doi.org/10.1103/PhysRevB.47.10601.

[126] W. A. Hofer, A. J. Fisher, and R. A. Wolkow. Adsorption sites and STM images of C_2H_2 on Si(100): a first-principles study. *Surface Science*, 475:83, 2001. URL http://dx.doi.org/10.1016/S0039-6028(00)01076-1.

[127] R. Terborg, M. Polcik, J. T. Hoeft, M. Kittel, D. I. Sayago, R. L. Toomes, and D. P. Woodruff. Local adsorption geometry of acetylene on Si(100)(2×1): Multiple sites and the role of substrate temperature. *Phys. Rev. B*, 66:085333, 2002. URL http://dx.doi.org/10.1103/PhysRevB.66.085333.

[128] Yoshitada Morikawa. Adsorption geometries and vibrational modes of C_2H_2 on the Si(001) surface. *Phys. Rev. B*, 63:033405, 2001. URL http://dx.doi.org/10.1103/PhysRevB.63.033405.

[129] Dan C. Sorescu and Kenneth D. Jordan. Theoretical Study of the Adsorption of Acetylene on the Si(001) Surface. *J. Phys. Chem. B*, 104:8259, 2000. URL http://dx.doi.org/10.1021/jp001353n.

[130] Wondong Kim, Hanchul Kim, Geunseop Lee, Young-Kyu Hong, Kidong Lee, Chanyong Hwang, Dal-Hyun Kim, and Ja-Yong Koo. Initial adsorption configurations of acetylene molecules on the Si(001) surface. *Phys. Rev. B*, 64:193313, 2001. URL http://dx.doi.org/10.1103/PhysRevB.64.193313.

[131] Pier Luigi Silvestrelli, Olivia Pulci, Maurizia Palummo, Rodolfo Del Sole, and Francesco Ancilotto. First-principles study of acetylene adsorption on Si(100): The end-bridge structure. *Phys. Rev. B*, 68:235306, 2003. URL http://dx.doi.org/10.1103/PhysRevB.68.235306.

[132] Jun-Hyung Cho and Leonard Kleinman. Adsorption kinetics of acetylene and ethylene on Si(001). *Phys. Rev. B*, 69:075303, 2004. URL http://dx.doi.org/10.1103/PhysRevB.69.075303.

[133] R. Miotto, A. C. Ferraz, and G. P. Srivastava. Acetylene adsorption on the Si(001) surface. *Phys. Rev. B*, 65:075401, 2002. URL http://dx.doi.org/10.1103/PhysRevB.65.075401.

[134] H. W. Yeom, S. Y. Baek, J. W. Kim, H. S. Lee, and H. Koh. Adsorption of C_2H_2 and C_2H_4 on Si(001): Core-level photoemission. *Phys. Rev. B*, 66:115308, 2002. URL http://dx.doi.org/10.1103/PhysRevB.66.115308.

[135] Pier Luigi Silvestrelli, Flavio Toigo, and Francesco Ancilotto. Acetylene on Si(100) from first principles: adsorption geometries, equilibrium coverages, and thermal decomposition. *Journal of Chemical Physics*, 114:8539, 2001. URL http://dx.doi.org/10.1063/1.1366713.

[136] P. Skytt, P. Glans, J.-H. Guo, K. Gunnelin, C. Såthe, J. Nordgren, F. Kh. Gel'mukhanov, A. Cesar, and H. Ågren. Quenching of Symmetry Breaking in Resonant Inelastic X-Ray Scattering by Detuned Excitation. *Phys. Rev. Lett.*, 77: 5035, 1996. URL http://dx.doi.org/10.1103/PhysRevLett.77.5035.

[137] Y. Ma, P. Skytt, N. Wassdahl, P. Glans, D. C. Mancini, J. Guo, and J. Nordgren. Core excitons and vibronic coupling in diamond and graphite. *Phys. Rev. Lett.*, 71:3725, 1993. URL http://dx.doi.org/10.1103/PhysRevLett.71.3725.

[138] Y. Harada, T. Tokushima, Y. Takata, T. Takeuchi, Y. Kitajima, S. Tanaka, Y. Kayanuma, and S. Shin. Dynamical Symmetry Breaking under Core Excitation in Graphite: Polarization Correlation in Soft X-Ray Recombination Emission. *Phys. Rev. Lett.*, 93:017401, 2004. URL http://dx.doi.org/10.1103/PhysRevLett.93.017401.

[139] P. Skytt, J. Guo, N. Wassdahl, J. Nordgren, Y. Luo, and H. Ågren. Probing symmetry breaking upon core excitation with resonant x-ray fluorescence. *Phys. Rev. A*, 52:3572, 1995. URL http://dx.doi.org/10.1103/PhysRevA.52.3572.

[140] P. Glans, K. Gunnelin, P. Skytt, J.-H. Guo, N. Wassdahl, J. Nordgren, H. Ågren, F. Kh. Gel'mukhanov, T. Warwick, and E. Rotenberg. Resonant X-Ray Emission Spectroscopy of Molecular Oxygen. *Phys. Rev. Lett.*, 76:2448, 1996. URL http://dx.doi.org/10.1103/PhysRevLett.76.2448.

[141] K. Gunnelin, P. Glans, J.-E. Rubensson, C. Såthe, J. Nordgren, Y. Li, F. Gel'mukhanov, and H. Ågren. Bond-Length-Dependent Core Hole Localization Observed in Simple Hydrocarbons. *Phys. Rev. Lett.*, 83:1315, 1999. URL http://dx.doi.org/10.1103/PhysRevLett.83.1315.

[142] P. Glans, P. Skytt, K. Gunnelin, J. H. Guo, and J. Nordgren. Selectively excited X-ray emission spectra of N2 . *J. Electron Spectrosc. Relat. Phenom.*, 82:193, 1996. URL http://dx.doi.org/10.1016/S0368-2048(96)03065-4.

[143] A. J. Merer and Robert S. Mulliken. Ultraviolet spectra and excited states of ethylene and its alkyl derivatives. *Chem. Rev.*, 69:639, 1969.

[144] StoBe-deMon version 1.0. K. Hermann, L.G.M. Pettersson, M.E. Casida, C. Daul, A. Goursot, A. Koester, E. Proynov, A. St-Amant, D.R. Salahub, et.al., StoBe Software, 2002.

[145] F. Gel'mukhanov, T. Privalov, and H. Ågren. Collapse of vibrational structure in spectra of resonant x-ray Raman scattering. *Phys. Rev. A*, 56:256, 1997. URL http://dx.doi.org/10.1103/PhysRevA.56.256.

[146] F. Gel'mukhanov, P. Salek, T. Privalov, and H. Ågren. Duration of x-ray Raman scattering. *Phys. Rev. A*, 59:380, 1999. URL http://dx.doi.org/10.1103/PhysRevA.59.380.

[147] W. Domcke and L. S. Cederbaum. Vibronic coupling and symmetry breaking in core electron ionization . *Chem. Phys.*, 25:189, 1977. URL http://dx.doi.org/10.1016/0301-0104(77)87075-4.

[148] Luciano Triguero, Alexander Föhlisch, Peter Väterlein, Jorgen Hasselström, Martin Weinelt, Lars G. M. Pettersson, Yi Luo, Hans Ågren, and Anders Nilsson.

Direct Experimental Measurement of Donation/Back-Donation in Unsaturated Hydrocarbon Bonding to Metals. *J. Am. Chem. Soc.*, 122:12310, 2000. URL http://dx.doi.org/10.1021/ja0016710.

[149] Faris Gel'mukhanov and Hans Ågren. Channel interference in X-ray Raman scattering: parity selection rules, dephasing and localization of core holes. *J. Electron Spectrosc. Relat. Phenom.*, 93:31, 1998. URL http://dx.doi.org/10.1016/S0368-2048(98)00155-8.

[150] P. Jakob and D. Menzel. Benzene multilayers: A model for their anisotropic growth from vibrational spectroscopy and thermal desorption . *Surf. Sci.*, 220:70, 1989. URL http://dx.doi.org/10.1016/0039-6028(89)90464-0.

[151] P. Salek, F. Gel'mukhanov, and H. Ågren. Wave-packet dynamics of resonant x-ray Raman scattering: Excitation near the Cl LII,III edge of HCl. *Phys. Rev. A*, 59: 1147, 1999. URL http://dx.doi.org/10.1103/PhysRevA.59.1147.

[152] StoBe-deMon version 1.0. K. Hermann, L.G.M. Pettersson, M.E. Casida, C. Daul, A. Goursot, A. Koester, E. Proynov, A. St-Amant, D.R. Salahub. Contributing authors: V. Carraveta, H. Duarte, N. Godbout, J. Guan, C. Jamorski, M. Leboeuf, V. Malkin, O. Malkina, M. Nyberg, L. Pedocchi, F. Sim, L. Triguero, A. Vela, StoBe Software, 2002.

[153] Tor Karlsen, Leif J. S'thre, Knut J. Brve, Nora Berrah, Edwin Kukk, John D. Bozek, Thomas X. Carroll, and T. Darrah Thomas. Vibrational Structure and Vibronic Coupling in the Carbon 1s Photoelectron Spectra of Ethane and Deuteroethane. *J. Phys. Chem. A*, 105:7700, 2001. URL http://dx.doi.org/10.1021/jp010863u.

[154] K. C. Prince, M. Vondr ek, J. Karvonen, M. Coreno, R. Camilloni, L. Avaldi, and M. de Simone. A critical comparison of selected 1s and 2p core hole widths . *J. Electron Spectrosc. Relat. Phenom.*, 101-103:141, 1999. URL http://dx.doi.org/10.1016/S0368-2048(98)00436-8.

[155] L. Triguero, L.G.M. Pettersson, and H. Ågren. Calculations of X-Ray Emission Spectra of Molecules and Surface Adsorbates by Means of Density Functional Theory. *J. Phys. Chem. A*, 102:10599, 1998. URL http://dx.doi.org/10.1021/jp980824r.

[156] H. Rabus, D. Arvanitis, M. Domke, A. Puschmann, L. Wenzel, C. Comelli, G. Kaindl, and K. Baberschke. The vibrational fine structure of chemisorbed C2H4 molecules in the (1s-1, *) state. *Phys. Scr.*, T31:131, 1990. URL http://www.physica.org/asp/TopicalArticleList.asp?Vol=T31.

[157] J.L. Solomon, R.J. Madix, W. Wurth, and J. Stöhr. NEXAFS and EELS Study of the Orientation of Sulfur Dioxide on Ag(110). *J. Phys. Chem.*, 95:3687, 1991.

[158] Y. Ma, C. T. Chen, G. Meigs, K. Randall, and F. Sette. High-resolution K-shell photoabsorption measurements of simple molecules. *Phys. Rev. A*, 44:1848, 1991. URL http://dx.doi.org/10.1103/PhysRevA.44.1848.

[159] P. F. Williams, D. L. Rousseau, and S. H. Dworetsky. Resonance Fluorescence and Resonance Raman Scattering: Lifetimes in Molecular Iodine. *Phys. Rev. Lett.*, 32:196, 1974. URL http://dx.doi.org/10.1103/PhysRevLett.32.196.

[160] A. Nilsson, P. Bennich, T. Wiell, N. Wassdahl, N. Mårtensson, J. Nordgren, O. Björneholm, and J. Stöhr. Direct probing of the adsorbate-substrate chemical bond using angle-dependent x-ray-emission spectroscopy. *Phys. Rev. B*, 51: 10244, 1995. URL http://dx.doi.org/10.1103/PhysRevB.51.10244.

[161] A. Nilsson, M. Weinelt, T. Wiell, P. Bennich, O. Karis, N. Wassdahl, J. Stöhr, and M. G. Samant. An Atom-Specific Look at the Surface Chemical Bond. *Phys. Rev. Lett.*, 78:2847, 1997. URL http://dx.doi.org/10.1103/PhysRevLett.78.2847.

[162] A. Nilsson, N. Wassdahl, M. Weinelt, O. Karis, T. Wiell, P. Bennich, J. Hasselström, A. Föhlisch, J. Stöhr, and M. Samant. Local probing of the surface chemical bond using X-ray emission spectroscopy. *Appl. Phys. A*, 65:147, 1997. URL http://dx.doi.org/10.1007/s003390050557.

[163] M. Weinelt, N. Wassdahl, T. Wiell, O. Karis, J. Hasselström, P. Bennich, A. Nilsson, J. Stöhr, and M. Samant. Electronic structure of benzene on Ni(100) and Cu(110): An x-ray-spectroscopy study. *Phys. Rev. B*, 58:7351, 1998. URL http://dx.doi.org/10.1103/PhysRevB.58.7351.

[164] H. Öström, A. Föhlisch, M. Nyberg, M. Weinelt, C. Heske, L. G. M. Pettersson, and A. Nilsson. Ethylene on Cu(110) and Ni(110): electronic structure and bonding derived from X-ray spectroscopy and theory. *Surf. Sci.*, 559:85, 2004. URL http://dx.doi.org/10.1016/j.susc.2004.04.041.

[165] M. J. S. Dewar. A Review of the π-Complex Theory. *Bull. Soc. Chim. Fr.*, 18: C71–C79, 1951.

[166] J. Chatt and L. A. Duncanson. Olefin co-ordination compounds. Part III. Infra-red spectra and structure: attempted preparation of acetylene complexes. *Journal of the Chemical Society*, pages 2939 – 2947, 1953. URL http://dx.doi.org/10.1039/JR9530002939.

[167] Y. Ma, N. Wassdahl, P. Skytt, J. Guo, J. Nordgren, P. D. Johnson, J-E. Rubensson, T. Boske, W. Eberhardt, and S. D. Kevan. Soft-x-ray resonant inelastic scattering at the C K edge of diamond. *Phys. Rev. Lett.*, 69:2598, 1992. URL http://dx.doi.org/10.1103/PhysRevLett.69.2598.

[168] C. Keller, M. Stichler, G. Comelli, F. Esch, S. Lizzit, W. Wurth, and D. Menzel. Ultrafast Charge Transfer Times of Chemisorbed Species from Auger Resonant Raman Studies. *Phys. Rev. Lett.*, 80:1774, 1998. URL http://dx.doi.org/10.1103/PhysRevLett.80.1774.

[169] P. A. Brühwiler, O. Karis, and N. Mårtensson. Charge-transfer dynamics studied using resonant core spectroscopies. *Rev. Mod. Phys.*, 74:703, 2002. URL http://dx.doi.org/10.1103/RevModPhys.74.703.

[170] T. Belling, T. Grauschopf, S. Krüger, F. Nörtemann, M. Staufer, M. Mayer, V.A. Nasluzov, U. Birkenheuer, and N. Rösch. PARAGAUSS, version 2.1, 2000.

[171] Th. Belling, Th. Grauschopf, S. Krüger, M. Mayer, F. Nörtemann, M. Staufer, C. Zenger, and N. Rösch. Quantum Chemistry on Parallel Computers: Concepts and Results of a Density Functional Method. In Hans-Joachim Bungartz, Franz Durst, and Christoph Zenger, editors, *High Performance Scientific and Engineering Computing*, volume 8 of *Lecture Notes in Computational Science and Engineering*, page 439. Springer, Heidelberg, 1999. URL http://www.springeronline.com/.

[172] Markus Staufer, Uwe Birkenheuer, Thomas Belling, Folke Nörtemann, Notker Rösch, Wolf Widdra, Krassimir L. Kostov, Thomas Moritz, and Dietrich Menzel. The vibrational structure of benzene adsorbed on Si(001). *J. Chem. Phys.*, 112: 2498, 2000. URL http://dx.doi.org/10.1063/1.480816.

[173] M. Staufer, U. Birkenheuer, T. Belling, F. Nörtemann, N. Rösch, M. Stichler, C. Keller, W. Wurth, D. Menzel, L.G.M. Pettersson, A. Föhlisch, and A. Nilsson. Interpretation of x-ray emission spectra: NO adsorbed on Ru(001). *J. Chem. Phys.*, 111:4704, 1999. URL http://dx.doi.org/10.1063/1.479232.

[174] deMon Basis set library, 2001. URL http://www.demon-software.com/public_html/BASIS.html. Website (2005-10-02).

[175] Thom. H. Dunning. Gaussian Basis Functions for Use in Molecular Calculations. III. Contraction of (10s6p) Atomic Basis Sets for the First-Row Atoms. *J. Chem. Phys.*, 55:716, 1971. URL http://dx.doi.org/10.1063/1.1676139.

[176] Sigeru Huzinaga. Gaussian-Type Functions for Polyatomic Systems. I. *J. Chem. Phys.*, 42:1293, 1965. URL http://dx.doi.org/10.1063/1.1696113.

[177] A. D. Becke. Density-functional exchange-energy approximation with correct asymptotic behavior. *Phys. Rev. A*, 38:3098, 1988. URL http://dx.doi.org/10.1103/PhysRevA.38.3098.

[178] John P. Perdew and Wang Yue. Accurate and simple density functional for the electronic exchange energy: Generalized gradient approximation. *Phys. Rev. B*, 33:8800, 1986. URL http://dx.doi.org/10.1103/PhysRevB.33.8800.

[179] J. P. Gauyacq and A. G. Borisov. Excited electron transfer between a core-excited Ar*($2p^{-1}_{3/2}4s$) atom and the metal substrate in the Ar/Cu(111) system. *Phys. Rev. B*, 69:235408, 2004. URL http://dx.doi.org/10.1103/PhysRevB.69.235408.

[180] S. Vijayalakshmi, A. Föhlisch, F. Hennies, A. Pietzsch, M. Nagasono, W. Wurth, A. G. Borisov, and J. P. Gauyacq. Surface projected electronic band structure and adsorbate charge transfer dynamics: Ar adsorbed on Cu(111) and Cu(100). submitted to PRL, 2005.

[181] L. G. M. Pettersson, H. Ågren, Y. Luo, and L. Triguero. Benzene adsorbed on Cu(110): theoretical X-ray absorption, emission and shake calculations. *Surf. Sci.*, 408:1, 1998. URL http://dx.doi.org/10.1016/S0039-6028(98)00085-5.

[182] Luciano Triguero, Lars G. M. Pettersson, Boris Minaev, and Hans Ågren. Spin uncoupling in surface chemisorption of unsaturated hydrocarbons. *J. Chem. Phys.*, 108:1193, 1998. URL http://dx.doi.org/10.1063/1.475481.

[183] H. Öström, D. Nordlund, H. Ogasawara, K. Weiss, L. Triguero, L.G.M. Pettersson, and A. Nilsson. Geometric structure and chemical bonding of acetylene adsorbed on Cu(110). *Surf. Sci.*, 565:206, 2004. URL http://dx.doi.org/10.1016/j.susc.2004.07.012.

[184] Mary Coville and T. Darrah Thomas. Molecular effects on inner-shell lifetimes: Possible test of the one-center model of Auger decay. *Phys. Rev. A*, 43:6053, 1991. URL http://dx.doi.org/10.1103/PhysRevA.43.6053.

[185] S. Vijayalakshmi, A. Föhlisch, F. Hennies, A. Pietzsch, M. Nagasono, and W. Wurth. In Manuscript, 2005.